FACULTY OF ELECTRICAL ENGINEERING

UNIVERSITY
OF WEST BOHEMIA

ELECTRO-MECHANICAL INTERACTION BETWEEN ELECTRIC DRIVE AND ITS MECHANICAL LOAD AND CONTROL INTERVENTIONS MITIGATING UNWANTED VIBRATION PHENOMENA

A thesis submitted for the degree of

Doctor of Philosophy

2018   Ing. Martin Brůha

ZÁPADOČESKÁ UNIVERZITA V PLZNI
FAKULTA ELEKTROTECHNICKÁ

ELEKTROMECHANICKÁ INTERAKCE MEZI ELEKTRICKÝM POHONEM A MECHANICKOU ZÁTĚŽÍ A ŘÍDICÍ ALGORITMY PRO JEJÍ POTLAČENÍ

Disertační práce

k získání akademického titulu doktor

v oboru

Elektronika

Autor:	Ing. Martin Brůha
Školitel:	prof. Ing. Zdeněk Peroutka, Ph.D.
Datum státní doktorské zkoušky:	04. 06. 2015
Datum odevzdání práce:	31. 08. 2018

Prohlášení autora

Předkládám tímto k posouzení a obhajobě disertační práci zpracovanou na závěr doktorského studia na Fakultě elektrotechnické Západočeské univerzity v Plzni. Prohlašuji, že jsem tuto práci vypracoval samostatně s použitím odborné literatury a pramenů, uvedených v seznamu, který je součástí této práce.

V Plzni 31. 08. 2018

_____

Ing. Martin Brůha

Prohlášení garanta projektu

Tato práce vznikla s podporou projektu LO1607 – RICE-NETESIS: New Technologies for Smart Industrial Systems (MŠMT) a projektu TAČR TE01020455, jejichž jsem řešitelem. Potvrzuji, že Ing. Martin Brůha je hlavním autorem částí, které jsou představeny v této práci.

V Plzni 31. 08. 2018

_____

prof. Ing. Zdeněk Peroutka, Ph.D.

Acknowledgement

Anotace

Frekvenční měniče se staly standardním technickým řešením pohonů s proměnnými otáčkami. Technický pokrok a cenový vývoj výkonové elektroniky umožnil jejich široké nasazení v nejrůznějších aplikacích a průmyslových odvětvích (od poměrně jednoduchých pohonů ventilátorů a čerpadel až po dopravníky, kompresory nebo dynamicky náročné pohony ve válcovnách). Mezi nesporné výhody otáčkové regulace patří zejména velmi vysoká energetická účinnost v širokém rozsahu otáček, významné energetické úspory a přesná regulace otáček a momentu s rychlou dynamickou odezvou. Kromě neoddiskutovatelných výhod řešení s měničem frekvence je třeba také zohlednit jisté minusy, např. harmonické zkreslení napětí sítě anebo zvlnění momentu. Právě kvalita momentu ve vzduchové mezeře a jeho frekvenční spektrum spolu s regulačními smyčkami a jejich zpětnovazebními efekty hrají důležitou roli z hlediska kmitání a torzních vibrací. Optimalizace poháněných zařízení z hlediska účinnosti a nákladů způsobila, že moderní systémy s turbostroji jsou citlivější než dříve. Vznikla proto logická potřeba detailního pochopení vlivu frekvenčního měniče na hřídelovou soustavu a zajištění stabilního a bezpečného chodu. Celá věc je navíc složitější díky tomu, že jsou do ni zapojeni elektroinženýři a strojní inženýři a je třeba najít společný jazyk.

Tato práce se zabývá elektromechanickou interakcí mezi frekvenčním měničem, napájeným elektromotorem a mechanickým soustrojím u pohonů středních a zejména velkých výkonů (řádově jednotky až desítky megawatt). Nejprve je analyzován moment motoru a jeho zvlnění, tj. jednotlivé pulsační složky momentu. Zkoumány jsou faktory mající vliv na tyto složky: topologie měniče, způsob modulace, nastavení regulátorů, interakce se zátěží a dále také specifické řídicí algoritmy.

Hlavní pozornost je zaměřena na způsob řízení pohonu resp. frekvenčního měniče a jeho vliv na interakci s poháněným zařízením.

Cílem práce je zejména optimalizace pohonu z hlediska minimalizace torzních kmitů a dále pak návrh a ověření algoritmů jejich aktivního tlumení. Nejperspektivnější metody jsou detailněji prezentovány pomocí simulací či v podobě měření konkrétních pohonů. Důraz je kladen také na analytické způsoby pro určení stability pohonu z hlediska torzního kmitání. S jejich pomocí je frekvenční měnič optimálně parametrizován předtím, než je uveden do provozu. Problematika elektro-mechanické interakce je demonstrována na několika reálných případech z praxe.

V závěru jsou zmíněny perspektivní algoritmy řízení pro tlumení kmitání a poskytnuty praktické rady, jak zohlednit elektrický regulovaný pohon s frekvenčním měničem jako součást torzního systému.

Klíčová slova

Vysokonapěťový pohon, zátěží komutovaný střídač (LCI), napěťový střídač (VSI), zpětná vazba, regulátor, přímé řízení momentu (DTC), vektorové řízení, elektromechanická interakce, pružný hřídel, vlastní frekvence, vibrace, simulace, experiment, aktivní tlumení

Abstract

Frequency converters have become a standard technical solution for variable speed drives. Technical progress and price development in the field of power semiconductors enabled its wide use in various applications and industrial branches (from simple fan and pump drives up to conveyors, compressor drives or dynamically demanding rolling mill drives). Among the major advantages of frequency control belong very high efficiency across wide speed range, significant energy saving potential and accurate speed and torque control with fast dynamic response. Besides those clear benefits, some drawbacks shall be considered as well, e.g. supply voltage harmonic distortion or torque ripple. The quality of air gap torque and its frequency spectrum together with control loops and their closed loop effects play important role from oscillation and torsional vibration point of view. Optimization of driven machines in regards to efficiency and cost reduction lead to a higher sensitivity of turbomachinery systems. Therefore, a logical need emerged to have a detailed understanding of the influence of frequency converter on the shaft string and ensuring of stable and safe operation. In addition, the whole thing is more complicated since it involves electrical and mechanical engineers and they need to find a common language.

This work deals with modern concepts of electric drives for medium and high power (megawatt range), particularly with electro-mechanical interaction between frequency converter, electric motor and mechanical shaft system. First the motor torque and its ripple is analyzed, i.e. the pulsating components of air gap torque. Factors influencing torque ripple such as converter topology, modulation scheme, controller settings, interaction with load and also specific control algorithms are investigated.

Focus is on the control strategy of the drive or frequency converter respectively, and the influence on the interaction with driven equipment.

The aim of this work is mainly an optimization of the drive from the point of view of minimized torque pulsations and development as well as verification of algorithms for active damping.

The most perspective methods are presented by means of simulations or measurements on specific drives. Focus is also given on analytic methods to determine stability from torsional viewpoint. With such aid, the parameters of the frequency converter are tuned prior to the commissioning phase. The problematic of electro-mechanical interaction is demonstrated on examples of several real field cases.

The summary shows selected active damping functions and gives some practical hints how to deal with variable speed drive with a frequency converter as part of a torsional system.

Keywords

Kurzfassung der Dissertation

Die Frequenzumrichter sind eine Standardlösung für drehzahlgeregelte Antriebe geworden. Der technische Fortschritt und die Preisentwicklung im Bereich von Leistungselektronik haben einen breiten Einsatz in verschiedenen Applikationen und Industriebereiche ermöglicht (von einfachen Lüfter- und Pumpenantrieben über Förderband-Anwendungen und Verdichterantriebe bis zu dynamisch anspruchsvollen Antrieben in Walzwerken). Zu den Hauptvorteilen von Frequenzregelung gehören ein hoher Wirkungsgrad über einen breiten Drehzahlbereich, bedeutende Energieeinsparungen und genaue Drehzahl- und Drehmomentgenauigkeit mit schneller dynamischer Antwort. Neben den klaren Vorteilen gibt es auch bestimmte Nachteile, wie z.B. die Netzrückwirkungen mit Spannungsverzerrung oder die Pulsigkeit vom Drehmoment. Die Qualität vom Drehmoment in der Luftspalt und sein Frequenzspektrum zusammen mit den Regelkreisen und denen Rückführungeffekten spielen eine wichtige Rolle aus Sicht von Oszillationen und Torsionsschwingungen. Die Optimierung von den Lastmaschinen führte dazu, dass heutige Turbomaschinen viel empfindlicher sind als früher. Ein logischer Bedarf ist entstanden, ein detailliertes Verständnis von dem Einfluss des Frequenzumrichters auf den Antriebsstrang zu haben und einen stabilen Betrieb zu garantieren. Das ganze Thema wird zusätzlich komplizierter, weil es Elektroingenieure und Maschinenbauer involviert und die eine gemeinsame Sprache finden müssen. Vorliegende Dissertation befasst sich hauptsächlich mit elektro-mechanischen Interaktion zwischen dem Frequenzumrichter, Elektromotor und mechanischer Last bei drehzahlregelbaren Antrieben von mittleren und hohen Leistungen (Megawatt-Bereich). Zuerst wird das Drehmoment der Maschine analysiert und vor allem dessen Welligkeit, d.h. einzelne Pendelmomente. Faktoren, die Einfluss auf die Pendelmomente haben, werden im Detail untersucht: Topologie des Frequenzumrichters, Modulationsverfahren, Einstellungen der Regler, Interaktion mit der mechanischen Last und spezifische Regelalgorithmen.

Die grösste Aufmerksamkeit wird den Regelungsstrategien des Frequenzumrichters gewidmet und der Einfluss auf die Interaktion mit der angetriebenen Last.

Das Ziel dieser Arbeit ist eine Optimalisierung des Antriebes aus Sicht der Minimierung von Torsionsvibrationen und weiter dann Entwurf und Verifikation von Algorithmen für aktive Dämpfung. Die perspektivsten Methoden werden detaillierter präsentiert mittels Simulationen oder Messungen konkreter Antriebe. Schwerpunkt ist in der analytischen Bestimmung der Antriebsstabilität aus Sicht der Torsionsschwingungen. Anhand von diesen Methoden wird der Frequenzumrichter optimal parametriert eher die reale Inbetriebsetzung anfängt. Die Problematik der elektro-mechanischen Interaktion wird anhand von mehreren konkreten Anlagen aus dem Feld demonstriert.

In der Zusammenfassung werden perspektiven Algorithmen für aktive Dämpfung erwähnt. Praktische Vorschläge werden vollbracht, wie man den drehzahlregelbaren Antrieb mit einem Frequenzumrichter richtig als Teil von Torsionssystem berücksichtigen soll.

Stichwörter

Mittelspannungsantrieb, lastkommutierter Wechselrichter (LCI), Spannungswechselrichter (VSI), Rückführung, Regler, direkte Selbstregelung (DTC), Vektorregelung, elektro-mechanische Interaktion, elastische Welle, Eigenfrequenz, Vibration, Simulation, Experiment, aktive Dämpfung

Contents

Nomenclature

List of Symbols and Abbreviations		
Symbol	Definition	Unit
AF	amplification factor	[pu]
AFD	adjustable frequency drive [1)	
AGT	air gap torque	[Nm]
AMB	active magnetic bearings	
ANPC	active neutral point clamped	
API	American Petroleum Institute	
ARF	anti-resonance frequency	
ASD	adjustable speed drive [1)	
AVR	automatic voltage regulator	
CLS	converter line side (rectifier)	
CMS	converter motor side (inverter)	
CSI	current source inverter	
$\cos\phi$	power factor	[-]
DOF	degree of freedom	
DTC	direct torque control	
η	efficiency	[-]
E	energy	[MWh]
FEA	finite element analysis	
FPGA	field programmable gate array	
FSC	floating symmetrical capacitor	
g	acceleration of gravity (9,80665 m/s^2)	[m/s^2]
GTG	gas turbine generator	
GTO	gate turn-off (thyristor)	
HVDC	high voltage direct current (transmission)	
I_{mM}	motor magnetizing current	[A]
I_{sdM}	motor direct (flux) component of stator current	[A]
I_{sM}	motor stator current	[A]
I_{sqM}	motor quadrature (torque) component of stator current	[A]
IEC	International Electrotechnical Commission	
IEEE	Institute of Electrical and Electronics Engineers	
IEGT	injection enhanced gate transistor	
IGBT	insulated gate bipolar transistor	
IGCT	integrated gate-commutated thyristor	
ISO	International Organization for Standardization	

List of Symbols and Abbreviations		
Symbol	Definition	Unit
$k_{\psi M}$	motor constant	[-]
L_{hM}	motor main (magnetizing) inductance	[H]
LCI	load-commutated inverter	
LNG	liquefied natural gas	
m	mass	[g]
M2C	modular multi-level converter (also written as MMC)	
MCS	maximum continuous speed	[rpm]
MMC	modular multi-level converter (also written as M2C)	
MMF	magneto-motive force	
MOS	minimum operating speed	[rpm]
MV	medium voltage	
n	speed	[rpm]
n_{pp}	motor pole-pairs	[-]
NPC	neutral point clamped	
ω	angular speed	[rad/s]
OEM	original equipment manufacturer	
OP	operating profile / operating point	[-]
ϕ	electrical angle between voltage and current	[-]
p	pole number	[-]
P	power	[kW]
PFC	power factor correction	
PDS	power drive system [2]	
PSS	power system stabilizer	
R	resistance	[Ω]
s_M	motor slip	[-]
S	apparent power	[kVA]
SM	separation margin synchronous motor	
SRC	silicon controlled rectifier	
SSCI	sub-synchronous control interaction	
SSR	sub-synchronous resonance	
SSTI	sub-synchronous torsional interaction	
t	time	[s]
T	torque	[Nm]
T_M	motor torque	[Nm]
TFA	transfer function analysis	

List of Symbols and Abbreviations		
Symbol	Definition	Unit
TNF	Torsional natural frequency	[Hz]
U	voltage or phase to phase voltage	[V]
U_p	phase to ground voltage	[V]
UIF	unit interaction factor	
VFD	variable frequency drive [1]	
VSD	variable speed drive [1]	
VSDS	variable speed drive system [2]	
VSI	voltage source inverter	
X	reactance	[Ω]
X_σ	leakage reactance	[Ω]
X_m	main reactance	[Ω]

Note 1: Use of abbreviations AFD/ASD/SFC/VFD/VSD.

[1] Abbreviations AFD, ASD, SFC, VFD and VSD are often used as synonyms to describe the same equipment, i.e. a frequency converter consisting of power electronic semiconductors. The meaning of each abbreviation is not exactly the same.

- Variable speed drive (VSD) is a general term for anything that varies the speed of motor driven load (AC drive, DC drive, eddy current clutch drive, hydraulic variable speed drive etc.). The speed is controlled electrically or mechanically.

- Variable frequency drive (VFD) is a smaller subset of VSD. It is an equipment controlling the speed of AC motor by altering frequency and voltage of the motor. Therefore, VFD is used for purely electrical speed control of motors. For example, DC drive is a VSD, but not a VFD.

- Adjustable speed drive (ASD) has similar meaning like VFD. The term ASD is typically used in North America.

Other terms are used as well: static frequency converter (SFC), frequency converter or just converter or drive (when understandable from the context). This work uses both abbreviations VFD and VSD.

Note 2: Use of abbreviations PDS/VSDS.

[2] Abbreviations PDS and VSDS have identical meaning. The term describes a drive system, i.e. not just the VSD, but also other system components such as isolation input transformer and motor; optionally also a harmonic filter, external cooler etc. IEC standards define the term PDS. However, the drive manufacturers and customers more frequently use the abbreviation VSDS.

General Indices		
Index	Definition	Examples
1	primary (input) side	Q_1
2	secondary (output) side	Q_2
a	armature	I_a
avg	average	T_{avg}
max	maximal value	n_{max}
min	minimal value	n_{min}
L	load	
M	motor	η_M
N	nominal value	P_N
OP	operating point	Q_{OP}
sc	short circuit	S_{sc}
pu	per unit value	T_{pu}
tot	total value	P_{tot}

Function Definitions		
Notation	Description	Examples
$f(x)$	function	$\eta=f(Q)$, $H = H(Q)$
$f_{IntersectLinIntArrays}(\mathbf{X1,Y1,X2,Y2})$	Find intersect of two discrete curves using linear interpolation represented by four one-dimension arrays.	

Note 1 – Array, matrix, vector notation: Highlighted by bold font.

Note 2 – Scalar notation: Highlighted by italic font.

Note 3 – Matrices multiplication: Matrix multiplication is marked by symbol: "*", matrix and array multiplication in the meaning element by element is expressed by symbol ".*" (Mathworks Matlab notation).

Note 4 – Matrices division: Matrix division is marked by symbol: "/", matrix and array division in the meaning element by element is expressed by symbol "./" .

Note 5 – Relation between per-unit ("pu") and "percentage" expression:

$$x_{percentage}[\%] = x_{per-unit}[-] \times 100$$

1   Introduction

Variable Speed Drive Systems (VSDS) have gained an increased popularity throughout the industry and their installed base is continuously growing. The factors driving growth in the VSDS market are energy prices, stringent efficiency regulations, power quality and often the process requirements. The advantages of VSDS are well known: significant energy savings, soft starting or precise speed and torque control and excellent dynamics (e.g. [1]). Among other specific features belong regenerative braking, power factor compensation etc. Besides these benefits, there are also some challenges. They are mainly related to the interaction of the power electronic converter with other equipment.

On the grid side, there is an interaction between the converter, input transformer and supply grid. The VSDS shall inject as little harmonics into the grid as possible. On the motor side, there is similar interaction between converter and motor (current harmonics, rapid dv/dt changes, bearing currents etc). The mentioned topics are known and there are efficient solutions how to mitigate the issues (e.g. reinforced motor insulation, use of multi-level converters, output dv/dt filter or sine filter). An area that still needs certain attention is the electro-mechanical interaction on higher system level:

On the line side between VSD and generators in local power generation and on the motor side between the VSD and the driven equipment (compressor, blower, pump, rolling mill etc.).
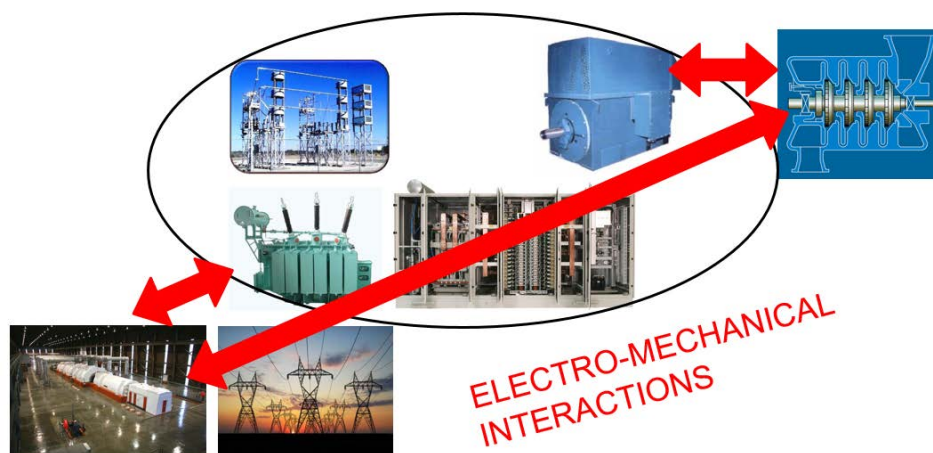
Figure 1-1: Electro-mechanical interaction within Variable speed drive systems (VSDS)

The torque pulsations generated by the variable speed drive system (VSDS) interfere with the mechanical shaft components. It causes increased torsional and lateral vibrations, audible noise, and accelerated aging or even component failure. In order to reduce the electro-mechanical interaction it is crucial to understand the phenomena of vibrations in VSDS.

A comprehensive study of the electro-mechanical interactions is a complex job since it combines different engineering fields, such as power electronics and electric drives, electric motor design, knowledge of rotordynamics, control theory and even basics of application engineering or process engineering. One person does normally not cover all the above disciplines. Instead, there are several specialists focusing on a dedicated field. A successful analysis of electro-mechanical interaction requires an interdisciplinary approach.

This work aims to explain the phenomena of torsional vibration of systems incorporating VSDs and fill in certain gaps in this field. A process is developed how to treat VSD from torsional point of view during engineering phase to ensure satisfactory system integration and system performance. Several mitigation methods are proposed in order to minimize the torsional risk. The methods shall be robust and easy to parameterize in order to enable their use in projects. The goal of such algorithms is to increase the overall damping by means of control. Examples point out the possibilities of passive damping as well as perspective active damping algorithms.

Some of the first torsional vibration issues in VSDS are mentioned in [2]. They were reported since 1970s when the semiconductor based VSDs started to be launched in various industries. At that time, current source inverter (CSI) type technology had been exclusively used. The engineers had to re-think the classical torsional analysis and consider the consequence of variable speed as well as additional excitations. Nowadays the topic is well known, but it still might be forgotten or misunderstood during the system integration. The torque ripple due to semiconductor switching and consequent non-sinusoidal current and voltage waveforms is understandable for most engineers. However, the effects related to closed loop behavior are less obvious and often underestimated, especially when people have their background on systems operating in open loop. It is also a question of system responsibility when integrating drive components from several manufacturers. Furthermore, as there is large variety of VSD topologies (nowadays with majority of voltage source inverters) and control techniques, a deeper knowledge of the specific VSD being utilized is required and VSD manufacturer shall support the torsional analysis by providing reliable and accurate data.

Finally, a successful electro-mechanical system integration requires a good collaboration between manufacturer of VSD and manufacturer of driven load and expertise of the system integrator.

1.1 Motivation

Applications incorporating VSDS may experience torsional vibration. If the issue is not considered in the system integration, excessive vibration may appear during normal operation. The consequences might be an impacted process quality (e.g. rolling mill drives), restricted performance (e.g. forbidden speed ranges), accelerated mechanical wear andl fatigue, unexpected downtimes and in worst-case failures or even hazard for personnel. A depth-in analysis is needed to mitigate risks of torsional vibration and excessive mechanical stress.

In order to successfully solve the problem we need to understand the root cause. It requires interdisciplinary approach combining several engineering fields such as power electronics and electric drives, control theory, rotordynamics etc. The challenge is nicely formulated in following quote:

"Electrical engineers see electrical problems. Mechanical engineers see mechanical. But many problems lie in the boundary between. An electromechanical perspective reveals the entire picture: the electrical, the mechanical and the complex interactions between the two."

Source: Lloyd's Register Consulting

The electro-mechanical interaction is especially important in systems with closed-loop control. When the electrical part influences the mechanical one, it is seen in the mechanical quantities, such as e.g. speed. When the mechanical quantity is sensed and used as feedback signal to control the electrical part then an electro-mechanical interaction is likely to happen. The basic principle of action and reaction was described by Sir Isaac Newton:

"For every action, there is an equal and opposite reaction"

Source: Newton's Third Law

Finally, the challenge for engineers dealing with oscillations in variable speed applications is summarized in the quote:

"If a drive system is able to oscillate, it will sooner or later start to oscillate"

Source: El. Eng. ETH Pieder Jörg and associated prof. Karel Zeman

Excessive torsional vibrations can result into gear wear, gear tooth failures, key failures, shrink fit slippage and broken shafts in severe cases.
The wide speed range increases the likehood that a coincidence between torsional natural frequency and excitation frequency exists at some operating speed. It also makes the torsional analysis more complex.

2   State of the art analysis

2.1   Technology evolution and general problems

2.1.1   Evolution

Oscillations and vibrations as undesired byproducts in electro-mechanical systems are known for decades. The issues are especially critical for high power turbo-machinery where the first torsional natural frequency tends to be low (typically below 20 Hz) and the inherent damping is almost negligible. The consequences of operation in resonance condition could be fatal. Therefore, it is no wonder that such systems are rigorously studied by rotordynamicists.

The classical approach is a forced response analysis. In this method the excitation sources of certain frequency and magnitude are applied and a response of the system is calculated. Magnitude of excitation is usually determined based on experiments and past experience. The method is an open loop type not considering system interactions. The evolution of power electronics was a game changer. It enabled the systems to operate efficiently at variable speed, allowed higher dynamics, but also brought new excitation sources with different signature. Moreover, the power electronic systems are non-linear devices. The open-loop analysis might not be able to cover the interactions in such systems anymore. Instead, an analysis considering the closed loop effects is needed.

Research for medium voltage AC drives started in the 1960s and industrial production in the 1970s. First medium voltage drive has been delivered in 1969. It was a 6.4 MW cyclo-converter working as gearless mill drive in a cement mill [3], [4]. The development continued rapidly. Cyclo-converters were used mainly for lower output frequencies. Sub- und super-synchronous cascades had been used as well. Then the era of current source inverters began. For high power range the load commutated inverter (LCI) became rapidly very popular in combination with synchronous machines, mainly because of its simple topology, robustness and easy scalability in terms of voltage and power. First LCI was delivered in 1974 [5], just five years after the pilot cyclo-converter. It was used as soft starter (LCI.SO) for gas turbines and pump storage plants. Very soon, a full drive for continuous duty followed (LCI.DR). The LCI drive is nowadays still a preferred choice in very high power range. In 1985 the worldwide first voltage source inverter (VSI) had been launched. Today, VSI is clearly the dominant drive technology on the market. Every leading drive manufacturer has a VSI drive in its portfolio. Most common topologies are listed below:

- 3-level neutral point clamped (NPC) or neutral point piloted (NPP) [6], [7], [8], [9], [10], [11], [12]
- 5-level NPC with cascaded H-bridge [13], [7], [14], [15]
- 5-level active neutral point clamped (ANPC) [16]
- cell-based multi-level (H-bridge) with multi winding transformer [6], [13], [7], [17]
- multi-level with multi capacitor-fed cells (flying capacitor clamped) [6], [7], [18]
- modular multi-level (MMC or M2C) converter [19], [20], [21], [22]

The selection of suitable topology depends often on process requirements. High performance drives typically have less voltage levels, but allow superior dynamics. Besides the various topologies, there are several modulation techniques. They both influence the spectrum of air gap torque and thus interaction with the shaft system. Frequently used modulation schemes are Pulse width modulation (PWM) [23] and hysteresis modulation as e.g. in direct torque control (DTC) [23] as well as optimized pulse pattern (OPP) [24], [25] sometimes also combined with model predictive techniques [26], [27]. Field oriented control (also known as vector control) frequently uses pulse width modulation (PWM) in its scheme. The spectrum contains characteristic harmonics and eventually non-characteristic harmonics as convolution products of carrier frequency and sampling times of the control loops.

Direct torque control (DTC) is based on hysteresis controllers for machine flux and torque. This control scheme is ideal for high dynamic applications as it allows extreme fast torque response. The pattern is inherently non-repetitive and the spectrum contains characteristic harmonics and broadband excitation of very low magnitude. With increasing switching frequency the magnitude of characteristic harmonics increases while the broadband noise gets smaller. In steady state operation the spectrum of DTC is similar like scalar or vector control with PWM modulator.

Optimized pulse pattern (OPP) is primarily used to eliminate specific harmonic orders from the harmonic spectrum. The pattern is pre-calculated offline. It naturally provides very distinct spectrum.

2.1.2 Oscillations in industrial applications

Lot of efforts have been put to investigate the mechanisms of oscillation and propose perspective countermeasures. Although the main focus of this work is on the electro-mechanical interaction between VSDS and the mechanical load (i.e. inverter-fed motor and driven equipment), it is very interesting and useful to make at least a short excursion into the other power electronic applications than just VSDS to see the challenges and the best practice to mitigate the oscillation problems. At a closer look, one can recognize that there are many analogies and some of them could be successfully transferred and re-used in a slightly different application. Studying the different approaches helps to understand the state of the art and might inspire for new ideas and solutions.

2.1.2.1   Traction applications

The development in railway transport goes into direction of larger interconnected systems. The use of modern locomotives driven by power electronic controlled motors brought a new requirement on interoperability and stability not known before. The "old" locomotives with dc motors and resistive control inherently had the behavior of positive damping in any circumstances. Modern locomotives, on the opposite, can act as negative damping at certain operating points. Such mechanism can destabilize the railway system and lead to a collapse [28], [29].

Learnings: The approach of positive equivalent impedance is a good idea and it could be principally used in industrial systems as well. Same principle was adopted e.g. for wind converters. It is also known as input admittance analysis.

2.1.2.2   Turbo-generators with super-conducting windings

The development of turbo-generators in power plants in 1970s and 1980s went towards larger and larger machines. A super-conducting rotor winding was proposed in order to get higher output power while keeping same machine dimensions and increasing the efficiency. This direction was considered as very perspective and followed by all major manufacturers. However, the dynamic performance and oscillation problems required a deep analysis [30].

- Transient behavior: The super-conducting field winding reduces inherent damping based on winding resistance.
- Control and regulation: The super-conducting field winding requires special concerns regarding control of field current and stability issues.

Special cylindrical winding layers have been proposed to maximize natural damping of torsional vibration and reduce the time variation of electromagnetic field.

Learnings: Systems with extremely low inherent electric damping have to be rigorously studied in terms of stability and controllability.

2.1.2.3 *Sub-synchronous oscillations*

Sub-synchronous torsional interaction as an instability phenomenon mainly associated with synchronous machines. The torsional mode of a turbine-generator shaft train is destabilized through the interaction with the load (large VSDS, HVDC terminals, static synchronous compensators). Resulting sub-synchronous oscillations might be large enough to trip the system or (if not protected) damage the equipment. The risk of sub-synchronous oscillations is significant if the power electronic load acts as negative resistance in certain frequency ranges. To ensure the stability a positive electrical damping at each torsional resonance as well as at low frequencies is necessary. Such (virtual) resistance can be provided by proper parameterization of power electronic converter. Positive electrical damping at each torsional resonance as well as at low frequencies in most cases implies stability [31], [32].

2.1.2.4 *Power generation*

In conventional power plants, dynamic interactions in power systems involving turbine generators are considered seriously and have been identified as potentially hazardous. According to [33] there are following types of interaction: Sub-synchronous resonance, Induction generator effect, device-dependent sub-synchronous oscillations, super-synchronous resonance, device-dependent super-synchronous oscillations and transient shaft torque oscillations.

The wind converters represent an interesting example to study, as there are two independent areas concerning stability and oscillations:

- passivity of wind converter towards the distribution grid (input admittance analysis)
- torsional vibration within wind turbine-generator variable speed shaft system

The grid has several resonances that could potentially be excited. Therefore, grid stability in wind parks is an important aspect. To ensure a smooth connection of large offshore wind park into a transmission grid an admittance analysis is recommended (approach from traction). The admittance is frequency dependent not equally important in all frequency regions. One approach used in the industry is enforced passivity within the frequency band of interest.

Another potential issue in the wind turbine-generator shaft system is torsional vibration. Damping strategies employ either passive or active damping systems. Passive systems use mechanical components with increased damping, e.g. rubber elements. Active systems utilize pitch control (adjustment of blades) or software algorithms to modify the torque of generator.

2.1.2.5   Power transmission

The High Voltage DC (HVDC) transmission is from topology point of view very close to an electric drive. It consists of a power electronics substation converting AC into DC, DC transmission line and another substation for the inverse conversion from DC to AC. The similarities have been described in [A2].
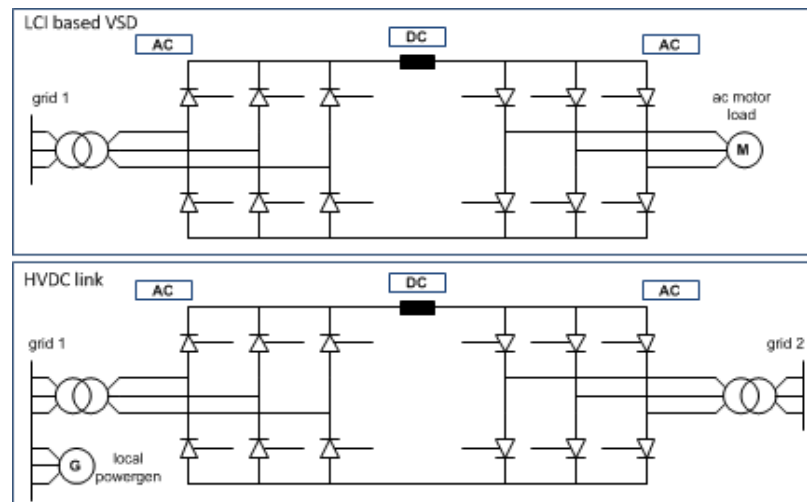
Figure 2-1: Simplest circuits representing an LCI based VSD (above) and a classic HVDC link with local power generation (below) [A2]

Nowadays, subsynchronous torsional interaction (SSTI) is a well-known phenomenon. To identify the risk of SSTI a screening study is always performed. First screening can be obtained by calculating so called Unit Interaction Factor (UIF) [34]. The empirical threshold is typically 0.1. Below that value there is small risk of SSTI, above that value the risk is higher and further studies and/or tests are recommended.

Learnings: Sub-synchronous torsional interaction might be a topic, especially in islanded networks with significant power electronics load. The experience comes mainly from HVDC transmission systems, but the same applies also for electric drive systems (e.g. large compressor drives with nearby power generation unit).

2.1.2.6   High-speed turbo compressors

Conventional solution for electric driven variable speed compressor trains is 4-pole motor with speed increasing gear. Since 1990s there is also the solution with compressor directly driven by high speed motor (gearless) [35], [36]. Depending on the rated speed the bearings are conventional (e.g. sleeve bearings) or active magnetic bearings (AMB). The AMB do not require any lubrication and allow operation in very wide speed range (e.g. 20…105% of nominal speed). There might be several critical speeds within the speed range. However, the control system can adjust the stiffness of the bearings depending on the speed. It allows shifting of critical speeds and avoiding vibration issues.

Learnings: Active adjustment of bearing stiffness allows shifting some of the critical speeds outside of speed range [30].

Summary of learnings is provided in table below:

Table 1: Oscillations across power electronics and motor drives applications

Application	Challenge	Solution	Limitation	Learning
Large turbo-generators in power plants (general)	- Power stability - Limited controllability	Power System Stabilizer (PSS)	Only for low frequencies (up to ca. 3-5 Hz); PSS shall not react on torsional vibration	System stability can be increased by suitable excitation control algorithms
Large turbo-generators with super-conducting windings (specific)	- Transient behavior due to low inherent damping - Control of field windings current - Stability issues	Special rotor construction with cylindrical layers to increase natural damping of torsional vibration		Systems with extremely low inherent damping need special attention in terms of stability and controllability
Power generation & Power transmission (HVDC)	SSTI between turbine-generator and HVDC terminal (destabilization of turbine-generator torsional mode)	Converter control to ensure positive damping	Only for low frequencies (up to ca. 3-20 Hz)	This approach of positive damping can be generalized as a stability criterion
Power generation & large power electronic load (islanded operation)	Sub-synchronous torsional interaction between turbine-generator and large VFD (destabilization of turbine-generator torsional mode)	Converter control to ensure positive damping	Availability of control algorithms for enhanced damping. Availability of plant data (especially resonance frequencies)	This approach of positive damping can be generalized as a stability criterion
Traction (rolling stock)	- Interoperability of rolling stock - Instability	Converter behavior as positive impedance/admittance throughout the control bandwidth	Passivity cannot be guaranteed at any frequency. However, it can be achieved for the critical frequency range.	This approach of positive impedance can be generalized as a stability criterion
Wind converters	- Stability of grid connected converters '- Interaction with weak grids	Same as traction, i.e. passivity and positive input admittance	Passivity cannot be guaranteed at any frequency. However, it can be achieved for the critical frequency range. Parallel operation of several active front end converters needs special attention.	This approach of positive impedance can be generalized as a stability criterion

2.1.3   Challenges

Due to increased operating speed range in VSDS systems and additional excitation mechanisms, variable frequency motor driven systems require special consideration when analyzed for torsional vibrations. The torsional analysis includes both steady state and dynamic torques coming from mechanical and electrical excitation. The electrical excitation components include the characteristic frequencies such as 6th, 12th, 18th and 24th orders of electric frequency. These characteristic (dominant) harmonics are injected by almost any VFD topology. However, there are also non-characteristic torque components. These harmonics and their behavior are linked to VFD topology, modulation scheme, inverter switching frequency, motor parameters, control algorithms and control parameter settings. A detailed information about the non-characteristic harmonics might not be easily accessible. Although the non-

characteristic harmonic components are much lower in magnitude compared to characteristic harmonics, they might still be dangerous for sensitive driven load equipment. To get reliable figures of excitation torques injected by VFD is a matter of proper system integration.

Another challenge is caused by the fact that torsional vibration is difficult to measure. It is therefore a very complex problem to setup a reliable condition monitoring. The indirect monitoring is based on measurement of lateral vibration that is a superposition of several excitation sources. The decomposition is not trivial making it hard to separate the vibration portion added through torsional-lateral transfer. In other words, it is difficult to distinguish between lateral vibration caused primary by torsional vibration and transferred through gear system and lateral vibration caused by other sources (unbalance, misalignment, effects inside the gear, hydrodynamic effects in sleeve bearings etc). The recalculation of lateral vibration magnitude into torsional stress is not easy either.

When developing advanced algorithms based on additional state feedbacks (load speed, load torque and shaft torque and eventually also their derivatives), the next challenge comes how to estimate these signals. Some authors consider e.g. the load torque as function of speed. However, this might not be 100% true. When the drive system operates within the design speed range, the load torque changes based on process requirements and cannot be assumed as simple function of speed.

2.2 Main problems under research and existing solutions

The main problems under present research are mainly the inherent torque pulsations due to converter topology and modulation technique, sub-synchronous torsional excitation due to presence of interharmonics and interactions associated with closed-loop control system.

2.2.1 State of the art in industrial applications

The problem with oscillations and vibrations appear in many industrial applications and some of the leading drive manufacturers spend significant effort in developing various control algorithms to increase the immunity of their system against those oscillations:

Oil and Gas [37], [38], [39], [40] , [41], [42], [43], [44], [45], [46], [47], [48], [49], [50]
The plant availability is key criteria. Modern compressors tend to be more efficient and better utilized, but at the same time less robust against vibrations. The compressor drive systems have very low inherent damping. Due to variable speed operation the torsional issues become more pronounced.

The authors investigate the phenomena of torsional vibration in large turbo-compressor trains, propose control modifications to reduce electro-mechanical interactions and describe prospective torsional dampers. The principle is often based on advanced PWM modulation strategies of the inverter and algorithms to increase the system damping (both passive and active damping). An analytical tool to predict torque pulsations in PWM modulated drives was presented in [44]. Discussions with some compressor manufacturers revealed a bit surprising fact to accept open loop scalar control. Despite of several disadvantages of open loop control they appreciate the inherent passive damping and no risk of closed loop interactions. Other compressor manufacturers prefer closed loop control since they understand that such method allows the use of algorithms suppressing the torsional vibration.

Besides conference papers also several case studies have been published. [45] presents a case study of 13.6 MW compressor system with vector-controlled induction motor drive. The authors find the root cause to be the speed feedback control together with purely parameterized controller gains (speed and current controller). They suggest the use of open loop V/f (scalar) control.

Generally, the Oil and Gas industry is traditionally very conservative segment and tends to be reluctant to use latest innovations that are not yet well referenced and proven in field.

High power VSI drive with fixed pulse pattern was introduced in [49]. The aim is to eliminate side bands in the torque spectrum and cancel any low frequency components. The pulse patterns are pre-calculated offline for the range of output voltages and stored in the memory of drive controller. The controller then selects suitable pulse pattern based on required output voltage. The method seems suitable for applications with slow dynamics such as compressors where the load changes gradually.

The report [50] presents two case studies with practical impact of electro-mechanical interaction in high power compressor trains. First case shows 10 MW VSI fed induction machine driving a centrifugal compressor. Interesting enough, efforts to tune the control parameters of VFD control did not help to reduce lateral vibration, but the mechanical modifications on the gearbox bearing reduced the vibration to an acceptance level. Second case is a large compressor train with gas turbine as main driver and 18 MW LCI drive as starter/helper. The electro-mechanical interaction is minimized by optimizing the current controller of LCI.

· Cement, mining and minerals [51], [52], [53]

Mechanical damages on large gears and pinions triggered investigations on torsional vibration in cement drives. These drives are either direct driven (low speed solution) or using speed reducing gear (high speed solution). Tandem motor drives have more complex mechanical system compared to single motor drives with larger number of resonant modes. Dual pinion mill drives are more pronounced to experience vibrations problems and mechanical wear when the control of both drives is not done properly [52]. In the past, the driver was often a wound rotor induction machine and the load sharing was inherently almost equal. Older papers describe the issue of large torque pulsations during direct on-line start of synchronous machine. Today's tools allow detailed numerical modeling of the dynamic torsional behavior. A study then points out the best direction of improvements (damping control, mechanical re-design, restricted speed ranges etc).

· Power generation & excitation systems [33], [54], [55], [56], [57]

The modern static excitation systems of synchronous generators make it possible to suppress torsional vibration at very low frequencies. So called power system stabilizers (PSS) are employed.

PSS shall not react on torsional natural mode of turbine-generator. [33] refers to a field case where PSS provided positive damping for the local mode of about 1.67 Hz, but destabilized the first torsional natural mode of turbine-generator of approx. 16 Hz. The solution was a re-location of speed sensor and introduction of torsional filter. Since then there are notch filters or other means inside PSS algorithms to avoid interaction with torsional modes.

Most recognized standard defining the transfer function of PSS is IEEE Standard 421.5 [5]. As input signals the combination of speed (or frequency) and electrical power is used.

Typically, a tuning study is performed to optimize the damping for specific plant and given range of frequencies. The four approaches frequently used are listed below:

1) phase compensated method, 2) root locus method, 3) state-space approach, 4) basic concept

Several active damping solutions are available, e.g. conventional band-pass filter with fixed parameters and model based damper structure. The authors in [58] propose model based damper as the preferred method. Licari et al. implemented a torsional damper based on state feedback controller in combination with Kalman filter.

In wind converter systems lot of attention is paid to torsional vibration of the shaft string with permanent magnet synchronous generator. This generator has no damper winding and the internal damping is inherently very small. An active damper was proposed e.g. in [56]. It is based on damping term added to the power reference or to the dc voltage reference (two structures). Somewhat similar compensator was described in [57], called stress damper controller (SDC). A challenging part might be the numerical differentiation of measured turbine speed, especially when accounting for certain noise in speed signal.

· **Metals** [59], [60], [61], [62], [63], [64]

Drives in metals industry, such as rolling mills, require high performance. Due to high dynamics the reduction of VSD bandwidth is mostly not acceptable and more sophisticated methods are needed. One approach is to include a multi-mass mechanical model in motor drive control so that unmeasured state variables can be observed and used as inputs for additional damping functions.

The optimization criteria for tuning of speed controllers of PI type in elastic systems were studied and compared in [59]. General recommendation is not possible, but the integrated absolute error (IAE) criteria seems to fit most practical cases.

Authors in [60] propose an additional torque feedback control for DC drive and claim to increase the damping by 50%-100%. The scheme measures the torque of the spindles and inherently requires a torque sensor. Ripple of speed sensor torque and sampling delays limit the improvements. Alternatively, a torque observer could be used instead, but the torque accuracy drops. The concept is expanded in [61] with improved torque estimator using a two-mass elastic model of the system implemented in the drive controller and executed online. The method does not require numerical differentiation and is more robust against signal noise.

[62] delivers a comprehensive analysis on origin of vibration in rolling mill drives using transfer functions, Bode diagrams or root locus. The work addresses many associated topics, e.g. controllability of rolling mill plants. In [63] the drive acceleration control is studied in detail in order to improve transient torsional dynamics. It uses acceleration between two strip-rolling sequences to minimize the gear backlash. The drive shortly accelerates when transiting from no-load operation into rolling and decelerates after rolling is finished.

2.2.2   State of the art in academic and research field

The academic research focuses on following main topics:

- Strategies to minimize the torque ripple

- o Ismail et al. proposed a modified direct torque control scheme for better capacitor voltage balancing and reduced torque ripple [9].

- Stability and positive/negative damping [65], [66], [67], [32]

  - o Already in 1982 Canay [65] presented the approach of complex torque coefficients to explain the torsional interaction and electric damping of the synchronous machines. To evaluate the torsional interaction the complex torque coefficients of the electrical and mechanical system or the values of electrical and mechanical damping can be used, respectively.

  - o Tabesh and Iravani use frequency response analysis to investigate the torsional dynamics [66]. The authors also further elaborated the complex torque analysis published by Canay and highlighted certain limitations of this approach [67].

  - o Harnefors provided the mathematical proof of positive net-damping stability criterion [32]. The analysis is a modified approach of the original method published by Canay. The stability of closed loop system is checked by means of Nyquist criterion. The proof shows that a linearized closed loop system is stable when the sum of mechanical and electrical damping is positive. It is introduced as positive net-damping stability criterion. This proof can be used as the basis of all control active damping functions on torsional vibration.

- Optimization of speed controller for elastic systems [59], [68], [69], [70], [71], [72], [73], [74], [75]

  - o Tallfors, Nordin and Isaksson compared the standard minimization criterias for synthesis of speed controller with respect of load disturbance rejection of the elastic mechanical system [59]. The outcome is that it is difficult to find one minimization criterion fitting for all applications. In most cases IAE (Integrated Absolute Error) is a suitable choice.

  - o Vukosavić and Stojić proposed a modification of speed controller suitable for high dynamic servo drives in systems with torsional resonance [68]. The solution consists of an anti-resonance compensator added at the output of speed controller (called series compensator). They have compared five-parameter notch filter with bandstop filter of FIR type and propose FIR filter due to its robustness and simple settings (one parameter). Authors also mention typical difficulties in realization of complex compensation schemes such as state controller or additional feedbacks.

  - o Szabat and Orlowska-Kowalska state in [69] that a classical PI speed controller tuned according to symmetrical optimum cannot damp the torsional vibration effectively. The paper studies different variants of additional feedbacks from state variables in order to improve the damping performance of vibration. As the state variables are often not measured nor estimated, a neuro-fuzzy controller [70] is introduced as an alternative

solution. The damping seems to work in the cases of unknown mechanical parameters, but the performance heavily depends on the selection of learning rates.

o Muszynski and Deskur focus on control optimization for high-dynamic drives with first torsional natural frequency often over 100 Hz. Such control systems are rather sensitive to any delays inside the control loops. Advanced control algorithms might be challenging to implement, especially if they implicate longer sampling time. Therefore, the authors recommend easier PI/PID control structure and provide guideline to design the controllers for elastic drive systems [72].

o Eloundou and Singhose use special input shapers to reduce the vibration of elastic mechanical system [73]. The shapers are designed considering the non-linearities of the system. The practical use for VSD applications is not fully clear.

o Yang and Wang came with interesting approach with a notch filter at the output of speed controller (similar to [68]) that is however parameterized online based on resonance frequency extracted from speed error [75].

o Saarakkala and Hinkkanen [74] propose analytical tuning of speed controller based on state-space control of elastic systems.

- Passivity based design and stability / admittance analysis

o Harnefors, Blaabjerg and Finger [76] published journal papers on passivity based stability using input admittance analysis. The converter must act passively, i.e. the real part of its input admittance must be nonnegative. This goal is difficult to achieve over the entire frequency domain, especially when taking time delays due to computation and modulation principle into account.

- Active damping methods [77], [78], [79], [80], [81], [82]

o Dutka and Orkisz showed methods for analysis and data-processing of vibration in rotating machinery. They have used state space represenation to describe the system with elastic shaft. Methods of detection of torsional oscillations are discussed, especially with regards to estimated speed and torque. The authors also introduced a damping controller based on band-pass filter [77].

o Pacas, John and Eutenbach listed several methods for passive (notch filter, FIR filter) and active damping (additional feedback of speed difference between motor and load speed, load side speed observer, combination of state-space and PI controller), mentioned their advantages and limitations and tested them on a high dynamic servo drive [78].

o Sarén and Pyrhönen presented an active vibration suppression implemented on a DTC drive for permanent magnet synchronous machine [79]. The shaft string is simplied into two mass elastic system. The authors use a Kalman filter to estimate the states of

mechanical system and the load torque. The work also considers automatic identification of certain system parameters.

- o Geng, Xu, Wu and Yang describe an active damping for wind energy conversion system based on band-pass filter and phase compensator in the voltage control loop [80]. It seems to be a hybrid solution between a band-pass filter and FIR filter.

- o Ji and Sul combined Kalman filter with LQ based speed controller to suppress torsinal vibration [81]. They have benchmarked this control with classical PI speed controller.

- o Sourkounis introduces active dynamic damping of torsional vibrations by using H∞-Control (H-Infinity) [82] and makes a comparison with classical PID controller. The viability of such method for industrial applications will be proved in near future.

- Model predictive control [83], [84], [85]
  - o Hours studied the possibilities of active vibration damping in variable speed drive systems using H∞ (H-Infinity) optimal control and model predictive control [83].

  - o Besselmann, Almér and Ferreau implemented model predictive control in load commutated inverter (LCI) type of drive and tested it successfully on a small-scale laboratory model [84]. As next step, Besselmann et al. utilized the model predictive control on a real 48 MW compressor drive [85]. The model predictive control is used especially to increase the immunity against voltage dips in supply network. The algorithms could principally be modified for damping of torsional vibration as well.

- Automatic identification of elastic shaft parameters [79], [86], [87], [88]
  - o Wertz, Bolognani et al. presented methods for commissioning of speed and position controlled electric drives. Part of the commissioning is automatic identification of parameters of the flexible shaft [86].

  - o Similar work had been done by Tallfors as part of his thesis [87].

  - o State variables of two-mass elastic system are identified by algorithms proposed by Sarén and Pyrhönen [79].

  - o Xu et al. described a method for on-line identification of system inertia using a load torque observer [88] in order to get more accurate speed control.

3   Main objectives of this thesis

Based on the state of the art analysis, this thesis focuses on overcoming of torsional vibration issues in VFDs. The main objectives of presented thesis are set as follows:

1. Explain the mechanisms of torsional oscillations in variable speed electric drive systems with focus on torque ripple and closed-loop electro-mechanical interaction.

2. Develop and validate simulation model of VFD with elastic shaft. Study the torsional response of elastic mechanics to steady state and transient excitation.

3. Perform closed-loop simulations. Determine the maximum alternating torques and to investigate the behavior of closed-loop control system and interaction between control loops. Explore the system damping and control damping.

4. Create frequency characteristics (Bode plots) of the system including elastic shaft and use them for offline optimization of controller settings and for determination of torsional stability.

5. Increase the damping of control loops for torsional modes by passive and active damping functions.

6. Perform experimental measurements on medium voltage VSDS. Use the experimental results to validate and confirm theoretical conclusions and perspective damping algorithms. Use the drive internal signals for diagnostic purpose and verify the parameterization of main controllers.

4   Methodology of the thesis

Following methodology is applied in the thesis:

Chapter 1 introduces the topic of electro-mechanical interaction in variable speed drive systems, describes the historical evolution linked with the development of power electronic based drives and stresses the importance of proper system analysis from torsional standpoint.

Chapter 2 starts with overview about oscillations in power electronic industrial and utility systems. This chapter further provides a detailed state of the art analysis mentioning both the development in industrial applications (chapter 2.2.1) and in research area (chapter 2.2.2).

The main objectives of the thesis are listed in chapter 3.

Chapter 5.1 describes the mathematical models of variable speed drive systems with focus on the modeling of elastic shaft. A state space model is introduced and described. The advantage is configuration flexibility that can be easily adjusted depending on the specific shaft system.

Chapter 5.2 gives theoretical background regarding vibration in variable speed drive systems, fundamentals regarding rotordynamics, torsional analysis and control damping functions. The analytical and numerical approach is briefly described.

The algorithms for control damping in LCI and VSI drives are outlined in chapter 6. Chapter 6.2 is dedicated to algorithms used in LCI drives. Focus is on analytical parameterization of current control loop using Bode diagrams and decoupling of control loops. Very perspective algorithms for torsional damping are the torsional damper introduced in section 6.2.6 as well as smart switchover at low speed described in section 6.2.5. Algorithms for VSI drives are proposed in chapter 6.3. Focus is on the speed control loop covering the speed controller and its analytic parameterization considering shaft elasticity and notch filter for passive damping.

Perspective methods are analyzed by means of numerical simulations in chapter 7. Section 7.1 shows the elastic shaft when excited by various different excitation signals. A simplified model is used to demonstrate the principal behavior. Section 7.2 is dedicated to LCI drives and the aim is to verify the optimizations with torsional damper, smart switchover in pulse mode and other improvements. VSI drives are simulated in chapter 7.3. There is an attempt to benchmark the torsional performance when operating in closed loop speed control and open loop (scalar). Finally, the algorithms are validated in chapter 8 by real measurements on drive systems ranging from 1.5 MW up to 38 MW and covering both LCI and VSI drive topologies.

Engineering guideline summarizing the best practice for drive systems sensitive to torsional vibration is provided in chapter 9. The work concludes in chapter 10 highlighting the main contribution of this thesis and pointing out perspective fields of future research.

Extensive tables, figures and background information linked with the subject is contained in Appendix and referred in the main body.

5   Theoretical analysis of the problem

5.1   Mathematical models for vibration analysis in VFD systems

5.1.1   Model of variable frequency drive

The model of LCI drive is described in previous work [89]. The models of VSI drives (with simple one-mass load model) were created by ABB during development stage of the corresponding products. All model are created in Matlab/Simulink environment.

5.1.2   Model of flexible shaft

Dynamic mechanical system can be described by using the simple analogies with electrical systems. This is well-known dualism within mechanics and electrodynamics [90], [91]. For interested reader a summary is provided in Appendix 3 – System analogies between electrical and mechanical systems.

Eigenfrequency Ω in mechanical translational systems with stiffness k and mass m (1):

$$\Omega = \sqrt{\frac{k}{m}}$$

(1)

Eigenfrequency in electrical systems with inductance L and capacitance C (2):

$$\Omega = \sqrt{\frac{1}{L \cdot C}}$$

(2)

Considering the simplest two-mass elastic model with lumped inertias J_M and J_L with torsional stiffness k in between of them, the resonance Ω_0 (3) and anti-resonance Ω_a (4) frequencies can be re-written:

$$\Omega_0 = \sqrt{k \cdot \frac{J_M + J_L}{J_M \cdot J_L}}$$

(3)

$$\Omega_a = \sqrt{\frac{k}{J_L}}$$

(4)

A mathematical model generally has either distributed characteristics where the parameters are distributed continuously or lumped (reduced) characteristics with concentrated parameters. The element in reduced model does not necessarily correspond to a physical element of real system. Lumped characteristics are often used to simplify the mathematical apparatus and replace partial differential equations by ordinary differential equations. To model the complex shaft string properly, a finite element approach based on a particular shaft-beam element type can be used. The number of nodes (called "stations") can vary between few hundred and several thousand. However, for the investigations of electro-mechanical interactions the finite element models are not usable. The detailed model is reduced to several dominant masses. A simplified lumped inertia model is usually sufficient. Therefore the simplified model needs to reproduce correctly the lowest one to three torsional modes (more

than three modes only in special cases with very complex shaft string). Higher torsional modes are much better damped and they are outside the bandwidth of the VFD controllers. The simplest model of elastic shaft is a two mass model (see Figure 5-1a). Such model is easy to understand and might be good enough for certain qualitative considerations. In Figure 5-1 following nomenclature is used:

(a) J_{mot}, J_{load} is motor and load inertia, K_{el}, C_{el} is the shaft stiffness and damping, m_{mot}, m_{load}, $m_{coupling}$ is motor torque, load torque and torque on coupling, ω_{mot}, ω_{load} is motor and load (angular) speed, ϑ_{mot}, ϑ_{load} is motor and load angle

(b) $J1$, $J2$,… represents the inertia of the given mass 1, 2, etc, $K1/2$, $K2/3$,… represents the stiffness of shaft element between masses 1 and 2, 2 and 3, etc and $C1/2$, $C2/3$ the damping of the shaft elements.

(a)

(b)
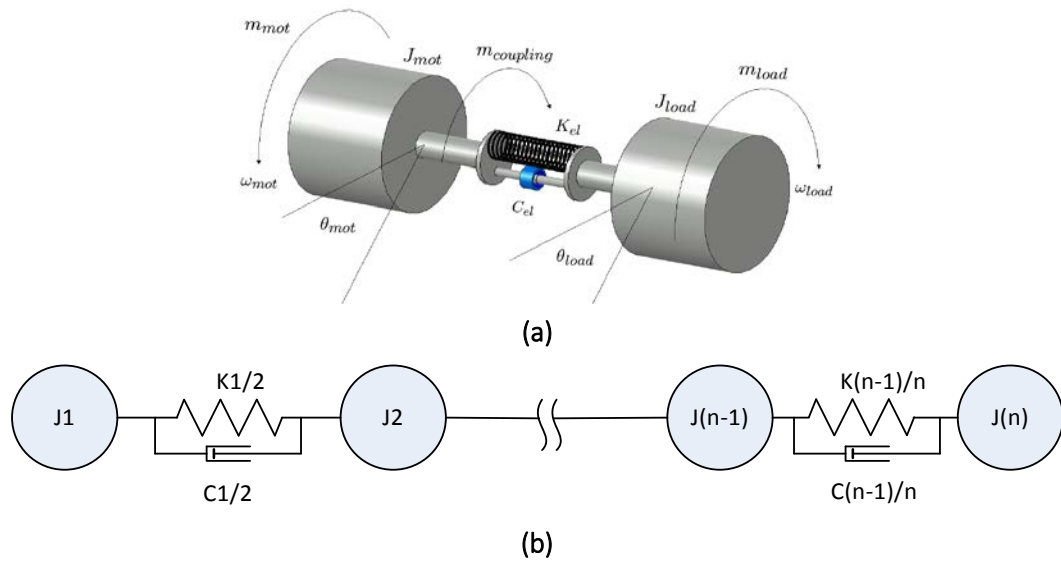
Figure 5-1: Elastic mass model; (a) representation of two-mass model with torsional spring; (b) multi-mass elastic model

The model from Figure 5-1a can be expressed in form of block diagram as shown in Figure 5-2.
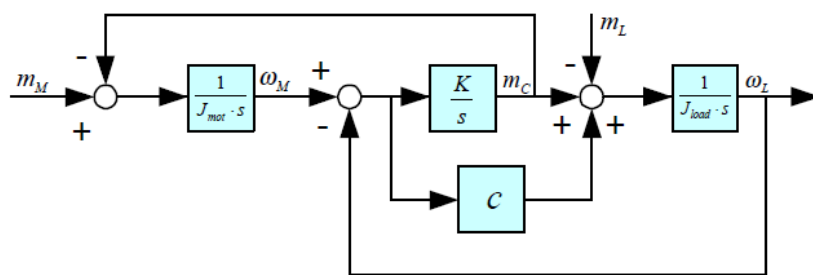
Figure 5-2: Block diagram of two-mass elastic model

The shaft system is called string. Main parts of the string are the driver (electric motor), couplings and driven load (compressor, pump, fan etc.). There is often a (increasing or decreasing) gear between driver and load. A simple compressor string is depicted in Figure 5-3. A speed increasing gear is located between motor and turbo-compressor. There might be several compressors on the same shaft (low, medium and high pressure).
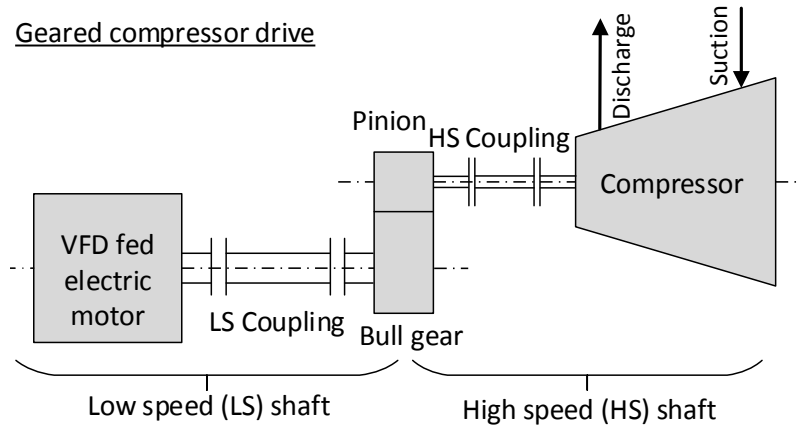
Figure 5-3: Diagram of motor driven compressor (geared solution)

5.1.2.1 Eigenvalue analysis

There are two types of eigenvalue problems: standard and generalized.

The generalized solution is based on equation of motion for free undamped oscillation;

$$M\ddot{x} + Kx = 0 \tag{5}$$

where M is the mass (inertia) matrix, K is the stiffness matrix and x is the motion vector. Assumed solution is in form (6) with Ω being the eigenfrequency:

$$x = x_0\, e^{i\Omega t} \tag{6}$$

And after substitution:

$$(K - \Omega^2 M)x_0 = 0 \tag{7}$$

$$(M^{-1}K - \Omega^2 E)x_0 = 0 \tag{8}$$

Necessary and sufficient condition of the equation is when the determinantion is equal zero.

$$det(M^{-1}K - \Omega^2 E) = 0 \tag{9}$$

Eigenvalues are the eigenfrequencies of the dynamic system (frequency spectrum). The eigenvectors are normalized based on unit matrix or mass (inertia) matrix. It uses the condition of orthogonality.

5.1.2.2 State space modeling

The state of a system represents the minimum amount of information about the system at any instant in time t_0 that is necessary so that its future behaviour can be determined without reference to the input before t_0 [55]. Standard state space description is used, i.e.

$$\dot{x} = A \cdot x + B \cdot u \tag{10}$$

$$y = C \cdot x + D \cdot u \tag{11}$$

where

x … vector of state variables (angle and angular speed)

u … input vector (motor and load torques)

y ... output vector (coupling torques)

A ... system matrix (feedback matrix)

B ... input matrix

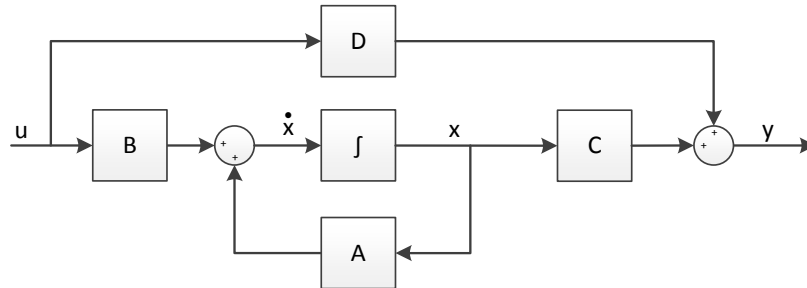C ... output matrix

D ... feed-forward matrix

Figure 5-4: Block diagram of state-space representation

The state vector contains relative displacements ϑ_1, ϑ_2, ..., ϑ_N between inertias and speeds n_1, n_2,..., n_N of each inertia.

$$x = [\vartheta_1, \ \vartheta_2, ..., \vartheta_n, n_1, n_2, ..., n_n]^T \tag{12}$$

Extending (5) with damping B and external excitation X we obtain:

$$M\ddot{x} + B\dot{x} + Kx = X(t) \tag{13}$$

Applying the state space description to the equation of motion following matrix form is received:

$$\begin{bmatrix} 0 & M \\ M & B \end{bmatrix}\begin{bmatrix} \dot{x} \\ x \end{bmatrix} + \begin{bmatrix} -M & 0 \\ 0 & K \end{bmatrix}\begin{bmatrix} \dot{x} \\ x \end{bmatrix} = \begin{bmatrix} 0 \\ X(t) \end{bmatrix} \tag{14}$$

Assumed solution is in form:

$$x = x_0 e^{\lambda t} \tag{15}$$

$$\lambda = \lambda_{Re} + i\lambda_{Im}$$

Real part of the complex eigenvalue represents damping and imaginary part defines the eigenfrequency of damped oscillation.

The multi-mass shaft string is modeled in following way:

1. Vectors of inertia (j_{data}), stiffness (k_{data}) and damping (c_{data}) in physical units are created. Inertia $[J] = kg \cdot m^2 = N \cdot m \cdot s^2$, stiffness $[k] = \frac{N \cdot m}{rad}$ and damping $[c] = \frac{N \cdot m \cdot s}{rad}$.

$$j_{data} = [J_1, J_2, ..., J_N] \tag{16}$$

$$k_{data} = [k_{12}, k_{23}, ..., k_{N-1,N}]$$

$$c_{data} = [c_1, c_2, ..., c_{N-1,N}]$$

where N is the total number of masses/inertias.

2. System matrices are created: inertia matrix J_{eqm}, stiffness matrix K_{eqm} and damping matrix C_{eqm}

$$J_{eqm}(n, n) = j_{data}(n) \tag{17}$$

$$K_{eqm}, C_{eqm}$$

if (n==1)

$$K_{eqm}(n, 1) = k_{data}(n), K_{eqm}(n, n + 1) = -k_{data}(n)$$

$$C_{eqm}(n, n) = c_{data}(n), C_{eqm}(n, n + 1) = -c_{data}(n)$$

if (n==N)

$$K_{eqm}(n, n) = k_{data}(n - 1), K_{eqm}(n, n - 1) = -k_{data}(n - 1)$$

$$C_{eqm}(n, n) = c_{data}(n - 1), C_{eqm}(n, n - 1) = -c_{data}(n - 1)$$

else

$$K_{eqm}(n, n) = k_{data}(n - 1) + k_{data}(n), K_{eqm}(n, n - 1) = -k_{data}(n - 1),$$

$$K_{eqm}(n, n + 1) = -k_{data}(n)$$

$$C_{eqm}(n, n) = c_{data}(n - 1) + c_{data}(n), C_{eqm}(n, n - 1) = -c_{data}(n - 1),$$

$$C_{eqm}(n, n + 1) = -c_{data}(n)$$

3. Modal analysis – undamped eigenfrequencies D_{eig} and eigenvectors V_{eig} are calculated based on system matrix of inertia and stiffness:

$$M_{dyn} = J_{eqm}^{-1} \cdot K_{eqm} \tag{18}$$

$$[V_{eig}, D_{eig}] = eig(M_{dyn})$$

4. State space matrices are created:

   System matrix A, input matrix B, output matrix C, feedthrough matrix D,

   size(A) = (2·N, 2·N), size(B) = (2·N, 2), size(C) = (4+N-1,2·N), size(D) = (4+N-1,2),

$$A = \begin{bmatrix} 0 & \cdots & 0 & 1 & 0 & 0 \\ \vdots & \ddots & \vdots & 0 & 1 & 0 \\ 0 & \cdots & 0 & 0 & 0 & 1 \\ -\left[J_{eqm}^{-1} \cdot K_{eqm}\right] & & -\left[J_{eqm}^{-1} \cdot C_{eqm}\right] \end{bmatrix} \tag{19}$$

$$B = \begin{bmatrix} 0 & 0 \\ \vdots & \vdots \\ 0 & 0 \end{bmatrix}$$

$$B(N + n_m, 1) = \frac{1}{J_{eqm}(n_m, n_m)} \ \dots \text{ motor torque}$$

$$B(N + n_l, 2) = \frac{1}{J_{eqm}(n_l, n_l)} \ \dots \text{ load torque}$$

$$C = \begin{bmatrix} 0 & \cdots & \cdots & \cdots & \cdots & 0 \\ \vdots & \ddots & & & & \\ \vdots & & \ddots & & & \\ \vdots & & & \ddots & & \\ \vdots & & & & \ddots & \\ 0 & & & & & 0 \end{bmatrix}$$

$$C\,(1, n_m) = 1 \dots \text{motor angle}$$

$$C\,(2, n_l) = 1 \dots \text{load angle}$$

$$C\,(3, N + n_m) = 1 \dots \text{motor angular velocity}$$

$$C\,(4, N + n_l) = 1 \dots \text{load angular velocity}$$

$$D = \begin{bmatrix} 0 & 0 \\ \vdots & \vdots \\ 0 & 0 \end{bmatrix}$$

where n_m is the position of motor and n_l is the position of load in the mass vector.

Equation (19) considered that external torque is applied to two inertias: motor inertia and load inertia. The model can be adapted to have additional external torques (e.g. several loads on the same shaft). Such model is universal and easily scalable.

5.1.2.3   Torsional natural frequencies and mode shapes

The determination of torsional natural frequencies and modes is a mathematical eigenvalue problem. There are numerous eigenvalue solvers that can be employed. The mode shape provides very important information how the mechanical shaft string is twisted when being excited. It reveals how critical the torsional mode is and how easy it can be excited from a given source. The mode shape also reveals information about controllability and observability. The first example in Figure 5-5 (system data as per Table 16) shows a mode that is observable and controllable.
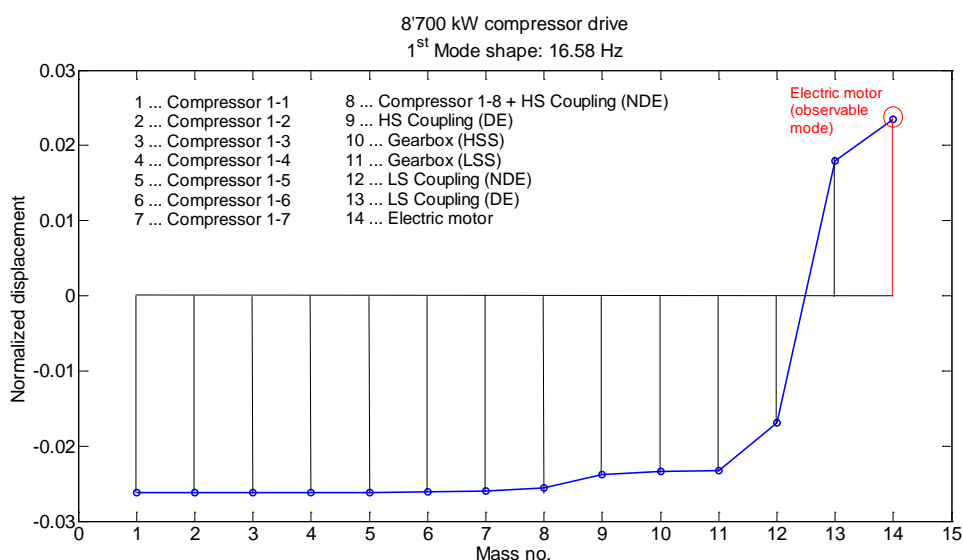

Figure 5-5: First mode shape of 8'700 kW compressor shaft string

The motor mass has the largest displacement and the torsional mode can be easily observed. A relatively small AC component in the air gap torque will be significantly amplified. In other words, such mode shapes couples the fluctuation in air gap torque very strong to the shaft torque.

The other example in Figure 5-6 shows a mode that is almost impossible to observe from motor side. The torsional twist does not involve the motor section of the shaft system. The motor quantities will not be disturbed by the torsional twist. In addition, any sensor located on the motor shaft or nearby will not provide any useful signal. It is the second mode shape of system described in Table 16.
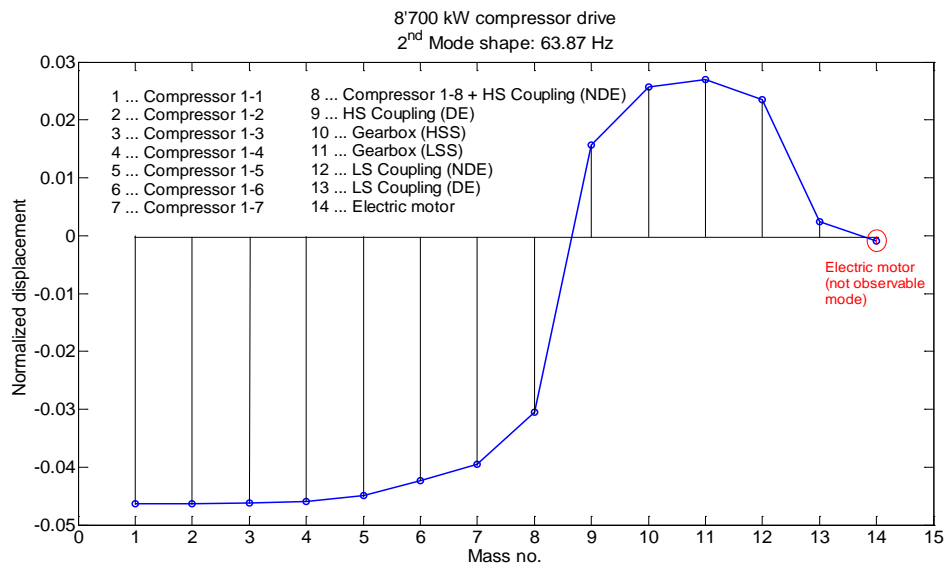
Figure 5-6: Second mode shape of 8'700 kW compressor shaft string

Several examples of typical mode shapes, all based on real projects, are shown in Appendix 12 – Torsional natural frequencies and mode shapes in variable speed drive systems. See also figure 9 in [47] for mode shapes of compressor trains. Characteristics of physical systems are often non-linear. If the input values are limited within a relatively narrow range, a linear model can be used that approximates the response of a non-linear model. Certain effects in rotordynamics can only be explained by considering non-linearity in the system.

5.1.3   Frequency characteristics and transfer functions

In the past DC motor drives dominated in variable speed applications. Modern AC motor drives employ induction or synchronous motors. The transfer function of those motors is more difficult (unless it is significantly simplified) and the analytical solution is often replaced by a simulation. However, for visualization of torsional behavior and evaluation of the severity of torsional vibration the frequency characteristics (Bode plots) are very useful. The method is also very practical since it requires much less time compared to detailed system simulations. Specific frequency characteristics of LCI drives are contained in chapter 6.2.1 and of VSI drives in chapter 6.3.1.

5.1.4   Impedance characteristics of VFD

The usage of impedance characteristics is an approach frequently used in modern traction drives. It emerged from the requirement to ensure inter-operability within various rolling stock equipment [28].

Similar analysis might be performed for HVDC transmission terminals in case of SSTI. The same approach can be adopted for medium voltage drives. It shall prove if the frequency converter acts as positive impedance throughout the whole frequency range or if there is any range where the converter acts as negative impedance and potentially destabilizes the system.

For this purpose three models of frequency converter have been studied: load-commutated inverter (LCI), 3-level voltage source inverter (VSI) of neutral point clamped (NPC) topology and 5-level voltage source inverter (VSI) of neutral point clamped (NPC) topology. Those three models cover some of the most common used topologies for high power drives (up to 40 MW and beyond).

5.1.5   Closed loop numerical simulations

Simulation is an alternative to analytic solution. Today's powerful computers make this method easier than ever before. Unlike the transfer function approach a simulation model can easily contain hundreds or even thousands of parameters. The author has performed in-depth sensitivity analysis for LCI type of VFD during his master thesis by means of computer simulations. Later on similar sensitivity has been performed using hardware in the loop technique.

Hardware in the loop (HIL) simulations represent the next level of simulation techniques. The real control hardware can be tested while the power section is modeled. Once the system is set up, the testing goes quite fast (compared to computer simulation). HIL testing shall also provide higher level of confidence as it is closer to real physical system. As example of HIL testing is shown in Figure 5-7 with following elements: ① master control board, ② slave board, ③ signaling interfaces, ④ interface board, ⑤ control display panel
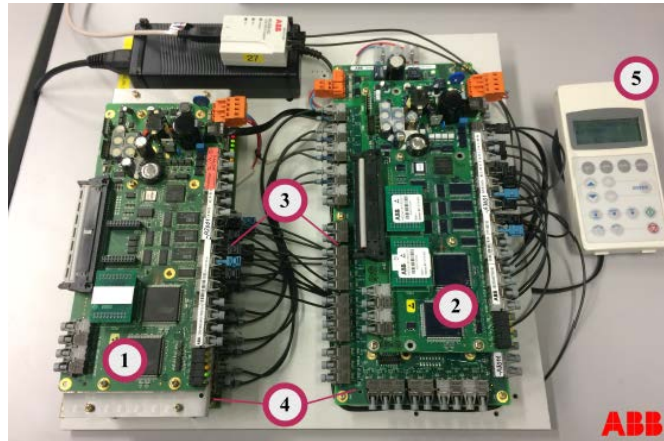

Figure 5-7: Environment for hardware-in-the-loop testing (courtesy of ABB)

5.2   Vibrations in VFD systems: A theoretical background

5.2.1   Torque considerations

5.2.1.1   Motor torque in general

In steady state condition the mechanical shaft torque T_{shaft} is the air gap torque $T_{air\ gap}$ minus mechanical losses $P_{loss,\ mech}$ divided by shaft speed ω_{mech}:

$$T_{shaft} = T_{air\ gap} - P_{loss,mech}/\omega_{mech} \qquad (20)$$

In generic electric machine following relations define shaft power P_{shaft} and torque T_{shaft}:

$$T_{shaft} = \frac{P_{shaft}}{\omega_{mech}} \tag{21}$$

The air gap torque has electromagnetic origin. It is a product of motor flux and current that is applied to the rotor bodies. The shaft torque is then determined by the dynamics of the rotor system. While both air gap torque and shaft torque are similar in steady state, they differ in dynamic operation. It is illustrated on example during short circuit fault (Appendix 11 – Motor transient torques).

Important is the quality of motor torque, namely torque ripple and frequency content. Factors influencing the torque quality are: converter topology, type of inverter output filter, switching frequency, modulation technique and enhanced control algorithms acting on torque.

If symmetrical three-phase voltage is applied to the stator windings, a constant DC torque component is created in the motor air gap [44]. The DC component is the one that is driving the load and the harmonic (AC) component is the one creating torque pulsations and not contributing to active power of the motor. DC torque component is equivalent to active power, AC pulsating components then equivalent to distortion power.

This harmonic transfer is essential for further considerations in the dissertation. More detailed mathematical background can be found e.g. in [92] and [93]. The latter one provides relatively simple set of harmonic transfer rules summarized in Figure 5-8:
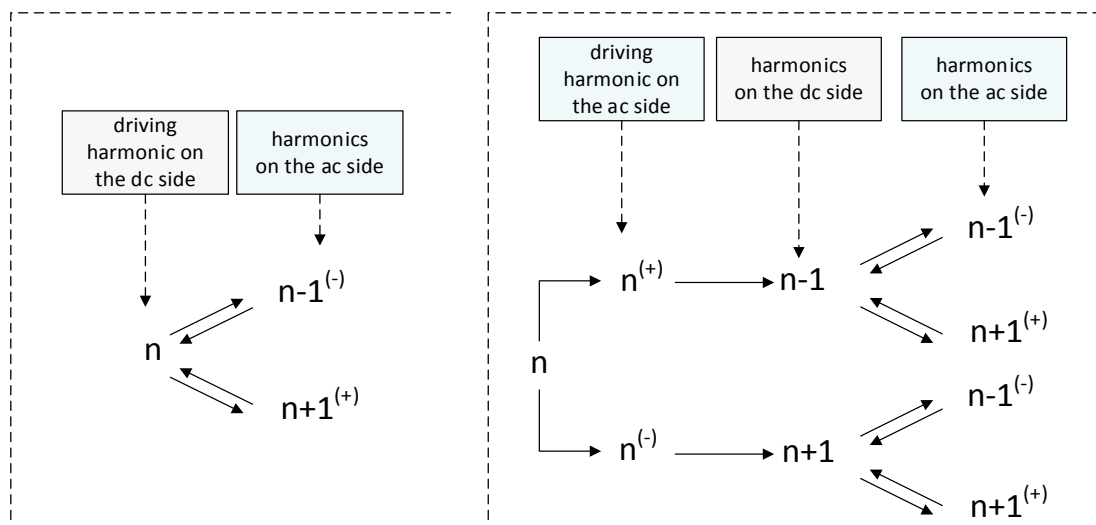

Figure 5-8: Harmonic transfer rules [93]

5.2.2   Rotordynamics and torsional analysis

Rotordynamics is the study of the dynamics of rotating equipment. The aim is to keep the rotating machinery out of excessive vibration, accelerated material aging and failures. A basic introduction into rotordynamics without equations can be found in [94]. For more theoretical background reader can also refer to Appendix 6 – Introduction in rotordynamics and torsional analysis.

The classical torsional analysis is of a feed-forward type, i.e. it is an open-loop analysis. It means that the excitation is defined, applied on the system and its response is analyzed. It is assumed that the excitation is invariant to the response. In other words, there is no back influence of the system on the excitation. Such simplification can be acceptable for passive systems without feedback loop. However,

actively controlled systems using closed control loops behave in a different way. A measured or esti-mated quantity is used as a feedback signal in the control loop. In electric drives utilizing VFDs the feedback signals in common control structures are motor speed (and sometimes also rotor position), motor current and voltage vector. The oscillations inside the system may affect the feedback signals and the reaction of the control system would change. It is obvious that the assumption of static exci-tation source is not valid anymore. The drive affects the driven load and the excited load has a back influence on the drive system. The traditional torsional analysis (open loop) cannot be used and ex-tended analysis covering the behavior of control system is necessary as illustrated in Figure 5-9. The label 'train' refers to a mechanical train or mechanical shaft string.
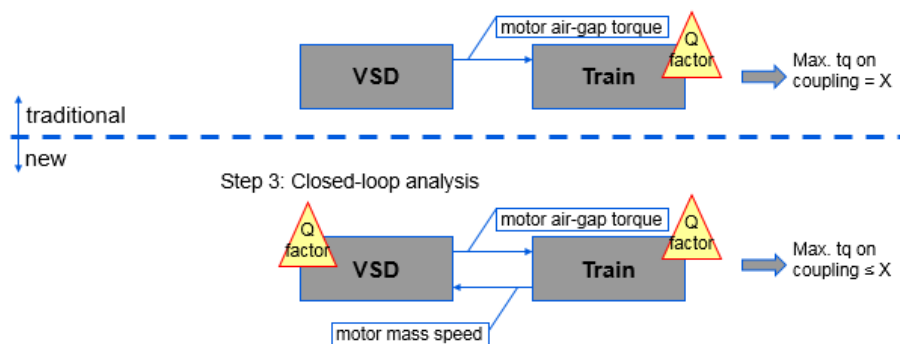
Figure 5-9: Torsional analysis – traditional and new form

5.2.3   Torsional excitation

From practical reasons, shaft systems cannot be manufactured ideally stiff. It is often a design purpose to create weak links in the shaft system. In case of excess mechanical stress, the system is expected to break in those links. Due to the elasticity of certain shaft components (such as couplings, spacers etc) the system has its natural frequencies. When there is a torque component of frequency equal the natural frequency, a resonance condition appears. The determination of relevant excitation sources is a central issue. The mechanical resonance can by excited by various sources. An overview of the most common excitation sources is provided in Appendix 6 – Introduction in rotordynamics and tor-sional analysis adopted from [95].

Some excitations have purely mechanical origin, such as unbalance or coupling misalignment. Those excitations are usually always present to some extent (residual rotor imbalance, not ideally aligned couplings) and therefore always considered in torsional analysis. Such excitations are not further de-scribed in this section. However, due to their frequent appearance in real drive systems, reader can refer to Appendix 4 – Unbalance, coupling misalignment and shaft eccentricity for some fundamen-tals. If the excitation is deterministic (e.g. in fix relation to fundamental speed), it is easy to include it in torsional analysis. However, there are some excitation sources with stochastic behavior. In that case the analysis is more complicated and requires some kind of "white noise" approach [47].

5.2.4   VSD as excitation source

The use of VSD allows an increased operating speed range that in turn means more possibilities for critical speeds. The VSD also introduces additional excitation mechanism.

Torque spectrum of VSD driven motor contains besides the 0 Hz component (mean value) also certain harmonics (seen as torque ripple in time domain). This is not a specialty of particular VSD, but rather a fact for any drive, disregarding the make, topology or control method. Diesel engines, gas or steam turbines also have such torque harmonics. It is impossible to design a VSD producing ideal torque without any harmonics the same as it is impossible to design a shaft string without any torsional natural frequency. However, the torque harmonics can be minimized by the modulation scheme, correct parameterization and utilization of software damping functions.

Generally, there are two principles how the excitation in VSD is formed. The nature of each of the principle is fundamentally different [A3]. One is the pulsating torque ripple, the other one is the electro-mechanical interaction with closed-loop effects. Each is them is explained in further sections.

5.2.4.1   Pulsating torque ripple

The pulsating torque ripple is a result of

- Spatial harmonics produced by electric motor (motor with its discrete windings), and
- Time harmonics produced by the frequency converter (discrete switching of power semiconductors).

The spatial harmonics are always present in the air gap torque of the motor no matter if the motor is operated direct on-line or fed from adjustable speed drive. They originate purely from the motor design. The amplitude of spatial harmonics depends on the motor type (induction versus synchronous motor, laminated versus solid rotor etc.). The frequencies of spatial harmonics are typically rather high and do not coincide with the lowest torsional natural frequencies of the driven mechanical system. They can often be neglected as source of excitation.

The time harmonics are the main source of torque pulsations. They are produced by the frequency converter due to discrete switching of power semiconductors and sometimes called induced torque pulsations. They can be a source of excitation of torsional resonance.

5.2.4.1.1   Current source inverters

There are current source inverter (CSI) topologies available for induction motors. However, this topology is nowadays quite seldom not investigated in detail in this thesis.

Current source inverters in combination with synchronous machines are available for more than four decades and still popular, especially for very high power or as a VSD soft starters. It is due to their easy scalability (both power and voltage) and excellent reliability records. The semiconductor bridges are commutated by external voltage source: line voltage for the rectifier and load voltage for the inverter). Therefore the name Load commutated inverter (LCI). The described principle is applicable above certain minimum speed where the LCI works in load commutated mode. At low speed (typically below 6...12% of motor nominal speed) the motor voltage is too low to commutate the motor side thyristor bridge (inverter) and another method has to be used. The most frequent solution is so called pulse mode where the dc link current is repetitively interrupted (forced to zero) before the next thyristor pair is turned on. Figure 5-10 illustrates the measurement of motor voltage, dc link current and motor speed during pulse mode. It is a real meausrement of drive system described in Table 7.
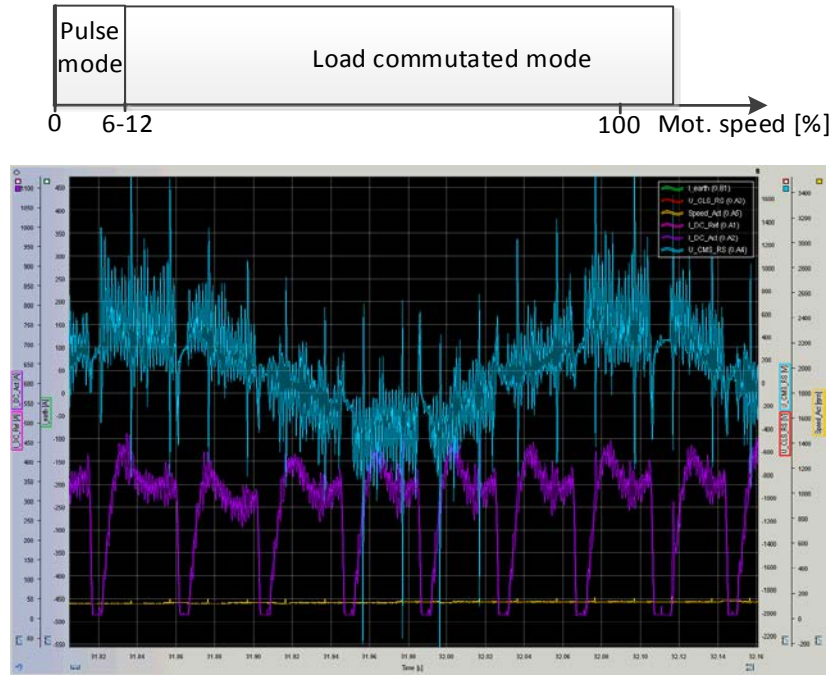
Figure 5-10: Machine ph-ph voltage (blue), dc link current (violet) and speed (yellow) during operation in Pulse mode

Let's analyze first the load commutated operation and then identify the specific topics of pulse mode. LCI consists of thyristor bridges decoupled by intermediate dc reactor. The reactor is smoothing the current and storing the energy. It provides the ‚current source' behavior. The rectifier commutates with line frequency (typically 50 or 60 Hz) and the inverter commutates with actual motor frequency. The thyristor bridges are mostly 6-pulse (smaller power drives and soft starters) or 12-pulse (larger drives or large soft starters). Topologies higher than 12-pulse are principally possible. However, their use is rather seldom. Figure 5-11 displays the most common variants.

For practical reasons (such as cost and dynamic response of VSD) the dc reactor has finite size in terms of inductance (range of several mH) and the current is not purely DC, but contains certain amount of ripple. The most dominant components are the integer multiples of the line frequency multiplied by pulse number:

$$f_{char} = 6 \cdot k \cdot f_{line}$$
$$f_{char} = 12 \cdot k \cdot f_{line}$$
$$f_{char} = 6 \cdot l \cdot f_{mot}$$
$$f_{char} = 12 \cdot l \cdot f_{mot}$$

(22)

Besides those dominant harmonics with larger magnitudes there are also interharmonics present in dc link current. The origin of the interharmonic components can be explained as convolution happening inside the dc link (see Figure 5-12). The current flowing through a coil can be generally expressed as in (23)

$$i_L = \frac{1}{L} \int u(t) \, dt$$

(23)

The current flowing through the dc link reactor of LCI can be expressed as per (24),

$$i_d = \frac{1}{L_d} \int (v_{CLS}(t) - v_{CMS}(t))\ dt \tag{24}$$

where v_{CLS} is the voltage across the rectifier (converter line side) bridge and v_{CMS} is the voltage across the inverter (converter motor side) bridge. Both voltages contain characteristic voltage ripple of frequency equal the fundamental switching frequency of the corresponding bridge multiplied by the pulse number of the bridge.
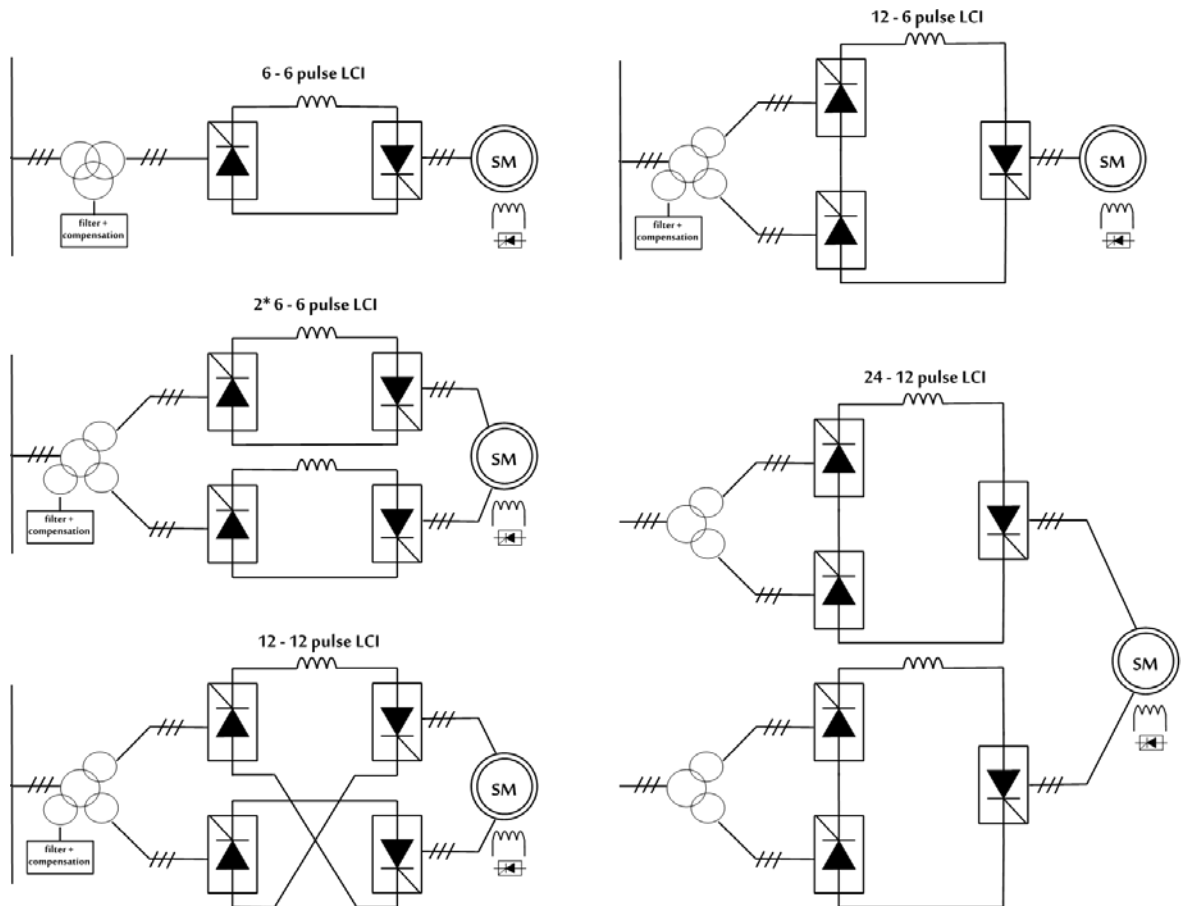

Figure 5-11: Typical configurations of LCI variable frequency drives*

Block with thyristor symbol in this case represents a full bridge with six thyristors (B6)
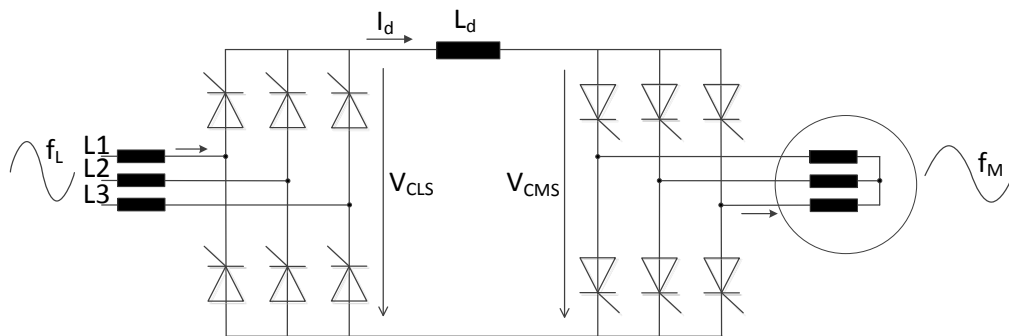
Figure 5-12: Origin of inter-harmonics inside dc link of LCI converter

Although the magnitudes of interharmonics are smaller compared to dominant components, the frequencies can interfere with dominant torsional modes and excite them. Therefore, the interharmonics need to be carefully considered in system design.

Due to the hardware simplicity of LCI drives it is possible to make a rough assessment of air gap torque analytically. For that purpose we will use the 6-pulse thyristor bridge as a fundamental building block (all LCI configurations consist of multiple such building blocks).

First let's assume an infinite size of smoothing reactor with purely DC current in intermediate circuit (i.e. no current ripple and fully decoupled line and motor side). Then the waveform of air gap torque depends on the firing angle of inverter bridge. This function is inherently strongly non-linear. The air gap torque is a cross product of motor flux and stator current. The flux is harmonic as it is integral of voltage. However, the voltage has only 6 discrete vectors in case of 6-pulse thyristor bridge. One cycle is 360 degree. Each vector will be applied for 1/6 of cycle when one thyristor pair is conducting the current, i.e. for 60 degree electrical. Refer to switching diagram below. From historical reasons thyristors are denoted V1 to V6 as common in the older literature; V stands for 'valve'.
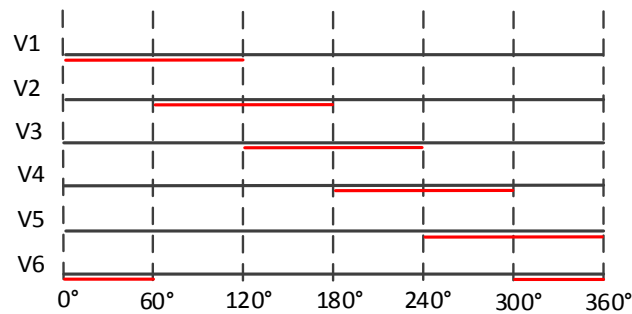
Figure 5-13: Switching diagram of 6-pulse thyristor bridge (red underlined the sector when thyristor is conducting)

Figure 5-14 shows the current flow within the rectifier bridge for three different switching combinations: V6-V1, V1-V2 and V2-V3. Other three combinations are analogous.
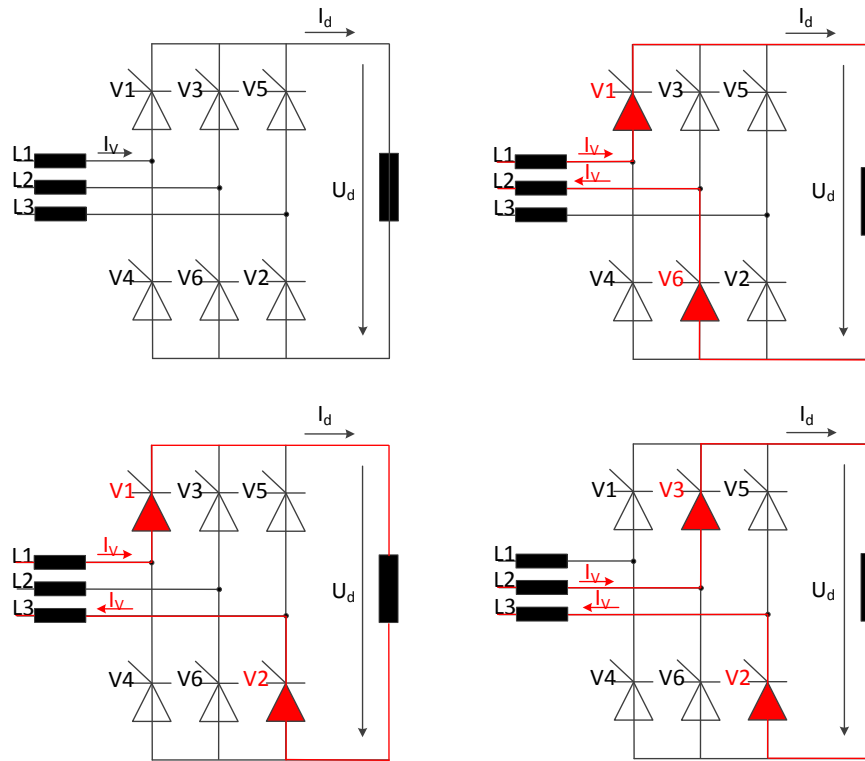
Figure 5-14: Current flow inside the thyristor bridge rectifier (inverter bridge is analogous)

The basic equation for the air gap torque is (25),

$$T_e = C_m \cdot I_{dc} \cdot \Psi_m \cdot \sin \varphi \tag{25}$$

where T_e is the electromagnetic (air gap) torque, C_m is the motor constant, I_{dc} is the dc link current of LCI, Ψ_m is the rotor flux and φ is the angle between stator current $\vec{I_s}$ and $\overrightarrow{\Psi_m}$ (where $\vec{I_s}$ has the same magnitude as I_{dc} and the vector orientation is given by the switching combination).

During the conduction window the angle between flux and current is variable. Even if current and flux have contant magnitudes, the resulting torque will have a ripple depending on firing angle (which is directly related to the angle between flux and current vectors).

The vector of stator flux has the same direction as the vector of stator current. To visualize the torque producing principle, (25) can be re-written as

$$T_e = C \cdot \Psi_s \cdot \Psi_f \cdot \sin \varphi \tag{26}$$

Ψ_s ... stator flux, Ψ_f ... rotor (field) flux

From (26) is obvious that the highest torque with lowest ripple is achieved when the vectors of motor flux and stator current are perpendicular. This corresponds to a firing angle of 180 degree. However, as explained, the angle is neither constant nor can reach 180 degree.
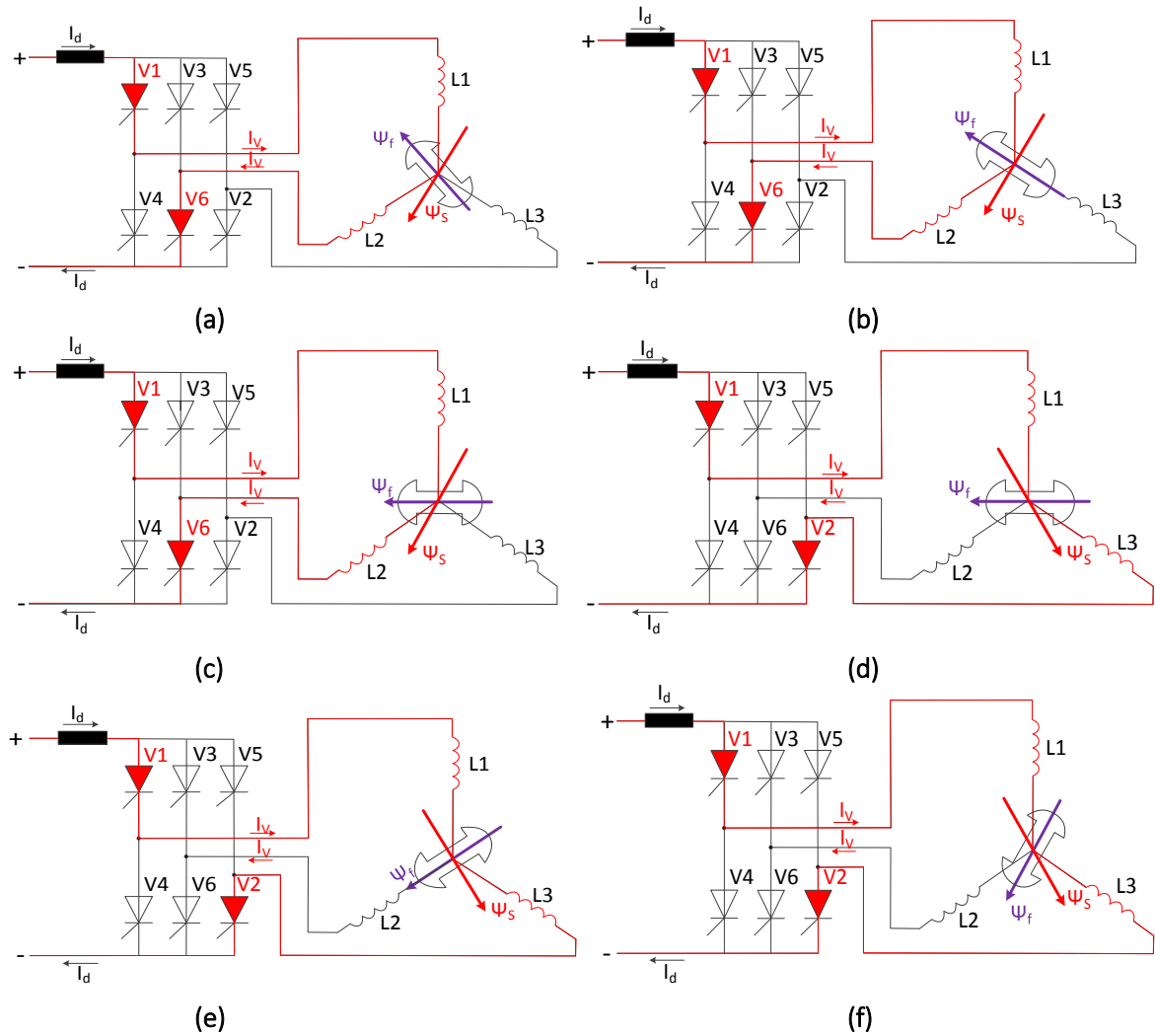
Figure 5-15: Switching vector and its relation to motor torque (Ψ_S is stator flux, Ψ_f is rotor flux)

Firing angle cannot reach 180 degree as the commutation time and recovery time (to renew blocking capability of thyristor) have to be respected. The upper limitation of firing angle depends on motor parameters (mainly the stator leakage inductance influencing the commutation length), actual load (the higher the motor current the longer the duration of commutation) and on the fundamental frequency (since for the recovery it is the voltage area which is important). Maximum firing angle that can practically be reached is approx. 150 to 160 degree. Due to the non-linear relationship is the torque ripple with 150 degree firing angle significantlly higher than with theoretical 180 degrees.

The torque ripple depending on adjustable firing angle can be expressed and calculated analytically. Analysis according to (25) in steady state condition (I_{dc} = const., Ψ_m = const.) can be simplified to (27) and solved by simple integration over the conduction period of one thyristor pair.

$$T_e \sim \sin \varphi \qquad (27)$$

a) Inverter firing angle $\alpha_{CMS} = 180 \ deg$

φ_1 = 120 deg, φ_2 = 60 deg

$$T_{e \ (AV)} = \frac{1}{T} \int_{\varphi_1}^{\varphi_2} \sin \varphi \ d\varphi \cdot T_{e(\max)} \qquad (28)$$

$$T_{e\,(AV)} = T_{e(\max)} \cdot \frac{3}{\pi} \int_{\frac{\pi}{3}}^{\frac{2\pi}{3}} \sin \varphi \; d\varphi \; = T_{e(\max)} \cdot \frac{3}{\pi} \; [-\cos \varphi]_{\frac{\pi}{3}}^{\frac{2\pi}{3}} \; = \frac{3}{\pi} = 0.955 \, T_{e(\max)}$$

For firing angle of 180 deg is the average air gap torque 0.955 (95.5%) of maximum torque.

$$T_{e\,(min)} = \; \sin \varphi_1 \, \cdot \, T_{e\,(\max)} \tag{29}$$

$$T_{e\,(min)} = \; \sin \frac{2\pi}{3} \cdot T_{e(\max)} = 0.866 \cdot T_{e(\max)}$$

$$T_{e\,(min)} = \frac{0.866}{0.955} \cdot T_{e(\mathrm{AV})} = 0.907 \cdot T_{e(\mathrm{AV})}$$

b) Inverter firing angle $\alpha_{CMS} = 165 \; deg$

φ_1 = 105 deg, φ_2 = 45 deg

c) Inverter firing angle $\alpha_{CMS} = 150 \; deg$

φ_1 = 90 deg, φ_2 = 30 deg

The Table 2 summarizes the dependencies between inverter firing angle, air gap torque ripple, average, minimum and maximum air gap torque. The same results are visualised in Figure 5-16.

Table 2: LCI torque as function of inverter firing angle (6-pulse configuration)

Firing angle α_{CMS} [deg]	Average torque $T_{e\,(AV)}$ [pu]	Min. torque $T_{e\,(min)}$ [pu]	Torque ripple $T_{e\,(ripple)}$ [pu]
180	0.9549	0.8660	0.1340
165	0.9224	0.7071	0.2929
150	0.8270	0.5000	0.5000
135	0.6752	0.2588	0.7071
120	0.4775	0.000	0.8660
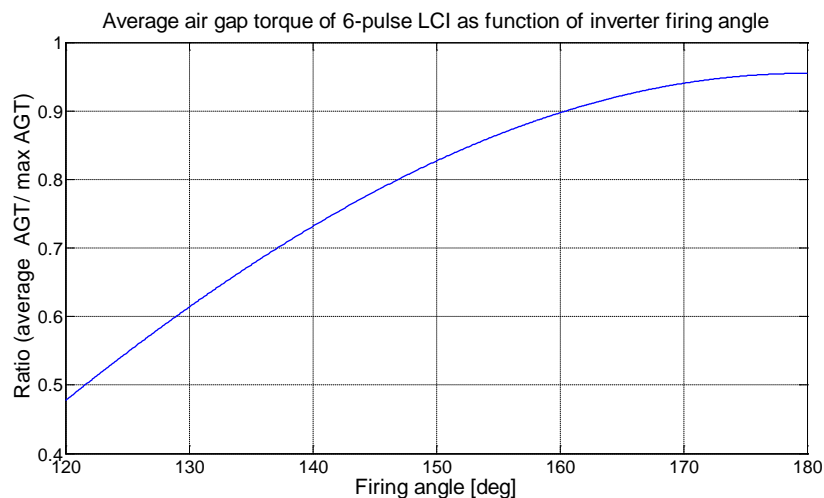
Figure 5-16: Average air gap torque as function of inverter firing angle (6-6 pulse LCI)
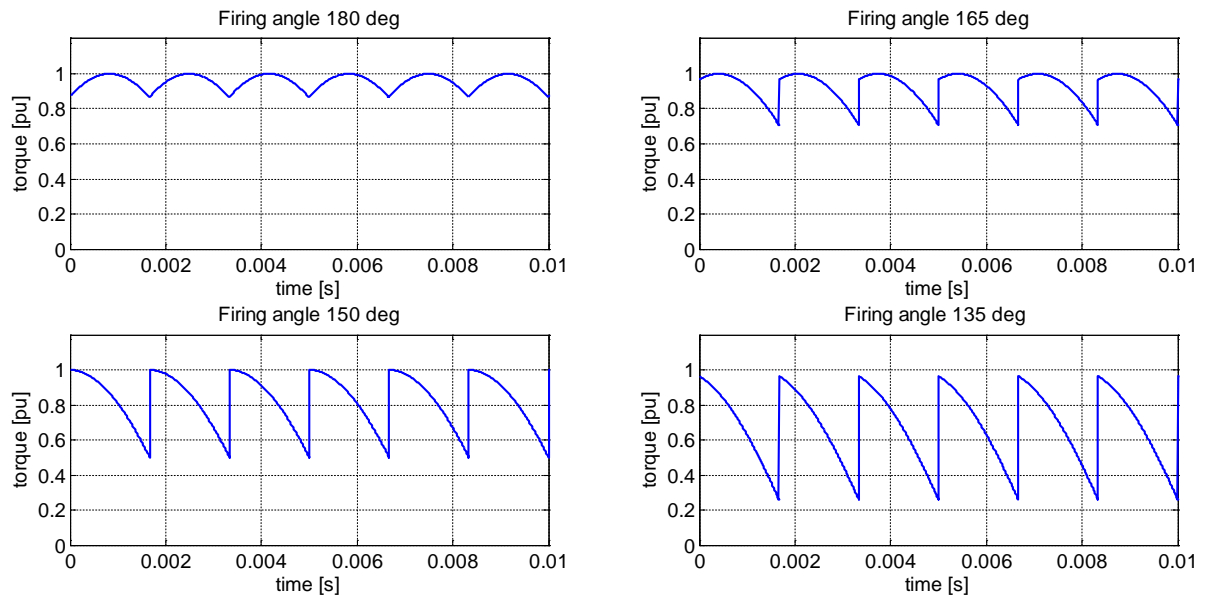
Figure 5-17: Pulsating air gap torque for typical firing angles of a 6-pulse inverter

As can be seen from above Figure 5-16, Figure 5-17 and Table 2, the torque ripple increases significantly with decreased firing angle. One way to minimize the torque ripple is a motor design with lower commutation reactance. A typical example of commutation notch in motor voltage is depicted in Figure 5-18. The larger the commutation reactance the wider the commutation notch and the lower inverter firing angle is required with implication on torque ripple as per Table 2.

Figure 5-18: Commutation notch in the inverter (CMS) voltage

Another way, very efficient, is the use of 12-pulse inverter in combination with dual winding machine. Both stator winding systems have relative phase displacement of 30 deg. Such configuration is very common for higher power drives and the torque ripple is reduced up to 3-times. The difference is obvious from the comparison in Figure 5-19.
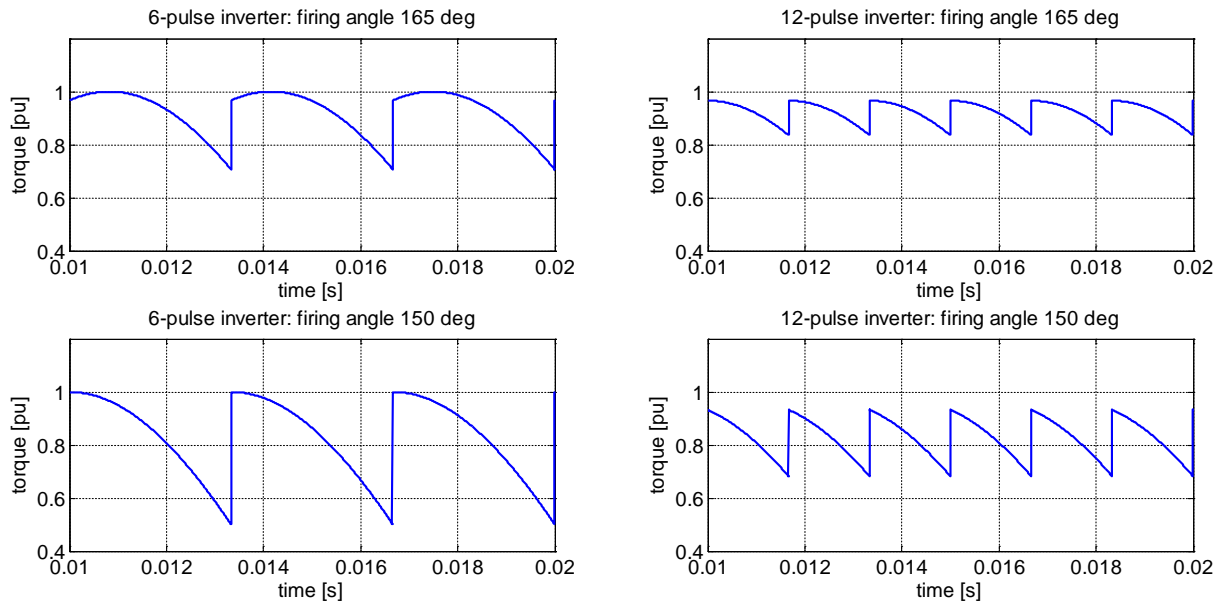
Figure 5-19: Pulsating air gap torque: Comparison between 6-pulse and 12-pulse inverter

Modeling, simulations and measurements of LCI drive has been published e.g. in [96].

The relationship between commutation reactance, length of commutation notch and dc current is given in (31):

$$d_x = x_\sigma \cdot I_d$$

(30)

So far the theoretical description has been simplified considering ideal dc link current without any ripple. Such ideally smooth dc link current cannot be reached in practice due to finite value of dc reactor. The current in dc link will have certain ripple. The frequency content is determined by the pulse numbers of rectifier and inverter and their actual fundamental frequencies. The magnitude is determined by the pulse number, ripple voltage over the dc reactor and size of dc reactor.

Above analysis was made for a 6-6 pulse LCI drive. A huge improvement of torque ripple is achieved when higher pulse number on motor side is used in combination with dual three-phase machine as per Figure 5-20. Large LCI drives most often have 12-12 pulse configuration and supply synchronous machine with two winding systems that are relatively displaced by 30 degree electric (see e.g. [96]).
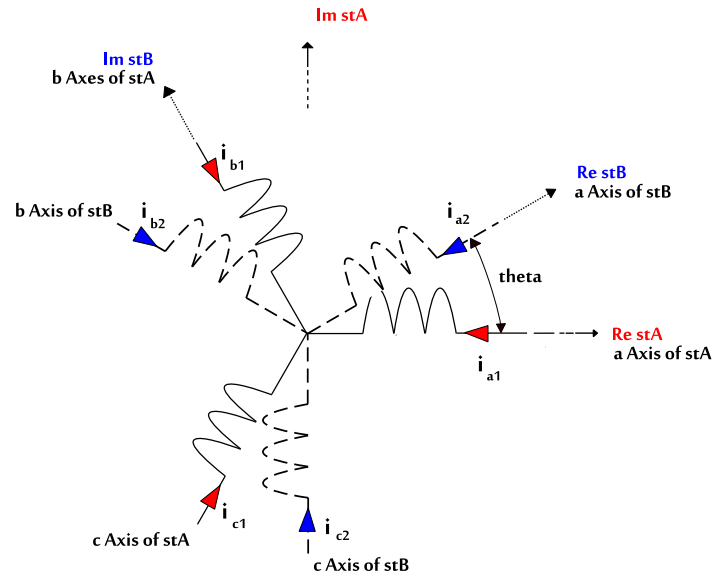
Figure 5-20: Schematic representation of dual three-phase machine

Pulsating torque components of LCI drive are depicted in Figure 5-21. This Campbell diagram is analytically derived and valid for any LCI drive with 4-pole machine connected to 50 Hz grid. Diagrams for LCI drives connected to 60 Hz grid or drives with 2-pole machines would look similar (see Appendix 5 – Campbell diagram for LCI and VSI drives for more details). On the x-axis there is the motor speed in rpm while the y-axis displays the frequency of the pulsating torque component. Multiples of line frequency (fN) are horizontal lines independent on motor actual speed. Multiples of motor frequency (fM) are lines rising with motor speed. Interharmonics are rising or falling depending on the motor speed (frequency) in relation to grid frequency. The interharmonics are well reproduced in simulations. The example below shows a setup with parameters acc. to Table 7. The motor is slowly accelerated up to 1'472 rpm (with very small overshoot of 0.5 rpm). At that speed the interharmonic component interferes with the 1st torsional natural frequency. The simulation model contains elastic model of the shaft string. The torsional vibration is visible in the motor speed – this is obvious in Figure 5-22.
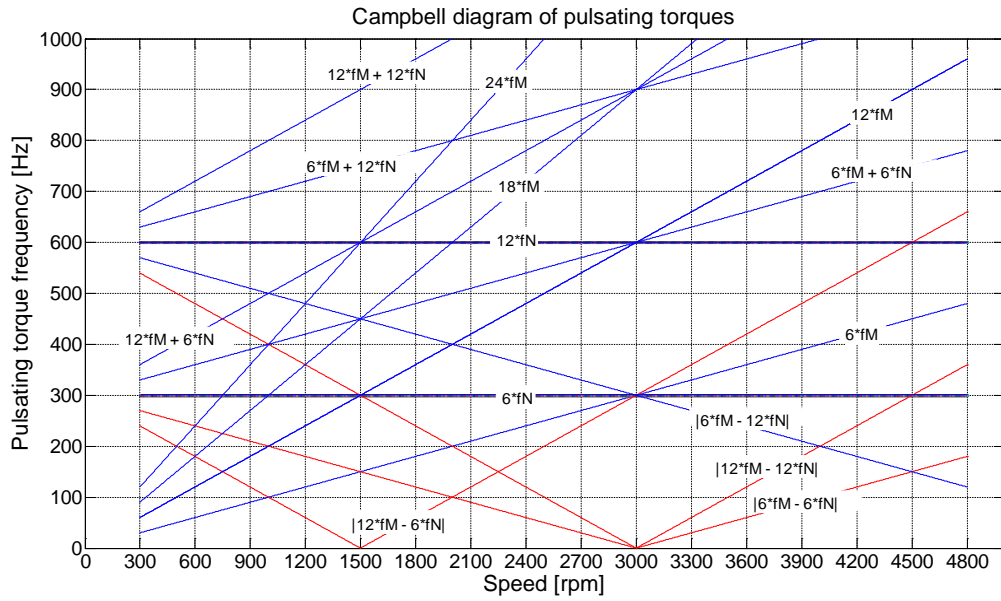
Figure 5-21: Campbell diagram of conventional drive system with current source inverter
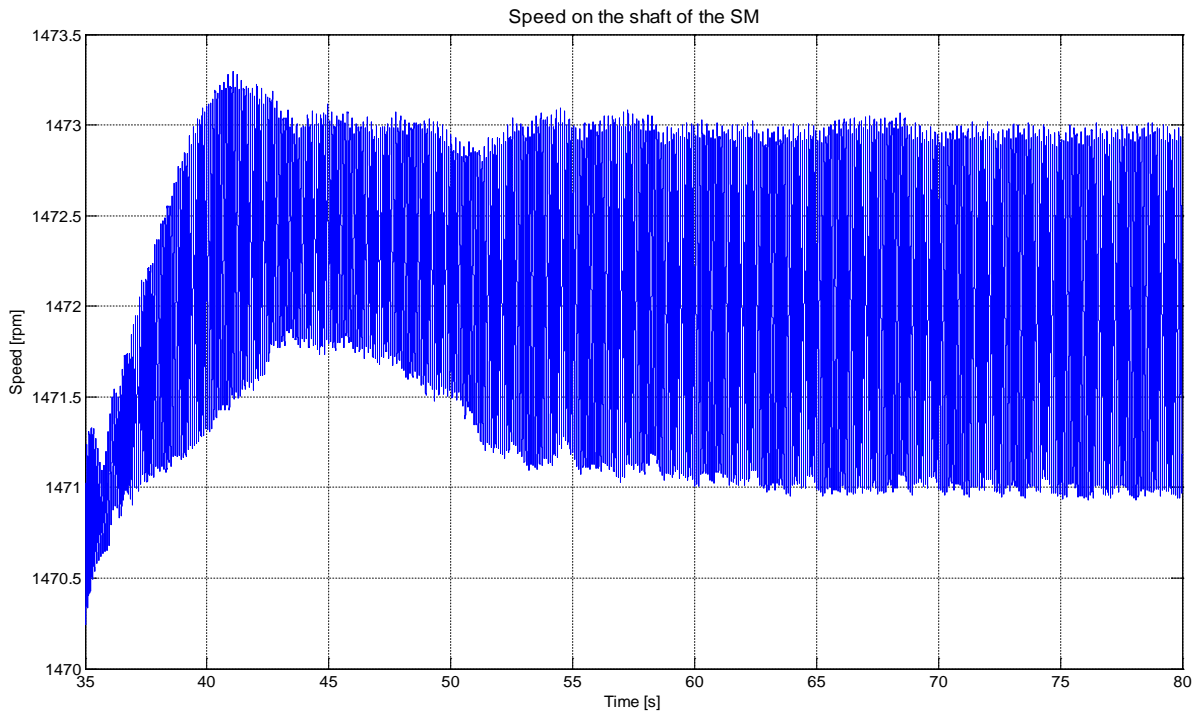

Figure 5-22: Motor shaft speed while driving into critical speed of 1'472 rpm

Figure 5-23 and Figure 5-24 show the spectrum of current in the dc link while the LCI drive slowly gets to 1'472 rpm and reaches a steady state operation. The dominant components of dc current ripple are not shown as these components are above 160 Hz. On the other hand the interharmonics are well visible. Figure 5-24 uses logarithmic scale for the magnitude (colorbar) so that also interharmonics with very small magnitude become easily recognizable.
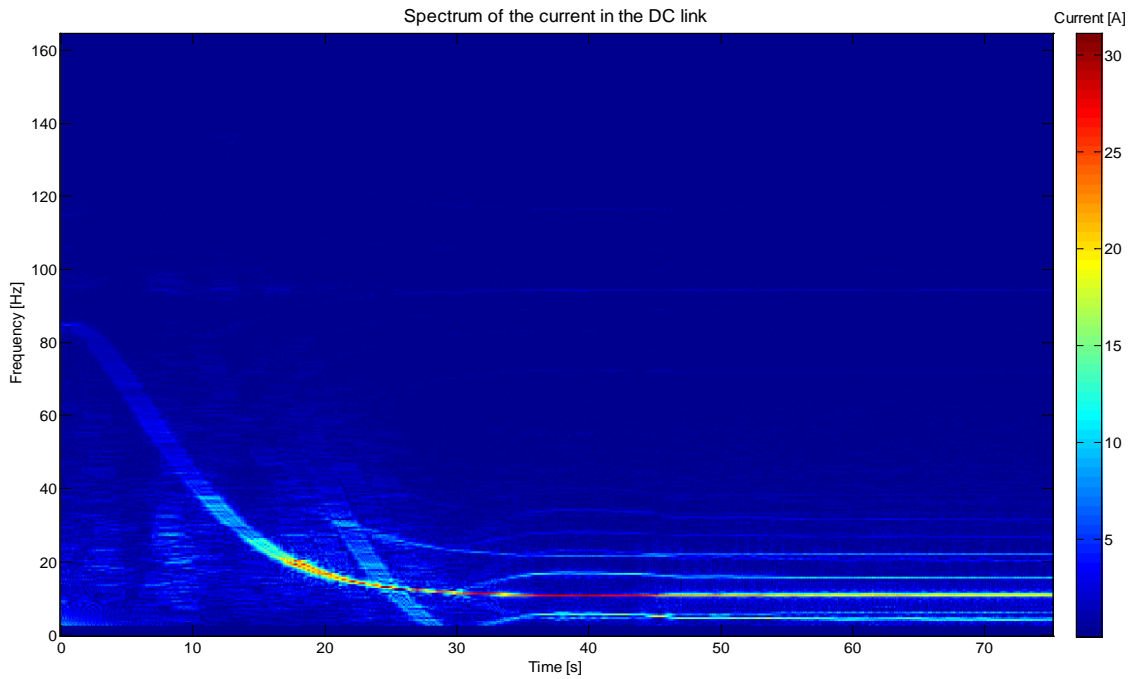
Figure 5-23: Waterfall plot of current in dc link while reaching 1'472 rpm (linear scale)
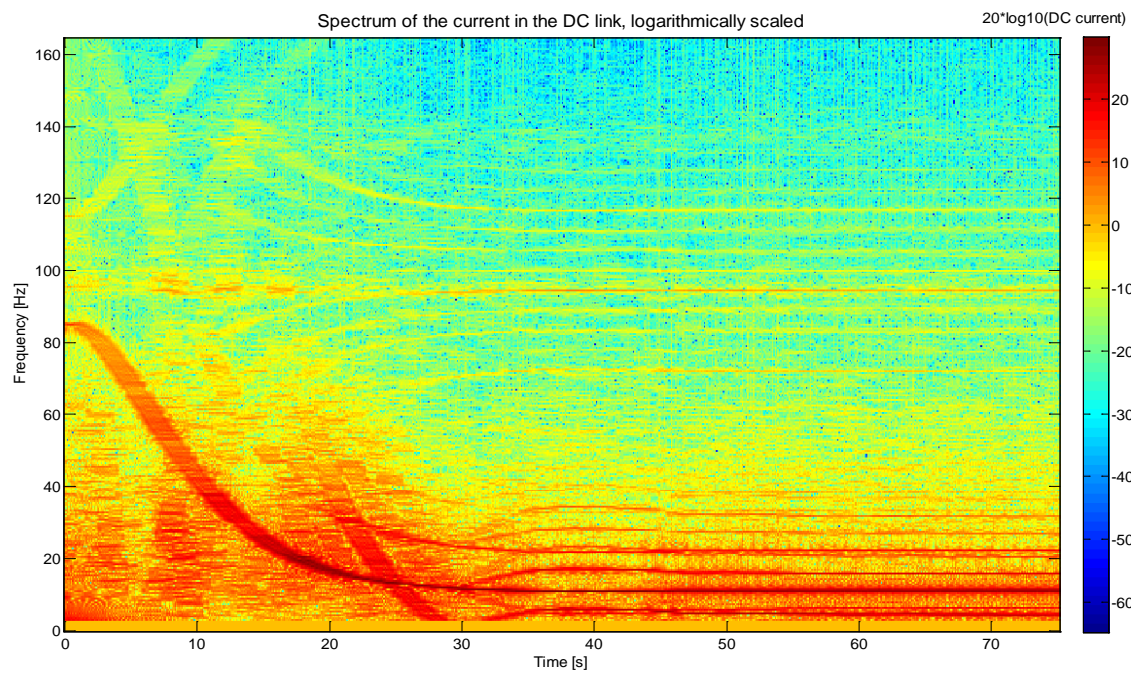
Figure 5-24: Waterfall plot of current in dc link while reaching 1'472 rpm (logarithmic scale)

These interharmonics are of concern from torsional perspective and the damping algorithms attempt to eliminate or at least reduce them.

5.2.4.1.2   Voltage source inverters

The advantage of current source inverters is the fact that for high power there is basically just one topology (LCI) used by main manufacturers and the behavior is more or less the same or at least very

similar (excluding algorithms for active damping etc). The LCI topology is being used for over 40 years and its harmonic content is usually well known.

The family of voltage source inverters is much larger and the products differ in their hardware circuitry as well as modulation principles. General analysis is therefore not easy. However, the basic pattern might be similar for most of them. The most frequent topologies are 3-level neutral point clamped (NPC) inverter, 5-level NPC/H-bridge inverter, multi-cell with cascaded H-bridge, 5-level flying capacitor inverter and others. The most common modulation methods are pulse width modulation (PWM) and hysteresis modulation used in direct torque control (DTC) strategy.

Despite the variety of product offerings, probably all of the VSI drives will have characteristic torque components integer multiples of six times fundamental motor electric frequency:

$$f_{char} = k \cdot 6 \cdot f_{mot\ el.}$$
$$k \ ... \ \text{integer (1, 2, 3,...)}$$

These torque harmonics usually have high frequencies and do not interact with the torsional modes of concern (below 100 Hz) within the operating speed range (see Campbell diagram below). Therefore, those harmonics shall only be considered as transient excitation during start-up. Besides these dominant harmonics in torque there are also other harmonics. These might be e.g. products (convolutions) of control task cycle and carrier frequency of PWM. Their magnitude is fairly small, but their frequency can enter the range 0...100 Hz and has the potential to excite the torsional modes. In most cases the response is very small. However, for s very sensitive driven equipment it could be an issue.
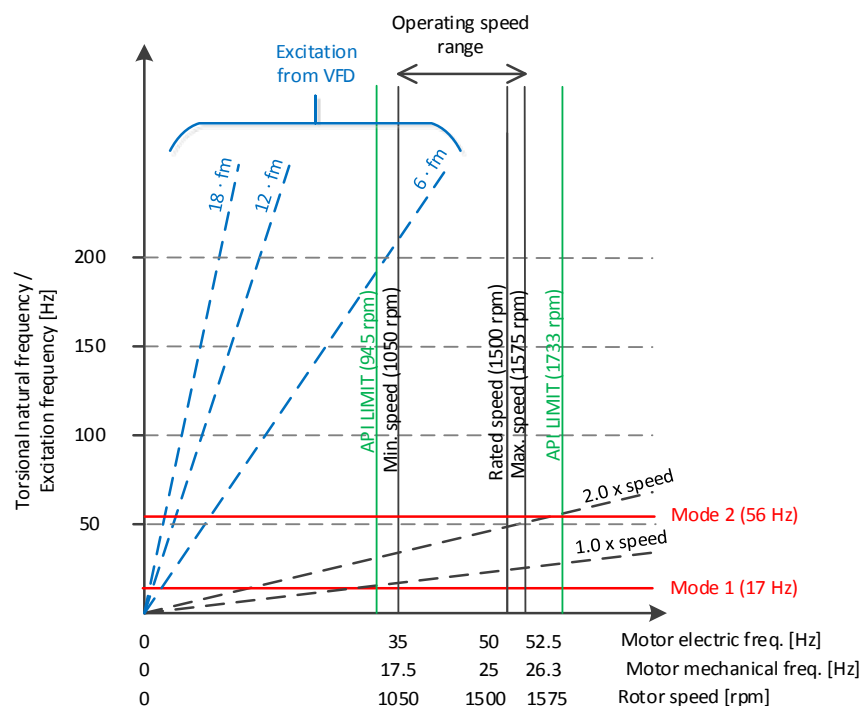

Figure 5-25: Campbell diagram of conventional drive system with voltage source inverter

Some VFD topologies offer option for so called N+1 cell redundancy in combination with bypass switch. In case of failure of one cell (cell usually refers to a low voltage IGBT switch), the cell is bypassed and the VFD continues in operation without tripping. The advantage for the user is that we can keep

his process running. However, it might introduce additional torsional risk. The torque might have increased ripple and eventually other frequency spectrum. It needs a special attention for the case of torsionally sensitive application.

5.2.4.2   Closed-loop interaction

The second source, the closed-loop interaction, is usually less obvious, but might often be the root cause of vibration problems on site. It is relevant for all drives using feed-back control. To understand the interaction, one must use closed loop (feed-back) thinking instead of traditional open loop (feed-forward) approach [38], [39], [40], [97], [98].

The traditional torsional analysis is open loop analysis. It defines the excitation (e.g. 2% rated torque at 1.0 x fundamental rotor frequency, and 1% rated torque at 2.0 x fundamental rotor frequency) and determines the torque response. What is totally ignored is the reaction of the drive control on the vibrations. This can be the reason why the traditional torsional analysis might not predict the torsional response correctly. The control system processes measured signals, such as motor speed, stator currents, stator voltages, etc. If these signals contain oscillations due to torsional vibration, it will directly affect the drive behavior.
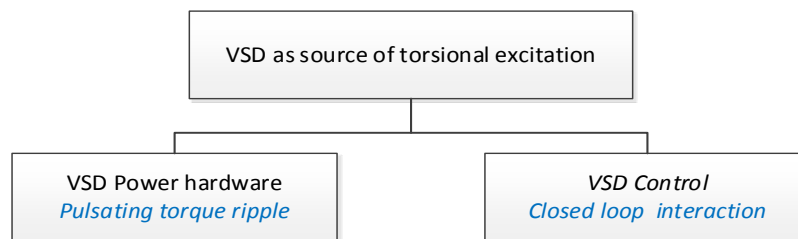

Figure 5-26: Mechanisms of torsional excitation in VSDS

5.2.4.3   Transient excitation

5.2.4.3.1   Excitation during fault condition

Transient torques originate from various conditions, such as

- High-speed automatic reclosing (31)
- Direct on-line start from standstill (32)
- 3-phase short circuit (33)
- 2-phase short circuit (34)

M_0, M_1, M_2 and M_{00} are constants (in pu) and τ_0, τ_1, τ_2 are time constants defined by motor manufacturer, ω is the motor (actual) frequency. The constants are only valid for specific operation point.

$$T_{e\ (reclosing)}(t) = M_0 \cdot e^{-t/\tau_0} + \left(M_1 \cdot e^{-t/\tau_1} + M_2 \cdot e^{-t/\tau_2} \right) \cdot \cos(\omega t - \varphi) + \qquad (31)$$
$$M_{00}$$

$$T_{e\,(DOL\,start)}\,(t) = \; M_0 \cdot \left(1 + e^{-t/\tau_1} \cdot e^{-t/\tau_2}\right) - M_1 \cdot (\cos(\omega t - \varphi) \cdot e^{-t/\tau_1} + \tag{32}$$
$$\cos(\omega t + \varphi) \cdot e^{-t/\tau_2})$$

3-phase and 2-phase short circuit transients are very rare conditions. They can appear in motor applications running either direct on-line (DOL) or with a variable frequency drive (VFD). In contrast, direct on-line start and automatic reclosing are only applicable for machines directly connected to supply network with fix frequency. They can be disregarded for VFD driven motors.

3-phase short circuit on motor terminals is very unlikely. However, a certain probability is there and it needs to be considered as transient excitation in torsional analysis. The transient torque contains only the fundamental electric motor frequency. Faults in the VFD might also result in 3-phase short circuit.

$$T_{e\,(3-ph)}\,(t) = \; M_0 \cdot e^{-t/\tau_0} - M_1 \cdot e^{-t/\tau_1} \cdot \sin \omega t \tag{33}$$

2-phase short circuit is more dangerous. The spectrum contains two frequency components: fundamental motor angular frequency (ω) and twice the fundamental frequency (2ω). Therefore, it is more likely to excite a mechanical resonance. In addition, the peak torque in 2-phase fault is generally higher than for 3-phase fault.

$$T_{e\,(2-ph)}\,(t) = \; M_{00} \cdot \left(1 - e^{-t/\tau_0}\right) + \left(M_0 + M_2 \cdot e^{-t/\tau_2}\right) \cdot \sin 2\omega t - M_1 \tag{34}$$
$$\cdot e^{-t/\tau_1} \cdot \sin \omega t$$

Reaction of VFD on 2-phase fault on the motor side can be a 3-phase short circuit. The VFD switches on all semiconductors inside the inverter which results in a symmetrical 3-phase fault. This is very beneficial. If the VFD reaction is fast enough, then 2-phase fault can be disregarded in VFD configuration and only 3-phase fault needs to be considered.

The worst case scenario would be if the fault happens at a motor frequency equal to one of the torsional natural frequencies. This condition should usually be automatically excluded in the continuous speed range (excitation from residual unbalance and misalignment), but it could appear during start-up. The probability is very low. However, if the risk is considered as too high, one possibility could be the inhibition of 3-phase short circuit as fault reaction at that specific frequency.

Refer to Appendix 11 – Motor transient torques for more details.

The peak transient torque also depends on the fundamental motor frequency (frequency dependent coefficients M_{00}, M_0, M_1 and M_2). The tendency is to have a higher peak at lower motor frequency. This fact might make the transient analysis more challenging for inverter driven motors compared to direct on-line applications where the motor frequency is fix (50 or 60 Hz). For more details refer to Appendix 11 – Motor transient torques.

5.2.4.3.2   Synchronization process

The bypass option is a frequent feature of VSD. There are two types: Asynchronous bypass is used to start the motor as direct on-line. Synchronous bypass is required for variable frequency soft starters. The motor is soft started up to its nominal frequency. When the conditions for synchronization are fulfilled (i.e. matching magnitude, frequency and phase angle of grid voltage and converter output

voltage), the motor is transferred from VSD supply to the grid. The synchronization can be of two types referring to the sequence of involved circuit breakers:

- Make before break (Close before open)

    The motor starting switch is closed and motor is supplied from the VSD. When the conditions for synchronization are fulfilled, first the motor breaker closes. For several tens of milliseconds both circuit breakers are closed. Afterwards the motor starting switch is opened and motor operates direct on-line. With this method the current supplied to the motor is not interrupted and the method is also called "bumpless synchronization". In this method, the VSD has to be protected against the maximum short circuit current from the grid as during synchronization it is directly connected to the grid. An output reactor is usually needed in order to keep an acceptable current ripple during synchronization.

- Break before make (Open before close)

    The initial phase is the same as the other method, i.e. motor starting switch is closed, motor is supplied from VSD and accelerated to nominal speed. When the synchronization conditions are fulfilled, the motor starting switch opens at first and short time later the motor breaker closes. The motor then operates as direct on-line. Since both circuit breakers are interlocked and never closed at the same time, the VSD is inherently protected against fault current from the grid. This fact might have a positive impact on the protection concept of VSD. The output reactor is not needed unless it is a standard part of the drive. On the other hand, the current interruption causes transient torque every time the motor is synchronized. The additional mechanical stress is much lower compared to direct on-line start of the motor. However, especially for torsionally sensitive applications, the torque during synchronization shall be considered for the dimensioning of mechanical components.

The difference between "make before break" and "break before make" options is analogous to the different arrangements of motor starting via auto-transformer:

One arrangement causes transient overvoltages when one of the breakers opens. These overvoltages can potentially damage the auto-transformer (Korndorfer – closed transition).

The other arrangement causes transient air gap torque because the motor current is interrupted for a short time (ABB – open transition).

5.2.4.3.3   *Insertion of harmonic filter*

This type of transient is usually applicable only for LCI type drive with harmonic and power factor correction filter. When the filter is inserted, the commutation impedance seen by the rectifier changes abruptly. The firing angle needs to be adjusted and during the transient a current peak accurs. This current peak causes a peak in the air gap torque as well. The situation is illustrated in Figure 5-27 where the harmonic filter is switched on at approx. 26 seconds. Clear spikes in current and torque are visible.
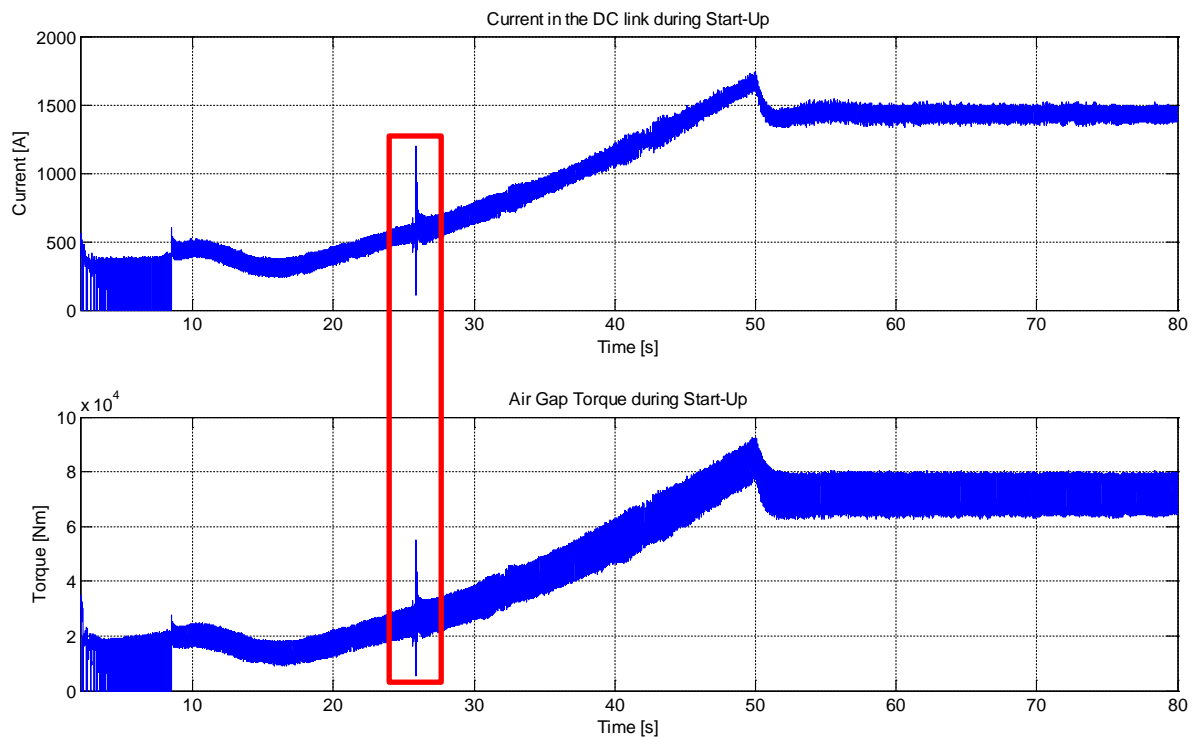
Figure 5-27: Current in dc link and air gap torque during start-up

If the filter is switched on before LCI starts to modulate, then this case can be disregarded. If the filter is switched on during operation (e.g. insertion at certain speed to avoid overcompensation), a small transient appears. The excitation is mostly not so significant and the torsional response is rather small. However, it is mentioned for completeness.

5.2.4.3.4   Undervoltage ride through

VFD might be equipped with so called undervoltage ride through (alternatively called kinetic buffer) functionality that allows to survive short time voltage dips in the supply [99]. This is very beneficial for the user as it prevents instantaneous tripping of drive system and increases immunity against disturbances in supplying grid. The VFD keeps the voltage in dc link at minimum level (typically 60-70% nominal voltage) and the inverter keeps modulating. When the grid voltage recovers, the drive system continues driving and accelerates to setpoint speed. The key for successful ride through is a fast removal of driving torque in order to avoid the discharge of dc link. The motor torque drops from initial value down to zero (or actually slight negative torque). Such dynamic change would potentially excite the torsional resonance as illustrated in Figure 5-28 below with parameters as per Table 16. The figure depicts the performance of compressor drive behavior before, during and after the supply undervoltage event.
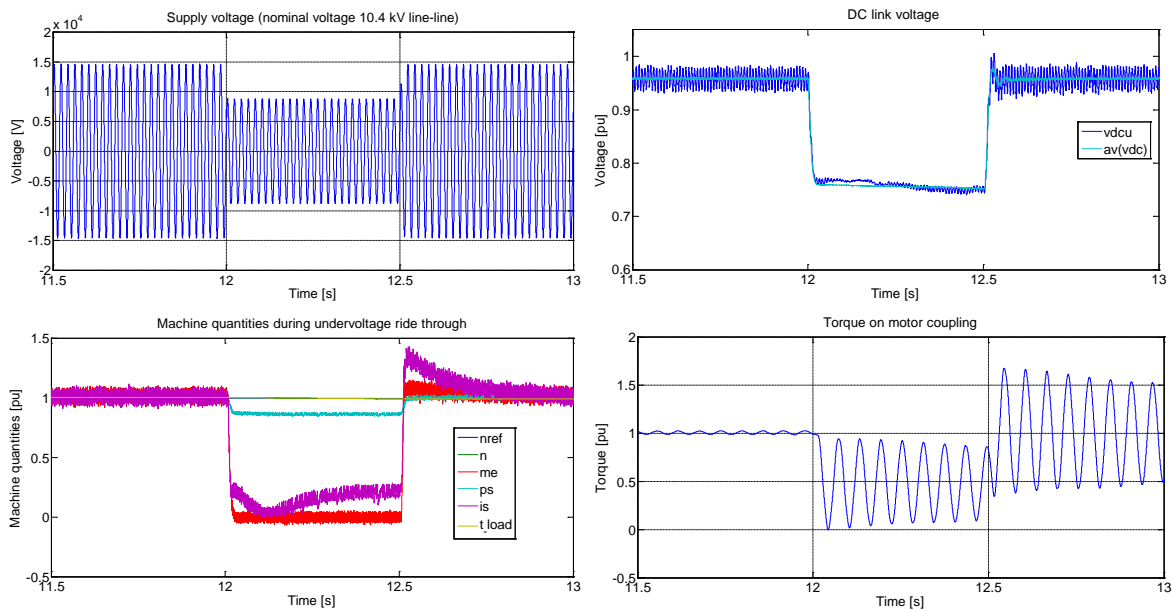
Figure 5-28: Transient torsional excitation during and after supply voltage sag

5.2.4.4   Sub-synchronous torsional interaction

Sub-synchronous interactions (SSI) is a general term that can be applied to the various subsynchronous phenomena where either series resonant circuits or control interactions can excite and amplify subsynchronous currents in the power system. Depending on the type of equipment and interaction this phenomena can be described as subsynchronous resonance (SSR), or subsynchronous torsional interaction (SSTI). The phenomena have also been referred to as sub-synchronous oscillations (SSO). This phenomenon is well known from the HVDC power transmission. In case of local power generation close to an HVDC terminal, there is a risk of interaction between the turbine-generator system inside the power plant and the power electronics within the HVDC terminal. The control loops of these active devices (semiconductors) can destabilize the torsional mode of the turbine-generator shaft string. The result is excessive vibration on the turbine-generator and consecutive trip reaction to protect the equipment.

5.3   Vibration measurement

As mentioned, direct measurement of torsional vibration is not an easy task and it is seldom utilized in industrial application. Instead, lateral vibrations are measured. The question emerges how to judge the severity of torsional vibration based on lateral vibration signals. Basically, observed lateral vibration is a superposition of multiple vibration sources. First problem is to decompose the vibration signal and separate the effect of torsional vibration from other sources (unbalance, misalignment, excitation from gearbox). Second problem is to estimate the coefficient of torsional-to-lateral vibration transfer. That might be actually the most significant uncertainty [100]. Some sources, such as [101], recommend six vibration related parameters:

1. Overall magnitude
     - indicates presence and severity of vibration problem

2. Frequency of vibration component
    - insight into root cause of vibration malfunction
3. Time-based waveform (unfiltered) and orbital paths
    - insight into nature of malfunction
4. Amplitudes and phase angles of orbital frequency-filtered components
    - phase angles to diagnose fluid whirl and fluid whip
5. Rotor centerline position at rest / during start-up / in steady state
    - insight into radial load status
6. Ratio of overall amplitudes to the filtered synchronous frequency amplitudes

There is sometimes a search for 'the best parameter' to observe a vibration phenomenon. In principle, several parameters can be measured. Typically used parameters are acceleration, velocity and displacement. The best parameter is such that requires the smallest dynamic range. In most cases it is the velocity. The modern equipment for vibration monitoring consists of several stages, such as:

1. Transducer
2. Preamplifier
3. Conditioning amplifier
4. Oscilloscope / Voltmeter / Pulse analyzer / Counter / Tape recorder / Transient recorder / Peak detector

The properties of above stages determine the suitability of equipment for measurement of specific vibration pattern.

5.4   Damping and amplification factor

Besides the excitation magnitude it is the damping that determines the severity of vibration. The oscillation magnitude is limited by damping. The torsional damping is usually much less than lateral damping. In majority of applications the damping is so low that it makes the avoidance of torsional critical speeds very essential for machine reliability and durability. Turbomachinery has especially low inherent damping since the equipment rotates in a gas atmosphere with very low friction. [102] reports that torsional damping of steam turbine-generator shaft system is approx. 0.1% or even lower. The amount of damping determines whether the intersection point can be ignored or becomes a design-sensitive critical speed.

Inverse value of the damping is so called amplification factor (another synonym is Q-factor). It defines how much the excitation is amplified, i.e. what is the magnitude of torque response.

There are many types of damping such as material and structural damping, fluid related damping, electrical damping, control damping etc. Further, the damping types can be classified in certain groups. Based on the location we can distinguish between internal and external damping. Based on the acting principle passive and active damping can be distinguished.

- material damping
- friction damping
- structural damping
- electric damping

- control damping

In rotordynamics the damping is frequently modeled as viscous damping:

$$\boldsymbol{B} = \alpha\boldsymbol{M} + \beta\boldsymbol{K} \tag{35}$$

where $\boldsymbol{B}$ is the damping matrix, $\boldsymbol{M}$ is mass (inertia) matrix, $\boldsymbol{K}$ is stiffness matrix and α, β are proportional coefficients. Note that coefficient α represents structural (construction) damping and β material damping. This expression does not consider either electric or control damping.

Damping forces are difficult to measure directly. In addition, rotor-bearing systems can have several different sources of damping. From those two reasons, the total damping is usually quantified as percentage of "critical damping".
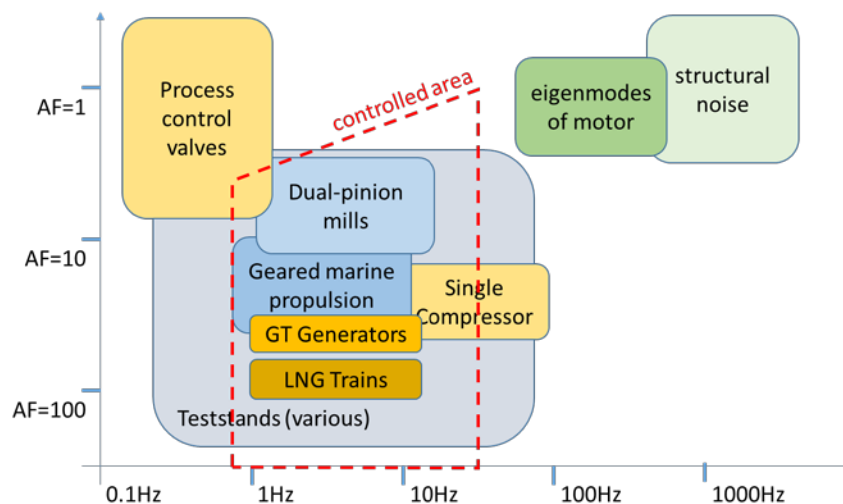
Figure 5-29: Typical application resonances in terms of frequency and damping/amplification factor [103] (x-axis: system resonance frequency, y-axis: amplification factor)

It seems that the amount of damping used in theoretical calculations in design stage is often overestimated and real damping in the system is actually smaller. Typical amplification factors (inverse proportional to damping) across various applications are summarized in [103].

Internal damping in rotating machinery, and particularly in turbomachinery, is inherently very low. It has several components, e.g. structural damping (hysteretic damping of the rotor material), damping of train couplings, natural motor damping (electro-magnetic) etc. The use of VFD might – depending of control parameterization – remove certain portion of the inherent damping. It is nicely illustrated on the comparison of DOL versus VFD driven induction machine.

DOL induction machine

- Medium voltage motor has high efficiency (1…5 MW range typically above 96% efficiency, power ratings above 5 MW typically larger than 97% efficiency). This results in very small nominal slip and stiff torque-speed characteristic.

- Small change of motor speed results in instant change of slip and steep increase or decrease of torque ("hard" torque characteristic).

- In stable part of torque curve the additional torque caused by speed deviation always has damping effect – natural damping of induction machine. The damping torque is produced

without any time delay unlike the control interventions that inherently contain latency and time delays (observer algorithm, sampling of signals, cycle tasks of control loops etc).

- At sub-synchronous frequencies there is a range where the electric damping is negative due to impact of electric forces on rotor body (see figures 5 and 6 in [97]). That frequency range is usually just slightly below the nominal frequency. For fix speed DOL motor this is obviously not a problem, but when the motor is fed by VFD, the reduced (in worst case negative) electric damping shall be taken into account. Note: Many turbomachinery manufacturers use empirical values of damping that are based on experience with direct on-line machines and might be too optimistic for variable frequency driven systems.

VFD driven induction machine, torque controlled

- In case of constant torque reference the VFD tries to maintain the motor torque constant and compensates any external disturbance.
- Small change of motor speed does not affect the motor torque when controlled to a fix reference value.
- The inherent electric damping of DOL induction machine is removed!

VFD driven induction machine, speed controlled

- Between previous cases, closer to DOL induction machine.
- Change of motor speed causes a change of motor torque. However, the change is not instant, but comes with certain delay due to control latency. Such latency removes part of the natural damping that DOL machine inherently has.

The major sources of external torsional damping are the characteristics or the load and/or its driver. Information on torsional damping is rare. There is no existing formula to obtain directly the damping value depending on the dimensions of the shaft, air gap and air flow in the air gap. Damping coefficient is determined empirically based on the magnitude in resonance and applied for machines with similar construction.

The load also contributes to increased damping. Load torque partly counter-acts the pulsations in motor air gap torque. No load condition is the worst case from that standpoint. Therefore, transient excitation during start-up might be more severe than thought.

In SSTI analysis, the electrical and mechanical damping is often analyzed as key criterion for stability. Based on a simplified transfer function model the damping can be expressed as real part of the corresponding transfer function.

$$D_e \left(\omega \right) = Re \left\{ G_e \left(j\omega \right) \right\} \tag{36}$$

D_e is the electric damping, G_e is the transfer function of electric sytem.

$$D_m \left(\omega \right) = Re \left\{ \frac{1}{G_m \left(j\omega \right)} \right\} \tag{37}$$

D_m is the mechanical damping, G_m is the transfer function of mechanical sytem.

When talking about VFD damping, it is not correct to state anything about the damping value without mentioning the frequency range. Typically, the VFD has positive electric damping in some frequency

range while it drops and becomes negative in other frequency range. Therefore, the admittance analysis is very important for the design and verification of VFD control system.

Passive damping is either physical (dissipative elements in power hadware) or control based (notch, lowpass or highpass filters). Dissipative elements limit the magnitude of oscillation in resonance and shorten the decay time. Passivity based control tries to avoid electro-mechanical interaction and potential amplifications inside the closed loop control.

5.5   Control

The VFDs incorporate two fundamental control methods based on the control loop architecture:

> a) Open-loop control (feed-forward)
>
> b) Closed-loop control (feed-back)

The open loop control uses a simple motor model or no model at all. Often it is assumed that the actual value is equal its reference. There is no feed-back signal providing information about system response. The method is typically good enough for application with no dynamic operation.

The closed-loop control has much better performance in transient operation. It introduces one or more feed-back loops. The control receives feed-back signals from the driven system. The control interventions depend on the feed-back signals. It is a question whether to use actual or reference signals for certain algorithms. The actual signals are more accurate, but may introduce oscillatory behavior and additional loops. Once the system oscillates, it can be very difficult to determine the root cause. Therefore the actual signals are often at least pre-filtered. The filtering slightly reduces the dynamic response, but it makes the system more robust against oscillations.

The aim of the control system with regards to oscillation and vibrations is to minimize the torque pulsations, avoid excitation of resonances and provide sufficient damping for the system. The damping can be either passive or active. The differences are discussed in following chapters.

5.5.1   Control damping functions

The control software is often the only "muscle" to mitigate vibration problems. Another advantage of control damping algorithms is that they can be parameterized and relatively easily adjusted on site. A hardware change in the system is often not possible or not practical so the only option remains the control functionality. Depending on the control mode of the drive, the damping algorithms can be placed in speed control loop, torque control loop or both of them.
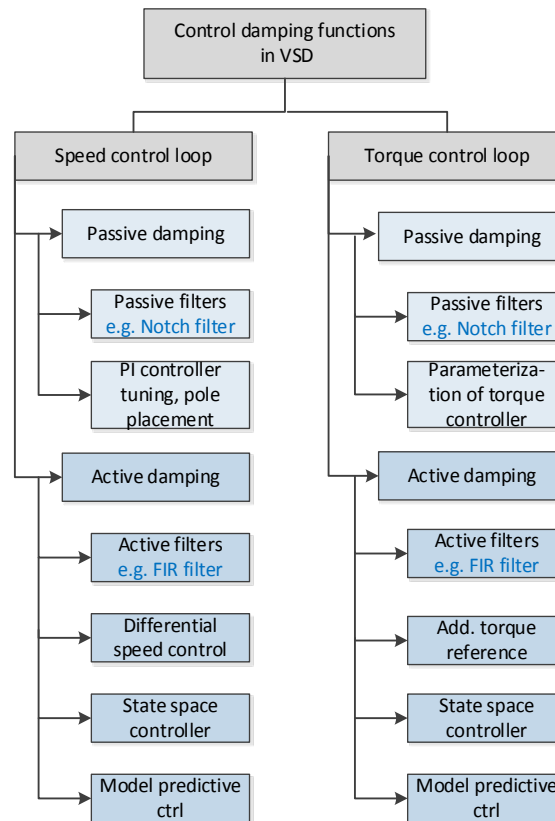
Figure 5-30: Classification of control damping functions

We can classify the damping functions according several criteria:

- way of acting (passive versus active)
- control loop (speed chain, torque chain, current chain etc)
- damping effect (direct / indirect)
- based on measurements / based on observers (sensorless)

Depending on the implementation the damping functions are either direct (acting in speed or torque control chain) or indirect (e.g. damping of dc link voltage or power).

5.5.2 Passive control damping and passivity based design

Passive control damping is an easy way to increase the robustness against vibrations. The strategies are typically based on some sort of software filters that shall remove specific frequencies from the signal. The system does not see those frequencies and does not react on them (certain frequencies are blocked). For most common filters used for passive damping refer to Appendix 14 – Software filters.

The passivity based design and stability analysis is something slightly different, although the basic principle is the same. The stability assessment can be done by modeling and analyzing the admittance in frequency domain. The converter shall have a passive behavior towards the grid or load side, i.e. the real part of its admittance must be nonnegative. It might be difficult to ensure passivity over entire frequency range, but it shall be possible to achieve this goal in a frequency range of interest. The

approach is mainly used for grid connected converters [104], [105], [106], [76]. It emerged from traction grids and was adopted for wind converters and HVDC. Therefore, in the literature it can be found under the keyword *input admittance*.

Latencies and time delays impact the passive (natural) damping that analog systems inherently have. The time delays are caused by sampling times and calculation delays inside the control loops. It impacts mainly fast control loops, e.g. current and torque regulation [105]. However, even the performance of speed control loop can be significantly affected by latencies. High-dynamic applications are especially sensitive to delays in control [72]. The total time delay consists of the particular delays of speed observer (encoderless operation) or speed digital filters (encoder operation) etc. The delays are usually not large enough to destabilize the control loop, but they reduce the natural damping [107]. Even a small delay can cause a frequency region where the converter appears as negative impedance [103] as illustrated in Figure 5-31.
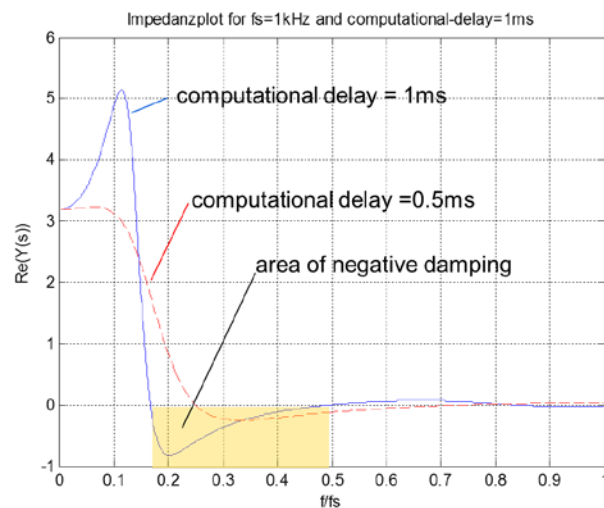
Figure 5-31: Converter impedance plot considering computational delays [103]

The switching frequency also influences stability. LV drives work with higher switching frequencies and the stability problem is inherently less pronounced. In contrast, MV drives typically use somewhat lower switching frequency and are less forgiving in respect of delays resulting from modulation. Up to delay of ¼ of signal period (90 deg phase lag), the system is still stable, but natural damping shrinks. A general recommendation is to minimize the latencies inside each control loop.

Modern torque meters also introduce certain time delay. The strain gauge is analog device with continuous operation (small hysteresis that can be compensated, but the internal signal processing of the torque meter (digital amplifier, digital filtering, and wireless transmission) causes small delay.

5.5.3   Active control damping

Dedicated control interventions are introduced in order to increase the overall damping. Such algorithms can contribute significantly to reduction of vibration and unlock a lot of potential. However, they also require more attention. When not properly parameterized (e.g. incorrect phase of additional signal), they can amplify the excitation and increase the vibration or even damage the rotating equipment. Therefore, the software functions shall be robust and fail-proof. The algorithms often require

much more details about the mechanical system. The data can be obtained from directly from the manufacturer of driven equipment (OEM), datasheets and reports or they can be estimated from experimental data [87].

In squirrel cage induction machine drives the VSD supplies just the stator. In wound rotor synchronous machine drives both stator and rotor windings are supplied from a controlled power electronics converter and the damping effect can be injected either through the stator winding, through the rotor winding or both of them. There is additional degree of freedom in regards to torsional damping. Damping functions based on interventions in rotor circuit typically have lower dynamics and are only suitable for low frequency oscillations (e.g. up to 5 Hz). Interventions in stator circuit usually allow higher bandwidth and can successfully damp oscillations up to 30-40 Hz.

Demanding applications such as rolling mills in metal industry have developed lot of advanced control functions in order to deal with oscillations and to damp vibrations not just in steady state, but also in high dynamic transient operation. The most important and most useful ones are drive train dynamic compensator, resonance frequency eliminator or adaptive oscillation damping.

6   Algorithms for minimized excitation and enhanced damping

6.1   General considerations

The goal is to ensure positive control damping throughout the control bandwidth. The algorithms are mostly based on certain feedback signals. At the beginning, it shall be defined:

- what signals (states) will be available as measurements
- what signals shall be estimated using observers
- what signals are not known

Additional measurements are often undesired since they mean additional cost, instrumentation and complexity. Some quantities (such as torque) are difficult to measure. The problem can be overcome by estimation techniques.

In recent years model predictive control (MPC) techniques emerged and became more attractive due to computational power of digital signal processors. The technique relies on estimation of several state variables. The models often assume certain type of load characteristic, e.g. quadratic load torque as function of speed (fans, majority of pumps and compressors). However, this assumption is normally true only for the start up to minimum speed. Afterwards the overriding control system adjusts the reference according to process needs (e.g. pressure, flow rate etc.) and the load curve is not strictly defined anymore.
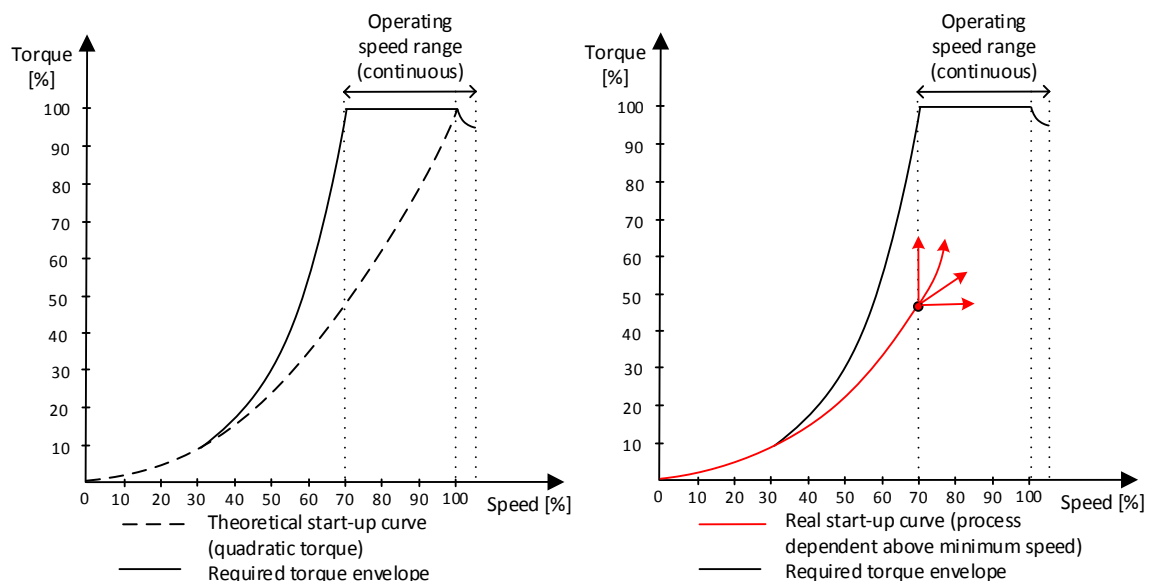
Figure 6-1: Torque-speed characteristic (start-up curve): Left – theoretical curve, right – real curve

This makes it more complex to estimate the load torque and other state variables.

6.1.1   Measured and estimated signals

Voltage source inverter measures current in two output phases towards motor and the voltage in the dc link. The output voltage is calculated from the dc link voltage and known switching state. Optionally the motor speed is measured using a speed encoder.

Current source inverter of LCI type measures currents and voltages at its input side. Current and voltage in dc link is calculated. Optionally the motor speed is measured using a speed encoder. As mentioned in [87], in many processes the measured quantity used as feedback signal is the motor speed, but actually it is the load speed which shall be controlled. In elastic (resonant) systems the motor and load speed may naturally not match, especially during transient operation.

Speed controlled drives can either use open loop control (scalar mode, simple V/f control) or closed loop control. Closed loop speed control is using a speed feedback loop. For this purpose a speed signal is required. The speed can either be measured (speed sensor, also called encoder) or observed (observer for sensorless control).

Most of the VFDs are speed encoder-less meaning that the motor speed is estimated from a motor model inside VFD control. It is very seldom that the motor torque is directly measured and it is often observed using the motor model already mentioned. The torque accuracy is mainly determined by the accuracy of the mathematical model of the motor (non-linearity, saturation effects).

6.1.2   Controllability and observability

Controllability and observability are important terms in control theory. Four combinations exist:
- torsional mode is controllable and observable
- torsional mode is controllable and observable
- torsional mode is uncontrollable and observable
- torsional mode is controllable and unobservable

When the actuator is placed at any node of vibration mode of elastic structure, the mode will be uncontrollable and when a sensor is placed at the node of a vibration mode, the mode will be unobservable. These statements represent limitations when considering active suppression of torsional vibration by means of VFD algorithms. The relationship is described e.g. in [108].

6.2   Torsional optimization and damping for LCI drives

6.2.1   Parameterization of speed controller

The considerations are generally identical to those described in chapter 6.3.1 for VSI drives. In addition, the parameterization of speed reference ramps (rate limiter) has an impact. When DOL motor is started, the intention is to cross the critical speed as fast as possible. The starting torque is not controlled and depends only on machine characteristics and supply voltage. When LCI starts, the situation looks different. Faster speed ramp requires higher acceleration torque and eventually also larger excitation torque. It might be more beneficial to use slower speed ramps, at least when crossing the critical speeds. The phenomena was investigated in [107] and in [A4] and confirmed in the field.

6.2.2   Parameterization of current controller

Current controller in LCI drives corresponds to torque controller in VSI drives with either vector control or DTC. The controller is of PI type and has two basic parameters to optimize. The specific implementation allows different settings in Pulse mode and in LCI mode. Tuning is done based on

bode plots. Transfer function description represents block diagram in Figure 6-2. Current sensor is not shown, the scaling from SI (ampere) into pu system is hidden in current controller with gain *1/I_{dc, nom}*.
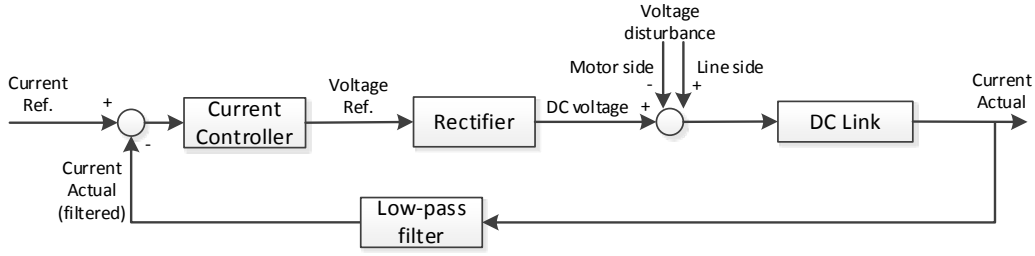
Figure 6-2: Block diagram of LCI current controller

Transfer function of the current controller is written in (46);

$$G_{PI\ Current}\ (s) = \frac{1}{I_{DC,nom}} \cdot K_{RI} \cdot \frac{1 + s \cdot T_{RI}}{s \cdot T_{RI}} \tag{38}$$

where K_{RI} is the proportional gain and T_{RI} integration time const.; $I_{DC,\ nom}$ is the nominal dc current.

Thyristor rectifier is non-linear and simplified as block with transport delay;

$$G_{Rect}\ (s) = \frac{U_{dio}}{1 + s \cdot T_D} \tag{39}$$

where U_{di0} is the ideal no-load rectified voltage and T_D is the average time delay (T/12 for 6-pulse rectifier and T/24 for 12-pulse rectifier; T is the period of line voltage, i.e. 20 ms for 50 Hz grid).

DC link is modeled as first order system with inductance and resistance;

$$G_{DC}\ (s) = \frac{1}{R_{DC} + s \cdot L_{DC}} \tag{40}$$

where R_{DC} is the resistance of DC link and L_{DC} is inductance of DC link.

The low-pass filter placed in the current feedback loop shall remove part of the current ripple;

$$G_{LP}\ (s) = \frac{1}{a_2 \cdot s^2 + a_1 \cdot s + a_0} \tag{41}$$

with filter parameters a_2, a_1 and a_0 defined in (50);

$$a_2 = \frac{1}{(2 \cdot \pi \cdot f_{co})^2}, a_1 = \frac{2 \cdot d}{2 \cdot \pi \cdot f_{co}}, a_0 = 1 \tag{42}$$

where f_{co} is the filter cut-off frequency and d is the filter damping.

Finally the transfer function of open current control loop is described in

$$G_{OC}\ (s) = G_{PI\ Current}(s) \cdot G_{Rect}(s) \cdot G_{DC}(s) \cdot G_{LP}(s) \tag{43}$$

Besides (51) used for control stability we define tracking (52) and disturbance rejection (53).

$$G_{ref\ tracking}(s) = \frac{G_{PI\ Current}\ (s) \cdot G_{Rect}\ (s) \cdot G_{DC}\ (s)}{1 + G_{PI\ Current}\ (s) \cdot G_{Rect}\ (s) \cdot G_{DC}\ (s) \cdot G_{LP}(s)} \tag{44}$$

$$G_{dist}(s) = \frac{G_{DC}\ (s)}{1 + G_{PI\ Current}\ (s) \cdot G_{Rect}\ (s) \cdot G_{DC}\ (s) \cdot G_{LP}(s)} \tag{45}$$

Up to now, the transfer functions were defined in continuous world while in reality some of them are discrete. The discretization significantly impacts the phase margin for otherwise same parameters as illustrated in Figure 6-6 with K_{RI} = 0.16, T_{RI} = 0.02 s, f_{co} = 500 Hz and system parameters acc. Table 7.
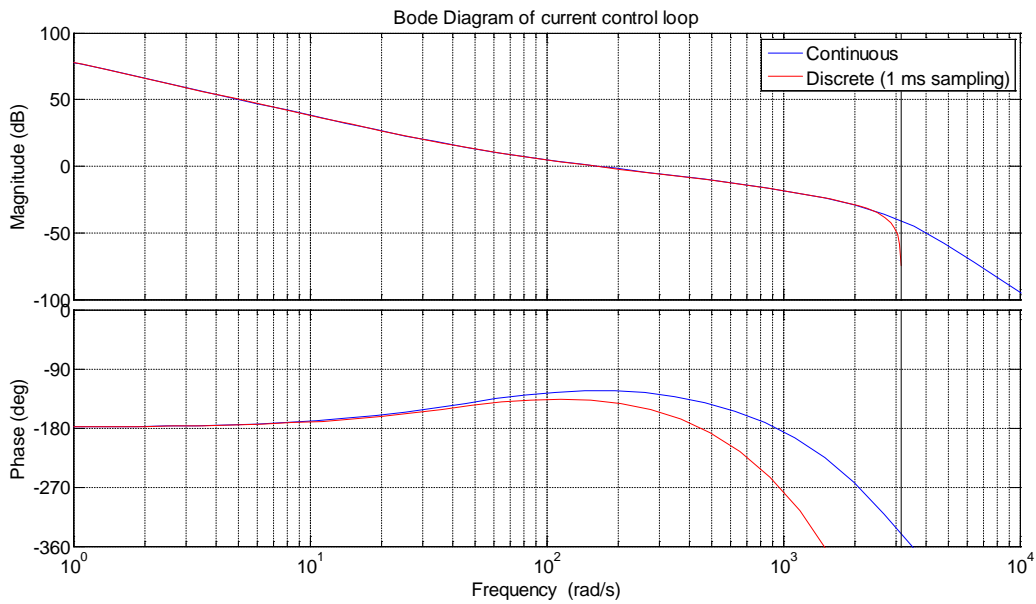
Figure 6-3: Bode of current control loop of system defined in Table 7

Alternative to Bode diagrams a root locus can be plotted as well. Besides the proportional gain the cut-off frequency of the low-pass filter has also a significant impact on stability - the lower the cut-off frequency the lower the maximum proportional gain for stable system. See Figure 6-4 for system acc. Table 7 with T_{RI} = 0.02 s and f_{co} = 500 Hz. For gain approx. 1.4 the system becomes unstable.
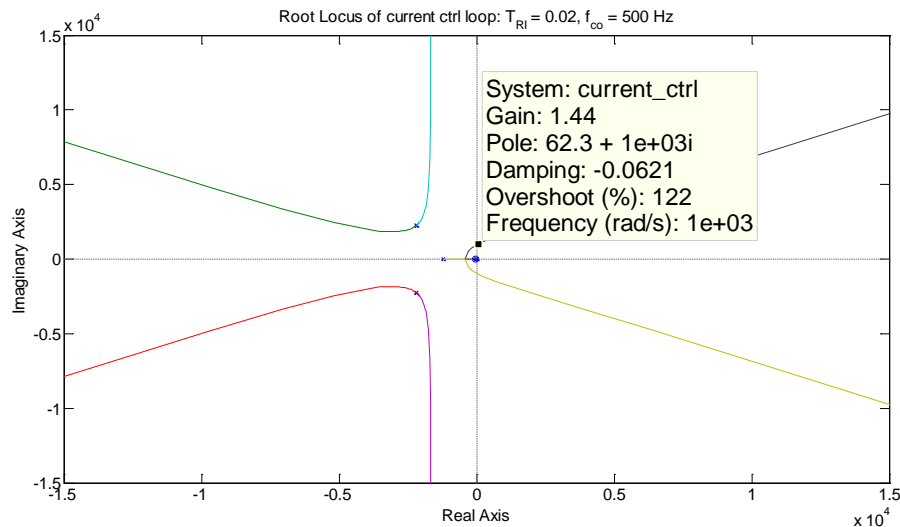
Figure 6-4: Root locus of current control loop of system defined in Table 7
For a large compressor drive system described in

Table 14 the current controller settings had been analytically optimized. The results are shown in Table 3. The table summarizes the current control loop from standpoint of stability (phase margin φ_{PM}) and disturbance rejection (f_{w0} is the frequency of external disturbance at 0 dB crossing). Suggested settings are highlighted green (two alternatives w/o active damping and one set of parameters with active damping).

Table 3: Parameterization of current controller for large compressor drive

Active damping OFF								
K_{RI} [-]	0.1	0.1	0.3	0.3	0.4	0.4	0.5	0.5
T_{RI} [s]	0.1	0.1	0.16	0.16	0.16	0.16	0.2	0.2
f_{co} [Hz]	250	500	250	500	250	500	250	500
L_{DC} [mH]	8.0	8.0	8.0	8.0	8.0	8.0	8.0	8.0
φ_{PM} [°]	65.8	69.8	34.2	46.2	17.0	33.0	0.4	20.3
f_{wo} [Hz]	13.9	15.7	27.0	30.2	31.8	35.4	36.4	40.2
Active damping ON (17 Hz)								
K_{RI} [-]	0.2	0.25	0.3	0.3	0.3	0.3	0.5	
T_{RI} [s]	0.16	0.16	0.16	0.16	0.16	0.16	0.2	
f_{co} [Hz]	250	250	250	250	500	500	250	
L_{DC} [mH]	8.0	8.0	8.0	9.6	8.0	9.6	8.0	
φ_{PM} [°]	33.6	28.1	21.4	28	34.3	38.6	-9.1	
f_{wo} [Hz]	22.5	24.8	27.2	24.7	28.4	25.5	37.2	

6.2.3 Synchronization of rectifier and inverter side

As explained earlier (chapter 5.2.4.1.1), in the operating speed range the interharmonics are the main concern and not the characteristic harmonics. The intersections appear when the inverter operates at frequency close to the rectifier frequency (e.g. 50 Hz grid, 49 Hz motor). One attempt was to synchronize the rectifier (converter line side) and inverter (converter motor side) when the frequencies are close enough and eliminate the interharmonic components inside the dc link. Synchronization of both modulators was programmed in the simulation for a 12-12 pulse LCI. A synchronization window was added to the rectifier modulator. The idea was that the rectifier adjusts the firing angle slightly so that both rectifier and inverter commutate simultaneously (i.e. rectifier commutates a little earlier or little later than it should without this function). The first results were not useful as the small correction of the firing angle on the grid side resulted in huge current and torque oscillation. In next attempts, the rectifier synchronized with virtual 24-pulse, 48-pulse and 96-pulse inverter. As the virtual pulse number is increased, the synchronization window and firing angle error get smaller and smaller. Correspondingly, the current and torque oscillations reduce as well. However, the performance is still significantly worse than without the synchronization. Finally, this approach had been disregarded. It was proven that even very small adjustment of firing angle causes large oscillations of current in dc link and motor air gap torque and the method cannot be used in practice. Figure 6-5 to Figure 6-8

below illustrate the drive behavior while attempting to synchronize the commutations of rectifier and
inverter. The motor shaft power is 17'500 kW, rated speed is 1'500 rpm, grid frequency is 50 Hz and
also rated motor frequency is 50 Hz. Modulators are synchronized when the frequency difference
between line and motor side drops below 5.2%. In the simulations, this condition is fulfilled at time
instant 18.58 s.
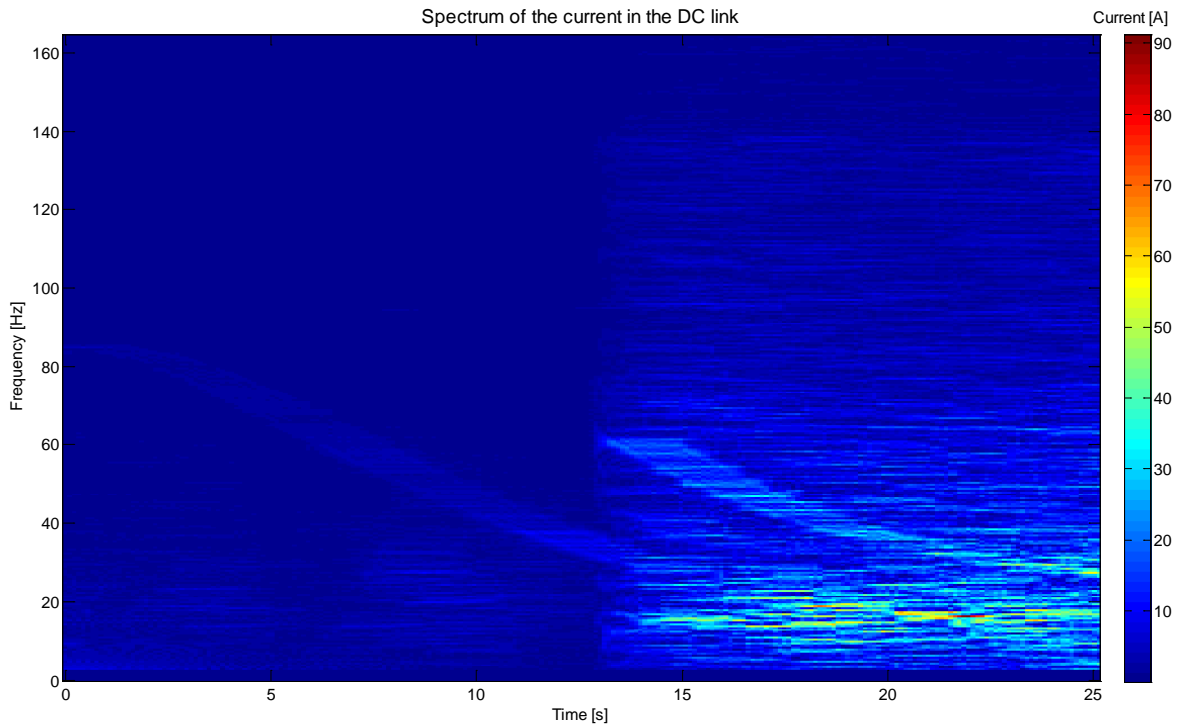
Figure 6-5: Spectrum of dc link current - Synchronization to virtual 24-pulse inverter
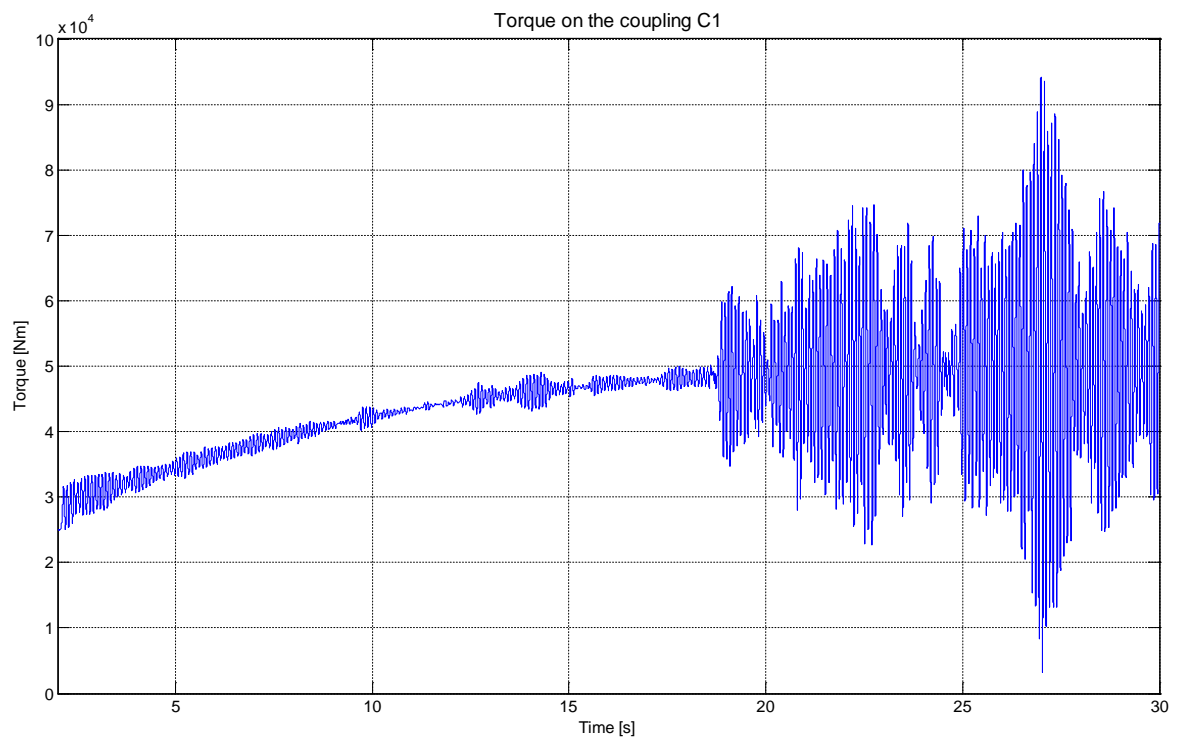
Figure 6-6: Torque on the compressor coupling - Synchronization to virtual 24-pulse inverter
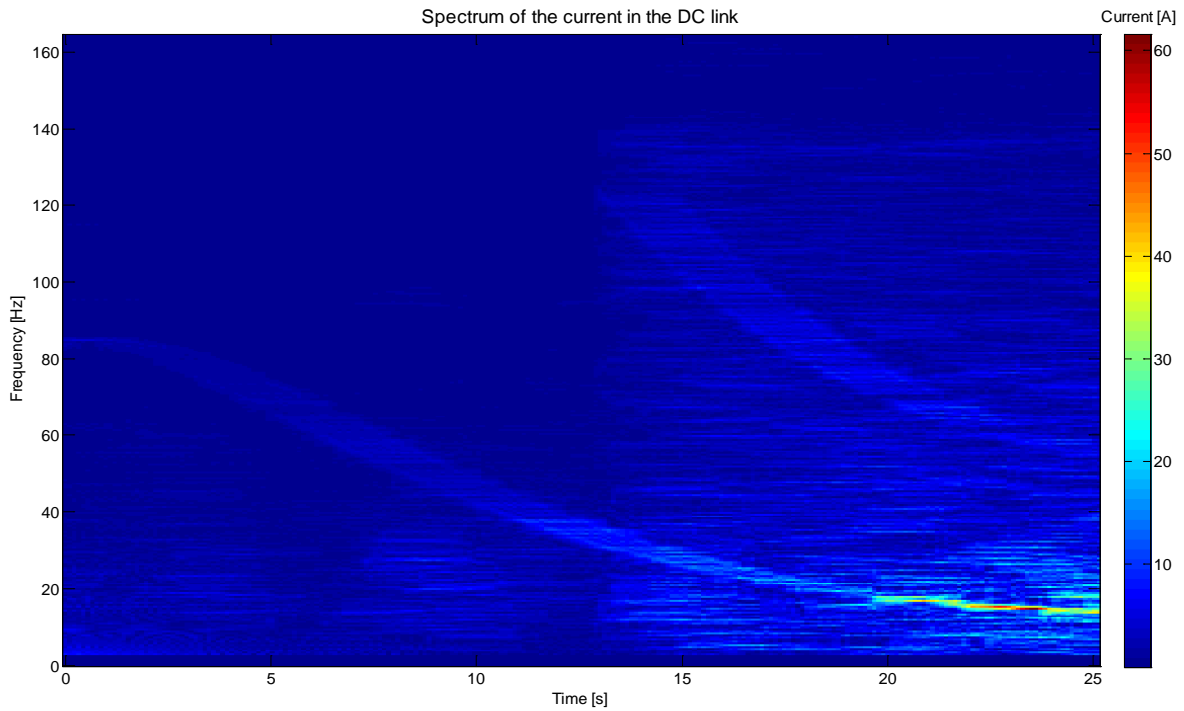
Figure 6-7: Spectrum of dc link current - Synchronization to virtual 48-pulse inverter
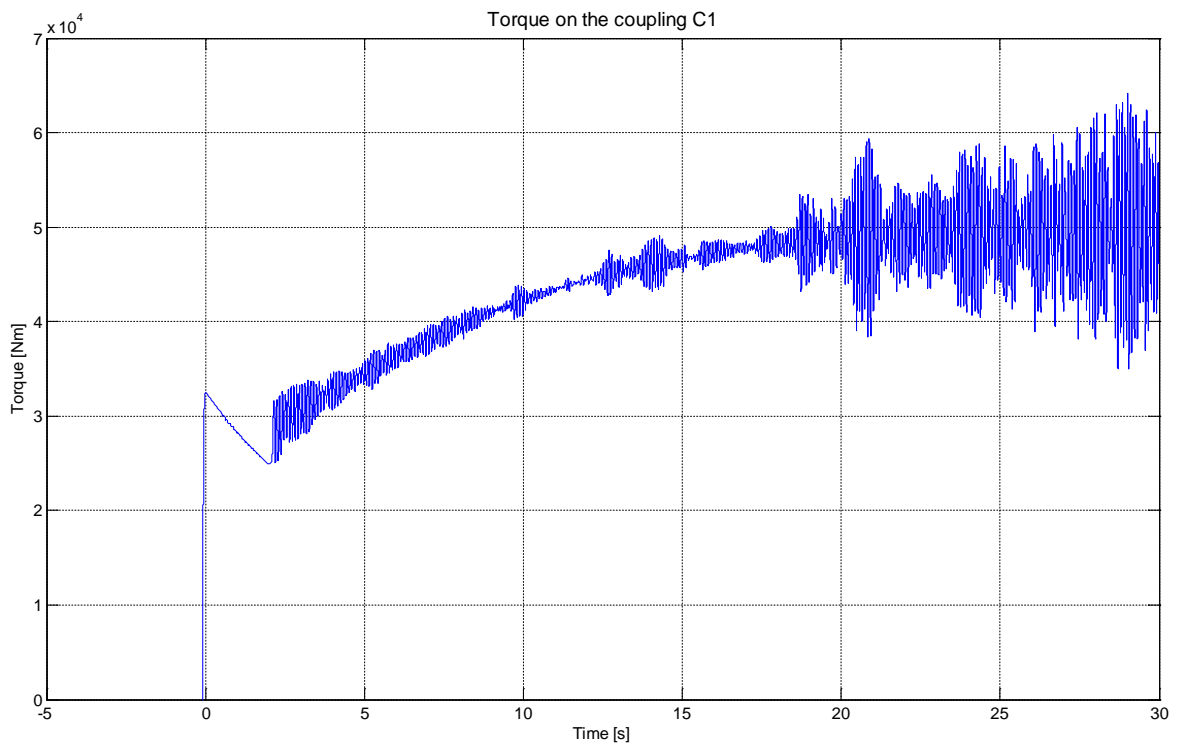
Figure 6-8: Torque on the compressor coupling - Synchronization to virtual 48-pulse inverter

6.2.4   Decoupling of control loops

The typical problem in complex control with several measured signals as inputs is that once there is an oscillation, it is propagated into many (if not all) control loops. In such situation, it is difficult to determine where the oscillation started. One way to minimize the electromechanical interaction is the decoupling of control loops, e.g. using reference signals or filtered signals instead of actual signals. An example of such decoupling is shown in Figure 6-9: It is a simulation of LCI drive with parameters as per Table 7. Although the reference signal for firing angle on motor side converter is not actively controlled, there is a small offset as function of dc link current. When the dc current oscillates, the firing angle will naturally follow this oscillation. A stabilization was achieved by using different rates of change to limit the variation of firing angle (slow rate of change for increment, fast rate of change for decrement). The function is internally called 'alpha CMS damping'.
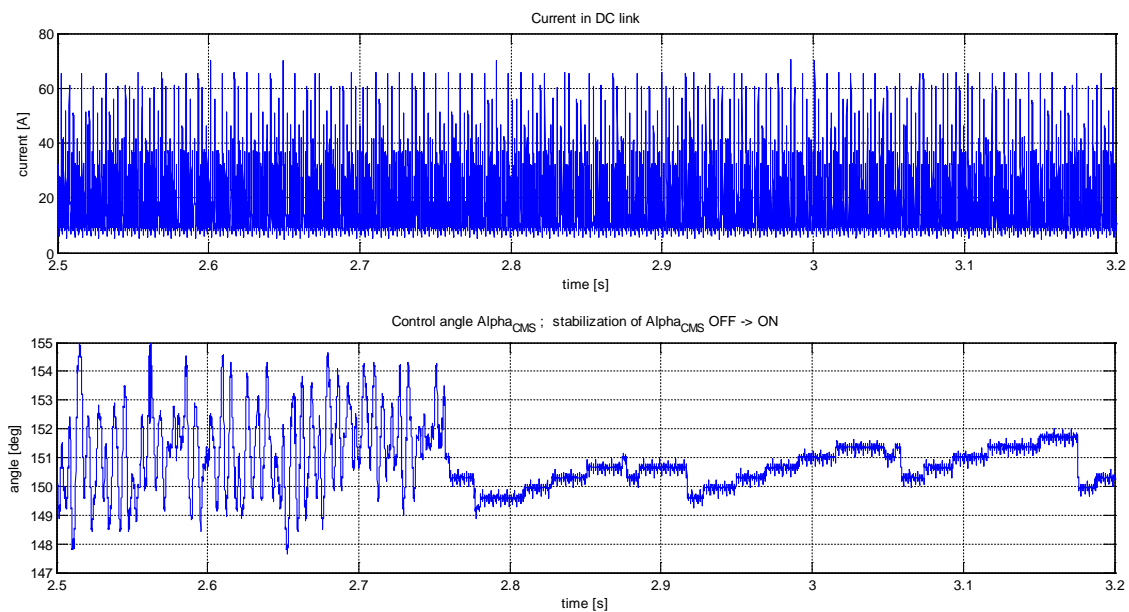
(a)
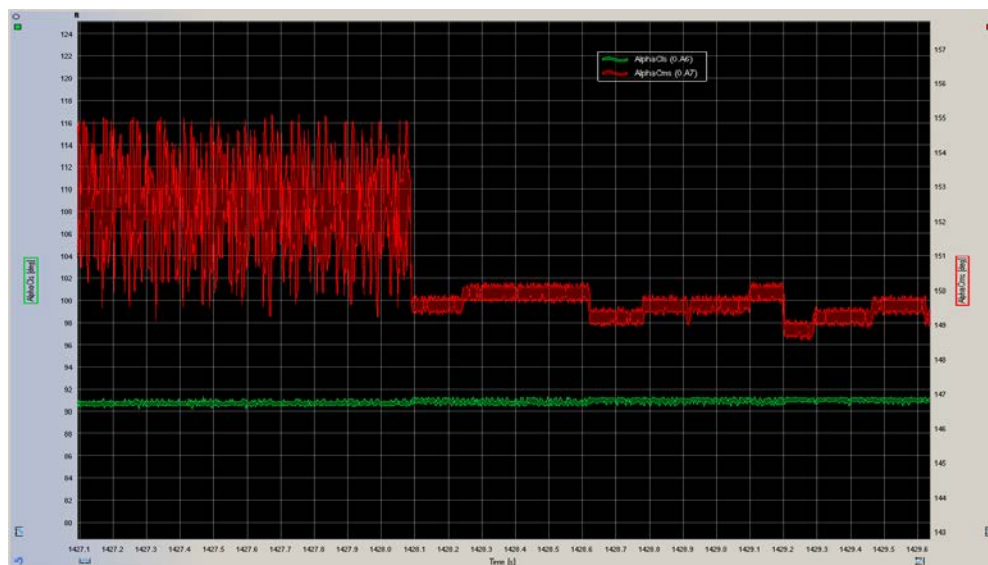
(b)

Figure 6-9: Stabilization of firing angle of motor side thyristor bridge;
(a) simulation, (b) measurement during string test

Another offset of firing angle is a function of motor speed. The background is again a safe commuta-tion, i.e. restoration of thyristor blocking capability. In case actual speed is used as input for offset calculation, the control potentially introduces oscillating offset signal.

6.2.5   Strategy for start-up

As explained before, the LCI cannot use the load commutated operation at very low speeds (from standstill up to 6...12%). So called pulse mode is frequently used in that speed range. The larger LCI drives are typically 12-pulse. It was believed that 6-pulse operation is the best at low speed in order to leave the pulse mode as soon as possible. However, a closer analysis shows that this is generally not the best method from torsional perspective.

6.2.5.1   Optimization of pulse intervals

During pulse mode a pair of thyristors is conducting for 1/6 (6-pulse inverter) or 1/12 (12-pulse inverter) of motor revolution. Before next pair of thyristors is fired, a short pause is necessary to renew the blocking capability of thyristors. However, introduction of additional pauses - sometimes called „inserted commutations" - will change the spectrum of air gap torque [98]. The closed loop simulations helped to optimize the period of of pauses for minimal excitation.

6.2.5.2   Switchover during pulse mode

Smart transitions between 6-pulse and 12-pulse operation during pulse mode can significantly reduce the excitation of the torsional modes. The principle is based on re-configuration between 6-pulse and 12-pulse inverter modulation as a function motor speed. As per the amplitude law, the lowest order of characteristic harmonics has the largest magnitude while the higher harmonic orders are smaller. The method proposes to start in 6-pulse configuration and accelerate above the speed where $12*f_M$ excites the 1st TNF. Afterwards the LCI is reconfigured to 12-pulse so that the intersection of $6*f_M$ and 1st TNF can be avoided. LCI either completes the pulse mode in 12-pulse configuration or changes over to 6-pulse operation in order to get higher average driving torque.

The principle is visualized in Figure 6-10. Larger asterix means dominant excitation, smaller asterix means less significant excitation.

A challenge requiring attention is the accuracy of observed speed during start-up (encoderless oper-ation). Since the speed is estimated from motor flux, the accuracy suffers a bit at low speed as seen in Figure 6-11 (simulation of system acc. Table 8).
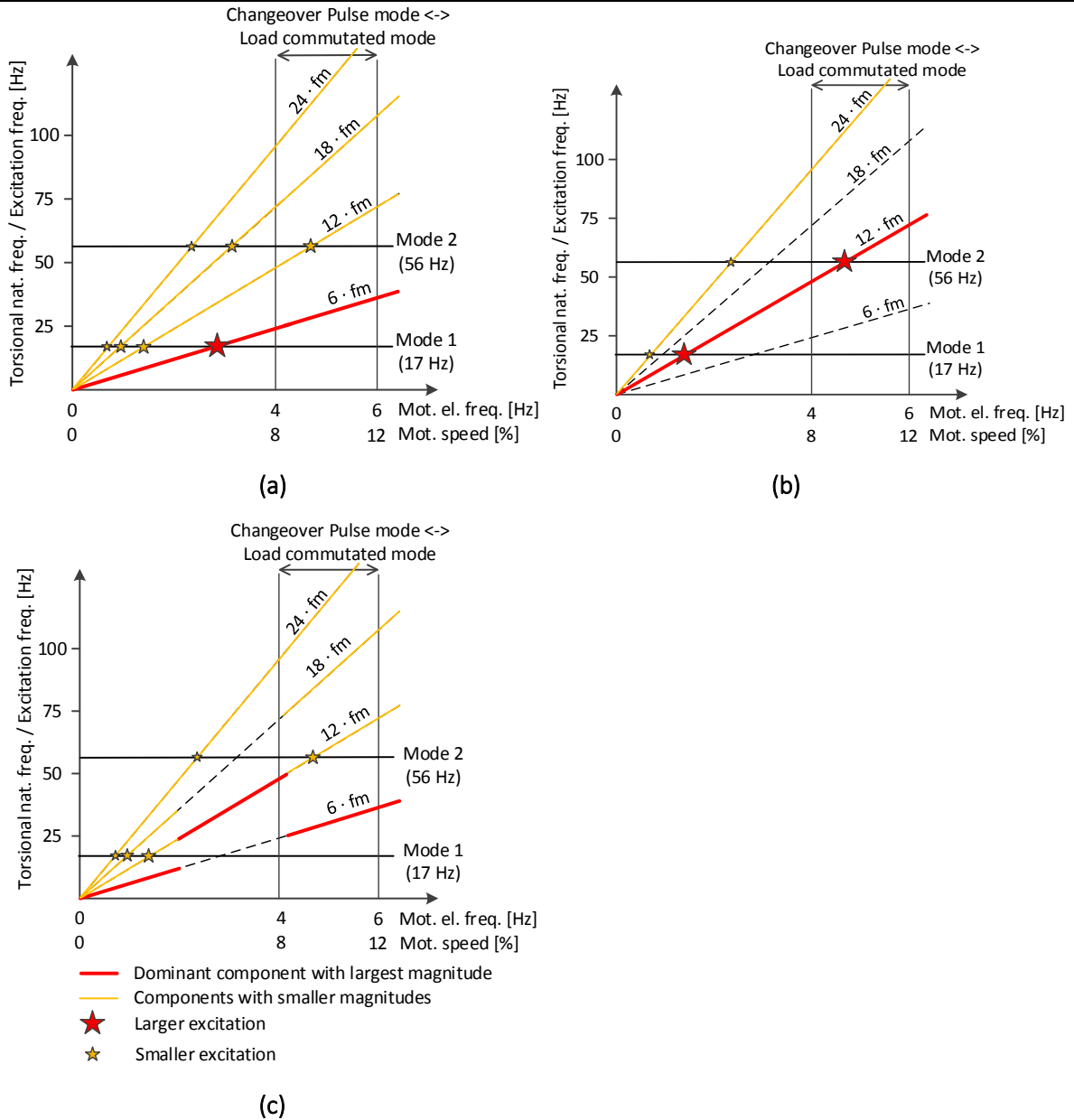
Figure 6-10: Operation of LCI in pulse mode and minimization of torsional excitation
(a) 6-pulse; (b) 12-pulse; (c) switchover 6-pulse <-> 12-pulse to minimize excitation
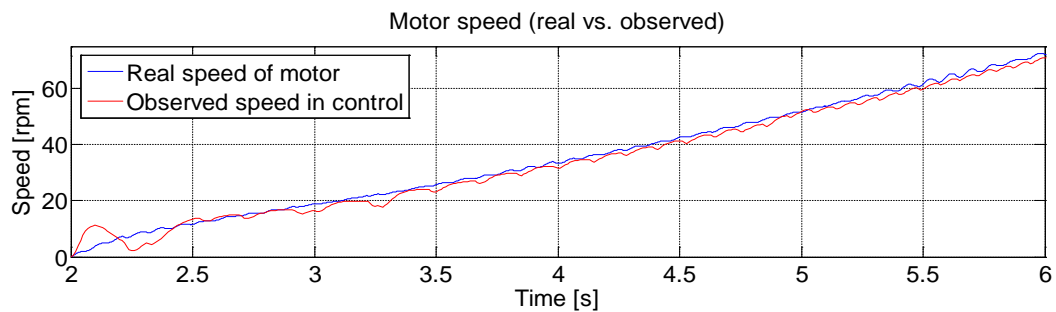
Figure 6-11: Motor shaft speed and observed speed in LCI control

Nevertheless, the simulations and measurements confirmed the positive effect of smart switchover.

Figure 6-13 and Figure 6-14 show the simulations in order to validate the functionality of switchover
during pulse mode. The parameters of the simulated drive system are provided in Table 7 and shaft
string is depicted in Figure 6-12 (EM = electric motor, GB = gearbox, CC 1 = centrifugal compressor 1,
CC 2 = centrifugal compressor 2).
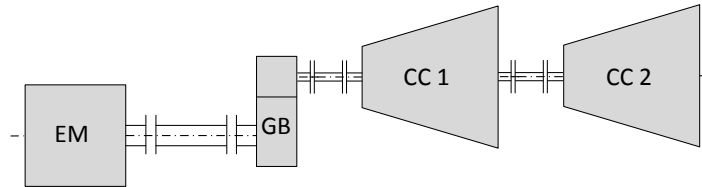
Figure 6-12: Compressor drive system used for simulations of switchover
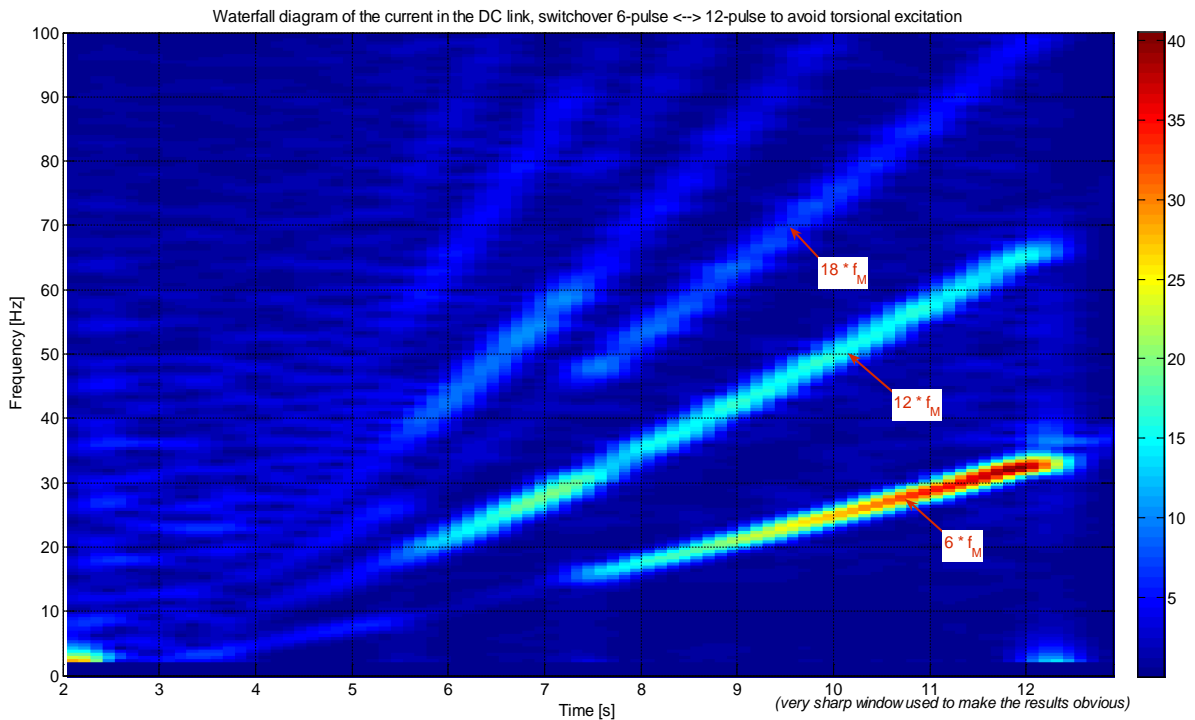
Figure 6-13: Waterfall plot of dc current (pulse mode) of LCI drive: changeover 6-pulse → 12-pulse →
6-pulse applied to eliminate torsional excitation
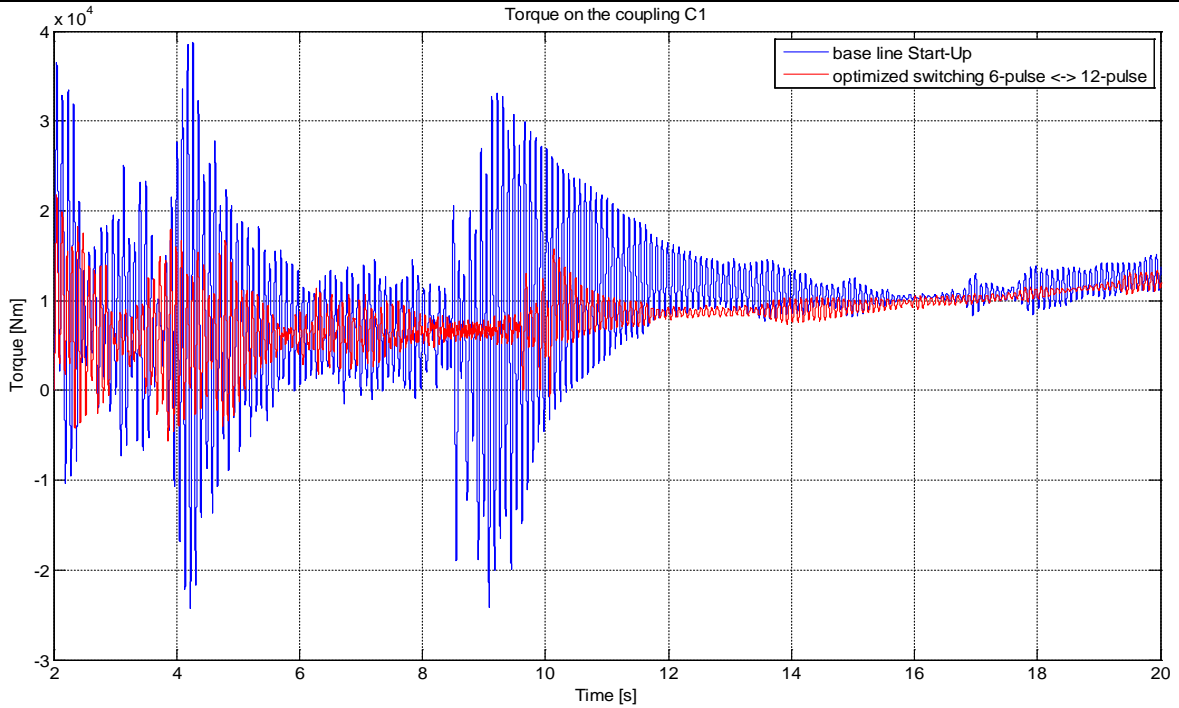
Figure 6-14: Torque on motor coupling during start-up (pulse mode) of LCI drive: blue curve – baseline settings; red curve – optimized settings for minimized excitation of 1st TNF
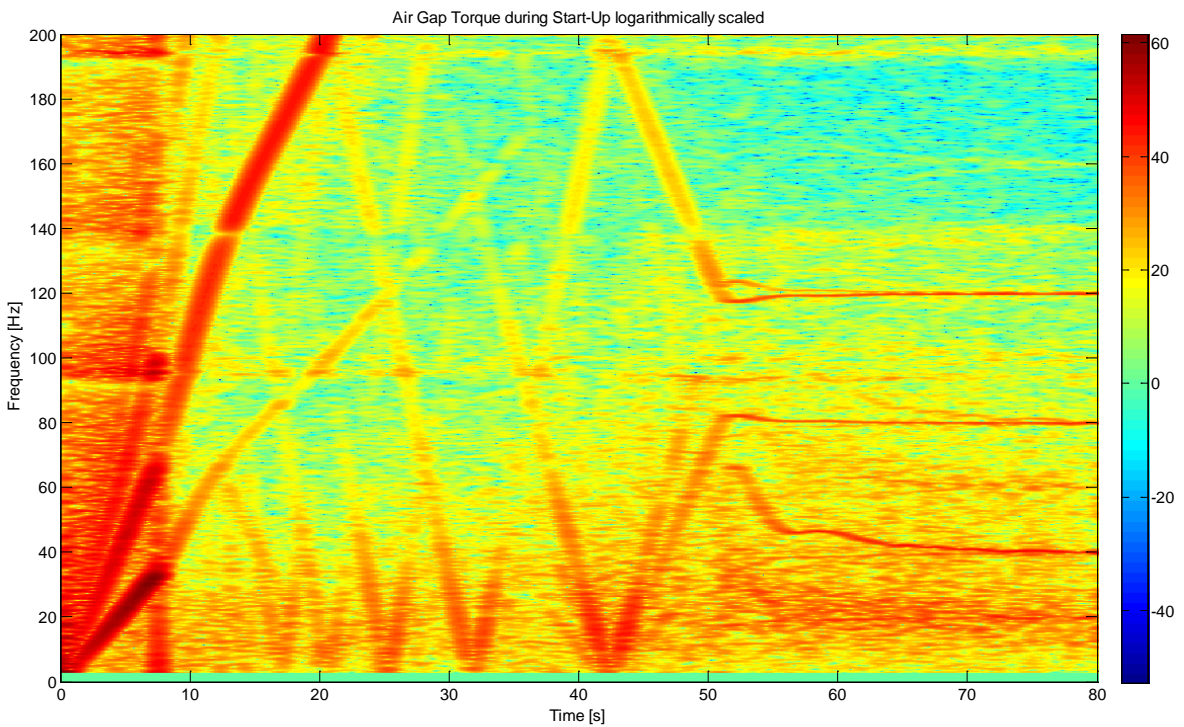
Figure 6-15: Waterfall diagrams of motor air gap torque during start-up of LCI drive (logarithmically scaled for better identification of harmonic and inter-harmonic components)

6.2.6   Torsional damper for LCI drives

A torsional damper had been developed for LCI drives. The principle is based on additional reference for the current controller (equivalent to torque controller in VSI drives). Active in this case means that

once enabled it searches the torsional natural frequency in the dc current using a bandpass filter. Once it is found, it is summed up with the actual dc current. The torsional damper is increasing the gain of current control loop locally in defined frequency range. The current controller can better coun-teract the interharmonics without increasing proportional gain across the whole frequency range. The damper can be disabled by setting the damping gain to zero. Basic implementation is shown in Figure 6-16 and the principle is illustrated in Figure 6-17 and Figure 6-18 using drive system parameters from Table 7.
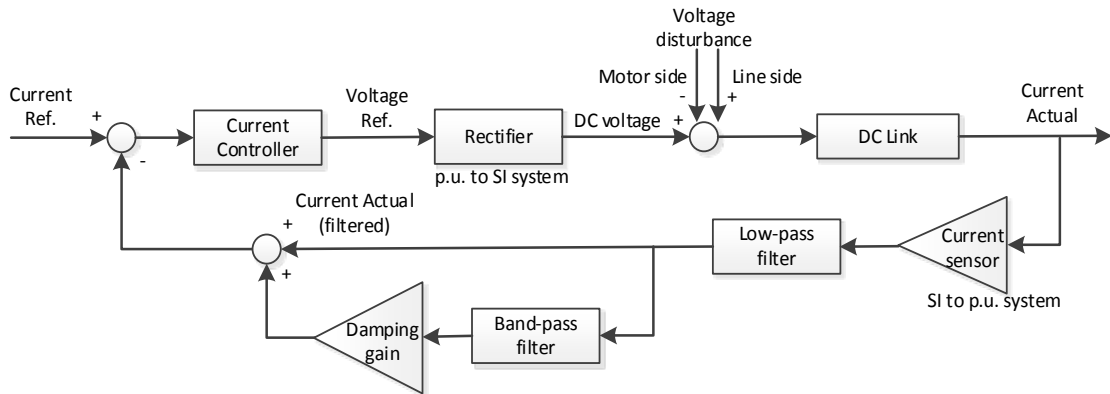
Figure 6-16: Implementation of torsional damper (simplified)

The current controller gain is set to 0.16 and integration time constant 0.02 s. The low-pass filter has cut-off frequency of 500 Hz. The blue curve of Figure 6-17 shows Bode plot without active damper, the red curve then with active damper parameterized for 11.6 Hz. The active damping provides ap-prox. 6 dB additional gain at the torsional natural frequency of 11.6 Hz. At the same time the phase margin is reduced by 6.3 degree. If the same gain at 11.6 Hz shall be achieved without active damping, the current controller gain needs to be doubled to value 0.32 and the phase margin is reduced by 19.6 dB as illustrated in Figure 6-18.
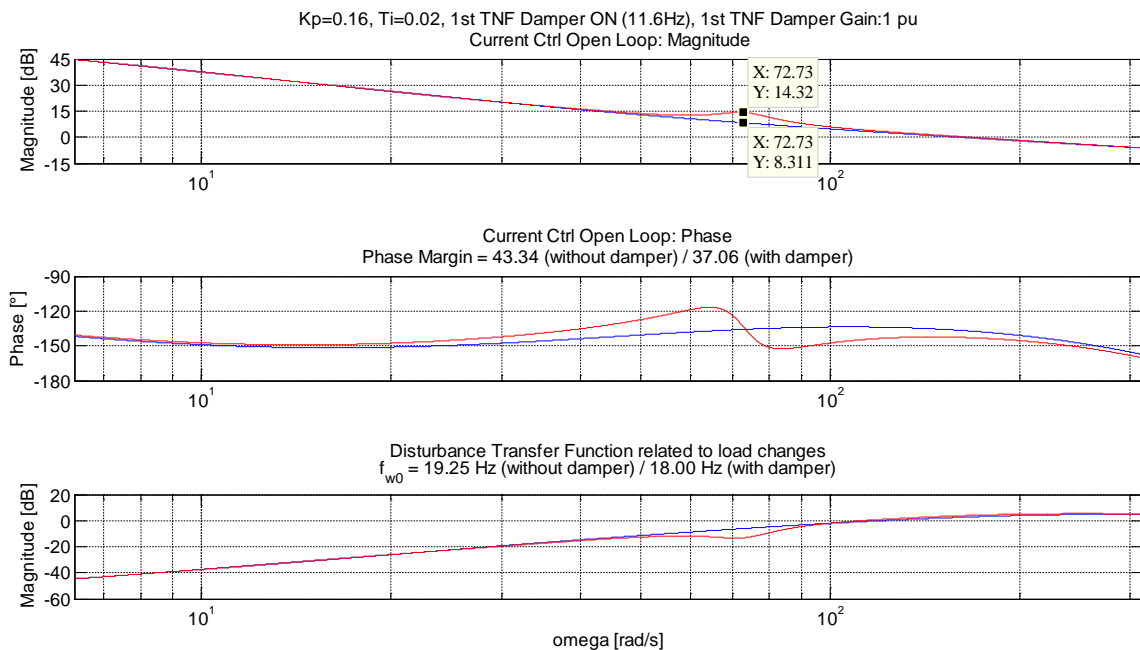
Figure 6-17: Bode plot of current control loop of LCI drive; blue curve – without active damper, red curve – with active damper
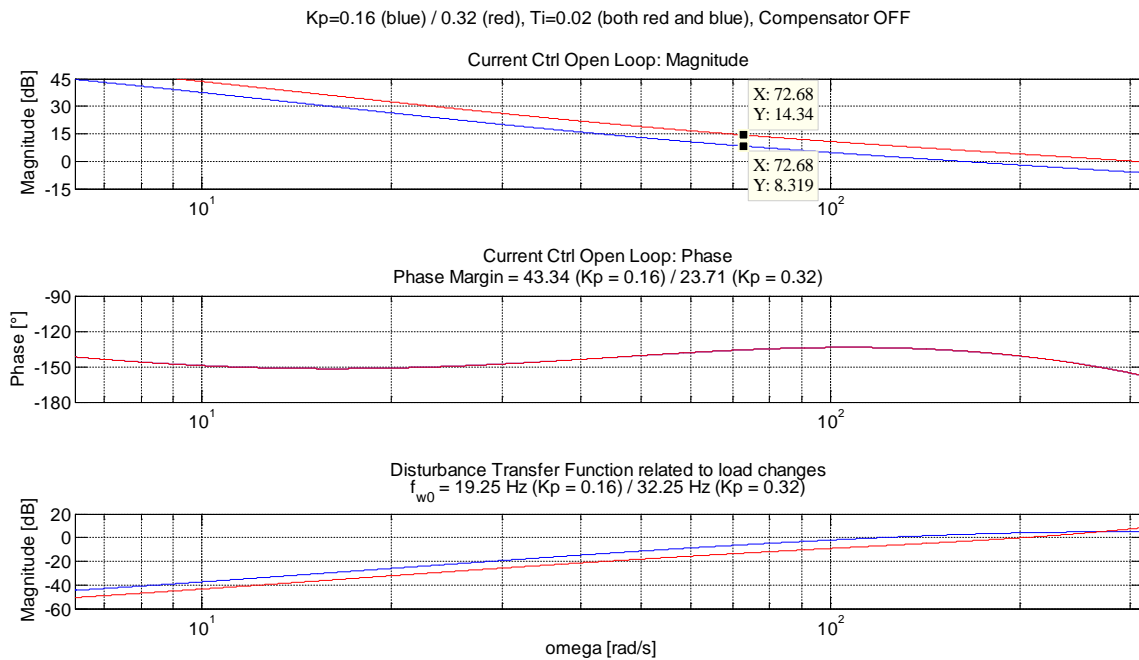
Figure 6-18: Bode plot of current control loop of LCI drive; blue curve – current controller gain 0.16 pu, red curve – current controller gain 0.32 pu

The functionality was confirmed by system simulations including the elastic mechanical shaft and by string testing in the field. The vibration magnitude is reduced approx. by factor 3.0.

The implementation allows paralleling of several dampers so that multiple interharmonic frequencies can be minimized as depicted in Figure 6-19 with two torsional dampers.
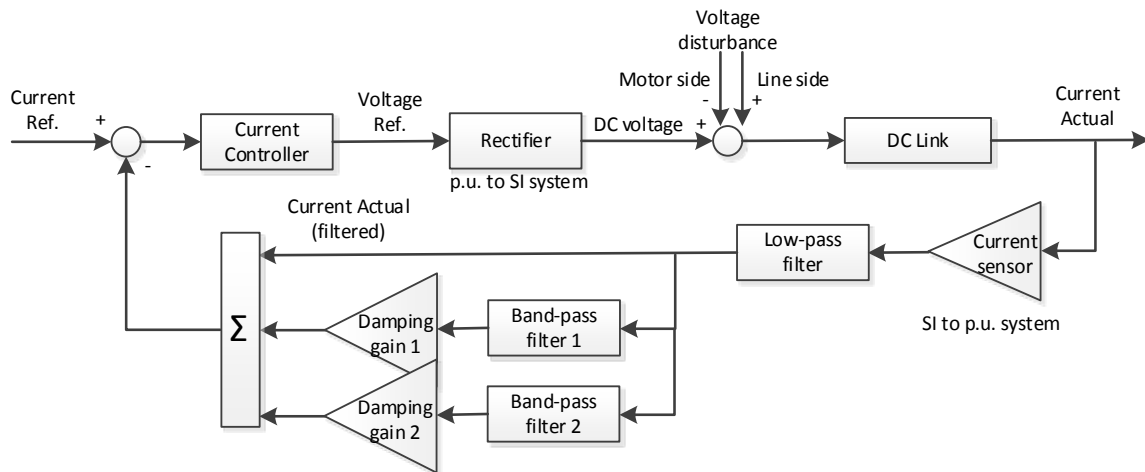
Figure 6-19: Implementation of multiple torsional dampers (simplified)

At the beginning the active compensator was "soft enabled" by ramping the gain gradually from zero to 1 as the simulation in Figure 6-20 shows. Later on this procedure was found unnecessary, i.e. active compensator can be enabled stepwise without any risk.
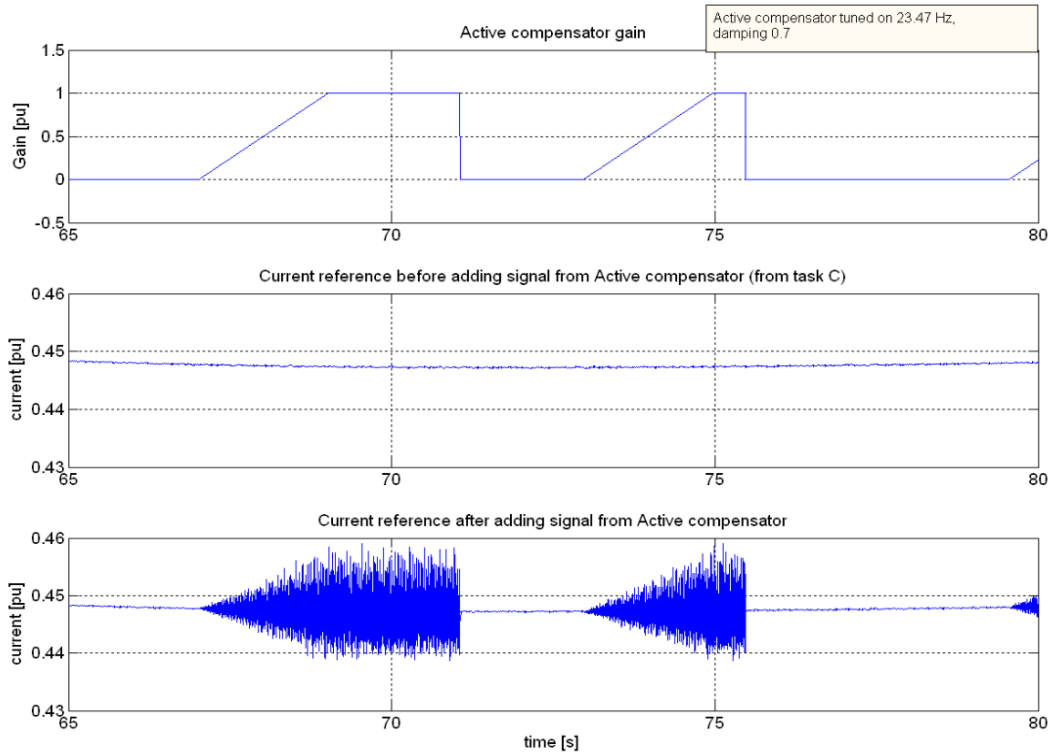
Figure 6-20: Soft enabling of active compensator by ramping the gain

Active damping was also studied for a specific project to investigate if the restricted speed ranges could be removed and drive could continuously operate at the resonance speed. Drive data are as per Table 10. The drive system slowly accelerates up to 1'462 rpm which is the critical speed. A steady state operation is reached. The damping function is first deactivated and then enabled. Immediate reduction of coupling torque ripple as well as speed oscillation is observed.
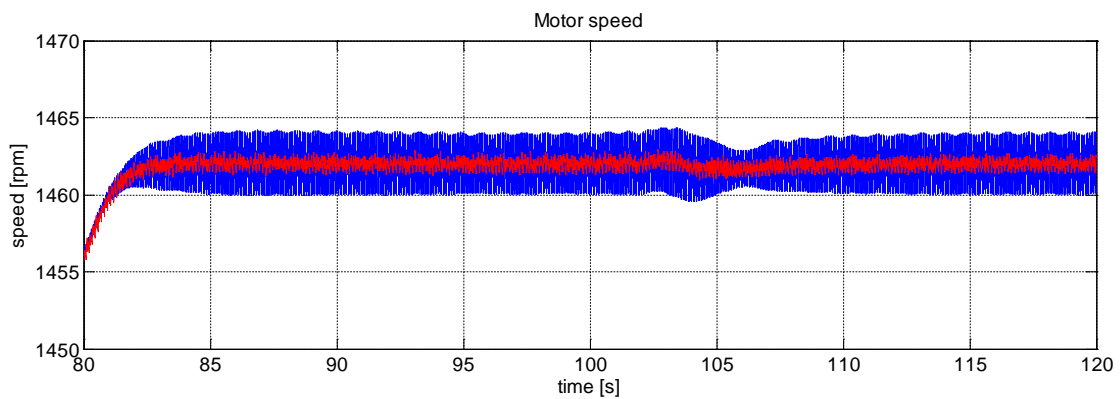
Figure 6-21: Motor speed (blue – actual motor speed from motor model, red – observed speed visible in drive control) – detail of steady-state
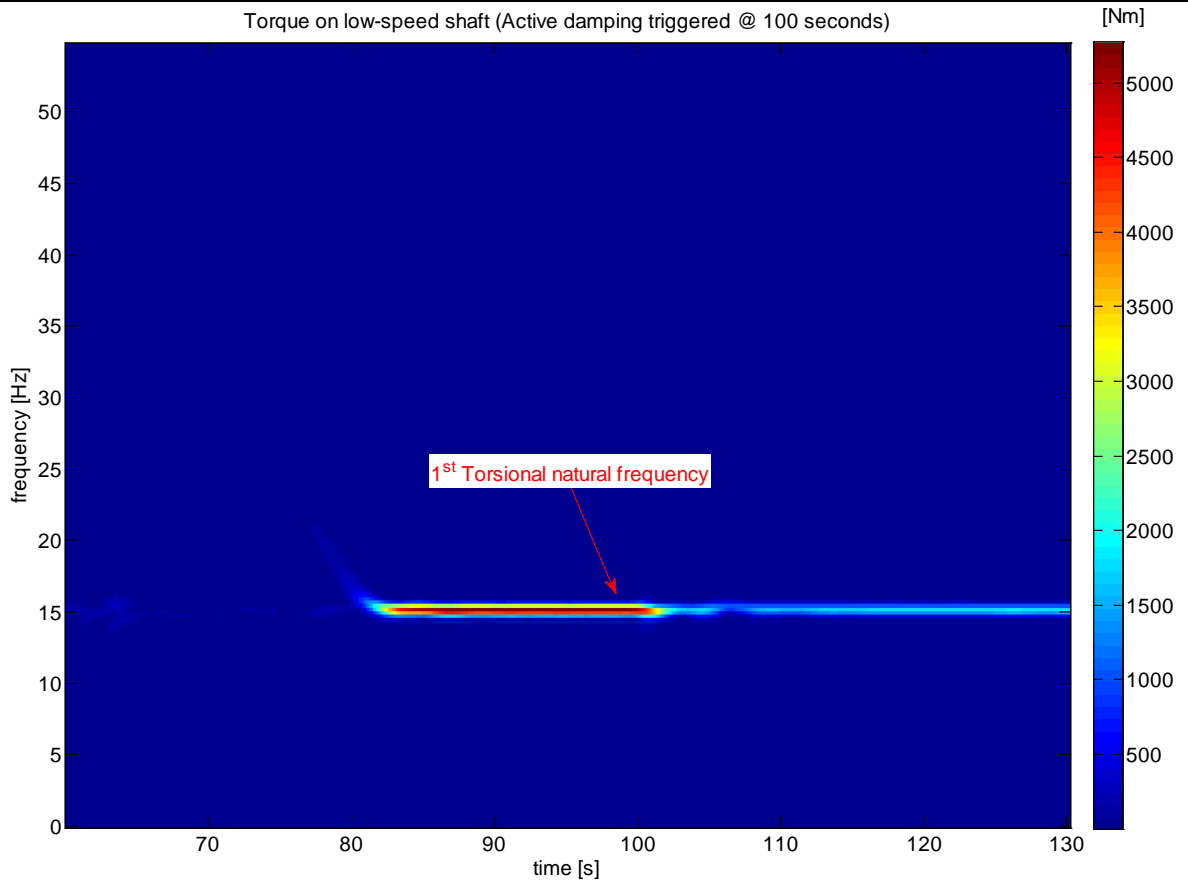
Figure 6-22: Waterfall of low-speed shaft torque (before and after Active damping was triggered)

Simulations results of model with elastic shaft and parameters according Table 11 are depicted in Figure 6-23 (EM = electric motor). The upper part shows coupling torque during start-up with disabled active damping, lower part shows coupling torque with enabled active damping. The resonance condition appears in both cases at simulation time approx. 17s. The peak coupling torque is reduced by 30-40%. Figure 6-24 shows the spectrum of dc link current at steady state operation without active damping (a), with active damping and gain 1.0 (b) and with active damping and gain 5.0 (c). It is a real measurement from string test of system acc. Table 7.
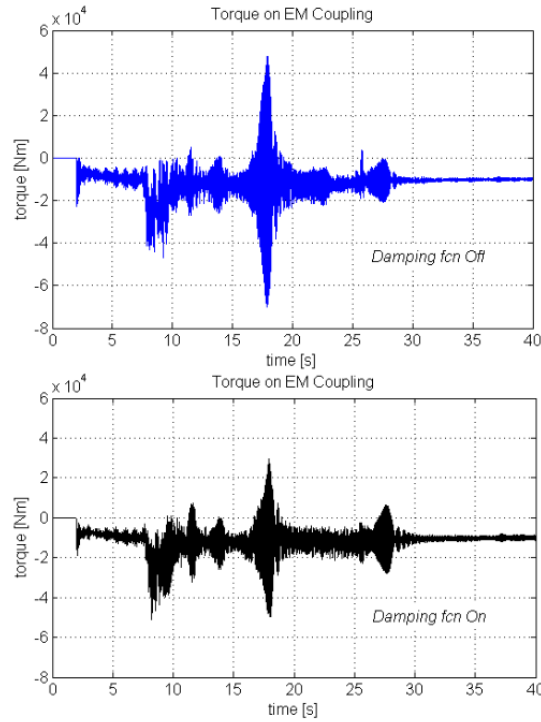
Figure 6-23: Torque on motor coupling in pulse mode during start-up
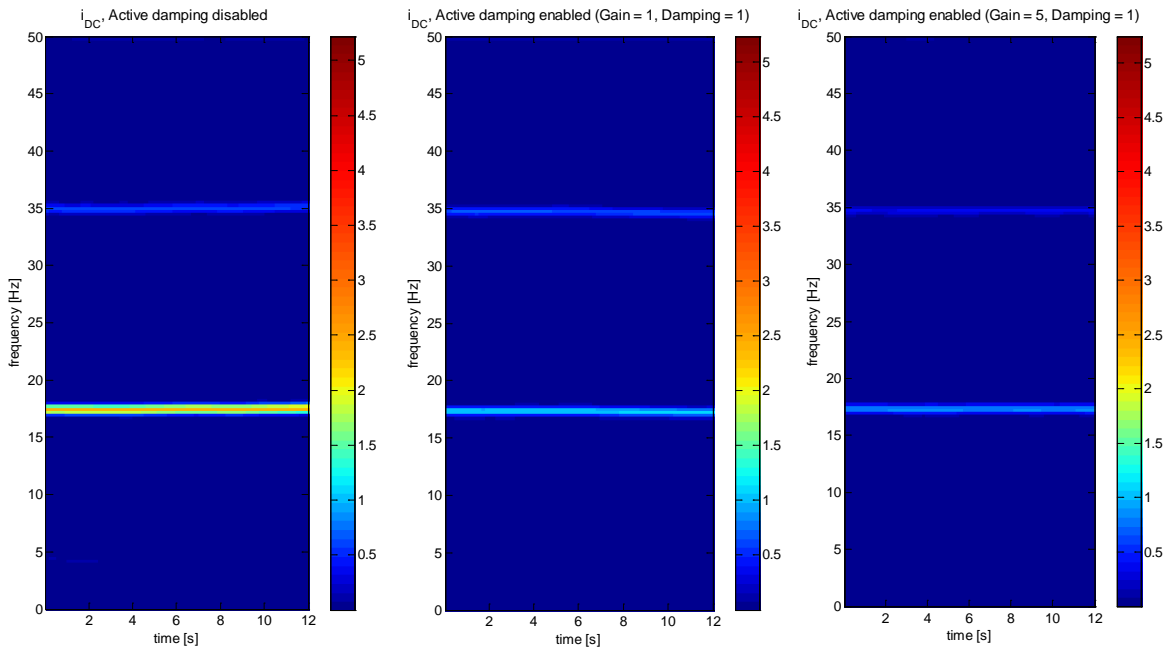
Figure 6-24: Waterfall diagrams of dc current of LCI
left – no active damping, middle – damping with gain 1 p.u., right – damping with gain 5 p.u.

6.3   Torsional optimization and damping for VSI drives

6.3.1   Speed control loop

6.3.1.1   *Parameterization of speed controller*

Conventional PI(D) type of speed controler (D-part mostly not used) has two basic parameters to optimize: proportional gain KPS and integration time constant TIS. The time constant TIS shall be selected depending on application dynamics. Rule of thumb recommends TIS to be at least 10-times shorter than fastest speed ramp. KPS shall be selected with care as the oscillation in speed feedback propagates through this gain directly into torque reference. Instead of high KPS additional feedbacks (such as inertia compensation) might be better approach from torsional standpoint. The optimization of speed controller is done based on transfer functions and bode plots.

The speed controller is a conventional PI type as already mentioned. The transfer function is;

$$G_{PI\,Speed}\,(s) = KPS \cdot \frac{1 + s \cdot TIS}{s \cdot TIS} \tag{46}$$

where *KPS* is the proportional gain and *TIS* integration time constant.

The torque controller is based on DTC. The control loop has high bandwidth of approx. 450 Hz which is faster than any mechanical time constant. A polynomial approximation [109] is used for description:

$$G_{DTC}\,(s) = \frac{1.936 \cdot 10^7}{s^2 + 5280 \cdot s + 1.936 \cdot 10^7} \tag{47}$$

The elastic mechanical model is described in state space as explained in chapter Model of flexible shaft that is transformed into transfer function (Matlab command "ss2tf").

$$G_{MECH}\,(s) = ss2tf(A_{mech}, B_{mech}, C_{mech}, D_{mech}) \tag{48}$$

Since (59) describes a multiple input/multiple output system, the row corresponding the motor mass shall be selected.
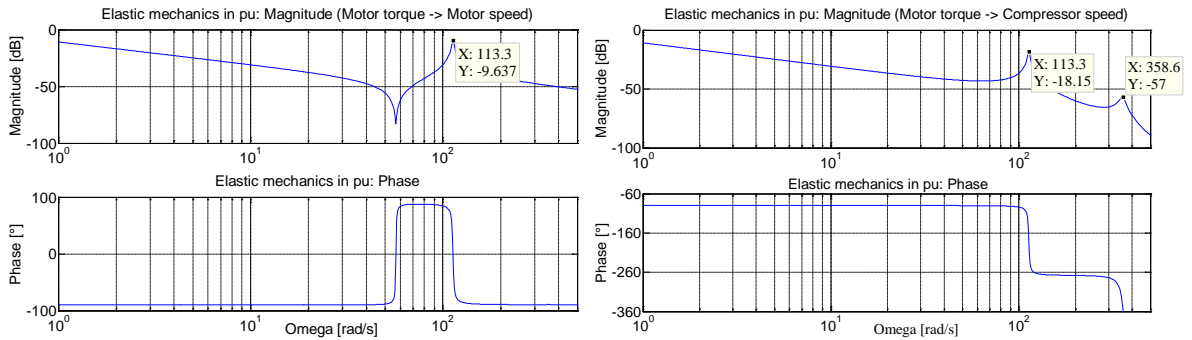
Figure 6-25: Bode plot of elastic mechanics; Motor torque to motor speed (left), Motor torque to compressor speed (right)

The speed and torque controllers are in per unit (pu) while the mechanical model is in SI units. Therefore scaling with nominal torque T_N, number of pole pairs *npp* and nominal speed ω_N is necessary. The open loop transfer function is then expressed in (59).

$$G_O\,(s) = G_{PI\,Speed}(s) \cdot G_{DTC}(s) \cdot T_N \cdot G_{MECH}(s) \cdot \frac{npp}{\omega_N} \tag{49}$$

The Bode diagram modelled is shown in with system data according Table 18.
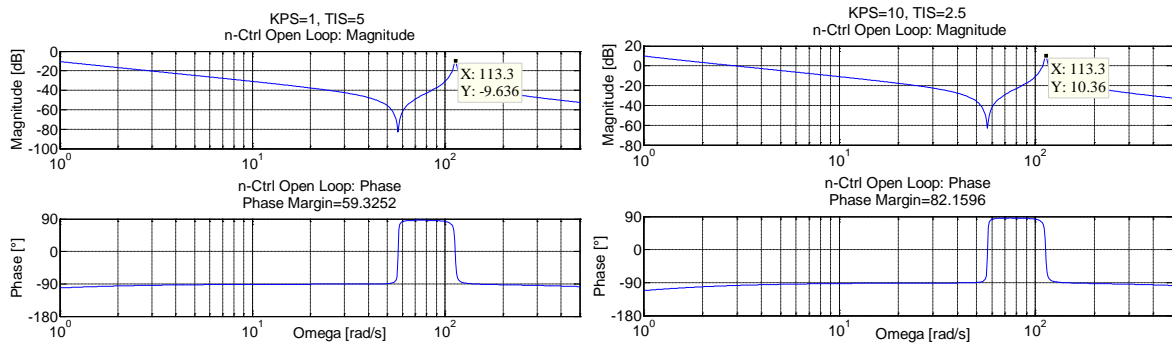
Figure 6-26: Bode plot of speed controlled drive system with elastic shaft; KPS = 1, TIS = 5s (left), KSP = 10, TIS = 2.5s (right)

While low proportional gain has positive effect on torsional interaction, the softer speed controller has degraded performance in terms of reference tracking. Such disadvantage can be compensated by additional feedforward terms known e.g. as inertia compensation (see Appendix 7 – Vector control and direct torque control schemes, section B).

6.3.1.2   Notch filter in speed control loop

The purpose is to remove specific frequency component (typically torsional natural frequency) from the speed feedback signal or speed error signal. The torque reference as output of speed controller shall not contain that specific frequency. The VFD shall not amplify the excitation through the closed loop.

(a)

(b)

(c)
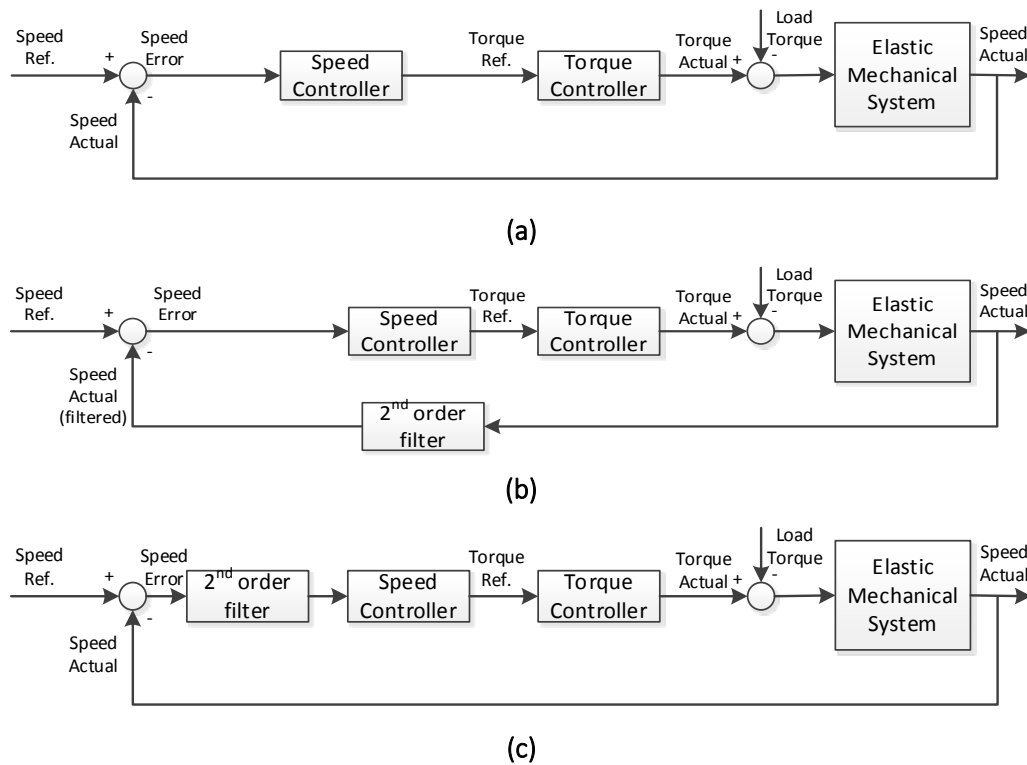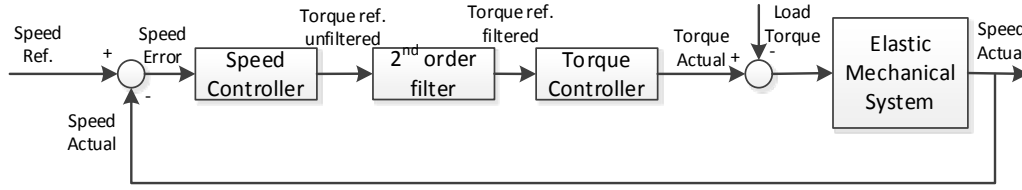
(d)

Figure 6-27: Block diagram of speed control loop; (a) no filter, (b) band stop on speed feedback, (c) band stop on speed error, (d) band-stop on torque reference

The bandpass (notch) filter can be also described with a transfer function like in previous chapter;

$$G_{BP}\,(s) = \left(\frac{\omega_P}{\omega_Z}\right)^2 \cdot \frac{s^2 + 2 \cdot d_Z \cdot \omega_Z \cdot s + \omega_Z^2}{s^2 + 2 \cdot d_P \cdot \omega_P \cdot s + \omega_P^2} \tag{50}$$

where ω_P, ω_Z is the frequency of pole and zero and d_P, d_Z is the damping of pole and damping of zero.

Bode plot of bandstop filter tuned for system acc. Table 18 is depicted in Figure 6-28:
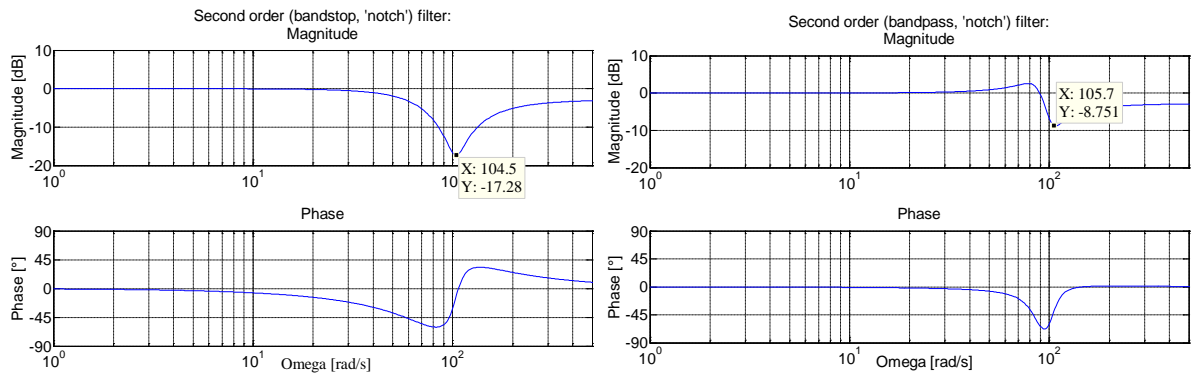
Figure 6-28: Bode plot of bandstop filter; higher pole damping (left), smaller pole damping (right)

Accordingly, the transfer function of the speed open loop incl.notch filter is expressed in (53) and plotted in Figure 6-29.

$$G_O\,(s) = G_{PI\,Speed}(s) \cdot G_{DTC}(s) \cdot T_N \cdot G_{MECH}(s) \cdot \frac{npp}{\omega_N} \cdot G_{BP}(s) \tag{51}$$
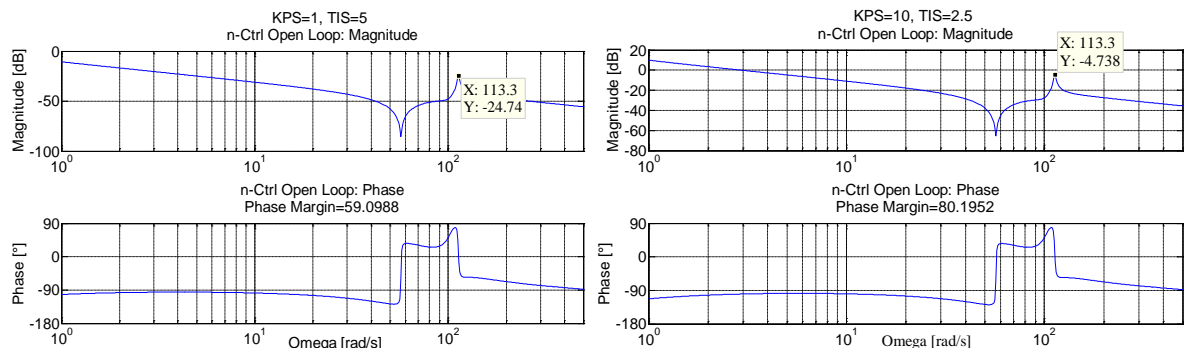
Figure 6-29: Bode plot of speed controlled drive system with elastic shaft and bandstop filter; KPS = 1, TIS = 5s (left), KSP = 10, TIS = 2.5s (right)

6.3.1.3   FIR filter in speed control loop

FIR filter is used for active damping. Unlike notch filter it does not remove specific frequency from the signal, but changes the phase of the particular frequency component and creates an additional reference summed up with the main torque reference from speed controller. Tuning of the phase is essential to ensure damping instead of amplification of vibrations.

6.3.1.4   Scalar control

Scalar control can be used for induction machine drives with low dynamics where it can be assumed that motor speed follows the changes in stator frequency. Torsionally sensitive turbomachines (compressors, blowers etc) typically do not require high dynamic response and scalar control is principally acceptable. In the literature many different scalar control schemes are described. The simplest form is without speed feedback loop while more advanced scalar control uses speed feedback as well.

In frame of this work a very simple scalar control without feedback loop has been investigated. The error due to slip is ignored. Such control seems to keep the natural damping of induction machine. More sophisticated variants of scalar control shall be checked to ensure that additional signals do not introduce oscillating behavior.

6.3.2   Torque control loop

6.3.2.1   Switching frequency

Changing the switching frequency affects the frequency spectrum of air gap torque. See Figure 7-23 and Figure 7-24 for comparison. Higher switching frequency tends to reduce torque components at lower frequencies while components at higher frequencies remain approximately the same or eventually increase.

6.3.2.2   Motor current in control

Both vector control and direct torque control use mathematical motor model in their algorithms. The inputs of the motor model are typically two motor phase currents, dc link voltage and switching combination (see Appendix 7 – Vector control and direct torque control schemes). The outputs of the model are actual values of speed (if encoderless), flux and torque. Distorted motor currents therefore affect the calculation of actual torque. It is benefitial when the control allows to adjust the ratio between measured and calculated current. Practically, when the measured current is very distorted, the calculated portion can be increased in order to reduce the signal noise.

6.3.2.3   Notch filter in torque control loop

The principle is the same as notch filter in the speed control loop (chapter 6.3.1.2). The filter shall remove specific frequency component from the spectrum and make the control passive to this frequency. The implementation of the filter shall consider much higher dynamics and sampling rate of torque control loop compared to speed control loop.

7   Simulation results

Numerical simulations can be performed offline (computer simulation) or online (hardware in the loop). This chapter presents the results of computer-based simulations. Hardware in the loop (HIL) simulations and testing had been used as well, but mainly for pre-commissioning setup. The results of HIL tests with elastic shaft so far could not 100% mimic the effects seen in the field.

7.1   Simulations of simplified model with elastic shaft

A simplified model acc. Figure 7-1 was developed in order to investigate the behavior of mechanical system with elastic shaft [A16]. The full VFD model is not included in this model. Instead, there is a selector to choose from various types of torsional excitations. These excitations were applied to the shaft model (as described in chapter 5.1.2) to investigate the response of elastic mechanics.

- excitation with variable frequency (sweep) – frequency response analysis (Figure 7-1b)
- driving mean torque with superimposed alternating component (Figure 7-1c)
- alternating torque components (Figure 7-1d)
- short circuit transient torque (same as Figure 7-1d)
- broadband random excitation of "white noise" type (Figure 7-1e)
- forced excitation with constant fundamental frequency matching torsional natural frequency and variable (random) magnitude (Figure 7-1f)

(a)

(b)   (c)

(d)   (e)

(f)
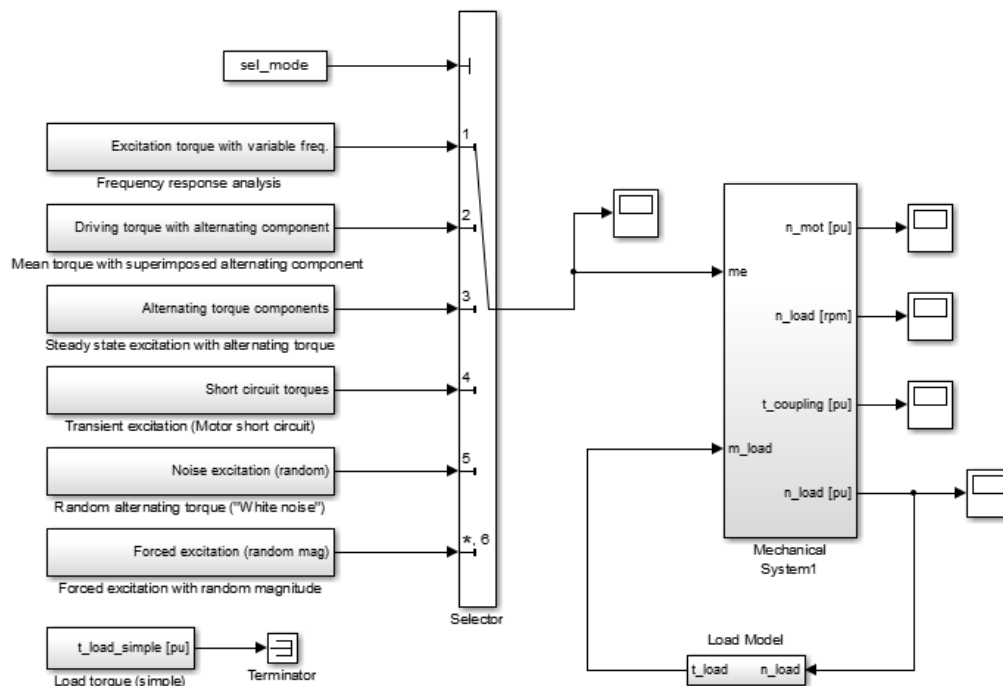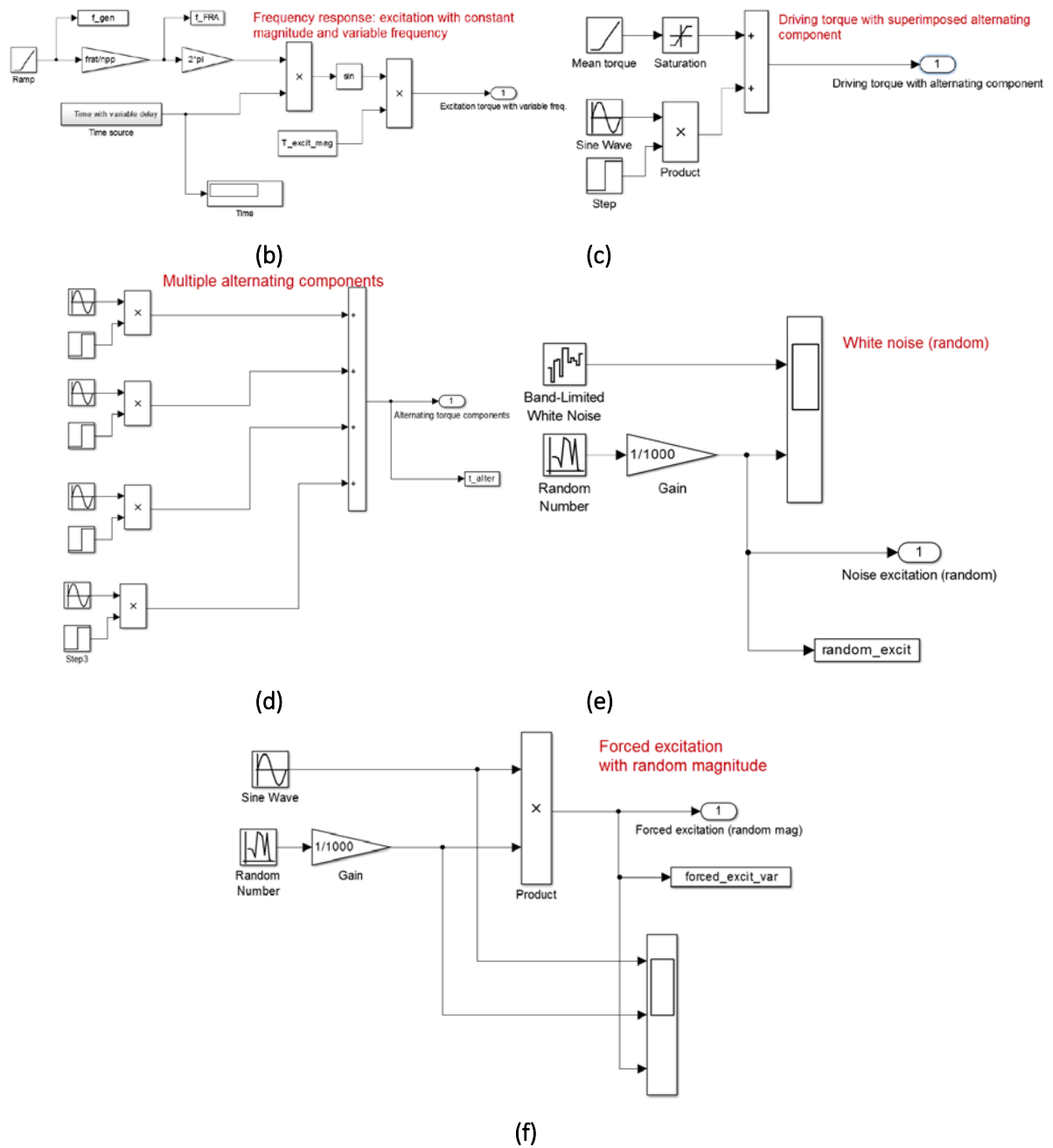
Figure 7-1: Model to test torque response to different kind of excitations

The torsional response is demonstrated in following paragraphs.

7.1.1   Frequency sweep of input torque

An alternating torque component with magnitude of 0.0141 pu (0.01 pu RMS value, i.e. 1% of rated torque) and variable frequency (sweep) is applied on the motor mass. The frequency is ramped line-arly from zero up to 25 Hz. Three frequency ramps with different rates of change are used: slow ramp (0.25 Hz/sec), medium ramp (1 Hz/sec) and fast ramp (5 Hz/sec). The first torsional natural frequency is 17.9 Hz. The observation is that due to low damping of torsional mode the peak torque on the

coupling does not significantly change with the ramp. Only at very fast ramp the peak torque is re-duced. The behavior is demonstrated in Figure 7-2 with rate of change 0.25 Hz/sec (left), 1 Hz/sec (middle) and 5 Hz/sec (right).
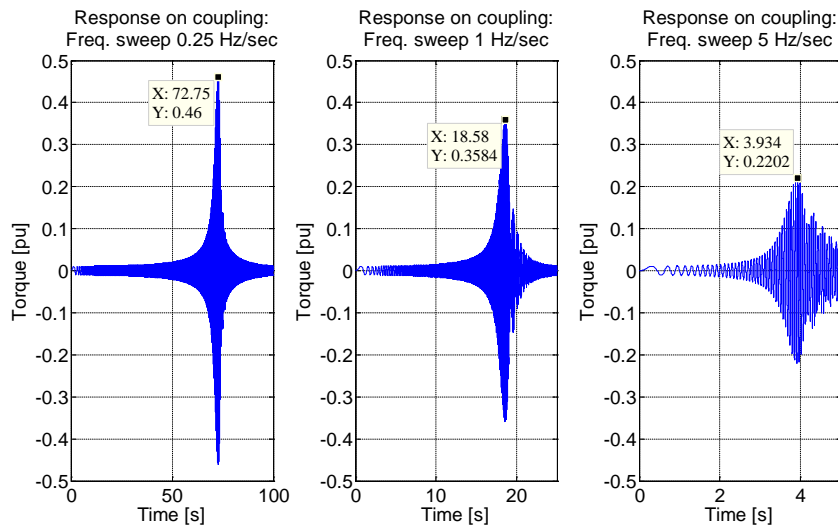
Figure 7-2: Torque response to harmonic excitation with frequency sweep

Figure 7-3 shows the dependence between torque excitation, frequency ramp and torque response on the coupling. In applications with direct on-line motor starting, it is recommended to accelerate as fast as possible in order to minimize the transient torque response. This is based on the fact that the motor torque is not controlled and dwell time in resonance shall be as short as possible (transient torque is then lower compared to steady state limit cycle). VFD driven system looks different. In order to accelerate faster a larger driving torque is required. In case the magnitude of pulsating torque com-ponents is certain percentage of mean driving torque, the faster acceleration ramp will cause larger excitation torque and consequently larger torque oscillation on the coupling.
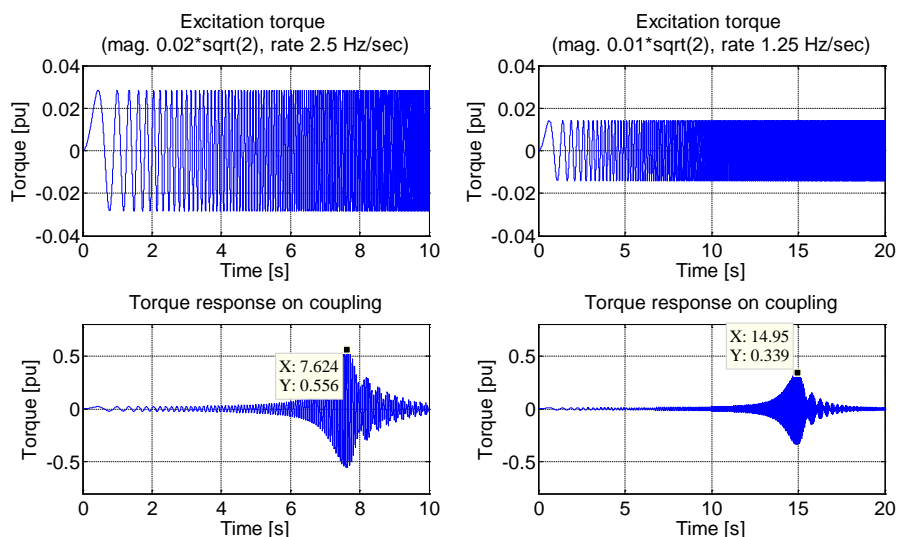
Figure 7-3: Torque response to transient excitation during start-up

Especially for LCI type of drive operating in so-called pulse mode at low speed it is often more benefi-cial to use slower starting ramp. Although the dwell time in resonance is longer, the smaller excitation

results in overall lower magnitude of alternating torque on coupling and consequently less mechanical stress. This is true for shaft systems with low damping (sharp resonance) and variable load torque (e.g. load torque proportional to the square of speed) which is normally the case in turbomachinery.

7.1.2   Mean input torque with alternating component

The driving torque consists of mean value corresponding to an ideal driver without any torque ripple. At certain point of time an alternating torque component is activated and modulated on top of mean value (superposition). The frequency of alternating torque component matches the first torsional natural frequency of the elastic shaft system.

In the particular test setup (Figure 7-4) the first torsional natural frequency is 17.9 Hz. The mean value of torque is 1 pu (rated torque) and the simulation runs until steady state is reached. Afterwards an alternating component with magnitude of 0.0141 pu (0.01 pu RMS value, i.e. 1% of rated torque) is modulated on top of the mean torque value. The torsional mode is excited and after several periods the coupling torque reaches its limit cycle. In the first scenario the driving torque is applied on the first mass of the elastic model which represents the electric motor. In the second scenario the driving torque is applied on the gear. The torsional response in both cases looks quite different due to mode shape.
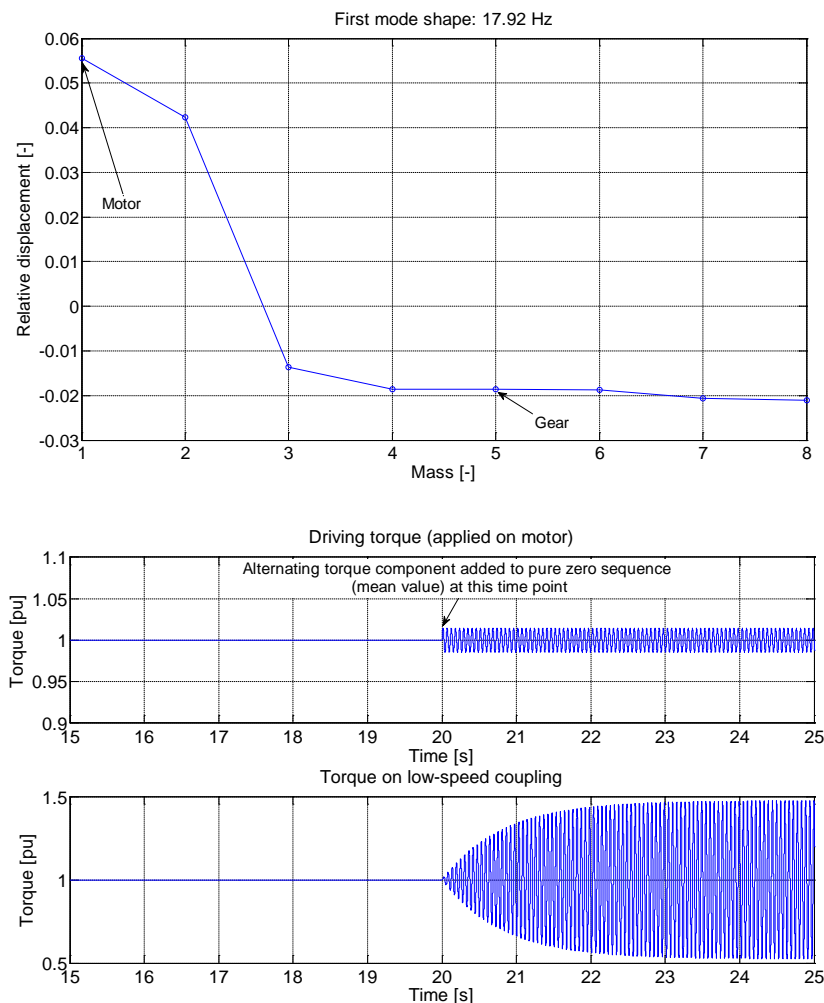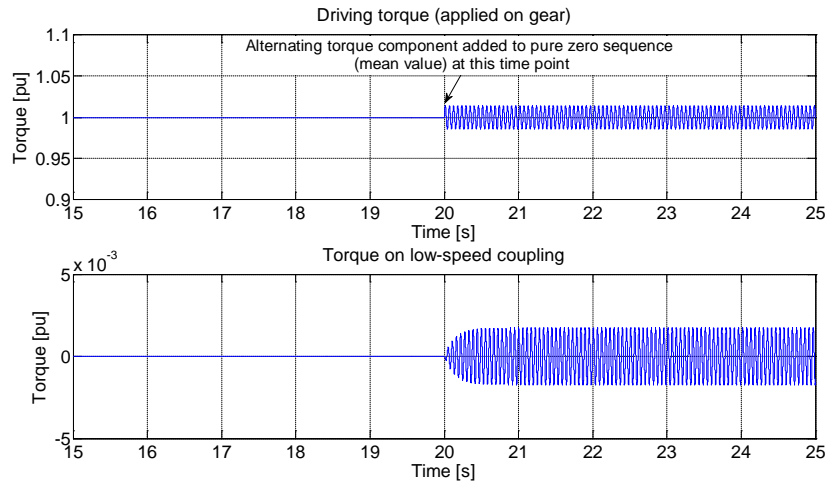
Figure 7-4: Torque response to excitation applied to different masses (disks)

Figure 7-4 demonstrates that mode shape determines whether the torsional natural mode can be excited from motor side or not and how large the torque response will be.

The torque response is also dependent on the load torque. Higher load torque provides more damping and lower envelope torque response while lower load torque provides less damping and the torque response is larger.
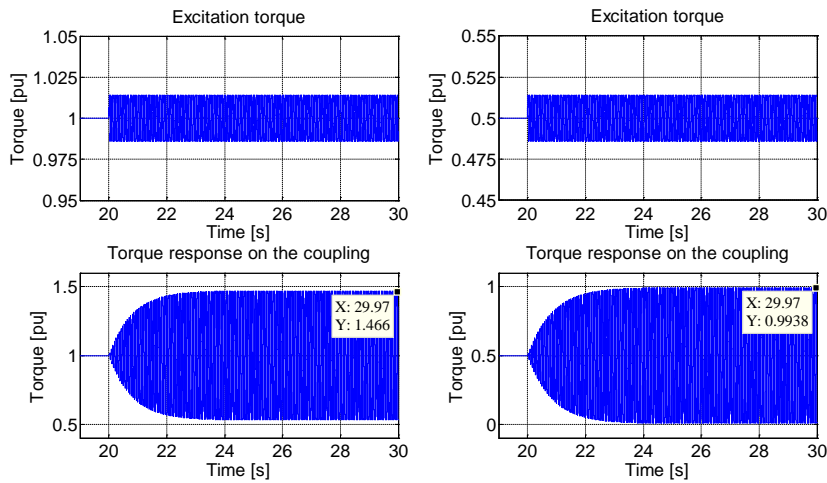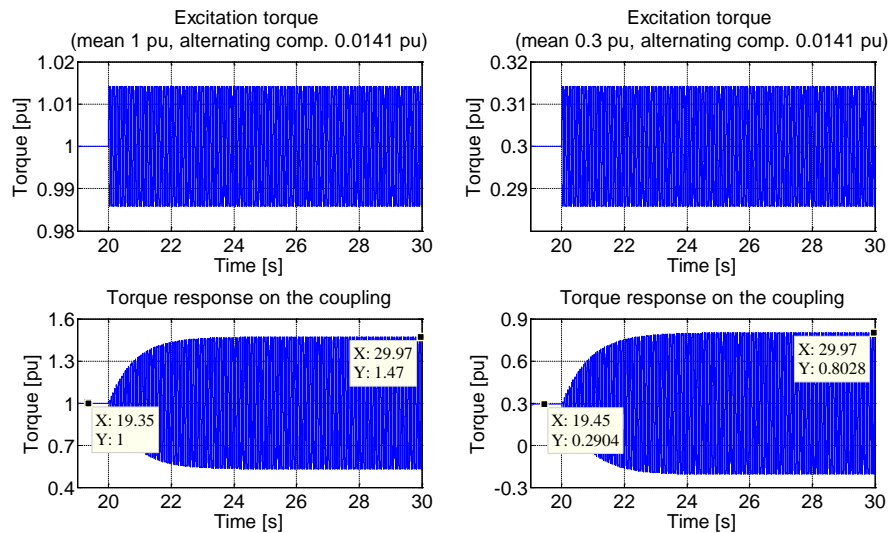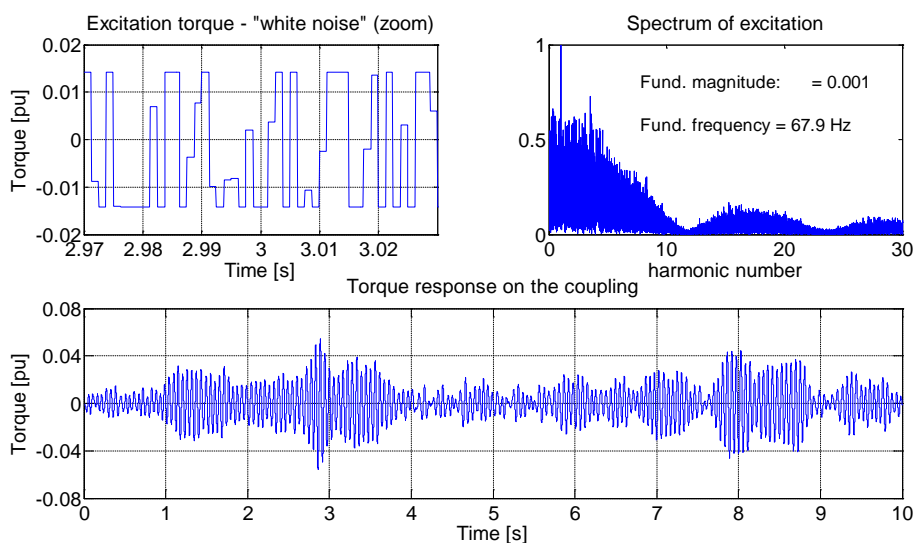
Figure 7-5: Torque response to excitation – impact of load torque

At 100% load the torque response to 0.0141 excitation is 0.47 pu (zero-peak) while at 30% load the torque response to same alternating excitation is over 0.51 pu. The difference is not so significant. However, the load torque has a significant impact on lateral vibration.

7.1.3   Random excitation (white noise)

As described in the theoretical part, some control methods (especially those with hysteresis modulator) inherently produce a broadband stochastic excitation with low magnitude. Other control methods may have such excitation as well, e.g. if there is a noise signal in measured quantities (e.g. output current or voltage). This type of excitation is sometimes referred to as "white noise".

Figure 7-6 shows a torque response to a white noise excitation with zero mean value and peak value limited to 0.0141 pu. The first case is configured with noise sampling time is 1.25 ms (sampling rate 800 Hz). The second case is configured with noise sampling time is 2.5 ms (sampling rate 400 Hz). The torque response displays typical fluctuation.
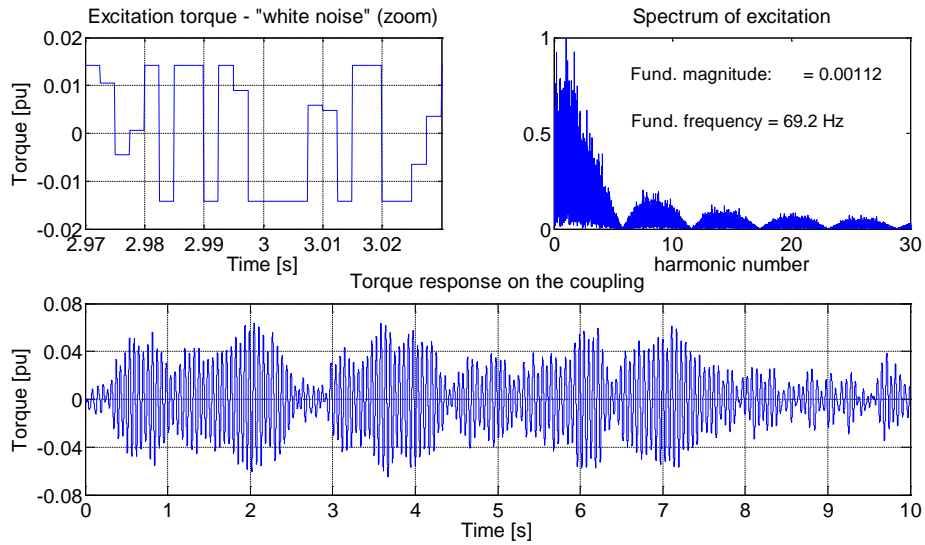
Figure 7-6: Torque response to white noise excitation

7.1.4   Excitation of resonance with random magnitude

This test case consists of excitation torque of fundamental frequency matching the torsional natural frequency (17.9 Hz), but with random time variant magnitude with limit set to 0.0141 pu. Noise sampling time is 2.5 ms (sampling rate 400 Hz). Torque response is reaching a quasi-steady state. Results are visualized in Figure 7-7.
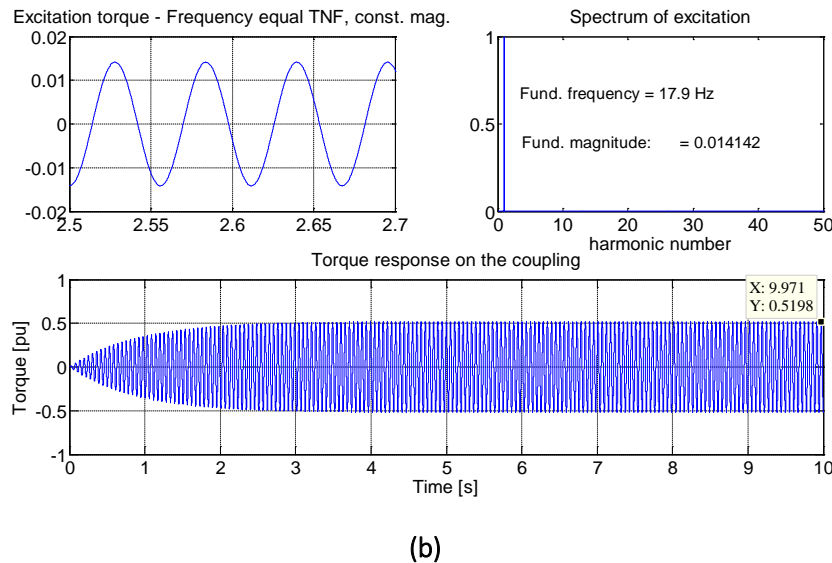

(a)

Excitation torque - Frequency equal TNF, const. mag.

Spectrum of excitation

Fund. frequency = 17.9 Hz

Fund. magnitude: = 0.014142

Torque response on the coupling

X: 9.971
Y: 0.5198

(b)
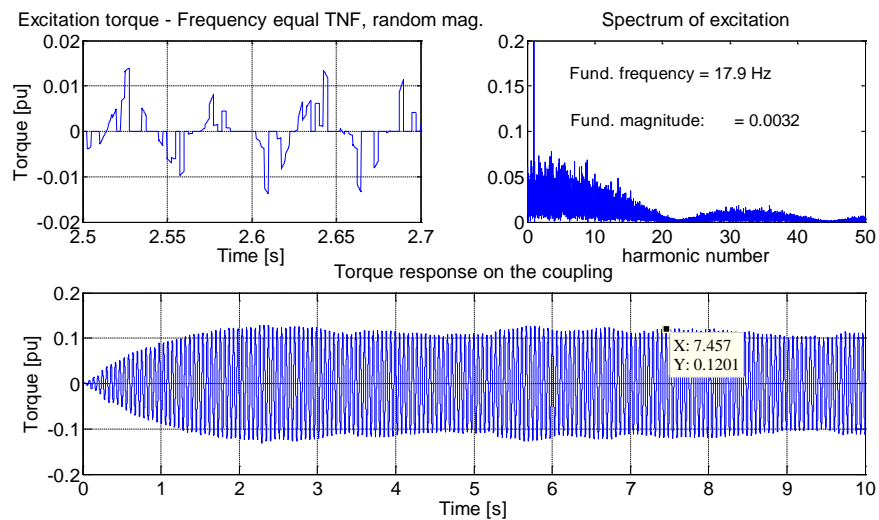
Figure 7-7: Torque response to excitation of torsional natural frequency with (a) variable (random) magnitude; (b) constant magnitude

The average magnitude of excitation is approx. 0.0032 pu (22-23% of magnitude limit) and also the torque response (envelope) is approx. 22% of the response when forced excited with constant magnitude of 0.0141 pu. Results are summarized in Table 4. The conclusion is that the mechanical system is (almost) linear in the sense that the ratio between average excitation and corresponding torque response is constant, i.e. the amplification factor is almost constant.

Table 4: Torque response to excitation with constant and random magnitude

	Random mag.	Constant mag.
MAX magnitude of excit. [pu]	0.0141	0.0141
AVG magnitude of excit. [pu]	0.0032	0.0141
Torque response (envelope) [pu]	0.1201	0.5198
Amplification factor (AF)	37.53	36.76

The conclusion is in line with the publications from rotordynamicists (e.g. [110] – see fig. 6).

7.2   Simulations of current source inverters (LCI drives)

Numerous simulations have been performed in order to understand the torsional behavior of LCI drive, obtain a sensitivity analysis and test and verify algorithms for active damping. The studies included steady state operating conditions as well as transient behavior.

First set of simulations considered full detailed model of LCI drive while the mechanical load was modeled just as single inertia (stiff mechanics) acc. left part of Figure 7-8 and Figure 7-9. Motor and load speed are identical in per unit system.
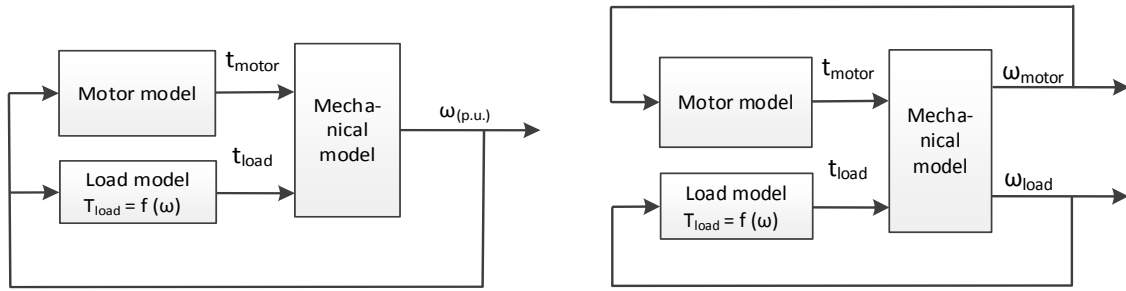
Figure 7-8: System with rigid (left) and elastic (right) mechanical model

Next set of simulations contains elastic mechanical model acc. Figure 7-8 and Figure 7-9 (right). Actual value of motor and load speed is different due to possible oscillations along the shaft string. A convenient modeling of elastic shaft is state-space representation. This method allows simple extension of number of masses depending on required model accuracy and easy configuration of input and output signals.
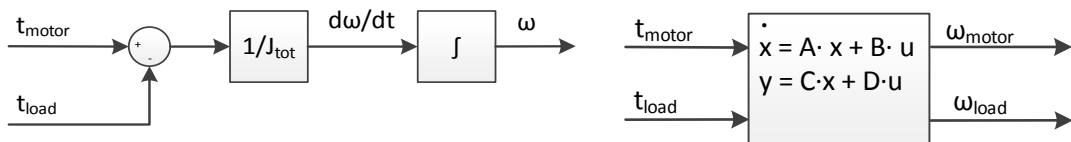

Figure 7-9: (a) Modeling of rigid shaft (left), (b) state-space modeling of elastic mechanics (right)

7.2.1   Start up from standstill up to minimum operating speed

7.2.1.1   Pulse mode operation

As described in the theoretical section, the pulse mode applies to operation at low motor speed from zero up to 6...12% of motor nominal speed. The exact threshold depends on the specific system and is influenced mainly by starting torque requirement and motor sub-transient reactance (the higher the reactance the longer time for commutation is required).

Pulse mode imposes significant pulsating torques on the shaft system. Since the load torque is usually low at low speed, a torque reversal might appear on the coupling. This situation is dangerous for the coupling and mitigations might be necessary. The closed loop simulations with elastic mechanical model reveal the torsional response on the couplings for the risk assessment and also for control optimization. Figure 7-10 illustrates the behavior of elastic shaft model during pulse mode. Current in dc link contains large portion of 6th harmonic and the same frequency is present in air gap torque. The first torsional natural frequency is significantly excited.

(a)

(b)

(c)

Torque on the GT coupling; torque magnitude logarithmically scaled
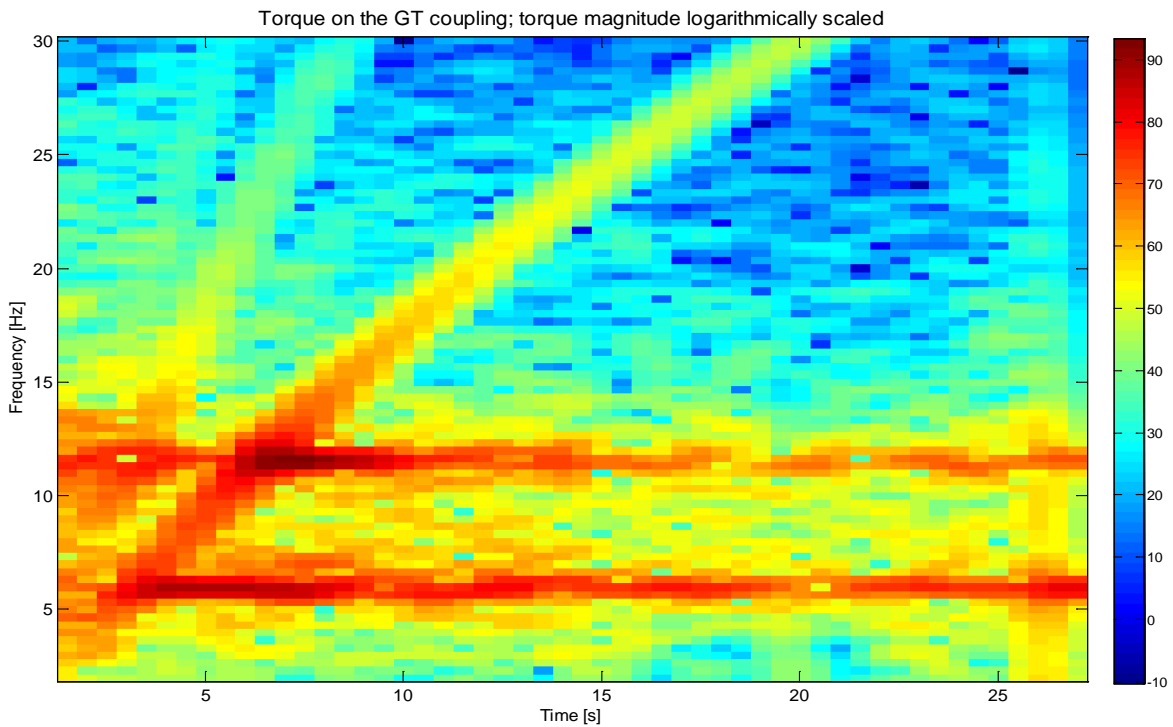

(d)
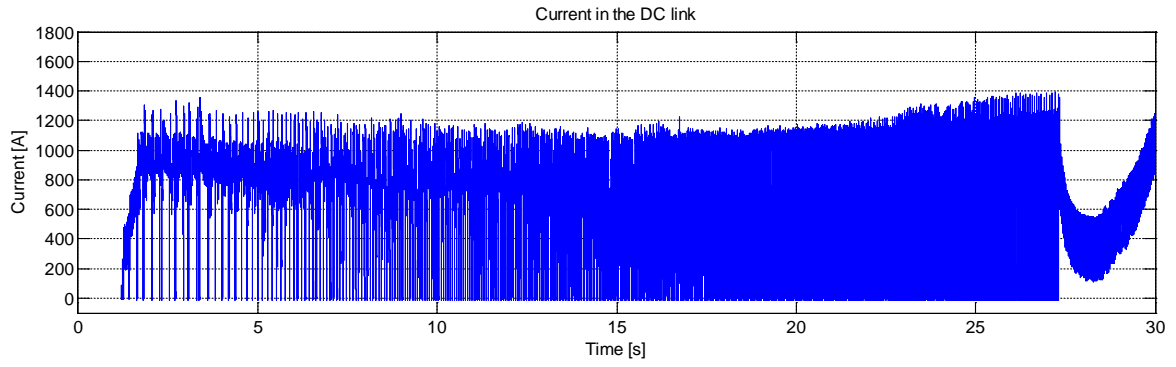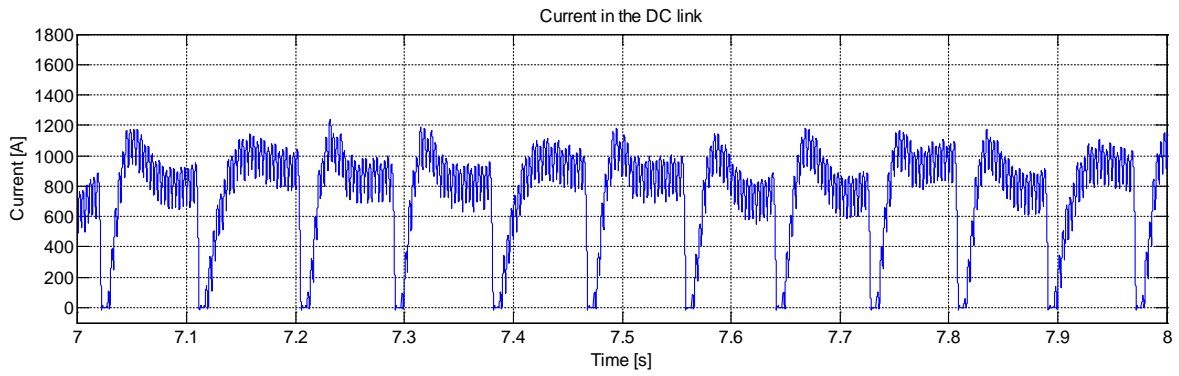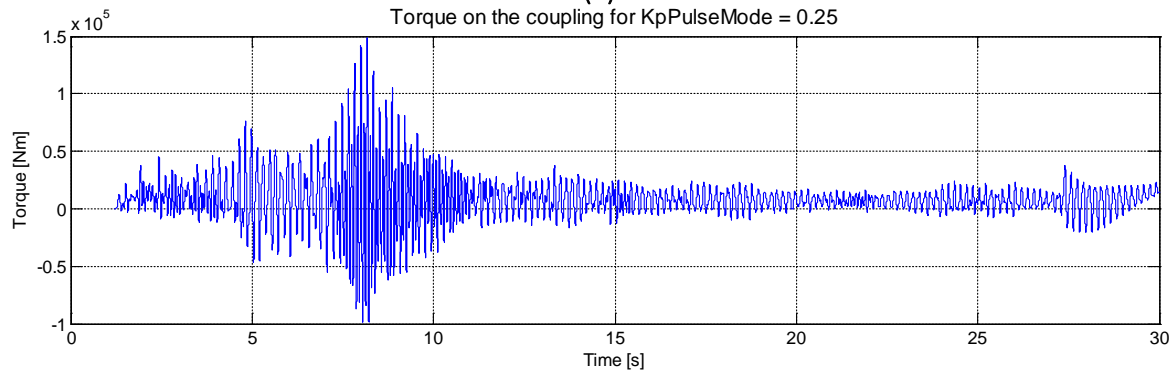
Figure 7-10: Current and torque during pulse mode;
(a) Current in the dc link (entire pulse mode), (b) Current in the dc link (zoom), (c) Torque on the cou-

pling, (d) Waterfall plot of torque on the coupling (logarithmic scaling of magnitude)

Such operation in pulse mode might be the most critical from torsional integrity point of view. Any

improvement achieved form control side is therefore much appreciated.

Torque on coupling during pulse mode operation of large mechanical train of drive system as per

Table 12 is shown in Figure 7-11. The first mode shape is practically not excitable from the electric

driver, but second torsional mode is significantly excited. Due to larger commutation reactance of the

motor the threshold between pulse mode and load commutated mode is increased to 12% of motor

rated speed.
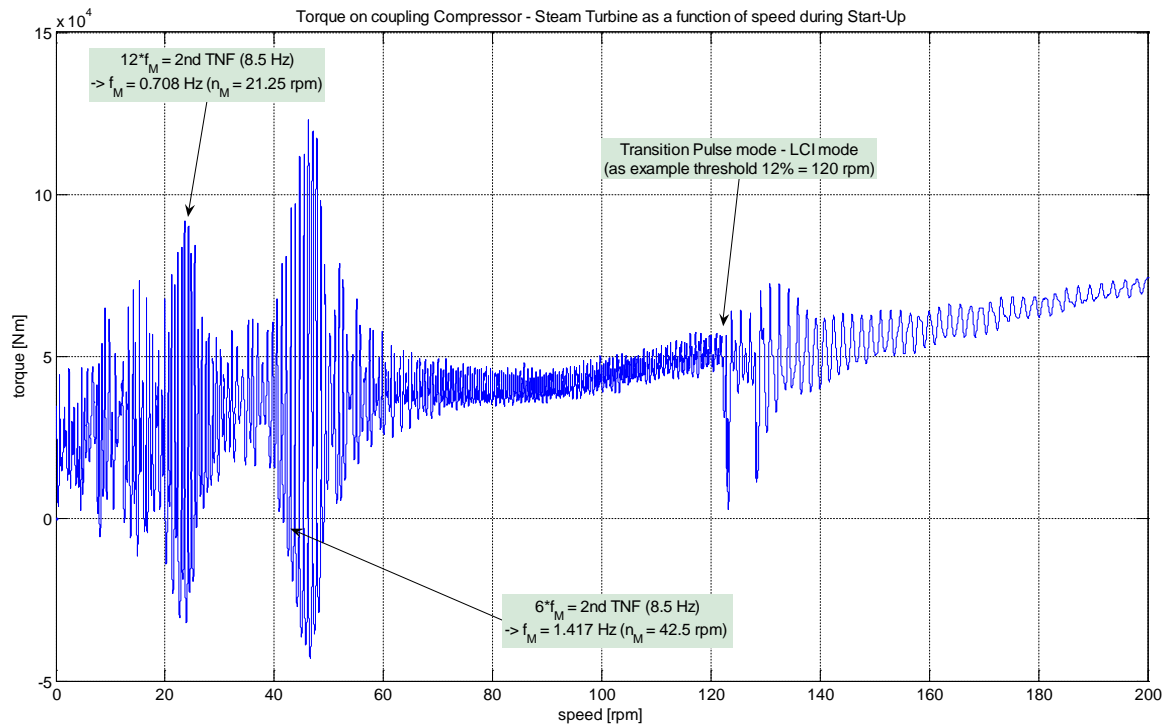
Figure 7-11: Torque on coupling between steam turbine and compressor during pulse mode

7.2.1.2   Entire start-up

During the start-up the LCI will excite all relevant TNFs. First excitation occurs in pulse mode when integer harmonics interfere with TNFs. At higher speeds in load commutated mode the interharmonics excite the TNFs. There might be additional transient excitation due to various events such as not smooth transition from pulse mode into load commutated mode, insertion of harmonic filter on the line side (in case not inserted prior to starting).

The excitations are identified in the torque on low speed coupling recorded during start up from zero to 1'200 rpm (80% of nominal speed). This starting is a benchmark prior to torsional optimization.
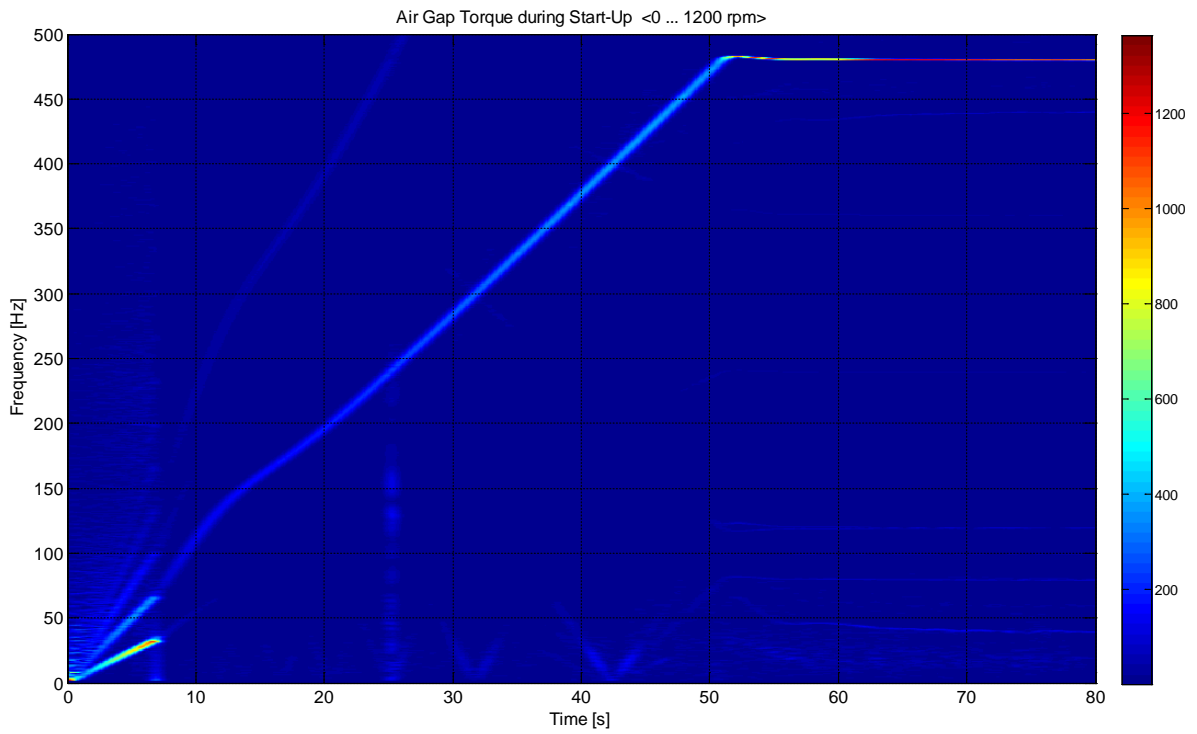
Figure 7-12: Waterfall of air gap torque during start-up
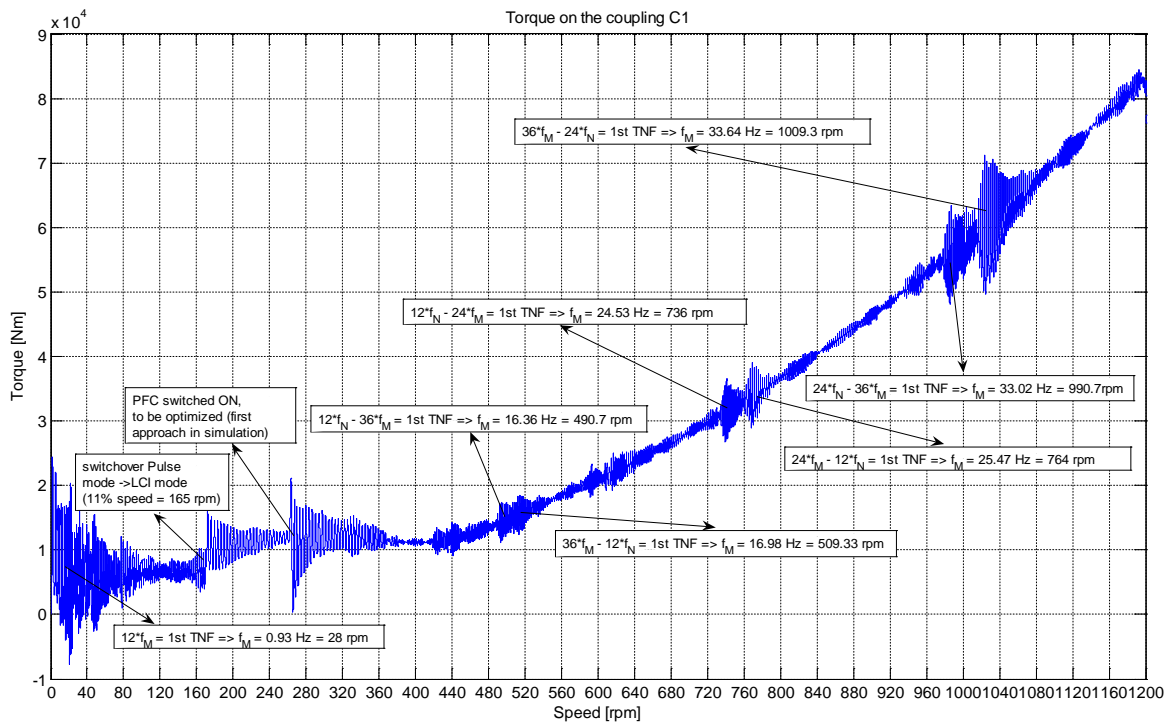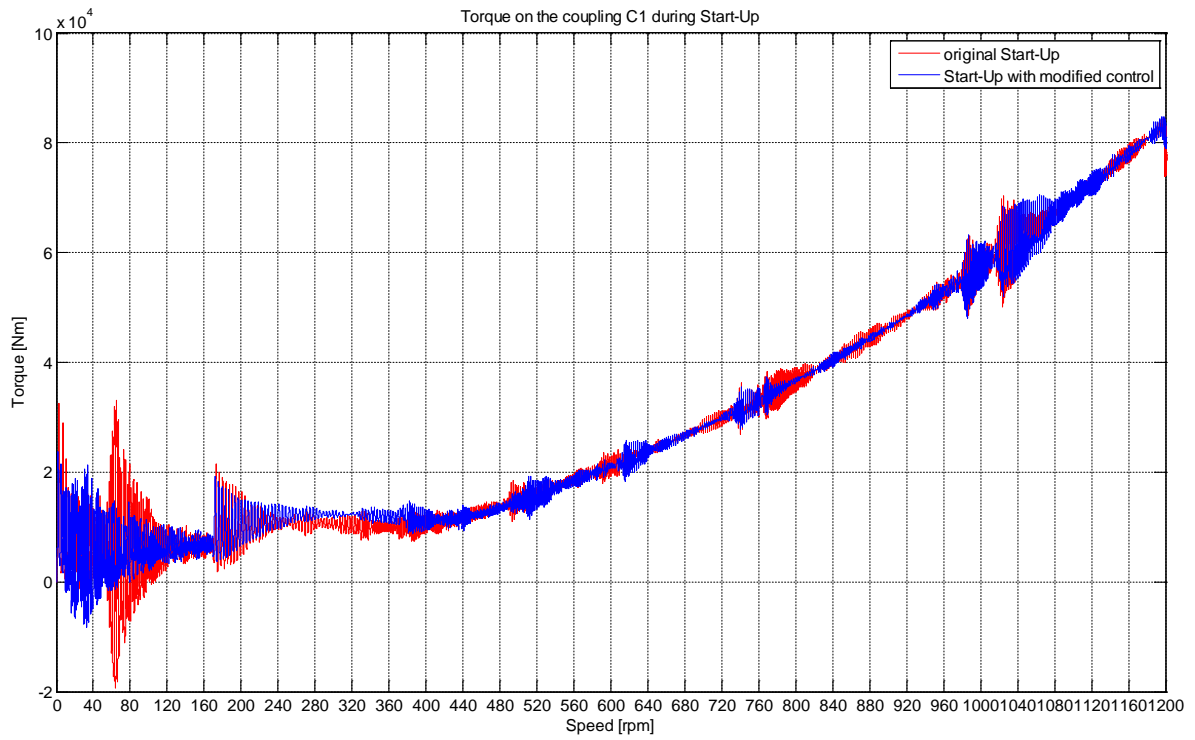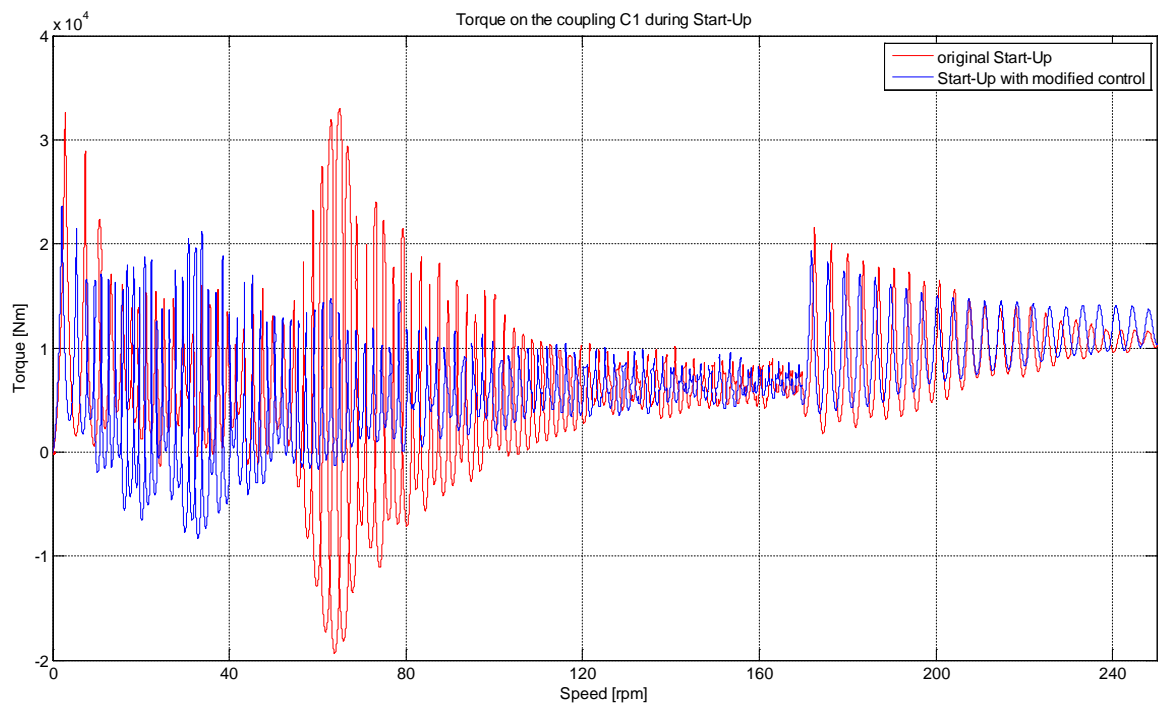

Figure 7-13: Torque on the motor coupling during start-up with identified excitations

(a) entire Start-up 0...80% speed

(b) detail of Start-up 0...16.7% speed

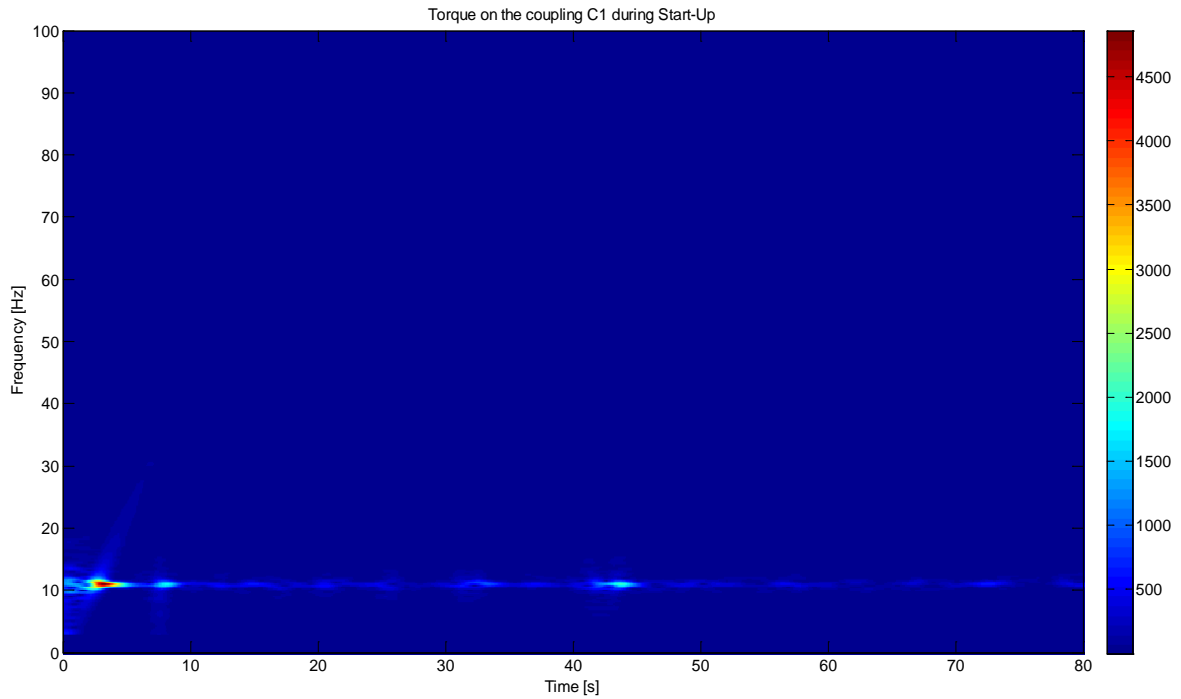Figure 7-14: Torque on the motor coupling - comparison of original and optimized control

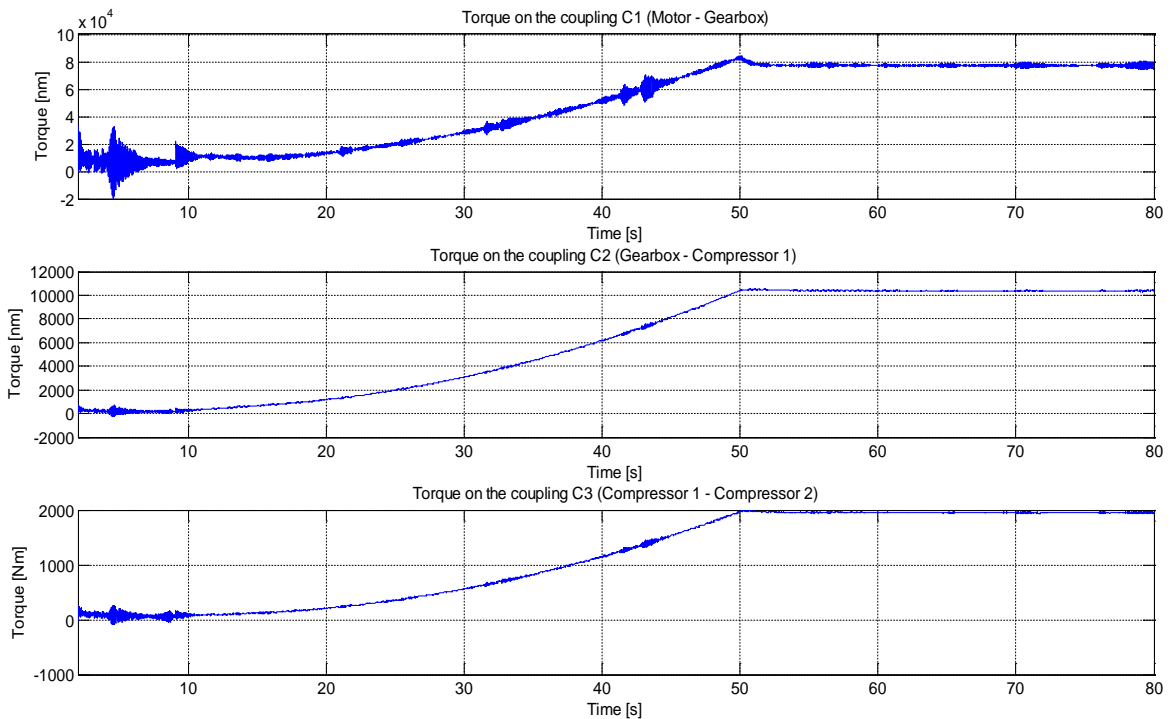Figure 7-15: Waterfall plot of coupling torque

Figure 7-16: Torque on all couplings during start-up (0 – 80% rated speed)

Example of air gap torque during start-up is depicted in Figure 7-17. The rated torque is shown as 2 pu. That is just a result of per unit definition of dual winding machine (2 x 3-phase). The start-up is valid for load with larger inertia where rated torque is applied to accelerate as fast as possible. Once

the reference speed is reached, the air gap torque is reduced to a level corresponding to load torque.
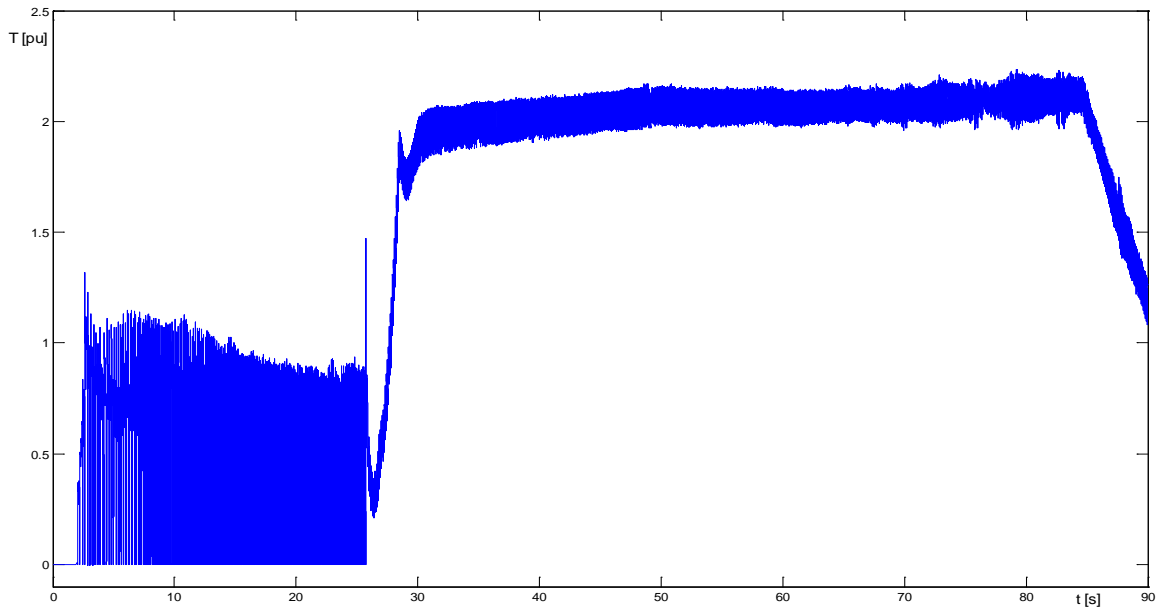

Figure 7-17: Motor air gap torque during entire start-up (case 1)

Another start-up is depicted in Figure 7-18. The example confirms the relationship between current in dc link and air gap torque.
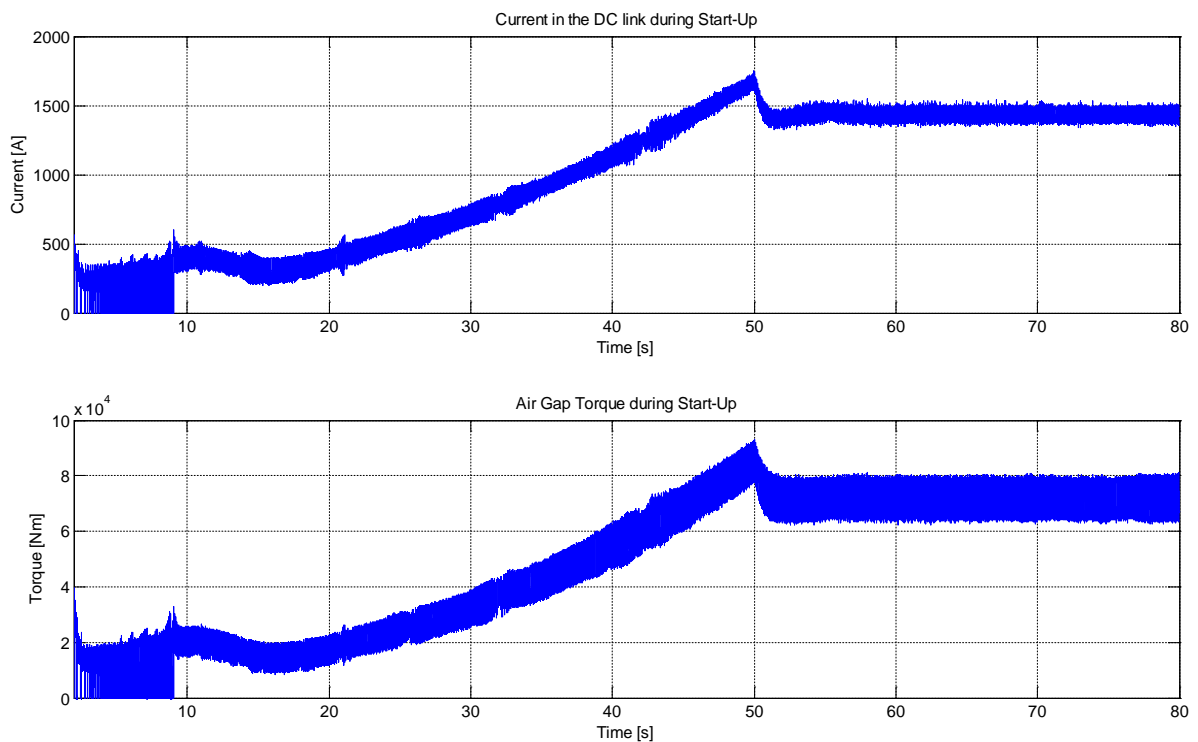

Figure 7-18: Current in dc link and motor air gap torque during entire start-up (case 2)

One more simulation example is in Figure 7-19. It shows the torque on motor shaft end and compressor shaft end during entire start-up. The system data is acc. Table 9.
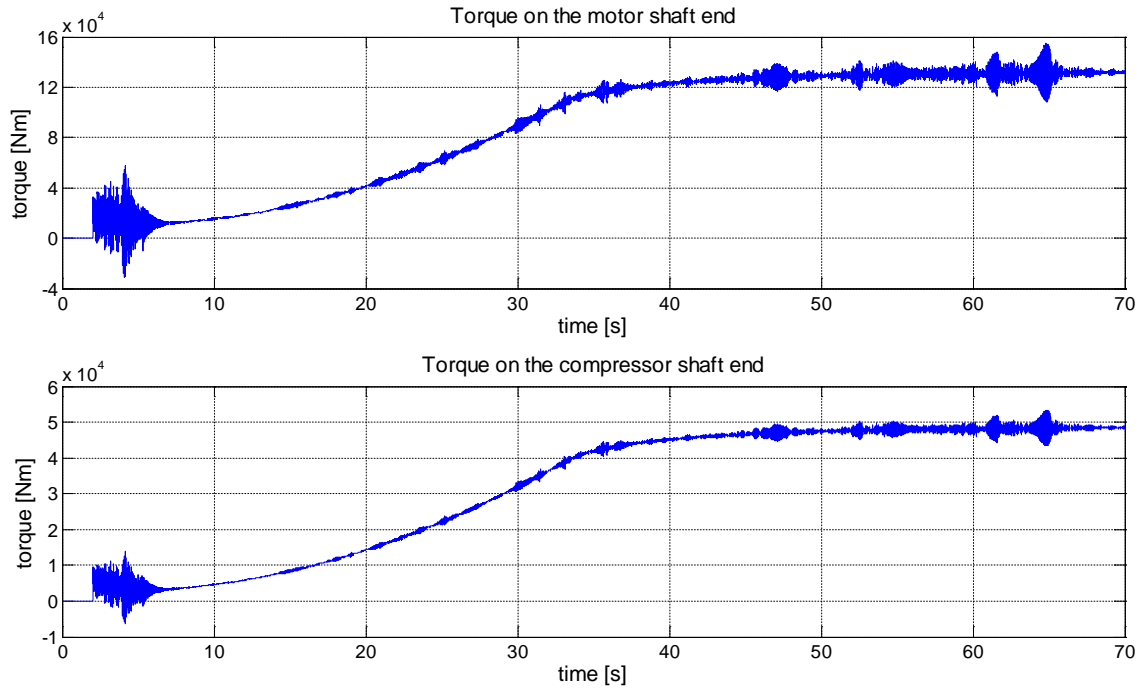
Figure 7-19: Shaft torque on the motor and compressor shaft end

7.2.2   Steady state operation at critical speed

In order to investigate the behavior of the drive in the mechanical resonance, the simulations were performed as follows:

1. Critical speeds are calculated based on knowledge of first and second torsional natural frequency.
2. Critical speed is set as speed reference for the drive system.
3. The simulation is initiated with speed slightly below the critical speed and runs into resonance. Simulation has to be long enough to ensure steady-state operation.

Table 5: Calculation of critical speeds
(intersections of interharmonics with torsional natural frequencies)

Inputs:			
network frequency	f_N	[Hz]	50
number of pole pairs	npp	[-]	2
rated motor speed	n_{rat}	[rpm]	1500
1st TNF	1st TNF	[Hz]	17.4
2nd TNF	2nd TNF	[Hz]	58.2
Critical speeds:	f_M [Hz]	n_{mot} [rpm]	n_{ref} in control [pu]
12*fN-12*fM vs. 1st TNF	48.550	1456.5	0.971
12*fM-12*fN vs. 1st TNF	51.450	1543.5	1.029
12*fN-12*fM vs. 2nd TNF	45.150	1354.5	0.903
12*fM-12*fN vs. 2nd TNF	54.850	1645.5	1.097
6*fN-6*fM vs. 1st TNF	47.100	1413.0	0.942
6*fM-6*fN vs. 1st TNF	52.900	1587.0	1.058
6*fN-6*fM vs. 2nd TNF	40.300	1209.0	0.806

6*fM-6*fN vs. 2nd TNF	59.700	1791.0	1.194
24*fN-24*fM vs. 1st TNF	49.275	1478.3	0.986
24*fM-24*fN vs. 1st TNF	50.725	1521.8	1.015
24*fN-24*fM vs. 2nd TNF	47.575	1427.3	0.952
24*fM-24*fN vs. 2nd TNF	52.425	1572.8	1.049
6*fN-12*fM vs. 1st TNF	23.550	706.5	0.471
6*fN-12*fM vs. 2nd TNF	20.150	604.5	0.403

Figure 7-20 shows the torque on the coupling when driving into the resonance (intersection of torsional natural frequency with $12*(f_N-f_M)$ interharmonic frequency in dc current and torque).
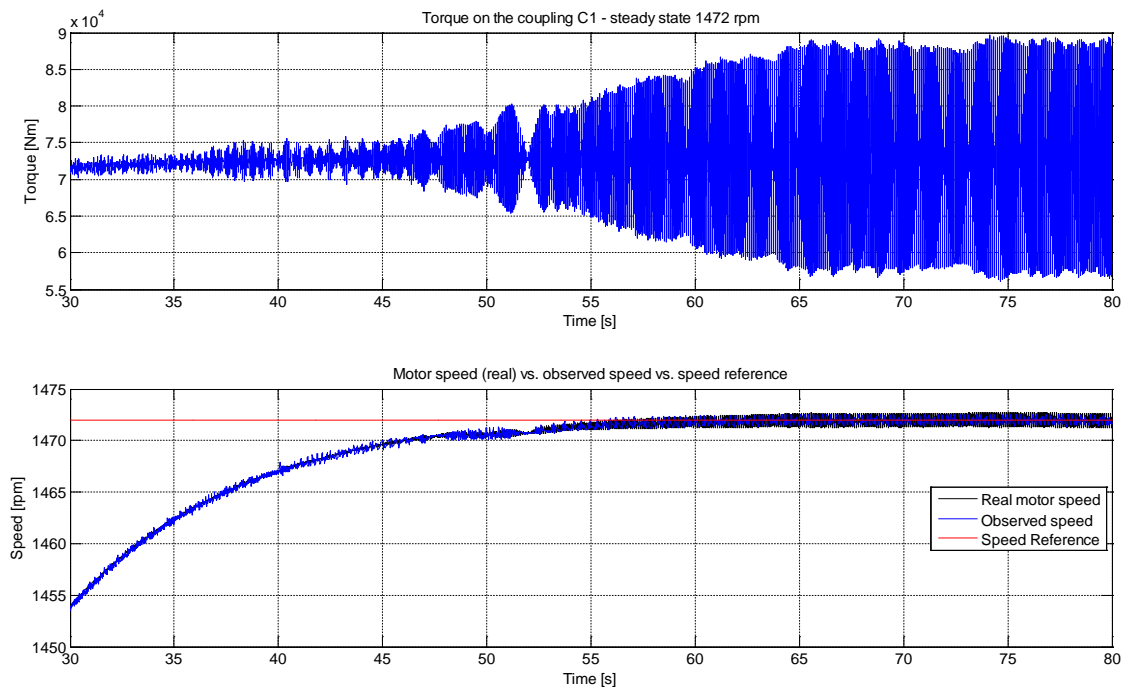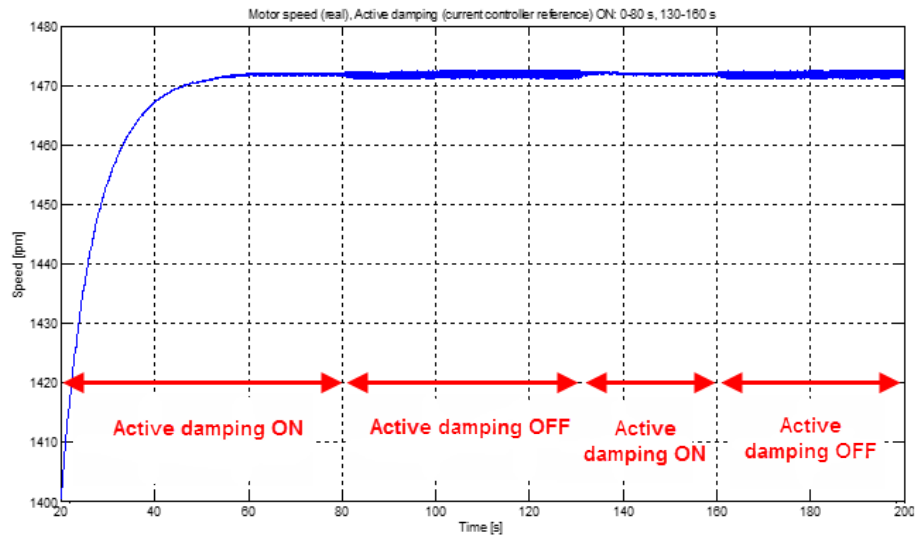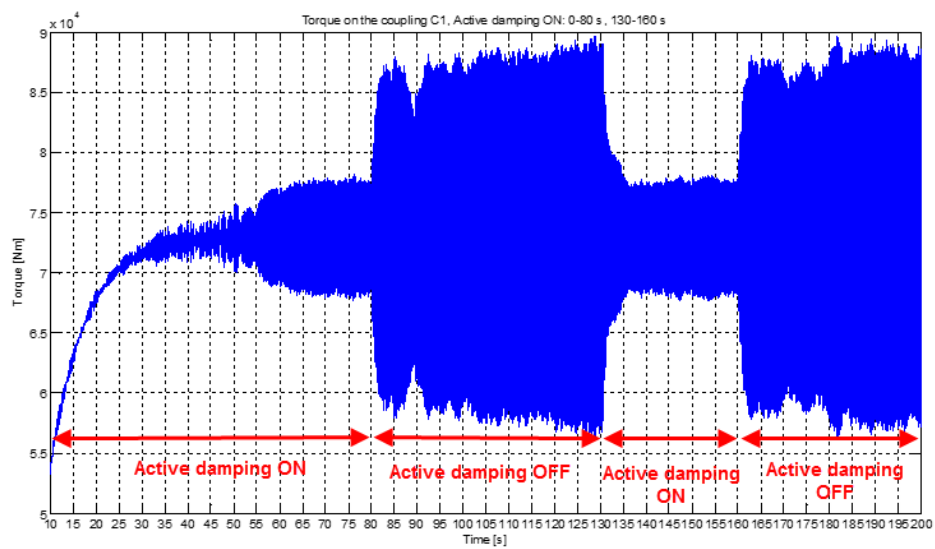

Figure 7-20: Torque on the coupling and motor speed in resonance condition

Figure 7-21 demonstrates the performance of torsional damper. While operating in resonance (at critical speed) the torsional damper is repeatedly activated and deactivated. The difference in the torque response on the motor coupling is significant. Figure 7-22 then shows the performance of torsional damper depending on the amplification factor AF (AF is indirect proportional to system damping).

(a)

(b)

Figure 7-21: Performance of torsional damper;
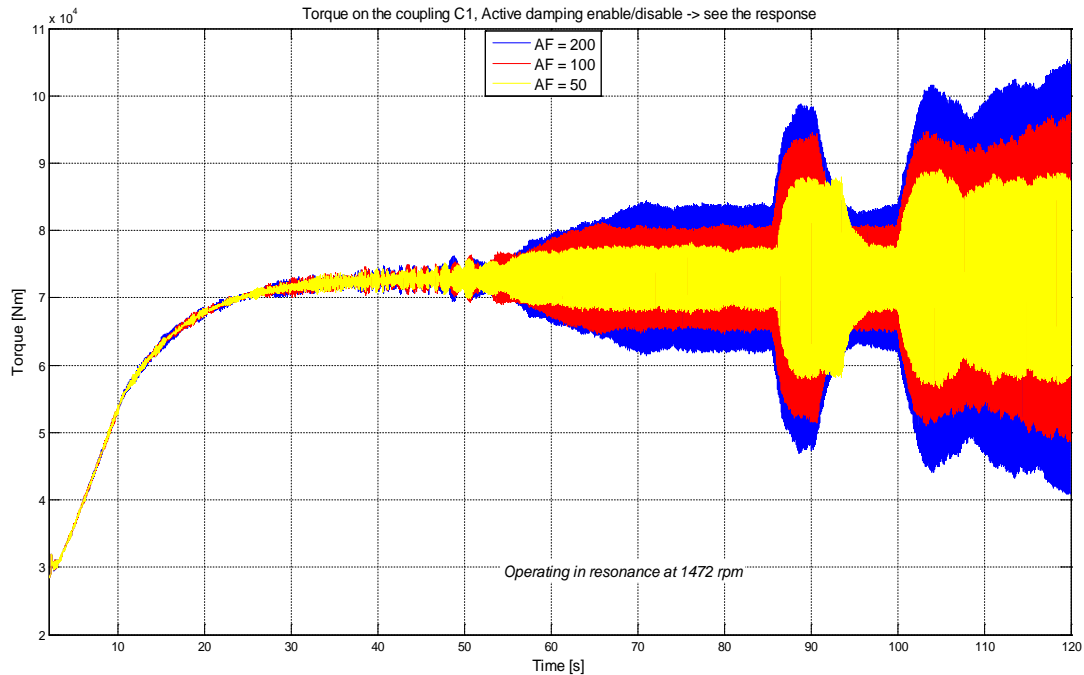(a) motor shaft speed, (b) torque on the coupling

Figure 7-22: Torque on coupling with and w/o active damping – impact of amplification factor

7.3   Simulations of voltage source inverters (VSI drives)

Similar simulations like for LCI drive have also been performed for VSI drives. The modulation scheme has an impact on torque spectrum of driven motor. For VSI drives the most common modulation techniques are Pulse width modulation (PWM) and Direct torque control (DTC). Both methods yield similar torque spectrum in regards to characteristic harmonics (integer multiples of motor fundamental electric frequency). In terms of interharmonics there is a difference:

- PWM generates interharmonic components as convolutions of fundamental output frequency (inverter frequency) and sampling frequency of the specific control loop. The mechanism has been described in [48]. These convolutions appear as sidebands of the drive output current (52) and consequently are contained in the spectrum of air gap torque.

$$f_{current\;SB} = \left| f_{ctrl\;samp} - n \cdot f_{inv,fund} \right| \qquad (52)$$

$f_{current\;SB}$ is the sideband frequency in the spectrum of VFD output current, $f_{ctrl\;samp}$ is the sampling frequency of the control loop, n is positive odd integer other than 3 and $f_{inv,\;fund}$ is the fundamental inverter output frequency.

According harmonic transfer rules the frequency in the air gap torque is determined by (53).

$$f_{torque} = \left| f_{ctrl\;samp} - (n \pm 1) \cdot f_{inv,fund} \right| \qquad (53)$$

Note that most of the VFD control systems have multiple different sampling frequencies resulting in several additional frequency components in the spectrum of air gap torque.

- PWM modulator might also generate interharmonic components as convolutions of carrier frequency of PWM and multiples of fundamental inverter frequency as per (54). Root cause is improper compensation of switching dead times.

$$f_{torque} = \left| f_{PWM\ carrier} - (n \pm 1) \cdot f_{inv,fund} \right| \qquad (54)$$

- DTC due to its hysteresis nature generates low-magnitude components across the frequency range. The magnitude is variable over time. This "noise" signal is equally distributed and in normal condition fully harmless. The noise level typically reduces with increased switching frequency. The only 'torsionally unsafe' condition appears if the natural frequency is excited by the noise signal and the closed loop control system locks the excitation due to its feedback loop.

Figure 7-23 and Figure 7-24 show the spectrum of air gap torque for two different motors (6'500 kW induction machine and 18'300 kW synchronous machine) for standard and increased switching frequency. With increased switching frequency the characteristic harmonics tend to have larger magnitude while the noise level drops down.
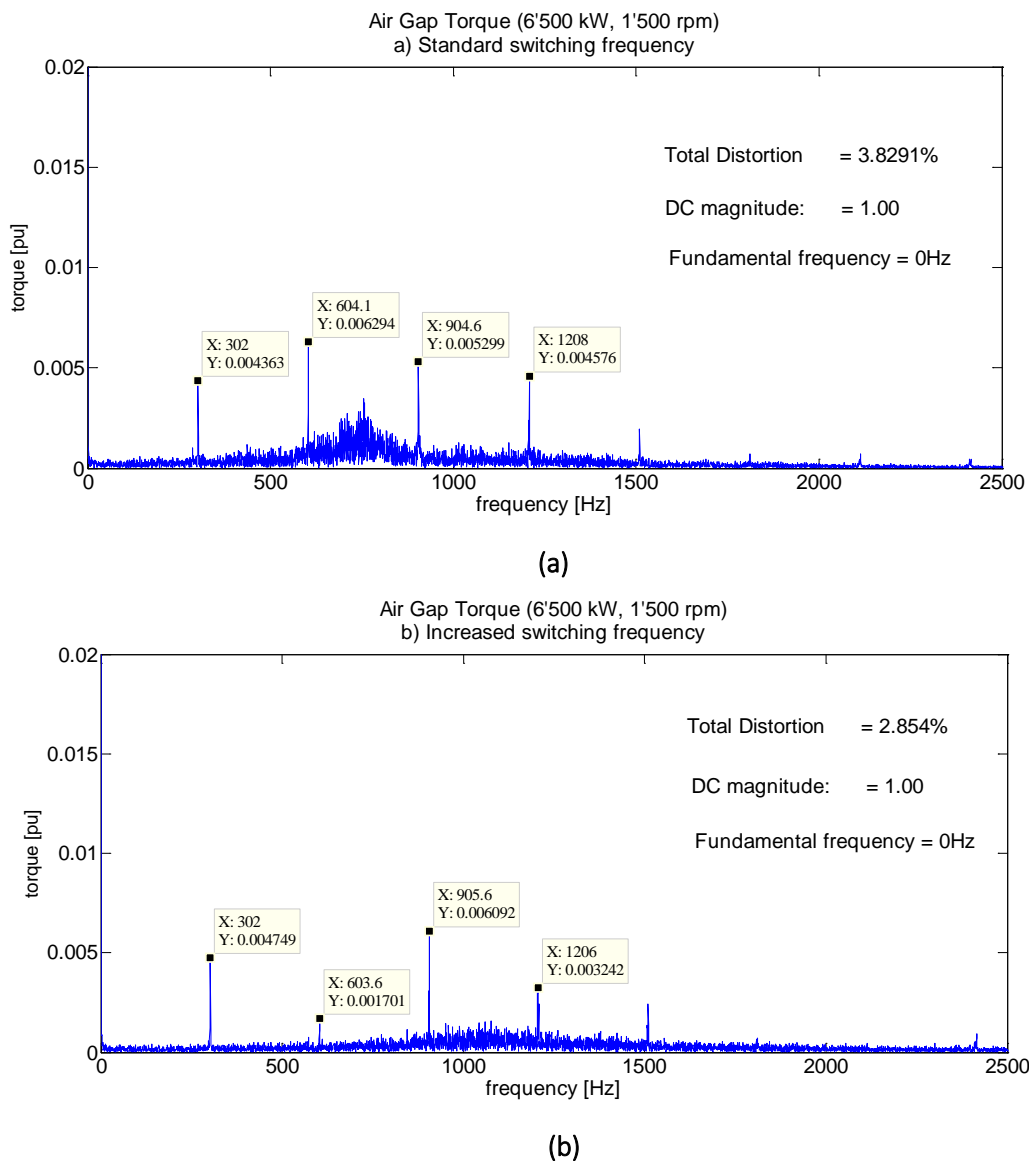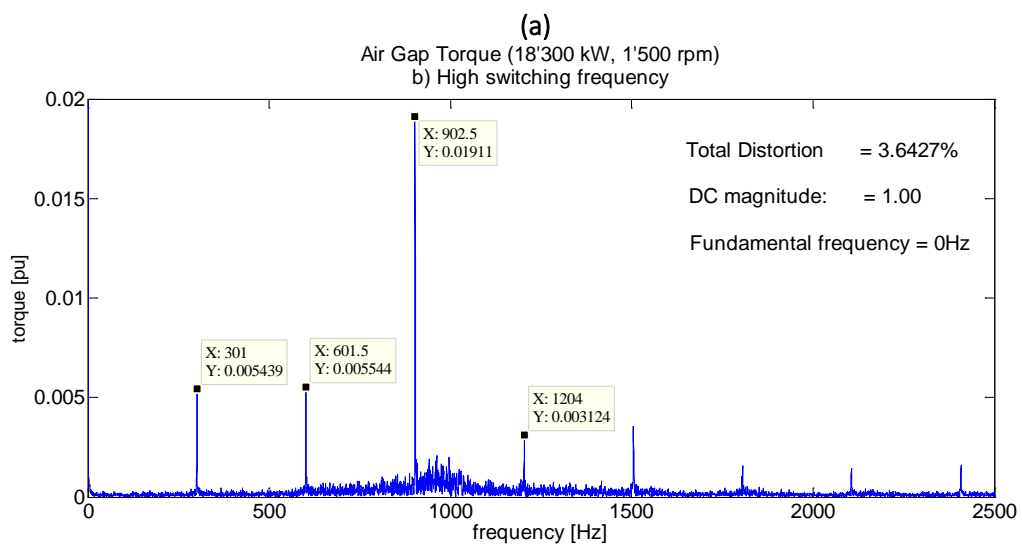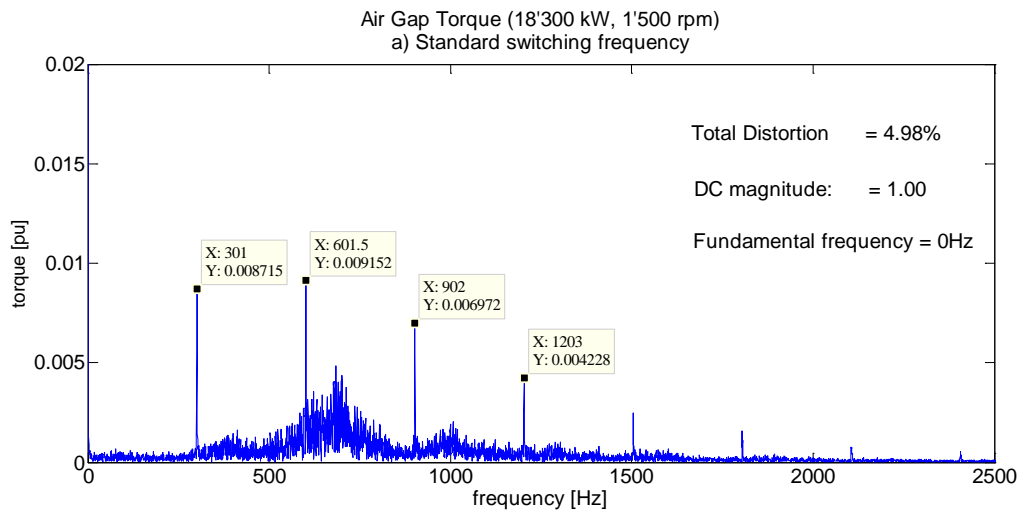

(a)

(b)

Figure 7-23: Spectrum of motor air gap torque (6'500 kW motor);
(a) standard switching freq., (b) increased switching freq.

Air Gap Torque (18'300 kW, 1'500 rpm)
a) Standard switching frequency

(a)

Air Gap Torque (18'300 kW, 1'500 rpm)
b) High switching frequency

(b)

Figure 7-24: Spectrum of motor air gap torque (18'300 kW motor); (a) standard switching freq., (b) increased switching freq.

Extensive simulations were performed for system described in Table 18. The focus was on torsional behavior of the drive when operating in closed loop (DTC) and in open loop (scalar) control mode. The spectrum of air gap torque and coupling torque was analyzed for several speed setpoints as seen in Figure 7-25 for selected speeds 1'000 rpm and 1'429 rpm. Torque is in pu of fundamental value (DC magnitude). It is a bit surprising that the improved torsional behavior of scalar (open loop) control observed in the field could not be reproduced in closed loop simulations.
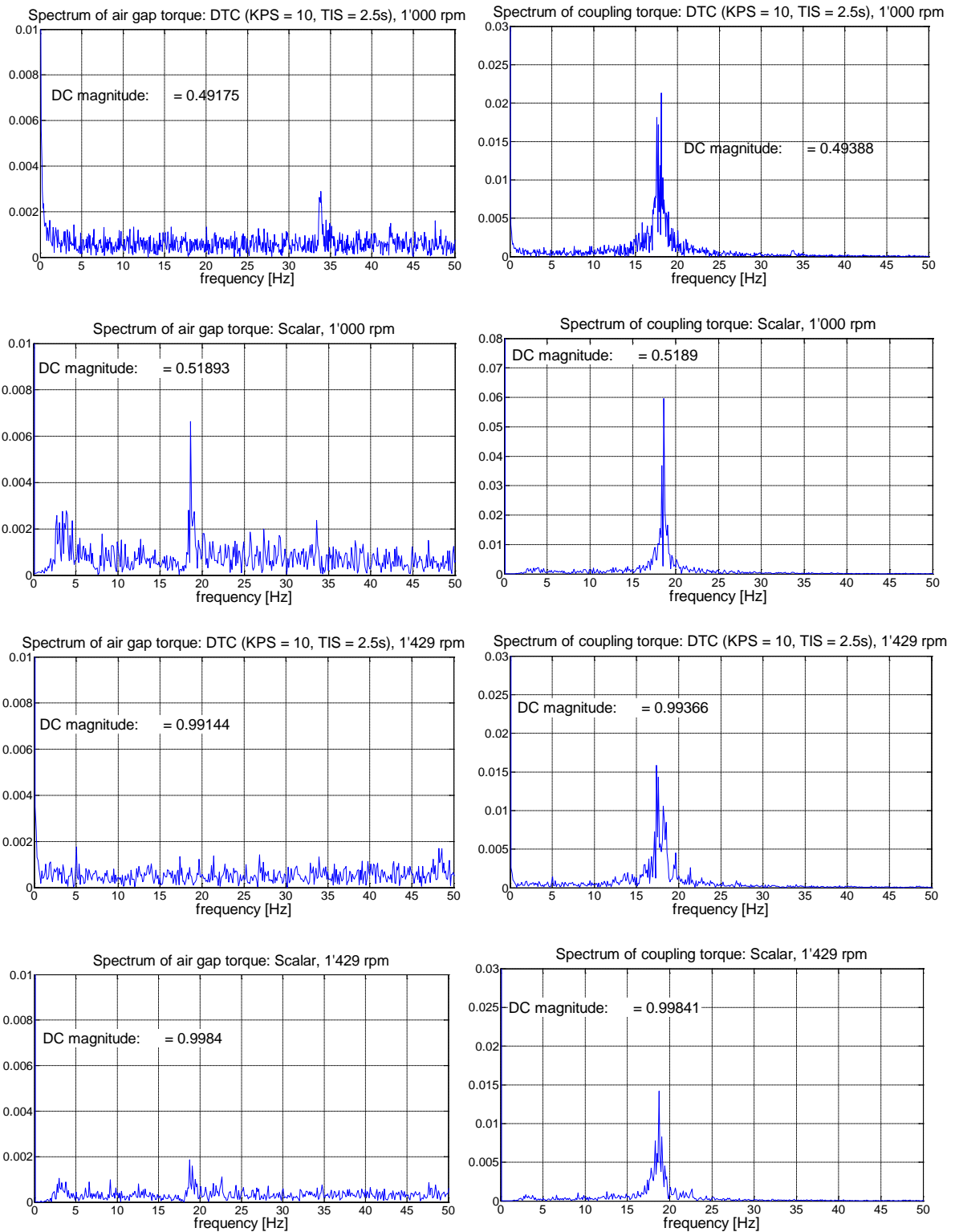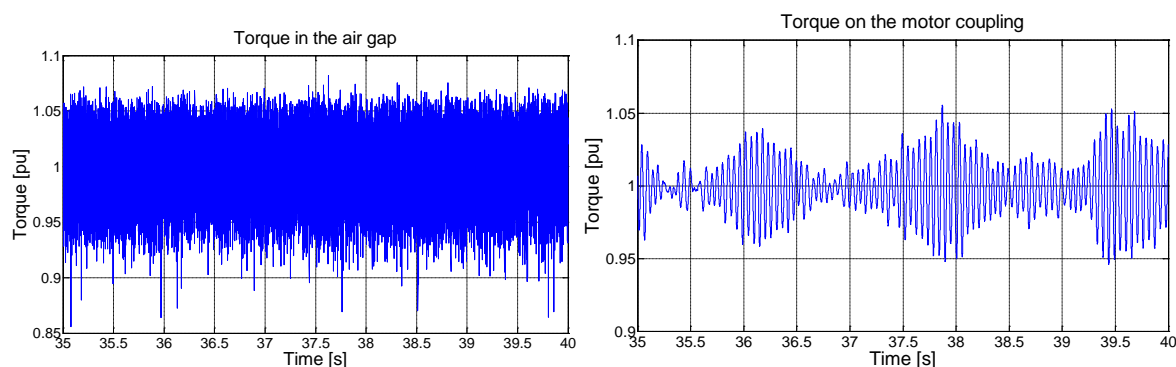
Figure 7-25: Spectrum of air gap torque and coupling torque: DTC versus Scalar mode

The overview of closed loop simulation results is summarized in Table 6. The peak-peak coupling torque at 17 Hz (1st TNF) is given in pu of mean value / pu of rated motor torque.

Table 6: Closed loop versus open loop control – Peak coupling torque

Setpoint	DTC: KPS = 10, TIS = 2.5s	DTC: KPS = 1, TIS = 10s	Scalar (Open loop DTC)
	Peak-peak torque on coupling - pu of mean value (pu of rated mot. torque)		
50% load, 1'000 rpm	0.044 (0.022)	0.024 (0.012)	0.12 (0.06)
70% load, 1'220 rpm	0.021 (0.015)	0.026 (0.018)	0.038 (0.027)
100% load, 1'429 rpm	0.032 (0.032)	0.031 (0.031)	0.028 (0.028)

Although the closed loop simulations couldn't reproduce the positive impact of scalar (open loop) control compared to closed loop, they reproduce the excitation due to 'white noise', i.e. broadband excitation with generally low time-variant magnitude. The excitation and response is shown in Figure 7-26 for the scalar mode. Alternating torque on the motor coupling is oscillating with frequency equal the dominant torsional natural frequency (17.5 Hz for the specific case) and variable magnitude.

Figure 7-26: Motor air gap torque and coupling torque in time domain

Same behavior was observed in the real operation as illustrated on examples in the next chapter.

8   Validation experiments

Proposed control interventions are validated by means of computer simulations, measurements of real plants or both. Results are presented in this chapter.

8.1   Technical data of simulated and measured drive systems

Tables below summarize fundamental technical data of simulated and measured (real) variable speed drive systems.

Table 7: Fundamental data of drive system 1

Driven load	Centrifugal compressors (2 units)
Motor type	Synchronous, salient pole rotor, brushless excitation, hazardous area
Stator winding	Dual star stator, 30 deg phase shifted windings
Motor rated power	13'550 kW
Motor rated voltage	2 x 3'300 V
Motor rated frequency	50.0 Hz
Motor min. / rated / max. speed	1'050 rpm / 1'500 rpm / 1'575 rpm

Compressor min. / rated / max. speed	7'704 rpm / 11'006 rpm / 11'556 rpm
Gear ratio	0.13
VFD topology	Load-commutated inverter (LCI)
VFD configuration	12-12 pulse, , n+1 thyristors per branch (72 thyristors in total)
Line frequency	50 Hz
Size of DC reactor	5 mH
Pulse mode operation	0 … 165 rpm / 0 … 11% of rated speed
Load-commutated operation	165 … 1'575 rpm / 11 … 105% of rated speed
Torsional natural frequencies (TNF)	11.6 Hz and 30.4 Hz (higher TNFs outside the speed range)

Project specific information:

The critical speeds, i.e. crossings of interharmonics with first torsional natural frequency are both inside the operating speed range (especially 1'473 rpm and 1'529 rpm). Validation of several control optimization functions was performed during string test of the entire drive system. The effect of torsional damper was verified by external measurement with torque meter.

Installation of drive system according Table 7 is shown in Figure 8-1. In the left picture dominates the synchronous machine with large cooler (due to design for 55°C ambient temperature on site) and there is also speed-increasing gearbox is visible. Compressor is not shown (confidentiality reasons). Figure 8-1b shows the view on the motor drive end and shaft towards gearbox. During the string test the drive system can be fully loaded. Inert gas with similar molecular weight is used instead of process gas.

Figure 8-1: String test of drive system as per Table 7 (courtesy of ABB)

Table 8: Fundamental data of drive system 2

Driven load	Centrifugal compressor
Motor type	Synchronous, salient pole rotor, 1'250 mm shaft height, brushless excitation, hazardous area
Stator winding	Dual star stator, 30 deg phase shifted windings

Motor rated power	17'000 kW
Motor rated voltage	2 x 6'000 V
Motor rated frequency	57.13 Hz
Motor min. / rated / max. speed	1'260 rpm / 1'714 rpm / 1'890 rpm
Compressor min. / rated / max. speed	7'026 rpm / 11'195 rpm / 11'755 rpm
Gear ratio	0.153
VFD topology	Load-commutated inverter (LCI)
VFD configuration	12-12 pulse, , n+1 thyristors per branch (120 thyristors in total)
Line frequency	50 Hz
Size of DC reactor	2 x 6 mH
Pulse mode operation	0 … 171 rpm / 0 … 10% of rated speed
Load-commutated operation	171 … 1'890 rpm / 10 … 110.2% of rated speed
Torsional natural frequencies (TNF)	10.8 Hz and 71.6 Hz
Project specific information: The critical speeds, i.e. crossings of interharmonics with first torsional natural frequency are inside the operating speed range. Active damping necessary otherwise coupling would have to be modified. First practical application of active torsional damper.	

Figure 8-2: LCI drive inside container of drive system as per Table 8 (courtesy of ABB)

Table 9: Fundamental data of drive system 3

Driven load	Centrifugal compressor
Motor type	Synchronous, salient pole rotor, 1'250 mm shaft height, brushless excitation, hazardous area
Stator winding	Dual star stator, 30 deg phase shifted windings
Motor rated power	21'000 kW
Motor rated voltage	2 x 3'030 V
Motor rated frequency	50 Hz

Motor min. / rated / max. speed	1'275 rpm / 1'500 rpm / 1'575 rpm
Compressor min. / rated / max. speed	3'412 rpm / 4'014 rpm / 4'215 rpm
Gear ratio	2.676
VFD topology	Load-commutated inverter (LCI)
VFD configuration	12-12 pulse, , n+1 thyristors per branch (72 thyristors in total)
Line frequency	50 Hz
Size of DC reactor	2.7 mH
Pulse mode operation	0 ... 150 rpm / 0 ... 10% of rated speed
Load-commutated operation	150 ... 1'575 rpm / 10 ... 105% of rated speed
Torsional natural frequencies (TNF)	17.6 Hz and 60.1 Hz

Project specific information:

Full load combined test / back to back test performed in dedicated test field. New control algorithms have been validated during the combined test. Further information regarding test setup for such systems can be found in [111].
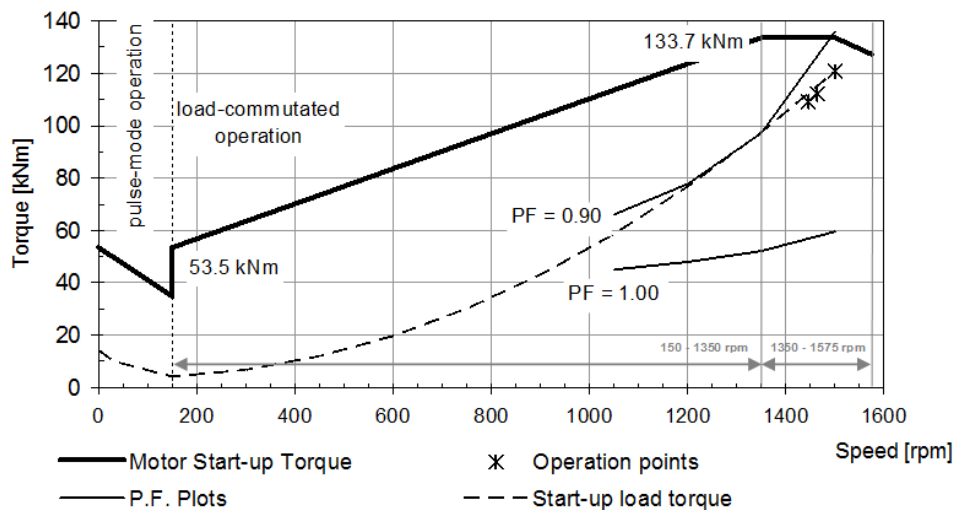

Figure 8-3: Speed – Torque characteristic of drive as per Table 9

Figure 8-4: Back-to-back test of drive system as per Table 9 (courtesy of ABB)

Figure 8-5: LCI converter with open doors (courtesy of ABB)

Table 10: Fundamental data of drive system 4

Driven load	Centrifugal compressor
Motor type	Synchronous, brushless excitation
Stator winding	Dual star stator, 30 deg phase shifted windings
Motor rated power	6'000 kW
Motor min. / rated / max. speed	1'050 rpm / 1'500 rpm / 1'575 rpm
Compressor min. / rated / max. speed	5'283 rpm / 7'547 rpm / 7'924 rpm
Gear ratio	5.0313 = 161/32
VFD topology	Load-commutated inverter (LCI)
VFD configuration	12-12 pulse
Pulse mode operation	0 … 150 rpm / 0 … 10% of rated speed
Load-commutated operation	150 … 1'575 rpm / 10 … 105% of rated speed
Torsional natural frequencies (TNF)	15.01 Hz and 77.81 Hz
Project specific information:	

Project specific information:

First torsional natural frequency is inside the operating speed range -> need to use restricted speed ranges. Elastic coupling with rubber elements had been used to provide more damping and operate at critical speeds. After upgrading with active torsional damper, the need for rubber coupling became obsolete.

Solution:

1. Torsional damper activated in order to expand controllable speed range.

Table 11: Fundamental data of drive system 5

Driven load	Three centrifugal compressors
Motor type	Synchronous, cylindrical rotor, brushless excitation, hazardous area
Stator winding	Dual star stator, 30 deg phase shifted windings
Motor rated power	20'000 kW
Motor rated voltage	2 x 3'930 V
Motor rated frequency	60 Hz
Motor min. / rated / max. speed	3'600 rpm
Compressor min. / rated / max. speed	not known

Gear ratio	not known
VFD topology	Load-commutated inverter (LCI)
VFD configuration	2 x 6-6 pulse
Line frequency	50 Hz
Size of DC reactor	2 x 7.5 mH
Pulse mode operation	0 … 216 rpm / 0 … 6% of rated speed
Load-commutated operation	216 … 3'960 rpm / 6 … 110% of rated speed
Torsional natural frequencies (TNF)	5.9 Hz, 11.6 Hz, 19.5 Hz, 23.2 Hz

Project specific information:

Large shaft string with multiple couplings. Mode shapes are complex with very low TNFs. Sub-synchronous torsional interaction with gas turbine generators (GTGs) located nearby → interactions on both grid and load side with conflicting requirements on current controller. Reference to conference paper [112].

Solution:

1. Optimized current controller based on frequency domain modelling. Compromise settings considering reference tracking and distrubance rejection.

2. Optimized feed-forward terms in control system to minimize interactions.

3. Torsional damper activated.

Table 12: Fundamental data of drive system 6

Driven load	Compressors
Motor type	Synchronous, brushless excitation
Stator winding	Dual star stator, 30 deg phase shifted windings
Motor rated power	24'500 kW (motor) / 23'650 kW (generator)
Motor rated voltage	2 x 4'500 V
Motor rated frequency	33.3 Hz
Motor rated speed	1'000 (const. speed) / 1'050 as max. speed (trip)
Compressor rated speed	1st stage: 4'651 rpm 2nd and 3rd stage: 6'511 rpm 4th and 5th stage: 9'767 rpm
Gear ratio	several gears
VFD topology	Load-commutated inverter (LCI)
VFD configuration	12-12 pulse, 3 thyristors per branch (72 thyristors in total)
Pulse mode operation	0 … 120 rpm / 0 … 12% of rated speed
Load-commutated operation	120 … 1'050 rpm / 12 … 105% of rated speed
Torsional natural frequencies (TNF)	4.55 Hz, 8.50 Hz, 19.70 Hz, 30.34 Hz

Project specific information:

The shaft string is very complex (see Figure 8-6) resulting in many torsional modes, not all of them controllable and/or observable. There is a steam turbine as main driver and expander and several compressor stages as loads. Motor rated frequency intentionally selected as 33.3 Hz (1'000 rpm) to avoid intersections with interharmonics. The drive system runs most of the time in generator mode feeding excessive energy back to electric grid. In dynamic operation, the drive system changes from generator to motor mode (power swing). Vibration is higher in generator mode – generally less damping. LCI torsional damper activated for 2nd and 3rd TNF.
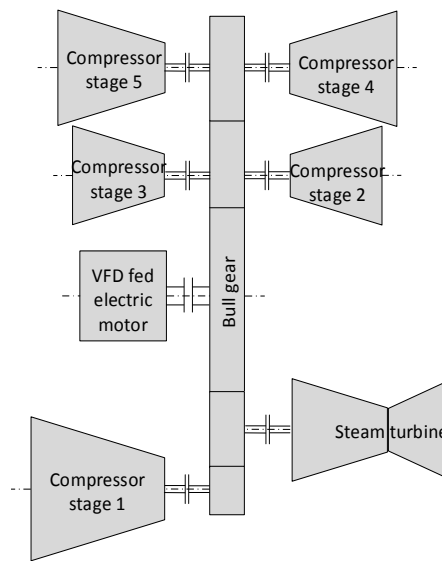
Figure 8-6: Shaft string of system as per
Table 12
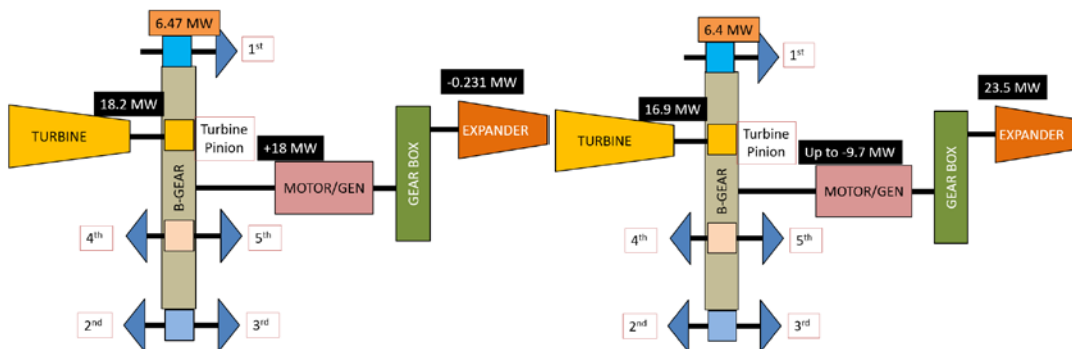
Figure 8-7: Average power distribution of system as per
Table 12 (left – gen, right – mot)

Table 13: Fundamental data of drive system 7

Driven load	Centrifugal compressor
Motor type	Synchronous, cylindrical rotor, 630 mm shaft height, brushless excitation, hazardous area
Stator winding	Dual star stator, 30 deg phase shifted windings
Motor rated power	20'000 kW

Motor rated voltage	2 x 3'930 V
Motor rated frequency	60.0 Hz
Motor min. / rated / max. speed	3'530 rpm / 3'600 rpm / 3'780 rpm
Compressor min. / rated / max. speed	not known
Gear ratio	not known
VFD topology	Load-commutated inverter (LCI)
VFD configuration	12-12 pulse, 3 thyristors per branch (72 thyristors in total)
Line frequency	50 Hz
Size of DC reactor	5 mH
Pulse mode operation	0 … 216 rpm / 0 … 6% of rated speed
Load-commutated operation	216 … 3'780 rpm / 6 … 105% of rated speed
Torsional natural frequencies (TNF)	8.5 Hz and 14.3 Hz (shaft train 1) 9.0 Hz and 15.1 Hz (shaft train 2)

Project specific information:

The shaft string is very complex – gas turbine as main driver, LCI used as starter/helper. Continuous operation range is rather narrow. There are multiple identical drives in this project. Some of them are speed controlled, others are torque controlled (from overriding control system).

Solution:

1. Detailed analytical modeling of drive system.

2. SSTI analysis performed by external company.

3. Small software modifications after first round of SSTI results.

The plant is in partial load operation and seems to work well. Full load operation not yet possible due to limitations on end user side (limited gas capacity).

Figure 8-8 depicts the motor during routine and type testing in the factory. This type of machine has low sub-transient reactance and allows exit from pulse mode at lower speed (6...8% nominal speed).
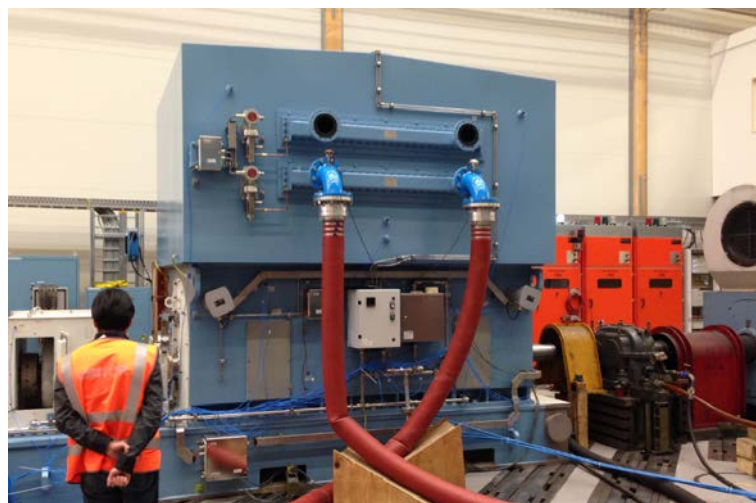

Figure 8-8: Factory motor test of drive system as per Table 13 (courtesy of ABB)

Table 14: Fundamental data of drive system 8

Driven load	Compressor
Motor type	Synchronous, brushless excitation
Stator winding	Dual star stator, 30 deg phase shifted windings
Motor rated power	37'000 kW
Motor rated voltage	2 x 6'100 V
Motor rated power factor	0.92 (capacitive)
Motor rated frequency / max. frequency	50 Hz / 63 Hz
Motor min. / base / rated / max. speed	1'260 rpm / 1'500 rpm / 1'800 rpm / 1'890 rpm
Compressor min. / rated / max. speed	5'549 rpm / 6'605 rpm / 7'927 rpm / 8'323 rpm
Gear ratio	4.4
VFD topology	Load-commutated inverter (LCI)
VFD configuration	12-12 pulse, 4+1 thyristors per branch (120 thyristors in total)
Line frequency	50 Hz
Size of DC reactor	2 x 4 mH
Pulse mode operation	0 … 150 rpm / 0 … 10% of rated speed
Load-commutated operation	150 … 1'890 rpm / 10 … 126% of rated speed
Torsional natural frequencies (TNF)	17.0 Hz (low speed coupling)
Project specific information: Large power drive system that underwent back-to-back test and string test before final installation at its destination. Model-based current controller.	

Table 15: Fundamental data of drive system 9

Driven load	Three (3) centrifugal compressors
Motor type	Induction, squirrel cage, 710 mm shaft height
Motor rated power	6'600 kW (110% overload for 180s every 30 min)
Motor rated frequency	85.5 Hz
Motor rated / max. speed	5'110 rpm / 5'588 rpm
Compressor rated / max. speed	same as motor
Gear ratio	N/A (gearless)
VFD topology	Voltage source inverter (VSI)
VFD configuration	36-pulse diode rectifier / 5-level inverter
Output filter	dv/dt filter
Torsional natural frequencies (TNF)	16.7 Hz and 63.9 Hz
Project specific information: Main driver is gas turbine (approx. 42 MW) and electric drive is used as starter/helper (see Figure 8-9). Vibration measurements performed with and without electric drive to quantify the impact of white noise. These measurements were neither performed nor evaluated by the author. However,	

the unique results illustrate the theory regarding white noise and experience from other drive systems with similar configurations and system designs where author was involved. Further information can be found in [38].
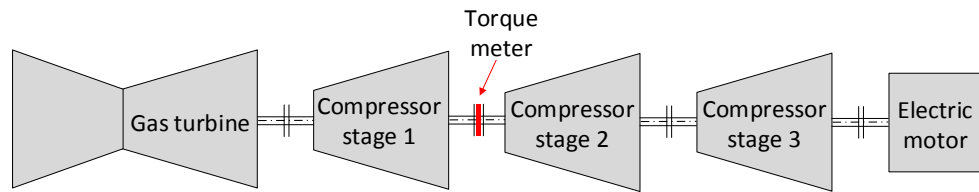

Figure 8-9: Shaft string of system as per
Table 15

Table 16: Fundamental data of drive system 10

Driven load	Centrifugal compressor
Motor type	Induction, squirrel cage, 800 mm shaft height
Motor rated power	8'700 kW (110% overload for 60s every 600s)
Motor min. / rated / max. speed	1'128 rpm / 1'318 rpm / 1'480rpm
Compressor min. / rated / max. speed	7'128 rpm / 8'332 rpm / 9'356 rpm
Bearing type on motor	Sleeve bearings
Gear ratio	6.32
VFD topology	Voltage source inverter (VSI)
VFD configuration	36-pulse diode rectifier / 5-level inverter
Output filter	dv/dt filter
Torsional natural frequencies (TNF)	16.7 Hz and 63.9 Hz

Project specific information:

Full load combined test was conducted before shipping the equipment to site for final installation. The setup is similar to the one described in [111]. Torsional analysis conducted for the test setup to verify the coupling selection. Calculation / simulation of transient torque during motor fault.

The full load combined test setup is illustrated in Figure 8-10. The project motor (grey painted), drive (bottom right) and transformer (top right) are loaded with two coupled induction machines working as generators and feeding power back to grid through 4-Q load converter.

Figure 8-10: Full load combined test of drive system as per Table 16

Table 17: Fundamental data of drive system 11

Driven load	Blower (axial compressor)
Motor type	Induction, squirrel cage
Motor rated power	8'400 kW (limitation to 7'600 kW)
Motor rated voltage	6'000 V
Motor min. / rated / max. speed	1'191 rpm / 1'492 rpm / 1'530rpm
Compressor min. / rated / max. speed	4'240 rpm / 5'313 rpm / 5'450 rpm
Gear ratio	3.561
VFD topology	Voltage source inverter (VSI)
VFD configuration	36-pulse diode rectifier / 5-level inverter
Output filter	dv/dt filter
Speed acquisition	Encoder / Observer (selectable)
Torsional natural frequencies (TNF)	17.5 Hz and 50.3 Hz

Project specific information:

Motor is designed for VFD as well as DOL operation and reconfigurable as 4-pole/6-pole. VFD equipped with synchronous bypass (continuous duty drive plus bypass as backup solution). However, due to vibration magnitude increasing with fundamental speed the rated speed for synchronization could initially not be reached. Motor is equipped with encoder; the drive can be operated with either encoder or encoder-less. First mode shape with torsional twist on high-speed coupling.

Solution:

1. Soft settings of speed controller (lower proportional gain, increased integration time constant).

2. Inertia compensation (add. feed-forward to main torque reference) used to eliminate speed overshoots during start-up.

3. Notch filter in the speed feedback loop activated and tuned for 17.5 Hz vibration frequency.

4. Compensation algorithm for long motor cables activated to stabilize the motor model.
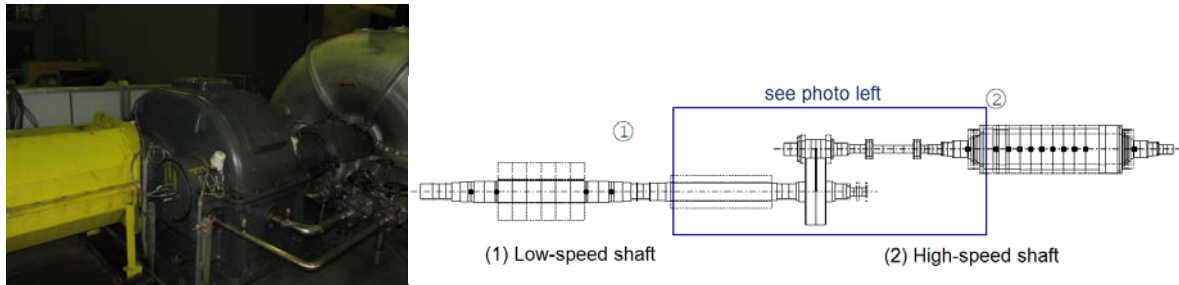
Figure 8-11: Coupling spacer, gear and compressor of drive system as per Table 17

Table 18: Fundamental data of drive system 12

Driven load	Centrifugal compressor
Motor type	Induction, squirrel cage
Motor rated power	6'100 kW (110% for 60s every 600s)
Motor rated voltage	3'100 V
Motor min. / rated / max. speed	1'200 rpm / 1'429 rpm / 1'500 rpm
Compressor min. / rated / max. speed	8'606 rpm / 10'249 rpm / 10'759 rpm
Gear ratio	7.17
VFD topology	Voltage source inverter (VSI)
VFD configuration	24-pulse diode rectifier / 3-level NPC inverter
Output filter	dv/dt filter
Torque control	DTC (scalar mode temporarily tested)
Speed acquisition	Observer (encoder-less)
Torsional natural frequencies (TNF)	17.0 Hz and 56.5 Hz

Project specific information:

Mitigation reached by reducing the gain of speed controller (PI type), activating bandpass (notch) filter is speed feedback loop, marginally increasing the switching frequency and optimizing the motor model with respect to long motor cables.

Problem description:

Initial very high vibration sustained due to high gain of speed controller.

Solution:

1. Soft settings of speed controller (lower proportional gain, increased integration time constant).

2. Notch filter in the speed feedback loop activated and tuned for 17.5 Hz vibration frequency.

3. Compensation algorithm for long motor cables activated to stabilize the motor model.

4. Marginal increase of switching frequency.

The solution approach was towards converter passivity, preservation of electric damping and minimization of electro-mechanical interaction.

Site successfully in operation since end of 2013 without any vibration issues.

Table 19: Fundamental data of drive system 13

Driven load	Centrifugal compressor
Motor type	Induction, squirrel cage, 630 mm shaft height
Motor rated power	3'900 kW
Motor rated voltage	3'300 V
Motor min. / rated / max. speed	1'050 rpm / 1'500 rpm / 1'575 rpm
Compressor min. / rated / max. speed	not known
Gear ratio	not known
VFD topology	Voltage source inverter (VSI)
VFD configuration	24-pulse diode rectifier / 3-level NPC inverter
Output filter	Sine filter
Torsional natural frequencies (TNF)	approx. 20.0 Hz
Project specific information: String test at compressor manufacturer conducted. Increased vibration observed. However, magnitude is variable and fluctuates even when operating in steady state. Rigorous fine-tuning of converter incl. changing the speed control from closed loop to open loop. Later on the drive system installed on an offshore platform and vibration issue never occurred again.	

Figure 8-12 shows the installation during string test at compressor manufacturer workshop.

Figure 8-12: String test of drive system as per Table 19 (courtesy of ABB)

Table 20: Fundamental data of drive system 14

Driven load	Centrifugal gas compressor
Motor type	Induction, squirrel cage, 500 mm shaft height
Motor rated power	2'500 kW (120% overload for 60s every 600s)
Motor rated voltage	3'300 V
Motor min. / rated / max. speed	1'176 rpm / 1'680 rpm / 1'764 rpm
Compressor min. / rated / max. speed	7'021 rpm / 10'249 rpm / 10'531 rpm
Gear ratio	5.97

VFD topology	Voltage source inverter (VSI)
VFD configuration	24-pulse diode rectifier / 3-level NPC inverter
Output filter	Sine filter
Speed acquisition	Observer (encoder-less)
Torsional natural frequencies (TNF)	17.01 Hz (calculated) / 17.5 Hz (observed)

Project specific information:

17.5 Hz vibration was visible across the speed range. Highest magnitude is at minimum speed (still significantly below alarm level). Tuning of speed controller and notch filter had small impact same as the increase of switching frequency. Active damping with FIR filter brought marginal improvement. Reduced flux reference increased motor damping. Scalar operation showed best results.

Table 21: Fundamental data of drive system 15

Driven load	Centrifugal compressor
Motor type	Induction, squirrel cage, 500 mm shaft height
Motor rated power	1'500 kW (110% overload for 60s every 600s)
Motor rated voltage	4'000 V
Motor rated torque	10'069 Nm
Motor min. / rated / max. speed	1'050 rpm / 1'422.5 rpm / 1'573.1 rpm
Compressor min. / rated / max. speed	not known
Gear ratio	not known
VFD topology	Voltage source inverter (VSI)
VFD configuration	24-pulse diode rectifier / 3-level NPC inverter
Output filter	Sine filter
Torque control	DTC
Speed acquisition	Observer (encoder-less)
Torsional natural frequencies (TNF)	19.7 Hz

Project specific information:

Speed controller optimized prior to commissioning using frequency characteristics. Notch filter in speed feedback recommended. Site measurements confirmed proper parameterization.

Table 22: Fundamental data of drive system 16

Driven load	Centrifugal compressor
Motor type	Induction, squirrel cage, 560 mm shaft height
Motor rated power	3'400 kW (110% overload for 60s every 600s)
Motor rated voltage	5'500 V
Motor rated torque	22'193 Nm
Motor min. / rated / max. speed	1'050 rpm / 1'463.0 rpm / 1'575.3 rpm
Compressor min. / rated / max. speed	not known
Gear ratio	not known

VFD topology	Voltage source inverter (VSI)
VFD configuration	36-pulse diode rectifier / 5-level NPC inverter
Output filter	dv/dt filter
Torque control	DTC
Speed acquisition	Observer (encoder-less)
Torsional natural frequencies (TNF)	22.15 Hz
Project specific information:	
Speed controller optimized prior to commissioning using frequency characteristics. Notch filter in speed feedback recommended. Site measurements confirmed proper parameterization.	

Table 23: Fundamental data of drive system 17

Driven load	Centrifugal compressor
Motor type	Induction, squirrel cage, 500 mm shaft height
Motor rated power	2'300 kW
Motor rated voltage	6'000 V
Motor rated torque	12'203 Nm
Motor min. / rated / max. speed	1'260 rpm / 1'800 rpm / 1'890 rpm
Compressor min. / rated / max. speed	not known
Gear ratio	not known
VFD topology	Voltage source inverter (VSI)
VFD configuration	36-pulse diode rectifier / 5-level NPC inverter
Output filter	dv/dt filter
Torque control	DTC
Speed acquisition	Observer (encoder-less)
Torsional natural frequencies (TNF)	26.1 Hz (twist on low speed coupling)
Project specific information:	
Speed controller optimized prior to commissioning using frequency characteristics and elastic shaft model. Notch filter in speed feedback activated. Site measurements confirmed proper parameterization.	

Table 24: Fundamental data of drive system 18

Driven load	Blower (compressor) with 4 stages
Motor type	Induction, squirrel cage, 710 mm shaft height
Motor rated power	4'620 kW
Motor rated voltage	6'000 V
Motor rated torque	29'628 Nm
Motor rated speed	1'489 rpm
Compressor rated speed	1st and 2nd stage: 14'672 rpm 3rd and 4th stage: 23'397 rpm

Gear ratio	9.85 and 15.71
VFD topology	Voltage source inverter (VSI)
VFD configuration	36-pulse diode rectifier / 5-level NPC inverter
Output filter	dv/dt filter
Torque control	DTC
Speed acquisition	Observer (encoder-less)
Torsional natural frequencies (TNF)	22.0 Hz

Project specific information:
Retrofit of fix speed motor operating inside heavy-duty plant. Polluted electric grid with frequent voltage dips. Compressor suffered from vibration induced from distorted grid into motor air gap torque. Another issue is critical speed close to nominal speed. The VFD shall decouple the grid from the motor. Careful VFD tuning required.

8.2   Methods of torque measurement

8.2.1   External torque meter

A direct torque measurement is not an easy task. While a shaft torque measurement is feasible at low power, it becomes a huge effort in large multi-megawatt drive systems. Direct shaft torque measurement requires an additional element on the shaft – surface mounted strain gauges or torque meter (used in drive systems as per Table 7 and Table 15 during internal tests). For torques above 2 kNm it is almost exclusively a flange type torque meter. Strain gauges might be used for temporary measurements during validation tests (see fig. 8 in [39]). In such case the overall torsional behavior of the string is modified due to the elasticity of torque flange. The measurement electronics consists of strain gauges in full bridge connection, a converter that converts torque into frequency (typically 60 kHz ± 30 kHz), analog amplifier, digital amplifier, digital filtering etc. The analog stage is crucial for the accuracy and weak analog stage cannot be compensated by the best digital stage. The torque flange is available in accuracy class from 0.1% up to 0.03% (referenced to rated torque). However, a torque meter that can measure rated torques of several kNm is a very costly device. Further to that, the maximum withstand torque limit is typically somewhere between 1.3 to 2.0 times rated torque. If this value is exceeded during transient overload, the torque meter is damaged or shows a permanent offset. Dimensioning the torque meter for the peak torques that can occur (e.g. during three-phase fault) might become unaffordable or impossible. An alternative is a protection ("mechanical fuse") which again adds cost and complexity. Mechanical safety coupling has response time of approx. 100 ms and the torque meter can still see 4.0 to 5.0 times rated torque. In other words, it might be too slow to protect the torque meter against overload. An alternative is a hydraulic safety coupling that is roughly 10-times faster, i.e. with about 10 ms response time.

The installation requires attention with regard to radial, axial and angular displacement.

A rough cost of torque meters (device itself, not considered installation cost):

- Up to 15 kNm, accuracy class 0.05:   20'000 EUR (status 2016)

- Up to 10 kNm, accuracy class 0.03:   30'000 EUR (status 2016)

Remark: A simple strain gauge sensor has virtually no time delay while a torque coupling has some small time delay due to internal signal processing. In the chapter related to control the impact of time delays and latencies is explained. Because of the challenges described above, direct measurement of torque is not always practical. Instead, several indirect methods have been developed. They usually rely on computation of torque as a product of current and flux.

8.2.2   Torque calculation by VFD

The air gap torque can be calculated directly in VFD motor control – see Appendix 7 – Vector control and direct torque control schemes. Then it is easy to trend it or synchronize the torque signal with other quantities measured or calculated by VFD.

Special applications such as ultrasonic wind tunnels or turbomachinery test stands may require very high torque accuracy. The VFD control can typically achieve high relative accuracy. Especially with direct torque control (DTC) the air gap torque is calculated with satisfactory accuracy. Relative accuracy related to reference and actual values of torque is extremely high and the frequency spectrum is typically accurate enough. Absolute accuracy (torque in Nm) is a bit lower, say about +/- 2…5% of nominal torque. If better absolute accuracy is required, then an overriding control system with a torque meter might be the recommended solution.

In the validation measurements described in next chapter the torque was calculated by VFD (in VSI drives the motor torque is calculated by the motor model in VFD controls, in LCI drives the dc link current is used and converter into torque). In some of the validation measurements an additional torque measurement by strain gauges was installed. Almost in all cases the lateral vibration level was measured. Although it is not a torque measurement, the lateral vibration in geared systems is closely linked to torsional vibration as explained earlier.

8.3   Validation measurements

The system acc. Table 7 underwent a string test before shipping to site. Due to critical speeds inside the speed range the torsional (active) damper was found to be necessary (based on closed loop simulations). One of the goals of string test was the validation of torsional damper on a real drive. The most interesting results are shown in Figure 8-13. The drive accelerates into resonance – critical speed at 1'530 rpm. The gain K_{RI} of current controller is temporarily reduced to half and increased back to original value (0.32 → 0.16 → 0.32). With lower gain the vibration slightly increases. Approx. 90 seconds later, the active damping is enabled. Immediate reduction of vibration magnitude is observed (color change from orange to yellow). The gain of active damper is gradually increased from 1.0 to 1.3. Then the active damper is switched off followed by immediate vibration increase. Some 120 seconds later the speed is increased from 1'530 rpm to 1'533 rpm. The system vibrates much less as the resonance window is very narrow (low damping). The torsional damper is once more activated and

deactivated. The colorbar on the right side of Figure 8-13 allows to determine the reduction of vibration. The magnitude is approx. 3-times less when the torsional damper is active. The result of string test is in line with simulations where same reduction of vibration was observed (compare with Figure 7-21 and Figure 7-22).
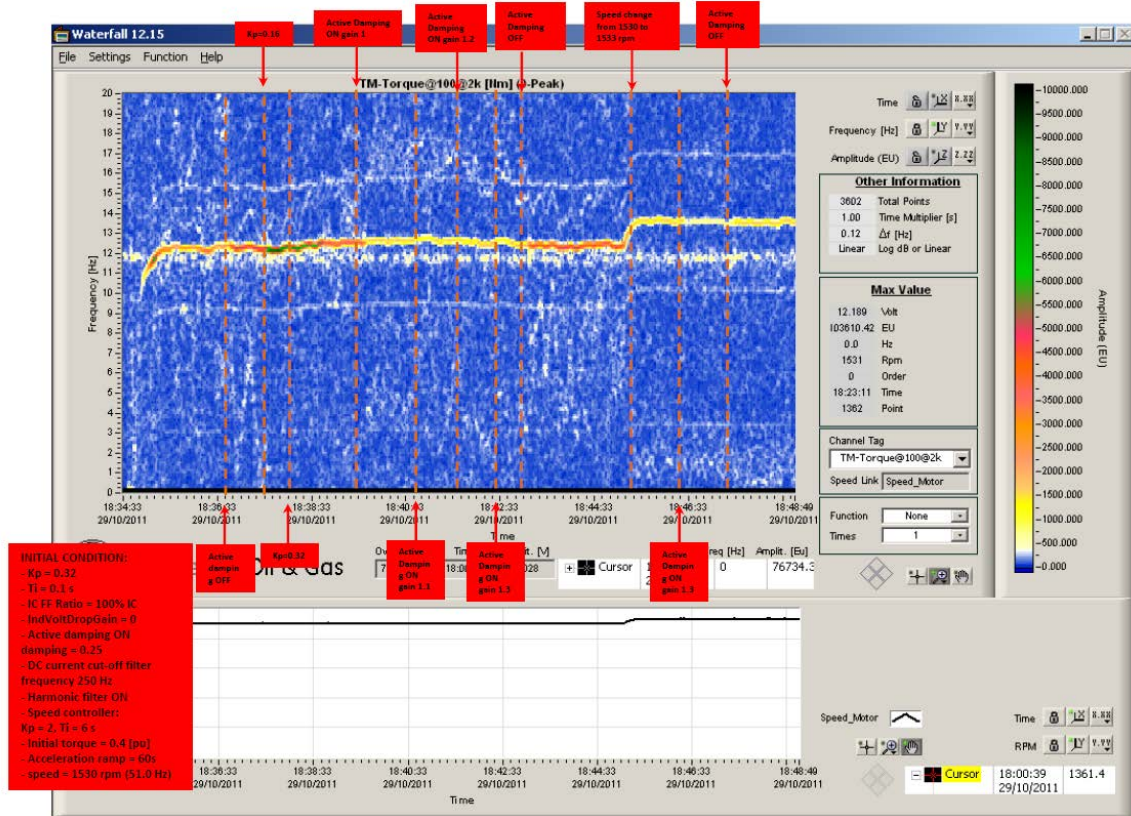
Figure 8-13: Validation of LCI torsional damper during string test

String test measurements of drive system as per Table 7 are shown below in Figure 8-14, Figure 8-15 and Figure 8-16. Figure 8-14 shows the line side and motor side alternating phase-phase voltages with characteristic commutation notches. Figure 8-15 shows the current in dc link with characteristic ripple. High frequency ripple (12*fN) of 600 Hz is visible as well as low frequency fluctuation (12*fN – 12*fM) of approx. 52 Hz.
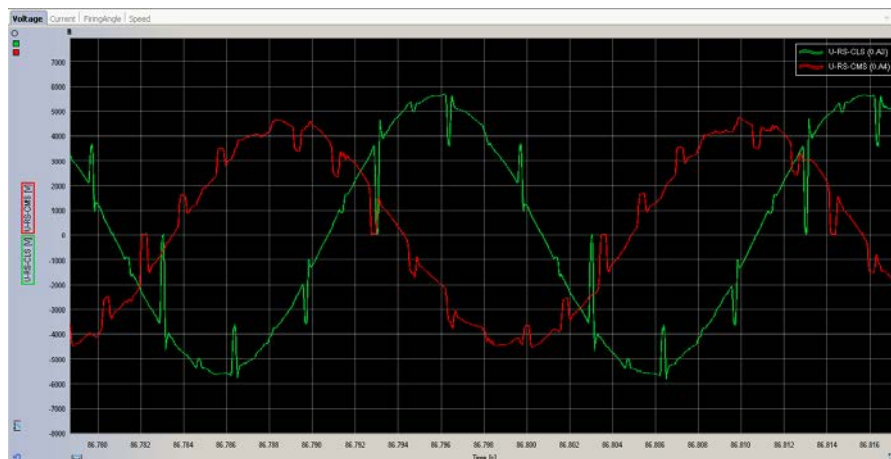
Figure 8-14: Line side and motor side voltages (green – line side, red – motor side)
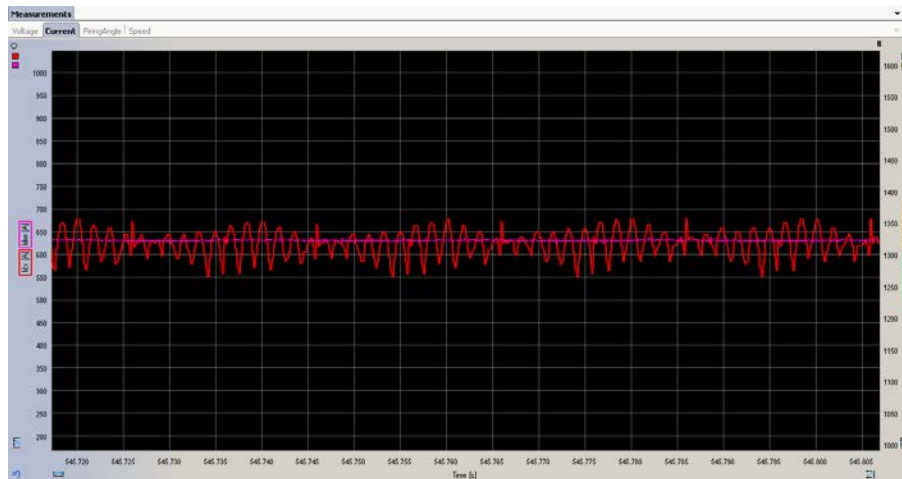
Figure 8-15: Current in dc link at 1'370 rpm (magenta – ref. value, red – actual value)

Figure 8-16 captures the start-up at low speed including transition from pulse mode to load commutated mode. Due to fix current reference in pulse mode there is a speed error between reference (yellow) and actual speed (green) which is then compensated as the drive accelerates.
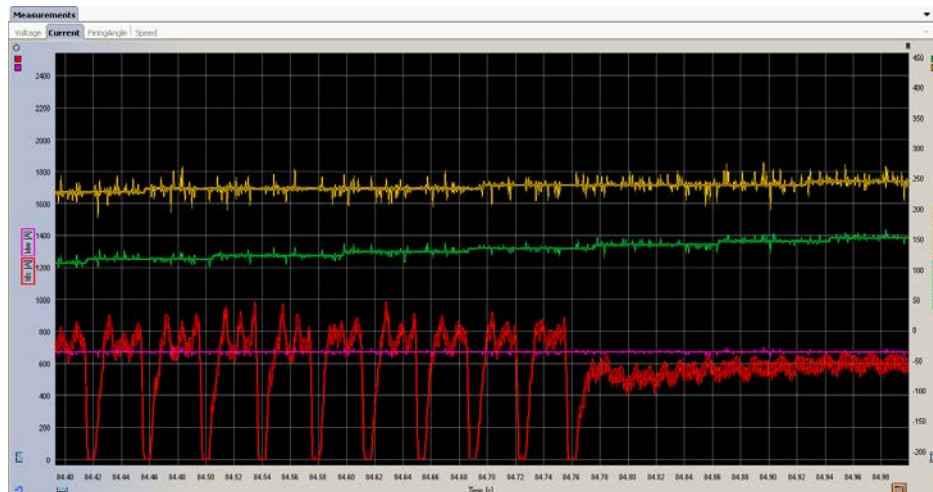
Figure 8-16: LCI start-up and transition from pulse mode to load commutated mode (magenta – current reference, red – actual current, yellow – speed reference, green – actual speed)

Measurements of system acc.

Table 14 during Back-to-back test can be seen in Figure 8-17. As this test is performed without driven load, the vibration performance could not be checked. However, the test validated the settings of current controller determined with model based approach. Figure 8-17a shows motor voltage and current for the rated point 37 MW / 1'800 rpm and Figure 8-17b shows the guarantee point.

(a) 37'000 kW, 1'800 rpm

(b) 30'500 kW, 1'761 rpm
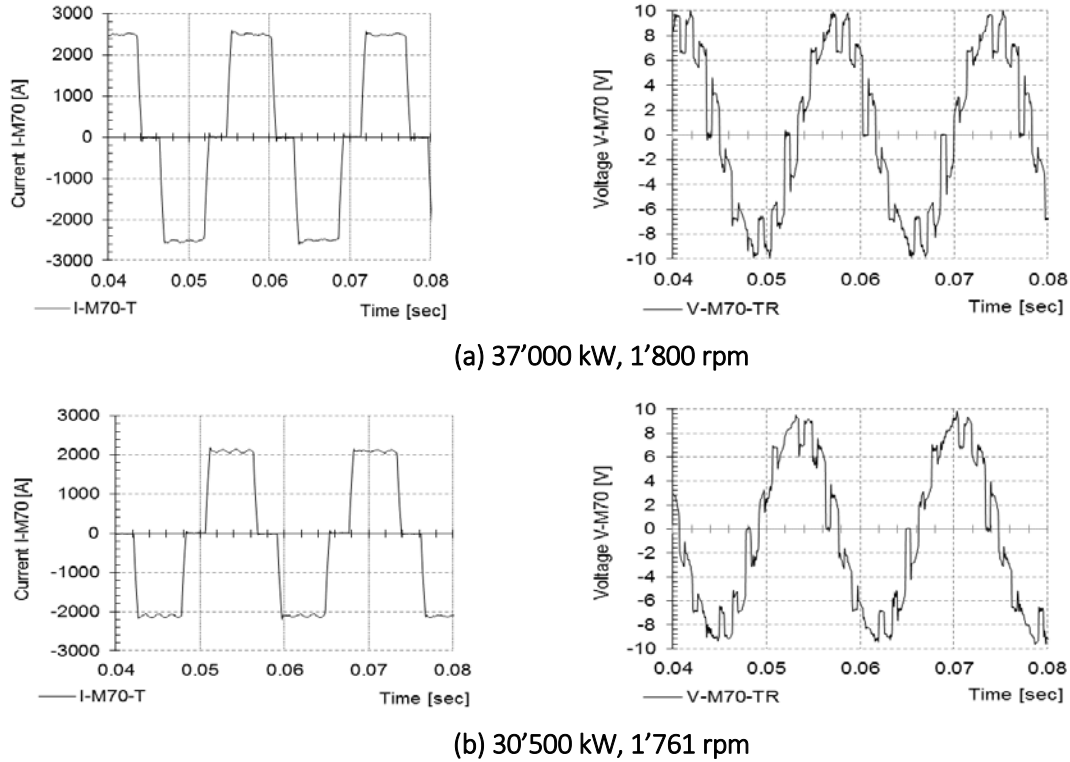
Figure 8-17: LCI motor current and voltage during back-to-back test

Torque measurement of drive system acc. Table 16 during combined test in shown in Figure 8-18. Torque fluctuation: Mean value: 91.8%, min. value: 86.8%, max. value: 96.3%. Although the peak-peak torque ripple is almost 10% of actual mean torque (9% of rated torque), the individual frequency components have small magnitude (all of them well below 1%).
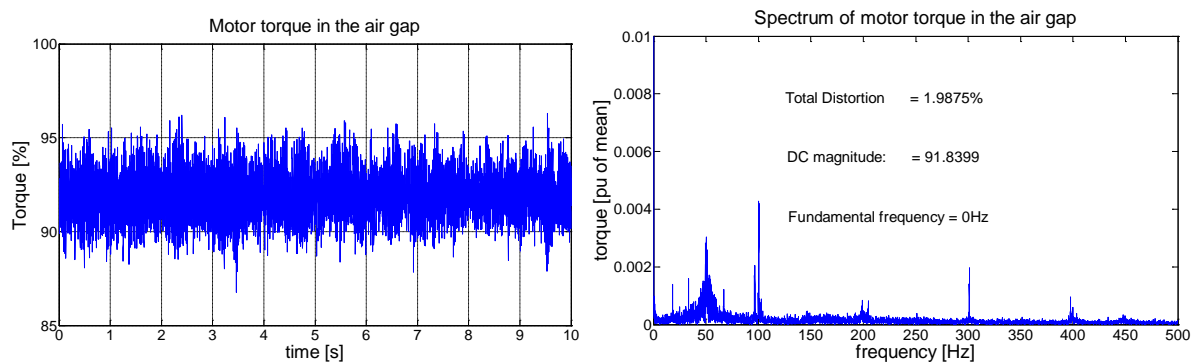
Figure 8-18: Torque trend from the VFD commissioning software and plotted in Matlab

Site described in Table 18 suffered from vibration and rigorous analytical and numerical study as well as extensive measurement campaign was conducted. The mitigation was done by changing settings of speed controller, introducing a notch filter in speed feedback loop, modifying the motor model with

regards to long motor cables (over 300 m) and increasing switching frequency. The final parameterization was verified by driving a speed and torque profile as shown in Figure 8-29. After a faster ramp the drive reaches 1'000 rpm and dwells shortly at that speed. Then the speed gradually increases up to nominal speed, reaches steady state and finally ramps down to 1'000 rpm again. The torque is given by the load. Since it is a centrifugal compressor, the load torque T_L is roughly proprotional to the square of speed n ($T_L \sim n^2$).
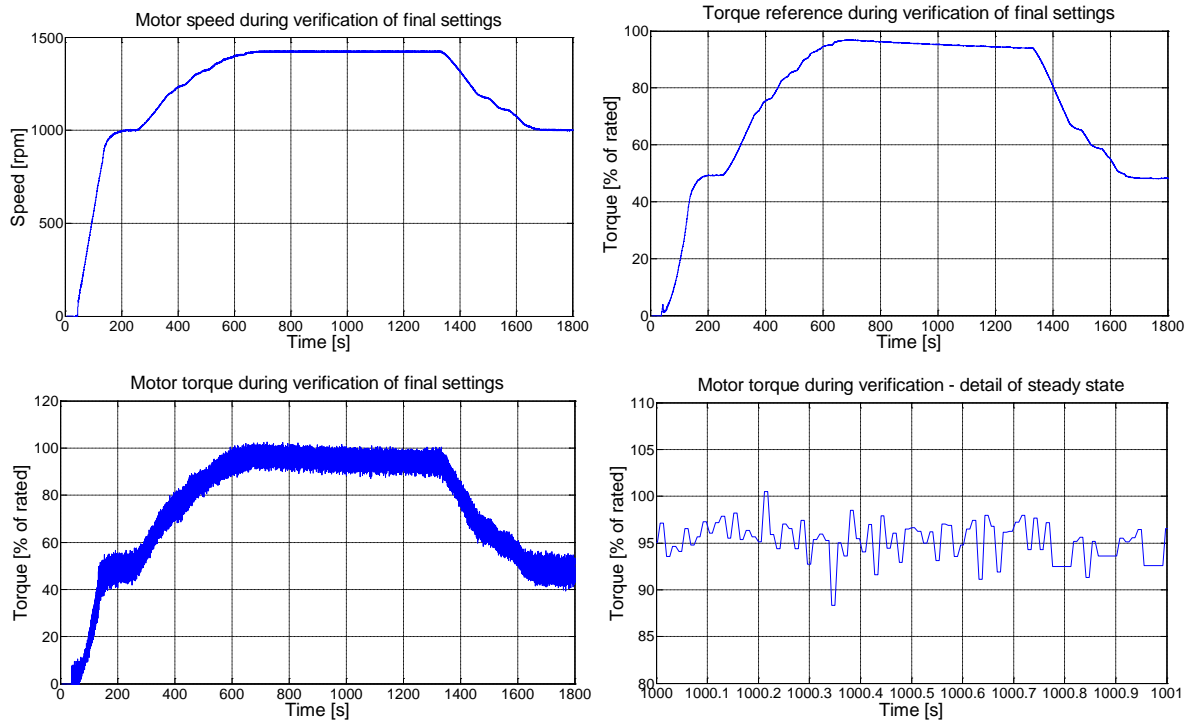
Figure 8-19: Speed and torque profile of system acc. Table 18 during site tuning

Distorted motor current due to long motor cables is depicted in Figure 8-20. Since the motor currents arte inputs of motor model, their distortion might disturb the model and the calculation of motor torque is affected as well. Increased calculated rate over measured portion might help to get smoother torque.
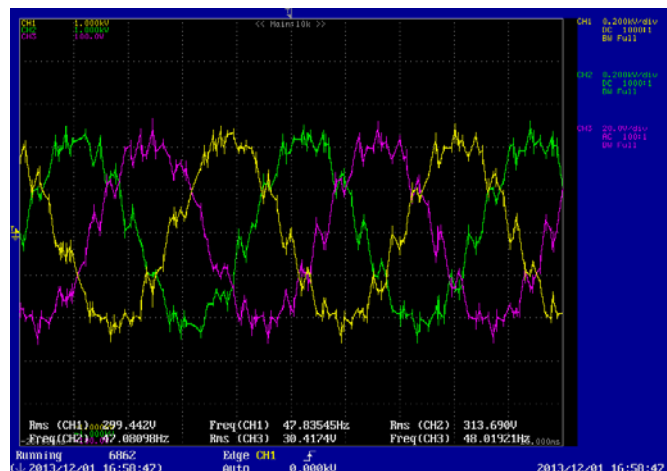
Figure 8-20: Motor current distorted due to long cables

The torque spectrum after final tuning on site is displayed in Figure 8-21. It is the steady state section at nominal speed in Figure 8-19. The focus is on low frequency components that could excite the 1st TNF (17.5 Hz). As this is just „white noise", the magnitude is not constant. FFT is actually defined for repetitive signals only. The numerical implementation works for stochastic signals as well. However, the results are inherently averaged. This is obvious in left part of Figure 8-21 (100 s interval) and right part (400 s interval).
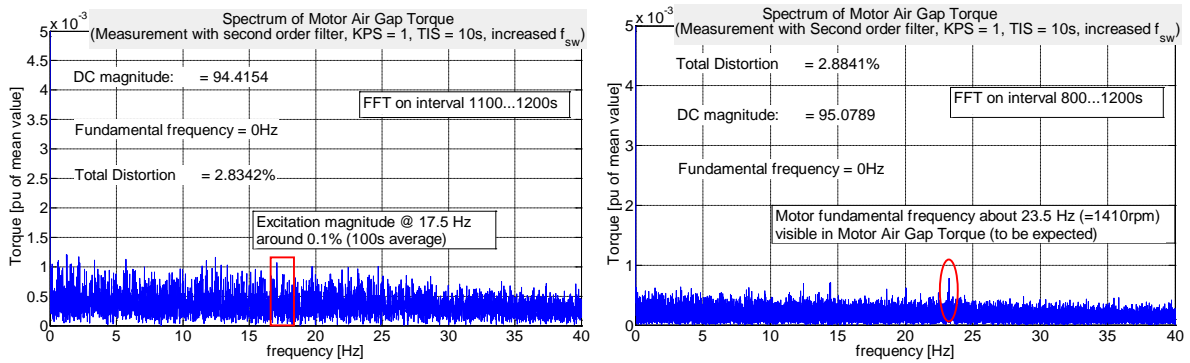
Figure 8-21: Spectrum of air gap torque of system acc. Table 18
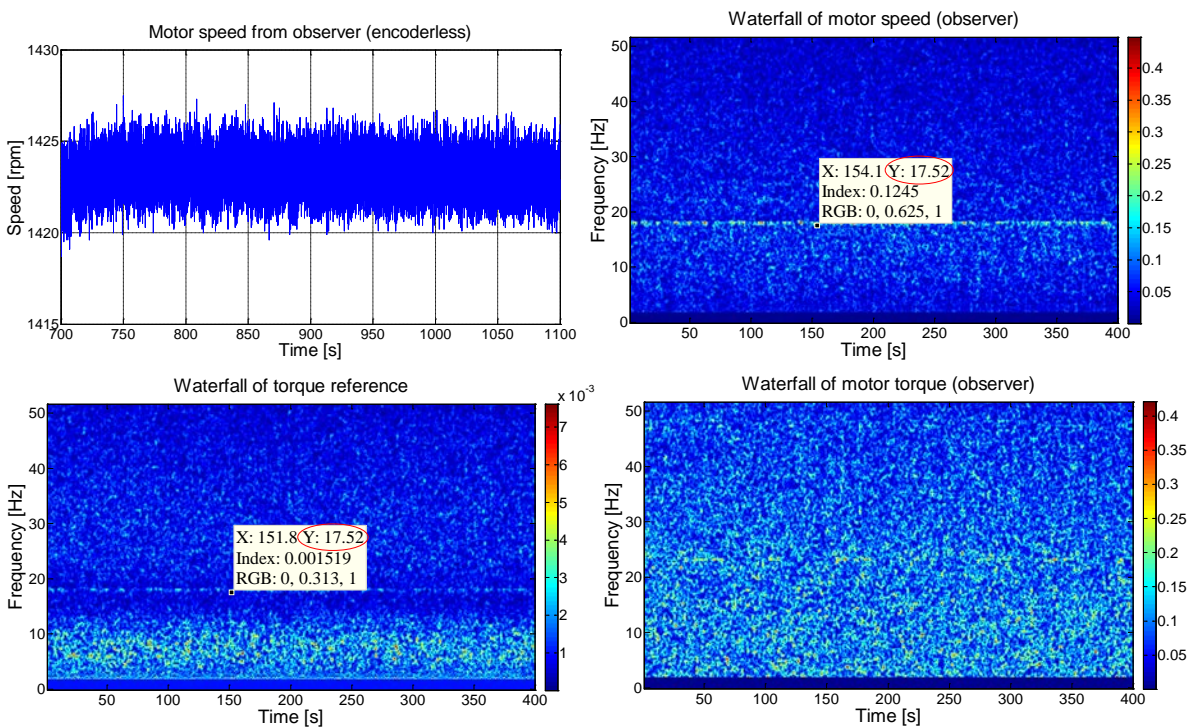
Figure 8-22: Waterfall of motor torque and speed of system acc. Table 18

The lateral vibration on the low-speed side of gear was measured in order to see the impact of drive parameter tuning. There are two sets of probes with geometric shift of 90 degree and therefore two plots for each measurement. Torsional and lateral vibration is coupled through the gear mesh. As seen in Figure 8-23 the vibration magnitude was drastically reduced when comparing plots on left side

(initial settings) and right side (final settings). The plots have frequency content on the x-axis while y-axis shows the fundamental speed.
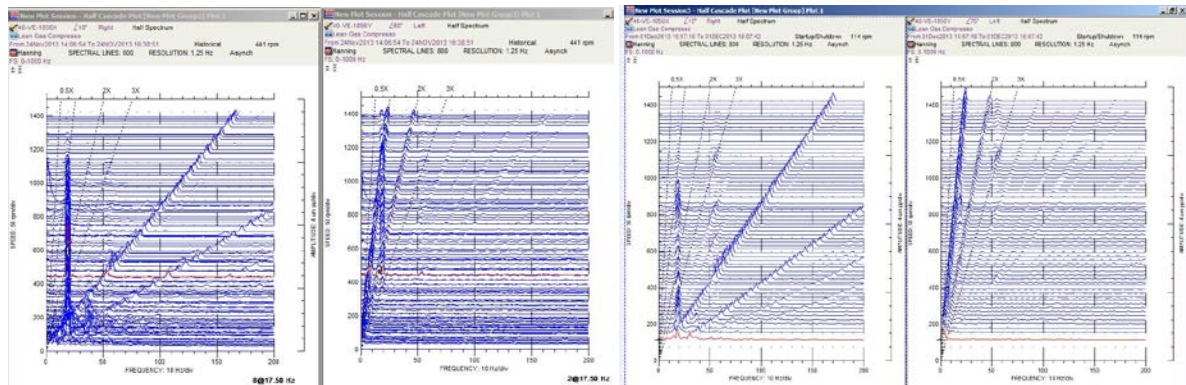
Figure 8-23: Lateral vibration of gear low-speed shaft of system acc. Table 18

Solution for system acc. Table 18:

1. Soft settings of speed controller (lower proportional gain, larger integration time constant).
2. Notch filter in speed feedback loop activated.
3. Compensation algorithm for long motor cables to stabilize motor model activated.
4. Marginal increase of switching frequency.

The solution approach was towards converter passivity, preservation of electric damping and minimization of electro-mechanical interaction.

Site measurements of system acc. Table 20 revealed a small imbalance on the shaft seen as '2X' component (2-times fundamental shaft frequency) summarized in Table 25. The imbalance was not the root cause of vibration, but it demonstrates the diagnostic possibilities of VFD (imbalance detected by motor model just based on motor current and dc voltage).

Table 25: Correlation between shaft speed and vibration component

Measurement [#]	Motor speed [rpm]	Motor frequency [Hz]	2X component (calculated) [Hz]	Motor torque (measured) [Hz]	Vibration component [Hz]	Vibration magn. [%]
1	1176	19.6	39.2	39.5	17.5	1.56E-03
2	1417	23.6	47.2	47.3	17.3	7.52E-04
3	1303	21.7	43.4	43.5	17.4	9.74E-04
4	1177	19.6	39.2	39.3	17.5	1.04E-03
5	1639	27.3	54.6	54.8	17.3	6.54E-04
6	1628	27.1	54.3	54.5	17.4	1.08E-03

The 2'500 kW compressor drive system experienced increased vibration at first TNF (17.5 Hz). The vibration was highest at the minimum speed (approx. 30 µm) and reduced at higher speed. This might be linked with the stiffness of the bearings that increases with load. The first mode shape is depicted in Figure 8-24. The frequency converter was already parameterized for slow dynamics / passive

behavior: low proportional gain of speed controller, notch filter blocking the vibration component from speed error.
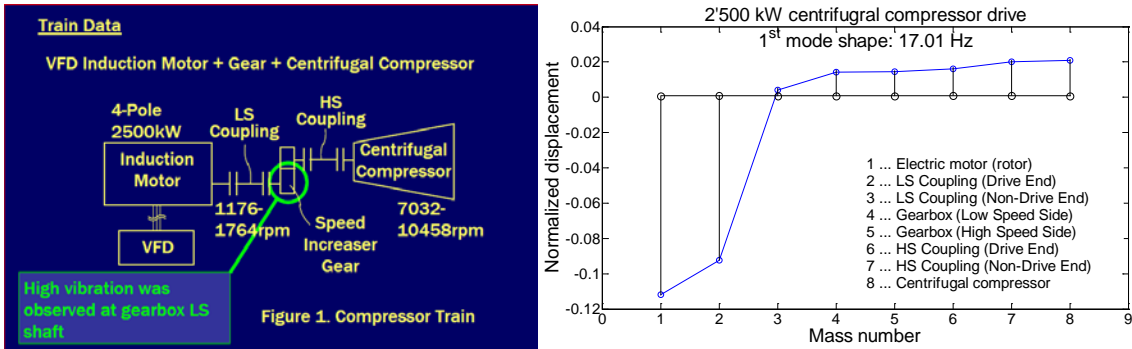
Figure 8-24: Shaft string data and first mode shape of drive system acc. Table 20

The tuning on site was performed in following steps:

Variation of switching frequency: 480...600 Hz (per switch) → no impact on vibration

FIR filter for active damping: Small improvement

Open loop (scalar) mode: Significant improvement (but loss of certain functionality -> changed back to closed loop) – see Figure 8-28.

Reduction of stator flux: Improvement (motor damping increased)

The vibration behavior practically did not change when varying the switching frequency as seen in Figure 8-25 and confirmed by lateral vibration measurement on the gearbox.
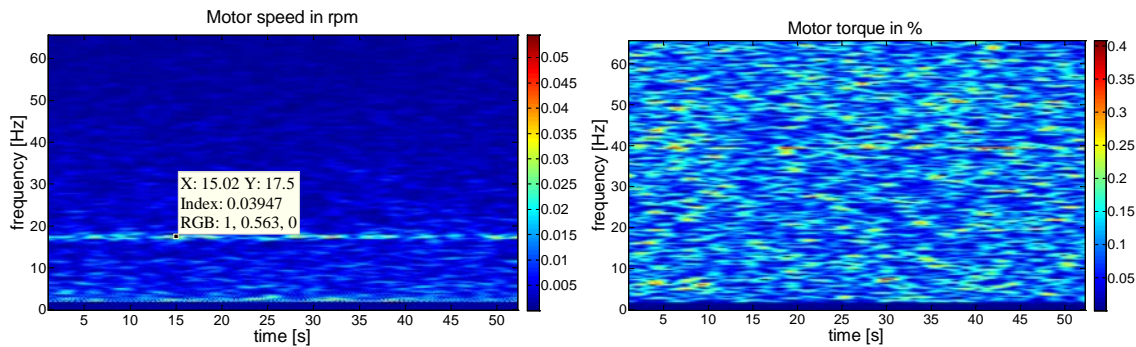
a) standard switching frequency
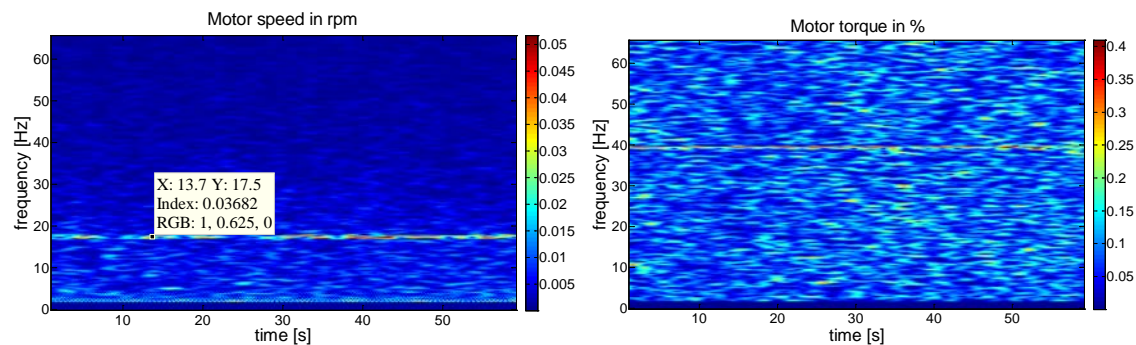
b) high switching frequency

Figure 8-25: Waterfall of motor speed and torque at 1'176 rpm

FIR filter was activated as attempt for active damping and the phase displacement was tuned. The output of FIR filter as additional torque reference summed up with torque reference from speed controller. The signal is seen in Figure 8-26. Since the magnitude of this additional torque reference is very small, the damping effect was very limited.
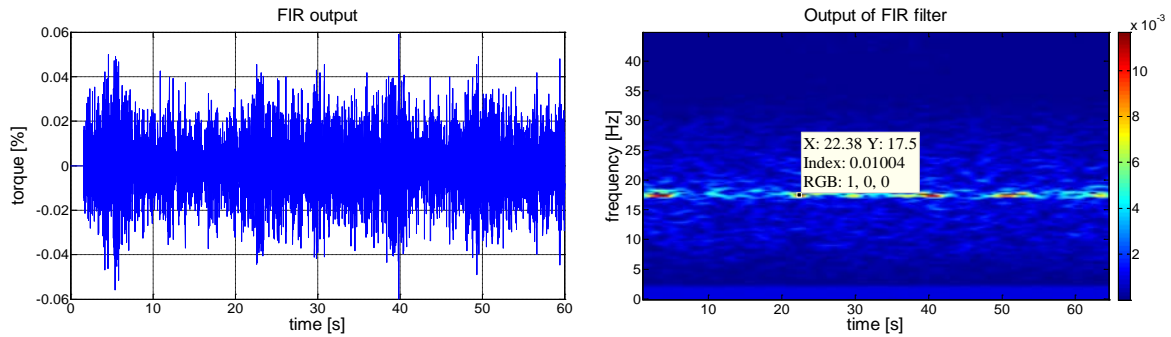
Figure 8-26: Output of FIR filter (add. torque ref)
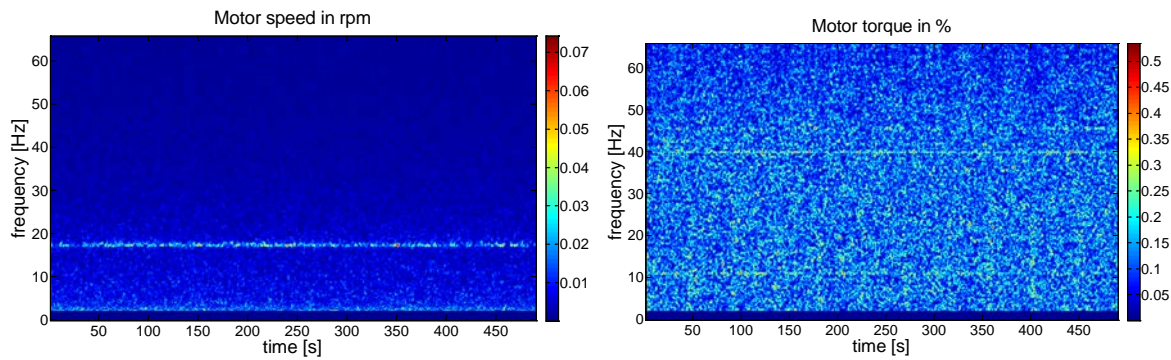
a) closed loop control (DTC)
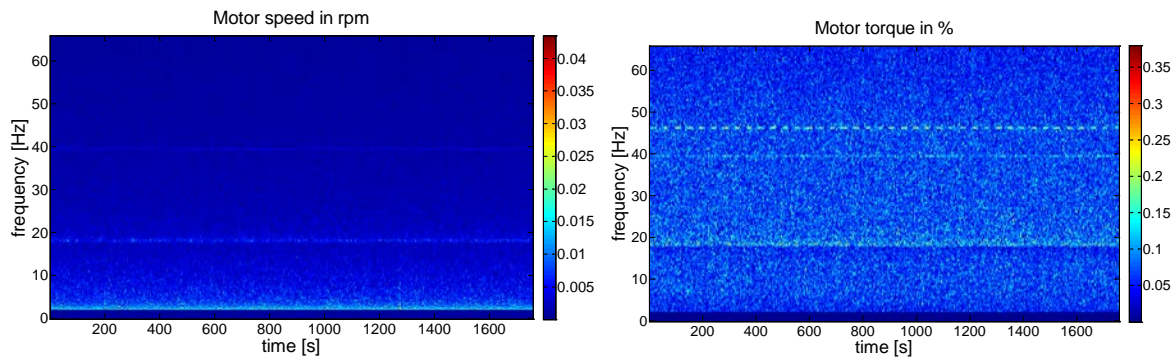
a) open loop control (Scalar)

Figure 8-27: Waterfall of motor speed and torque at 1'176 rpm

Final modification was the change of control mode from closed loop DTC into open loop (scalar) mode. There was a very positive impact on the vibration as seen in Figure 8-27. Note that the motor model is still running in the control in scalr mode and the calculated motor torque and speed is available. Figure 8-28 shows the vibration measurements over several days - the complete tuning excercise on site. Pink line represents the speed of the motor. Black and blue curves are the gear vibration signals (two sets of vibration probes). There is an obvious trend of higher vibration at lower speed. At the end of third day the drive control mode was changed from DTC to scalar. The vibration was immediatelly

reduced. However, due to other performance limitations the control was changed back to closed loop and drive was fine tuned and finally found acceptable. Note that initial vibration was up to 30 µm and final vibration 15-20 µm. The alarm level was set to 90 µm and trip level 120 µm.

Solution for system acc. Table 20:

1. Active compensation (damping) of visible speed oscillations.
2. Reduced stator flux reference -> increased electric damping.
3. Open loop (scalar) speed control (temporarily for test purpose).
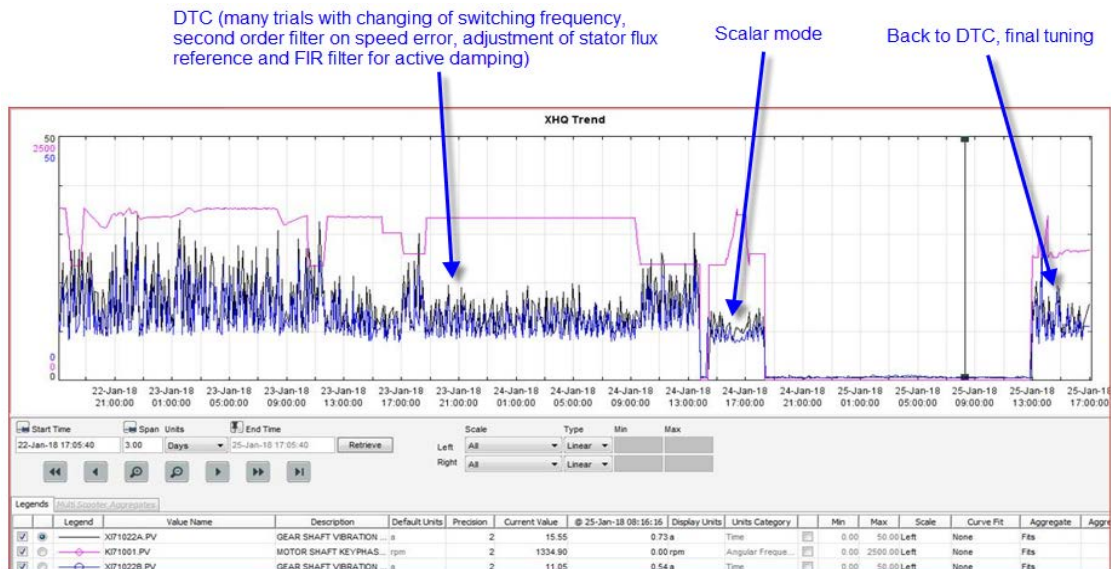
Figure 8-28: Vibration measurement in DTC and scalar mode of drive system acc. Table 20

The solution approach was first towards converter passivity. Since it was not sufficient, active damping was enabled as well. Due to the fact that vibration on the gear was increased, but motor vibration was fairly low, the potential improvement using active damping was very limited.

Examples of real measurements without and with notch filter inserted before speed controller (on speed error) are presented for comparison:

Example 1 with system data acc. Table 21: 1'500 kW compressor drive with VSI converter; first TNF expected at 19.7 Hz. Bandstop filter on speed error disabled during first measurement. Speed sweep performed in almost entire speed range for better correlation between motor fundamental frequency and components in torque and speed spectrum.

Motor speed

Motor speed in rpm (no filter)

Torque reference in % (no filter)
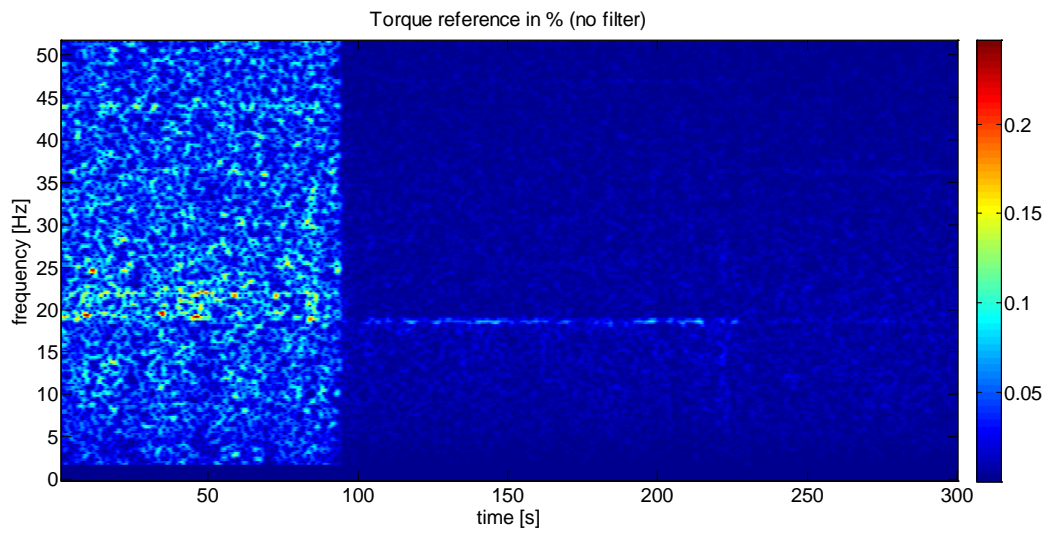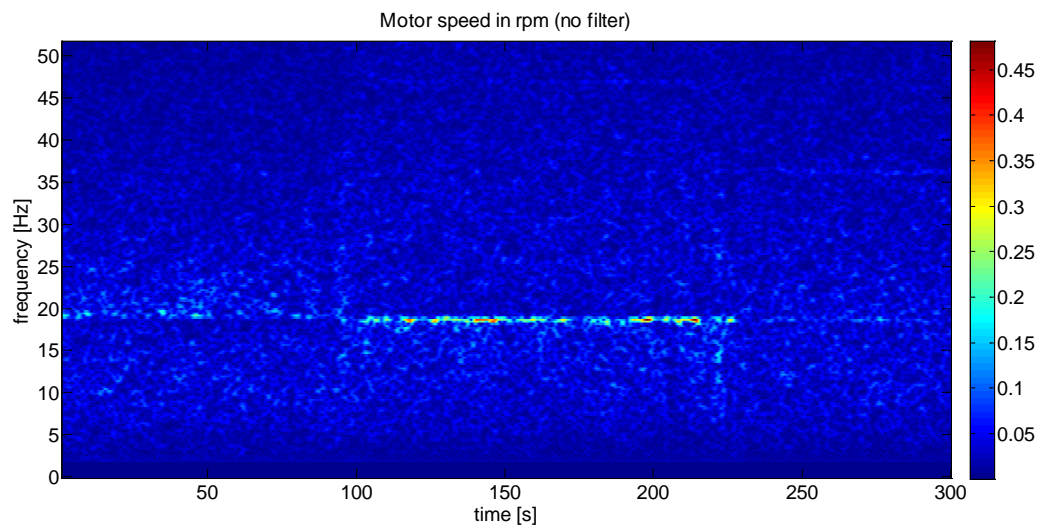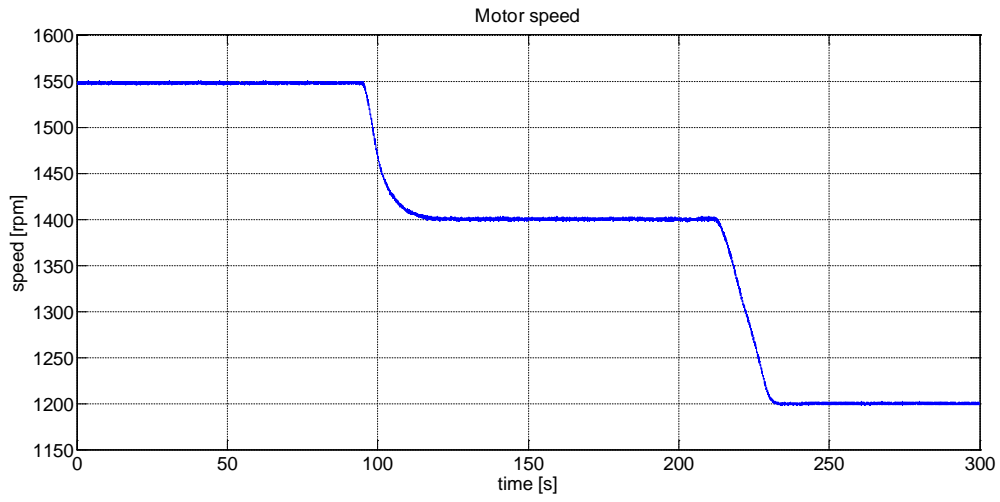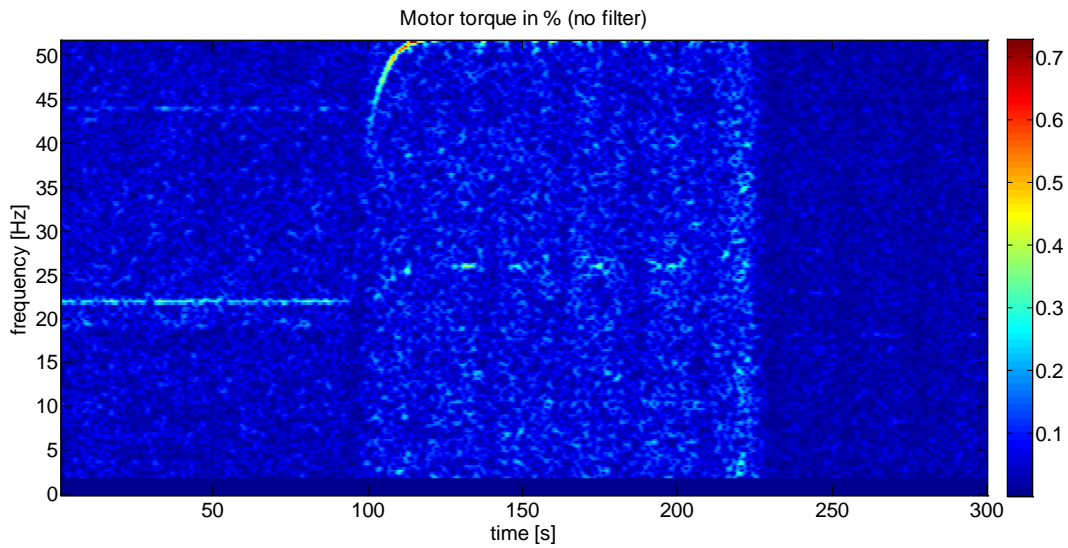
Figure 8-29: Motor speed, torque ref and motor torque with disabled band-stop (notch) filter

Example 2 with system data acc. Table 22: 3'400 kW compressor drive with VSI converter; first TNF expected at 22.15 Hz. Bandstop filter on speed error enabled during measurement.
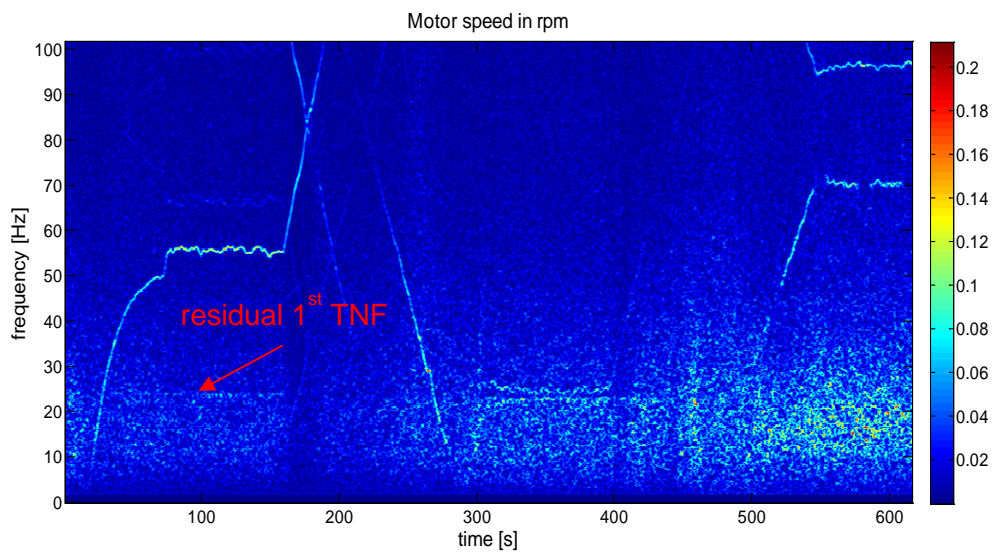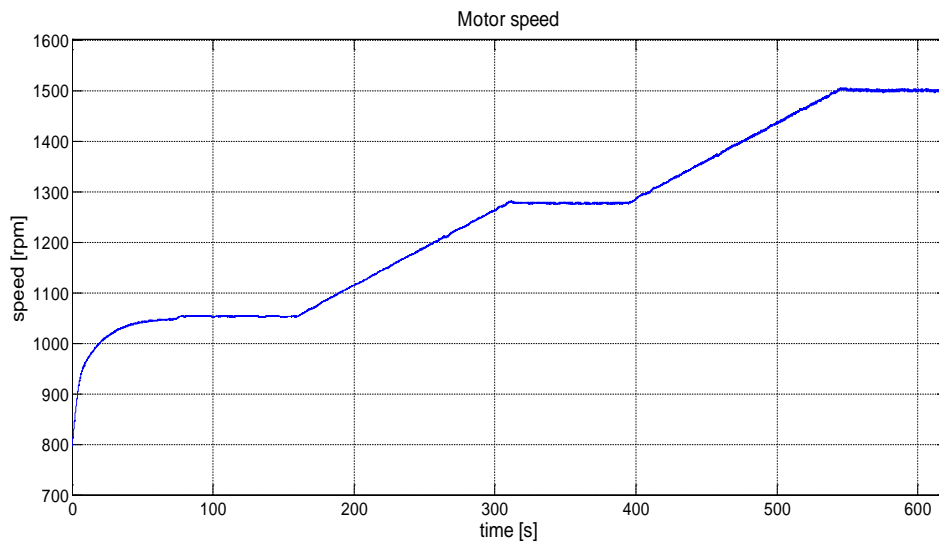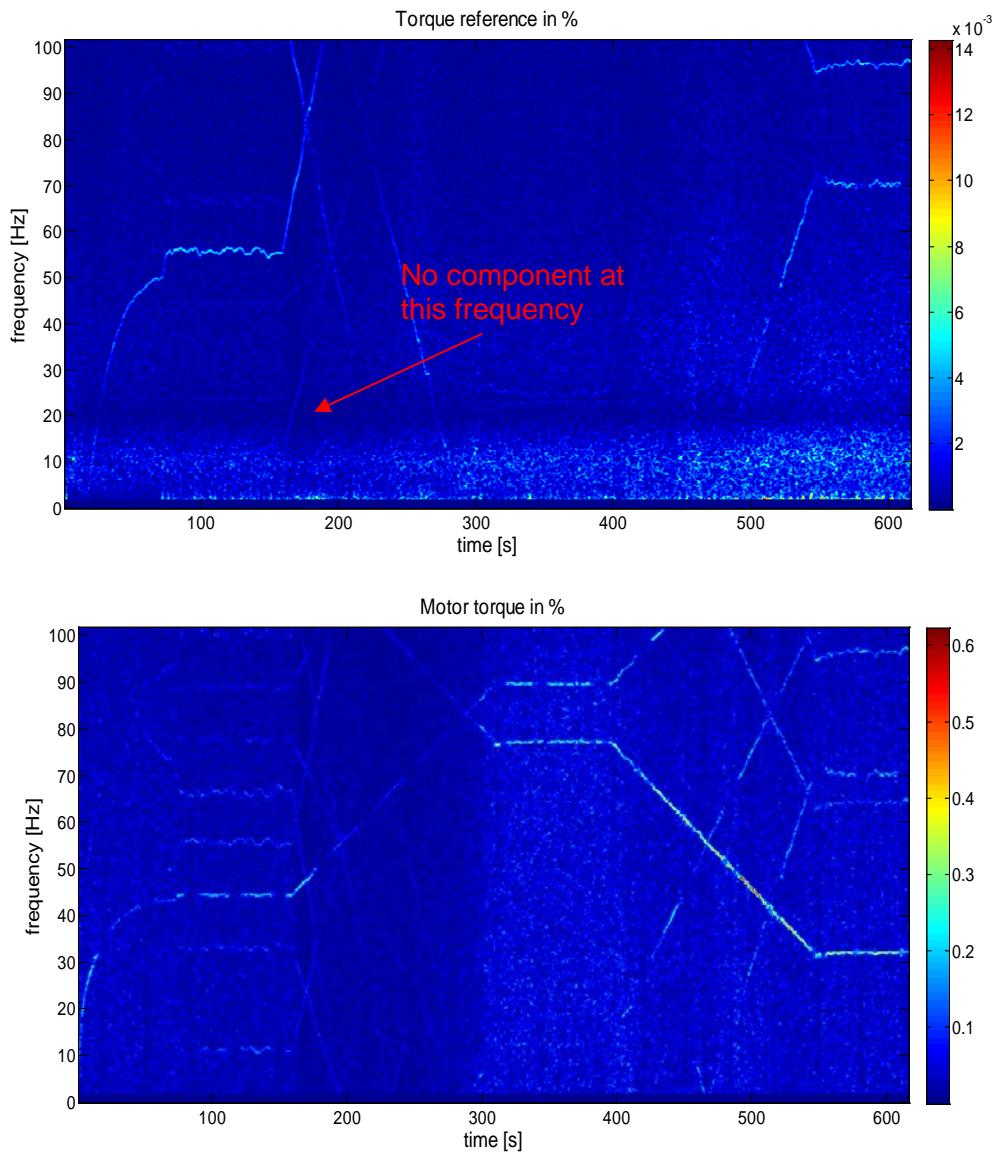
Figure 8-30: Motor speed, torque ref and motor torque with enabled band-stop (notch) filter

Next set of measurements represents the system acc. Table 23. The measurements were performed for setpoints 1'260 rpm, 1'350 rpm, 1'440 rpm, 1'710 rpm and 1'800 rpm with and without the notch filter in the speed feedback loop. Since the speed controller was soft tuned, there is not a significant difference when running with and without notch filter. The measurements without notch filter at 1'710 rpm are depicted in Figure 8-31.
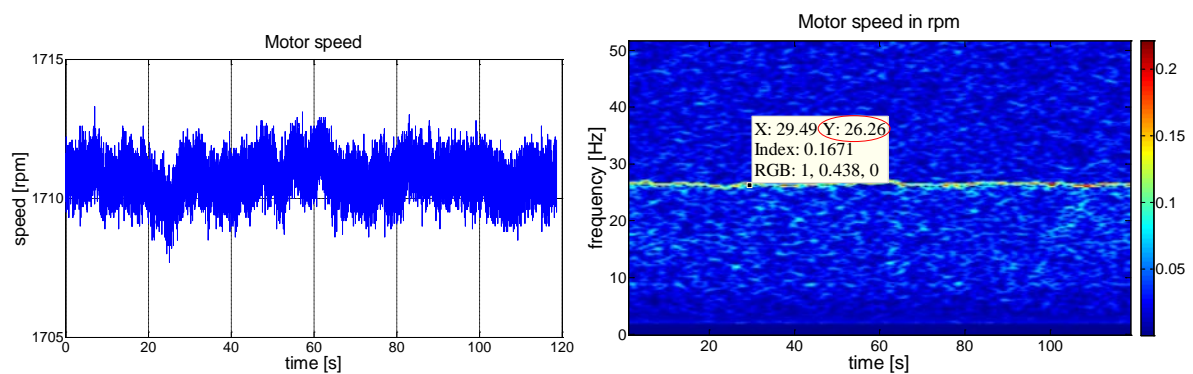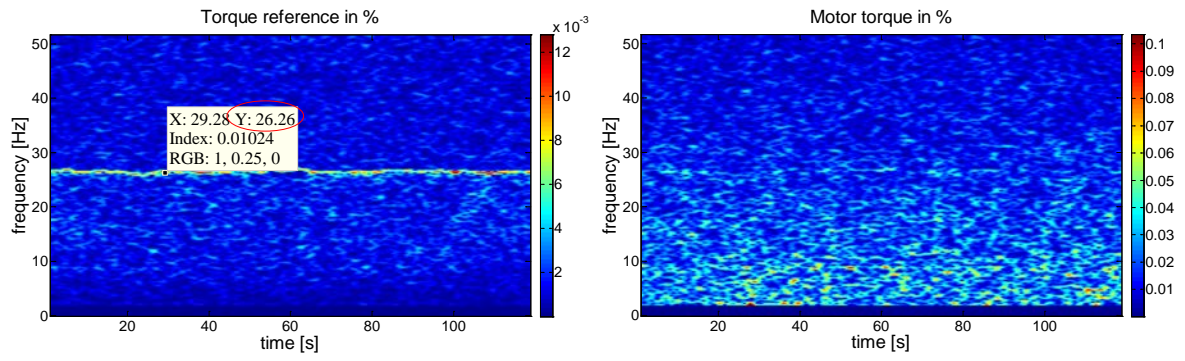
Figure 8-31: Motor speed and torque with disabled notch filter at 1'710 rpm

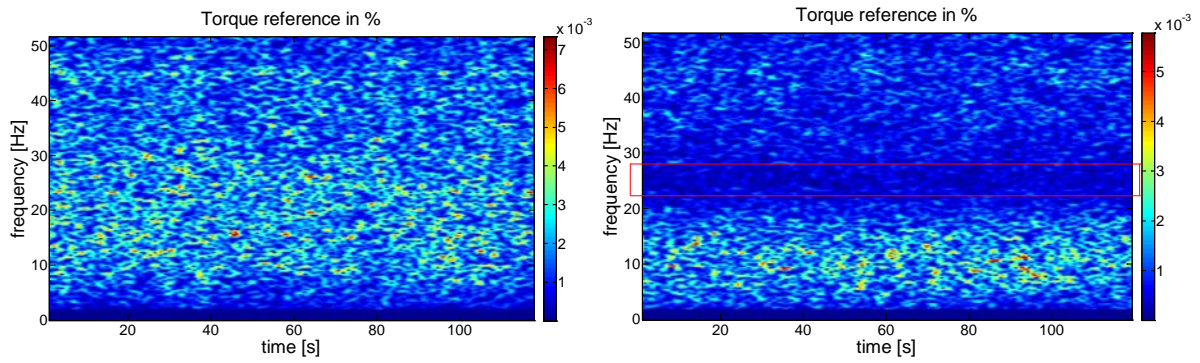The measurements with notch filter at 1'710 rpm are depicted in Figure 8-32.
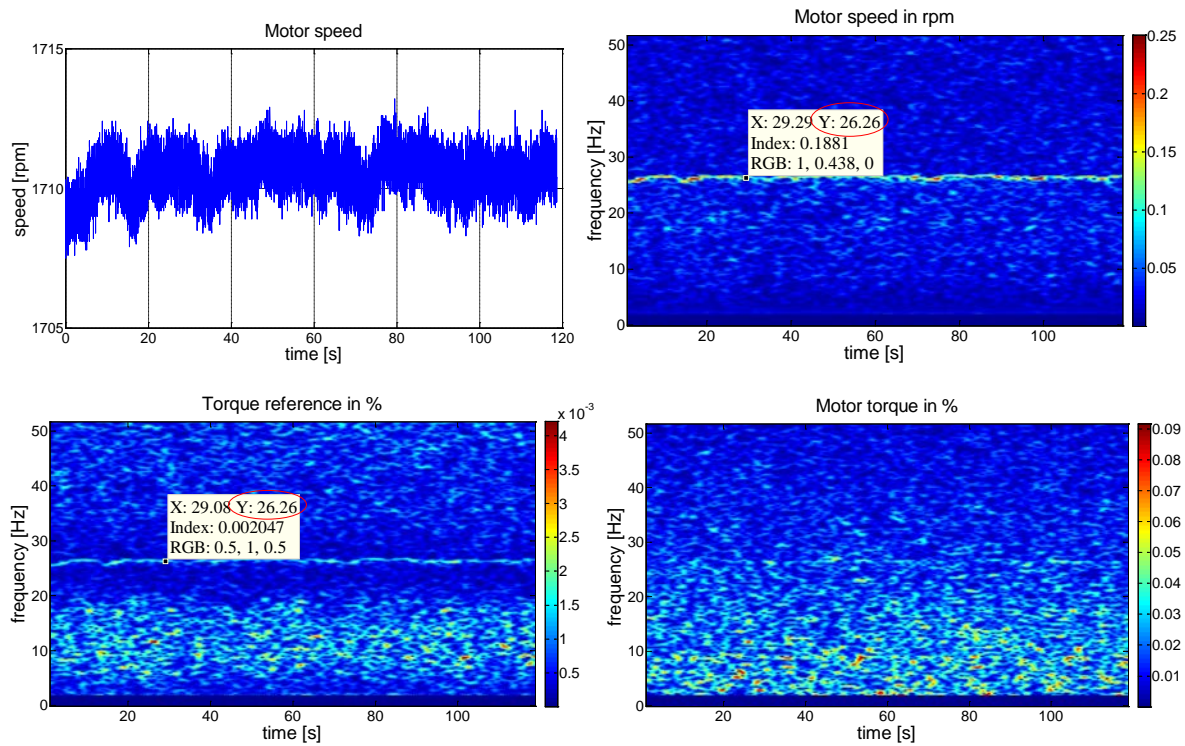
Figure 8-32: Motor speed and torque with enabled notch filter at 1'710 rpm

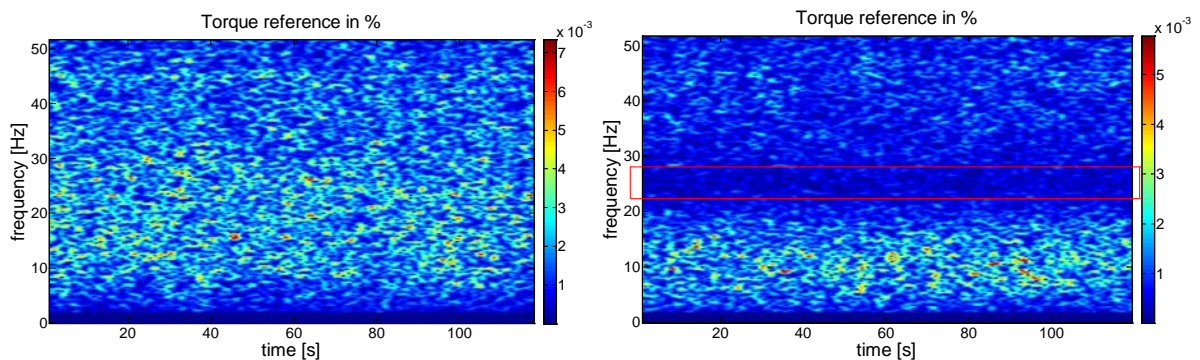(a) 1'260 rpm; left side – w/o filter, right side – with filter
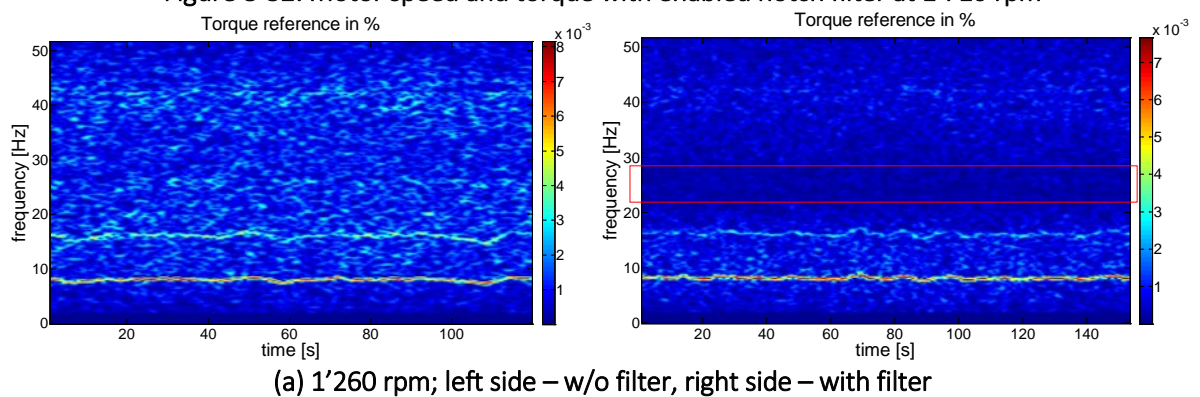
(b) 1'350 rpm; left side – w/o filter, right side – with filter

Figure 8-33 compares the torque reference without (left) and with notch filter (right). Figure 8-33a is captured at 1'260 rpm and Figure 8-33b at 1'350 rpm. At 1'260 rpm there are components at approx. 8.5 Hz and 17 Hz that cannot be explained. Nevertheless, in the frequency range 22 to 30 Hz (red rectangular frame) the torque reference with notch filter is very clean. At 1'350 rpm there is no distinct component in torque reference spectrum; it is just a white noise. The frequency range 22 to 30 Hz is again clean due to notch filter.
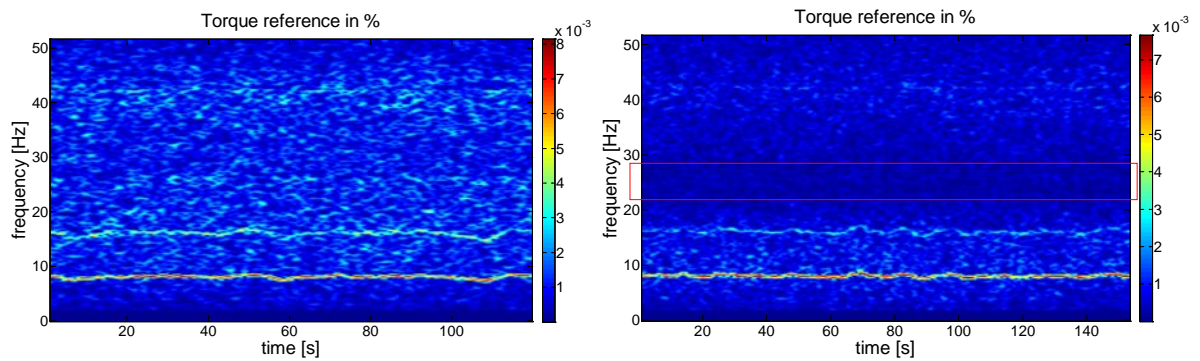
(a) 1'260 rpm; left side – w/o filter, right side – with filter

(b) 1'350 rpm; left side – w/o filter, right side – with filter

Figure 8-33: Torque reference with disabled and enabled notch filter

Unique measurements (not by the author) had been performed during string test of system described in

Table 15. Multi stage compressor system is driven by gas turbine and electric drive is used as starter/helper. A torque meter was temporarily installed between stage 1 and stage 2 of compressors. The shaft string is depicted in Figure 8-9. The vibrations in Figure 8-34 were measured when a) only

VFD was driving partial load of compressors, b) only gas turbine was driving with VFD idle and c) both gas turbine and VFD were driving.

a) VFD only

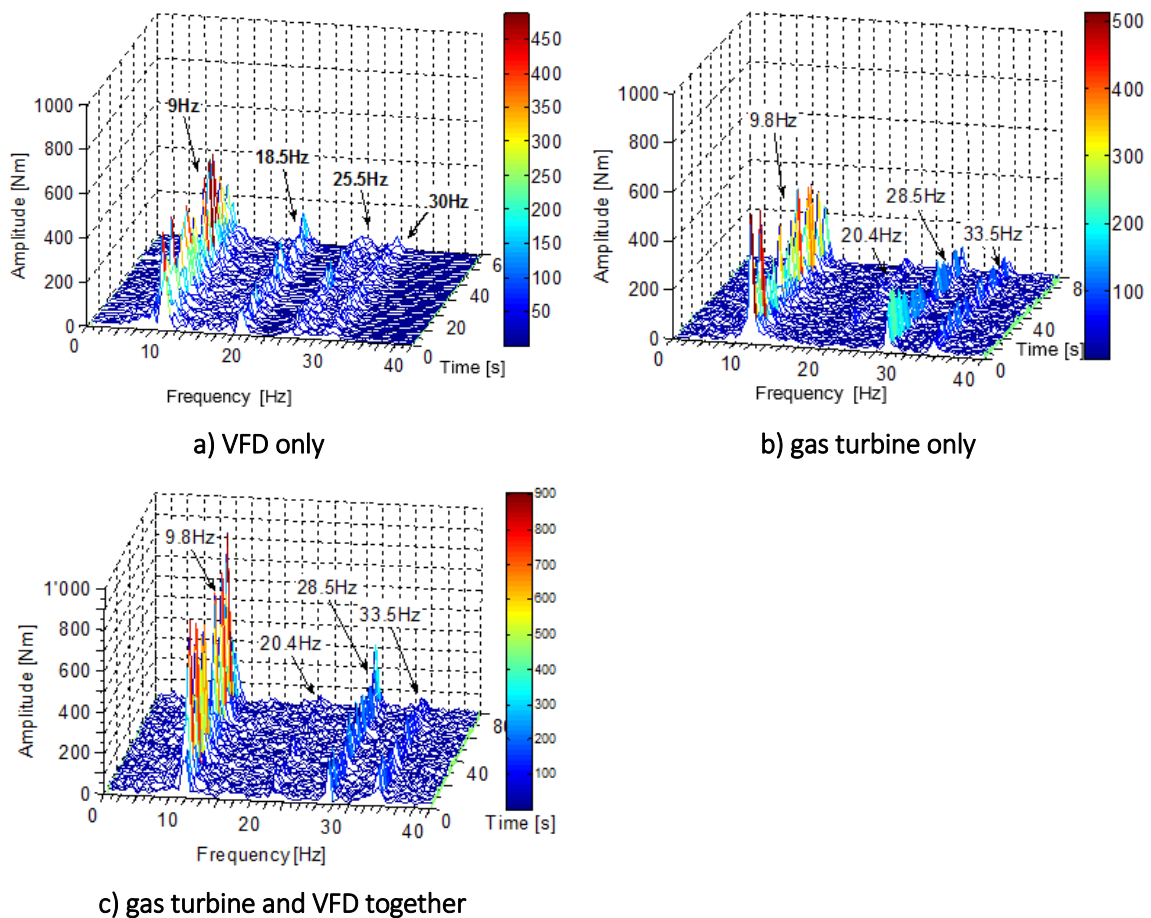b) gas turbine only

c) gas turbine and VFD together

Figure 8-34: Shaft torque spectrum from string test

Conclusions from Figure 8-34:

- Measured torsional natural frequencies are often slightly higher than theoretically calculated values (up to +10% tolerance)

- Computer simulation results correspond well with real vibration measurements (see [38]).

- Gas turbine is also a source of random broadband excitation ('white noise'). In case of VFD and gas turbine on the same shaft string, the total excitation is a sum of excitation from gas turbine and excitation from VFD (superposition of all sources).

System acc. Table 24 is a special case of fix speed motor retrofitted for VFD operation. The motivation was to decouple the motor from the grid that is much distorted from other non-linear loads and these disturbances induced vibrations on one of the compressor stages. First step was to change the speed controller settings – reduced proportional gain and longer integration constant. Next, the notch filter was tuned for the vibration frequency captured from measurement of lateral vibration. Third step was to increase the nominal speed to get more separation margin from TNF at approx. 22 Hz. Figure 8-35 shows the 21.5 Hz frequency that propagates from the motor speed into torque reference. Motor torque contains a strong component at 34.3 Hz that is not related to speed controller.
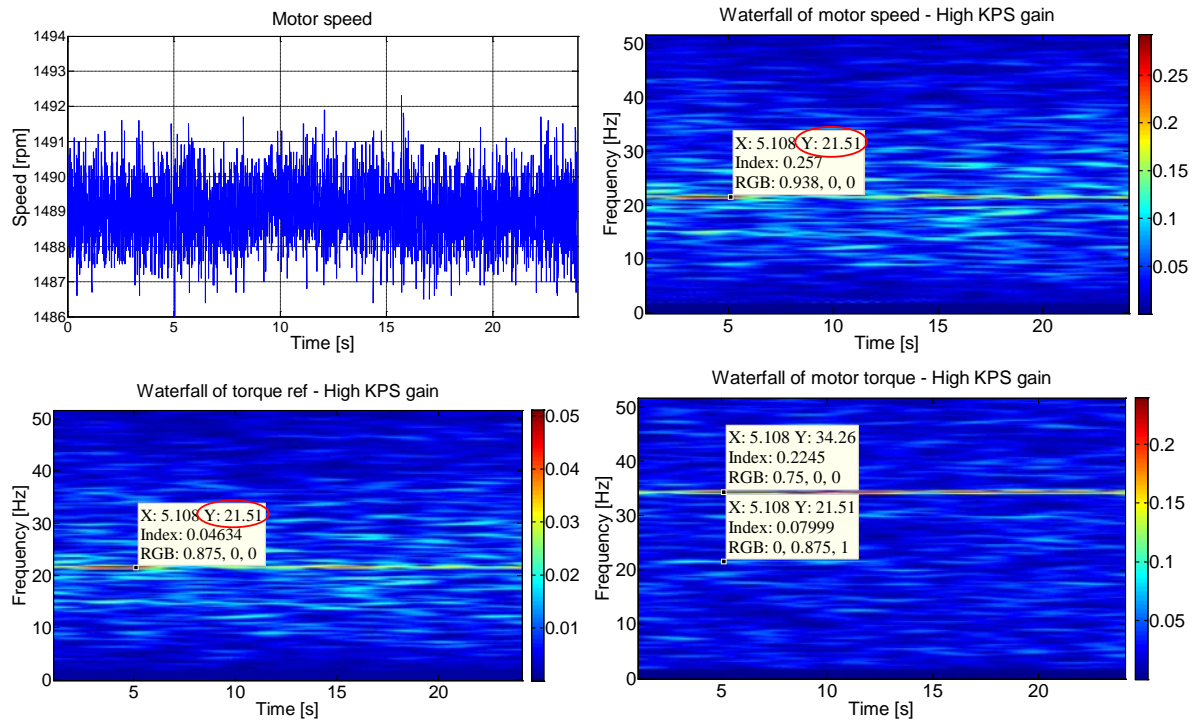
Figure 8-35: Motor speed and torque with initial settings of speed controller

Figure 8-36 demonstrates the vibration improvement when changing the motor speed from 1'489 rpm to 1'495 rpm.
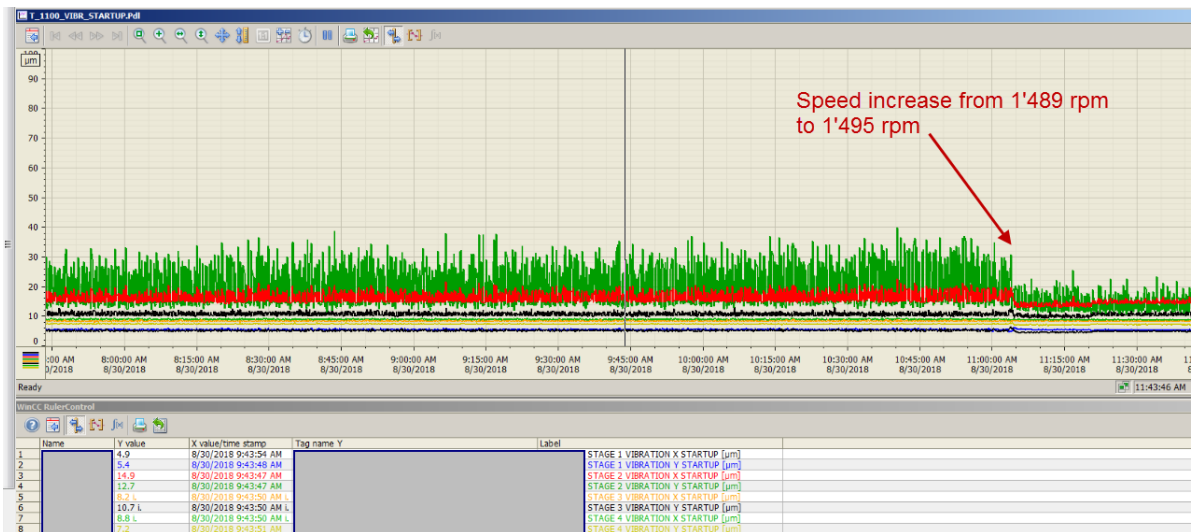

Figure 8-36: Lateral vibration measurement on system acc. Table 24

8.4   Author's involvement

In order to transparently show author's contribution and added value, Table 26 shows a summary of author's involvement.

Table 26: Author's involvement in referenced drive systems

System according to:	Author was involved in / mainly contributed to:				
	Torsional specific calculations or simulations	Preparations for commissioning	Measurements (on site, back to back test, string test)	Evaluation of measurements	Trouble-shooting
Table 7	Yes	No	Yes	Yes	No
Table 8	Yes	Yes	No	Yes	No
Table 9	Yes	No	No	Yes	Yes
Table 10	Yes	No	No	No	No
Table 11	Yes	Yes	No	Yes	Yes
Table 12	Yes	No	No	Yes	Yes
Table 13	Yes	No	No	No	No
Table 14	No	Yes	No	Yes	No
Table 15	No	No	No	No	No
Table 16	Yes	Yes	Yes	Yes	Yes
Table 17	No	Yes	Yes	Yes	Yes
Table 18	Yes	No	Yes	Yes	Yes
Table 19	No	No	Yes	Yes	Yes
Table 20	No	Yes	Yes	Yes	Yes
Table 21	No	Yes	Yes	Yes	No
Table 22	No	Yes	Yes	Yes	No
Table 23	No	Yes	Yes	Yes	No
Table 24	No	Yes	No	Yes	Yes

System acc. Table 15 was analyzed, simulated and tested by author's predecessor (tests in 2008 and published paper in 2009). The results are shown in this thesis due to their unique nature. In all other systems the author had been involved directly in different stages as shown above.

9   Engineering guideline

9.1   Torsional risk mitigation

Excessive torsional vibration might have fatal consequences and the risk mitigation plays an important role. Some of the principles are listed below:

1. Collect relevant information in early stage

   Receive data from mechanical vendor (calculated TNFs, mode shapes, damping, eventually copy of torsional analysis). Note that measured TNFs are often slightly higher compared to calculated values as shown in Table 27. One reason might be additional electromagnetic stiffening when motor field is applied.

Table 27: Correlation between calculated and measured TNFs

Calculated	Measured
10.79 Hz	11.2 Hz [1] (System acc. Table 8)
8.88 Hz	9.5 Hz [1]
17.87 Hz	18.6 Hz [1]
9.83 Hz	10.3 Hz [2]
23.47 Hz	24.3 Hz [2]
16.90 Hz	17.3 Hz [1] (System acc. Table 17)
17.01 Hz	17.5 Hz [1] (System acc. Table 18)

   [1]   Measured on site

   [2]   Measured during string test

2. Avoid excitation at frequencies equal to dominant torsional modes.

   a) Selection of motor speed range – mainly LCI drives and their interharmonics (refer to Appendix 5 – Campbell diagram for LCI and VSI drives)

   b) Change the pulse number online during starting – mainly LCI drives in Pulse mode operation

   c) Change the inverter pulse pattern depending on output frequency / motor speed – mainly VSI drives with optimized pulse pattern (OPP)

3. Minimize the magnitude of excitation torque

   a) Size of dc reactor (in terms of inductance)

      Applicable for LCI drives. Larger inductance value helps to smoothen the current in dc link and ultimately the interharmonic frequencies in torque spectrum. On the other hand, the integer harmonics will still be there with approx. same magnitude.

   b) Increase inverter pulse number plus use of dual winding machine

      This principle is often used in LCI drives with dual star synchronous machine. Minimization of torque ripple is significant, roughly by factor 3.

   c) Motor stray reactance optimized for given drive:

      a. small stator stray reactance in case of LCI drives (shorter commutation notches)

         i. better inverter firing angle in load commutated mode – less torque ripple

         ii. earlier exit of pulse mode operation (at lower speed)

      b. larger stator stray reactance in case of VSI drives (smoothing the stator current)

   d) Settings of current control loop – for LCI drives

      a. proportional gain and time constant of PI controller

         i. settings for load-commutated mode

         ii. settings for pulse mode (might be different than with load commutation)

       b. cut-off frequency of low-pass filter

          i. higher cut-off frequency means more ripple in dc current

          ii. lower cut-off frequency decreases the phase margin of control loop

    e) Use of output reactor or output filter (dv/dt filter, sine filter) – for VSI drives

4. Avoid closed loop interaction

    a) De-couple control loops that could otherwise propagate the oscillations

    b) Remove oscillations from feedback signal by digital filtering

    c) Tune the speed controller (proportional gain, additional feed-forward terms)

    d) Use reference values instead of actual signals for certain control loops

        It helps to decouple the loops (if possible). Write the software flexible so that certain feedback loops can be disabled if needed. Sometimes it is the only way to find a root cause in a system with several oscillating signals.

5. Maximize control damping

    a) Increase passive damping by use of digital filters (mainly selective higher order filters)

    b) Parameterize the main controllers properly considering application requirements

    c) Use additional feed-forward terms to improve dynamics while keeping lower proportional gain of PI/PID speed controller

    d) Minimize latencies in control loops (reference to [72], [105] and [107]) - latencies eat up damping

    e) Use algorithms for active damping

    f) Use state space controllers together with simplified models of mechanical system

    g) Use model predictive control algorithms together with simplified models of mechanical system

6. Use control software with freedom in parameterization

    a) Demanding projects shall be pre-parameterized in engineering stage (before going to site)

    b) Control functions shall allow flexibility for fine tuning (change of parameter value, activation/deactivation of certain feedback or feed-forward loops, select between actual and reference signals)

7. Verify torsional performance on site

    a) Early verification during commissioning and/or testing

    b) Commissioning manual for loads sensitive for torsional vibration – Follow the tuning rules based on theory and practical experience.

8. Compare (benchmark) drive performance from various sites and applications

    a) Collect know how to get insight about severity of vibrations

    b) Benchmark sites to see if there is any abnormality

9. Implement processes and learning mechanisms and define best practice

9.2   Initial drive analysis during string commissioning

"Lateral vibration is easy to measure and difficult to predict. Torsional vibration is difficult to measure and easy to predict."

Quote: Malcom Leader [113]

Torque and its quality can be observed by VFD. Direct torque measurement is seldom available, but the VFD has a torque signal that is being calculated by the motor model. It does not require any additional instrumentation or complex measurement campaign. The verification of torque and speed waveforms during commissioning can be very useful. In case the signal quality does not correspond the expectations, a parameter tuning can be done. It is recommended to perform this check before the site is handed over to end user. This 'torsional check' has been performed for several projects during commissioning phase. It is inexpensive method how to verify that there is no dangerous torsional excitation from the VFD. The captured signals are:

- motor speed (direct measured or observed in encoder-less operation)
- torque reference (output of speed controller)
- motor torque

See Figure 9-1 for location of internal drive signals for "torsional diagnostics". The figure is simplified showing only the main blocks.
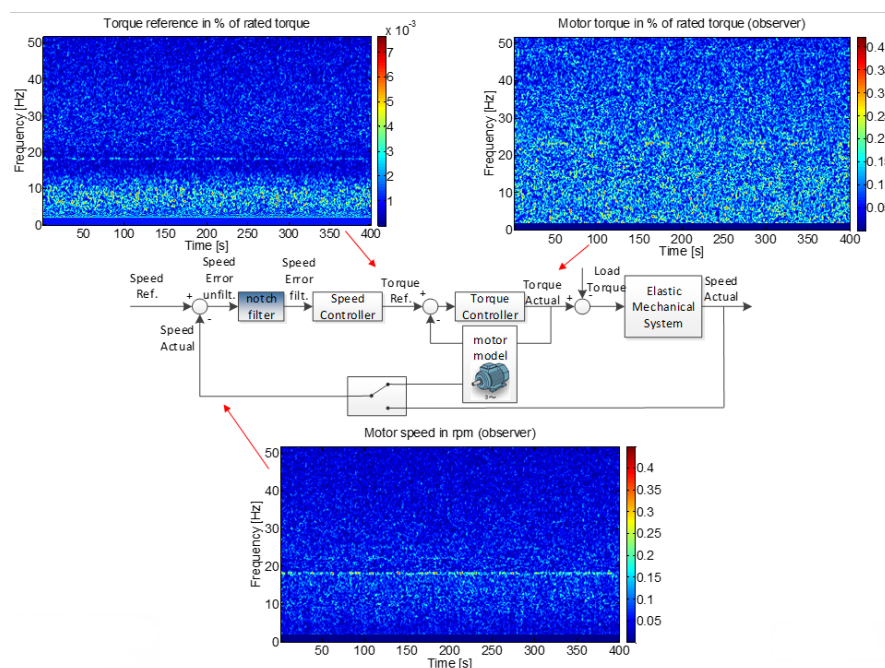
Figure 9-1: Drive internal signals with corresponding waterfall trends

The recommended length of each steady state section is at least $20 - 30$ seconds. Shorter measurement is not representative enough. Longer measurement is generally fine, but the measurement data files might get too large. Afterwards the speed setpoint is changed and again same period of steady state signal captured. This kind of speed sweep helps to determine the relationship between excitation components and fundamental motor frequency / motor speed. It is also useful to distinguish between real frequency components and components that might appear due to aliasing effect. In

ideal case there is a speed sweep throughout the whole speed range. If this is not possible, then at least a sweep within the continuous operating range.

During signal processing it is important to respect the sampling rate of measured signal and if necessary use suitable windowing functions (Hann, Hanning or Blackman-Harris window etc). If the frequency components of interest have very small magnitudes, then a logarithmic scale can be used instead of linear.

LCI drives with synchronous machines have another simple possibility that is the frequency analysis of the motor voltage. If the shaft string experiences torsional vibration and the torsional mode involves the motor (which is mostly the case for the first TNF), then the vibration frequency will be seen as sidebands symmetrical around the fundamental electric frequency. This simple check was found useful in numerous troubleshooting cases.

Therefore, in order to verify the actual value of torsional natural frequency and confirm the calculated value, following simple check is possible:

a) In case of voltage source inverters (VSI):

- FFT or waterfall diagram of motor speed (measurement or observed signal) → TNF directly visible in frequency spectrum of speed signal as seen in Figure 9-2. It shows a torque trend of approx. 140 seconds of system acc. Table 18. The horizontal line at 17.5 Hz shows the torsional natural frequency. The magnitude is represented by the color (see colorbar on the right side).
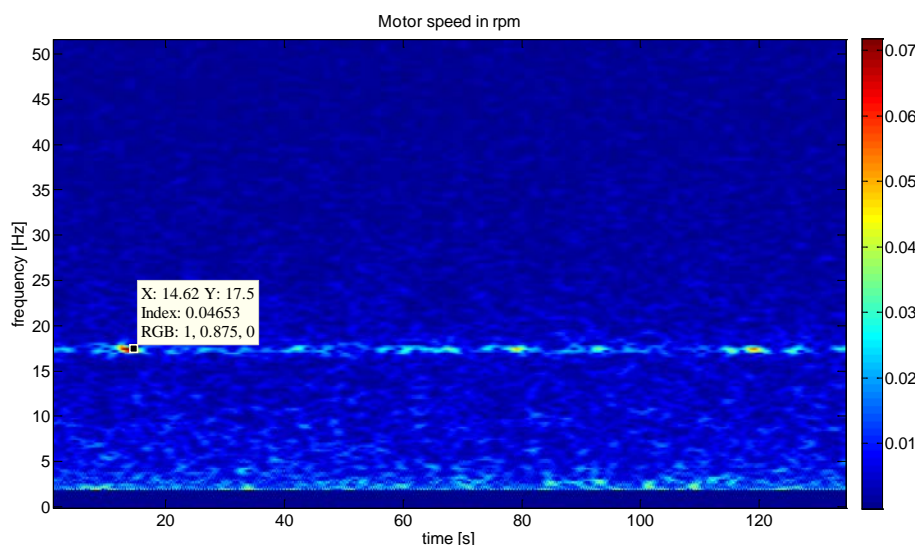
Figure 9-2: Waterfall diagram of motor speed (visible 1st TNF)

b) In case of load commutated inverters (LCI):

- FFT or waterfall diagram of stator voltage → TNF appears as side bands of the fundamental motor electric frequency ($f_M - f_{TNF}$ and $f_M + f_{TNF}$)

Example in Figure 9-3 (drive system acc. Table 8, real measurement from string test): Motor operates in steady state at frequency of approx. 51 Hz. This is the fundamental component in FFT spectrum. There are also visible components at approx. 38.5 Hz and 63.5 Hz (side bands). The TNF can be easily identified as (51 − 38.5) Hz = 12.5 Hz or (63.5 − 51) Hz = 12.5 Hz. In this way, the real values of the TNFs can be verified.

Examples in Figure 9-4 and Figure 9-5 (drive system acc. Table 11): The motor slowly accelerates. Waterfall plots show the fundamental frequency as dominant component with two parallel lines as constant distance from fundamental motor frequency (see arrows). Figure 9-4 has time on the x-axis while Figure 9-5 is reversed (x-axis shows frequency, y-axis shows time).
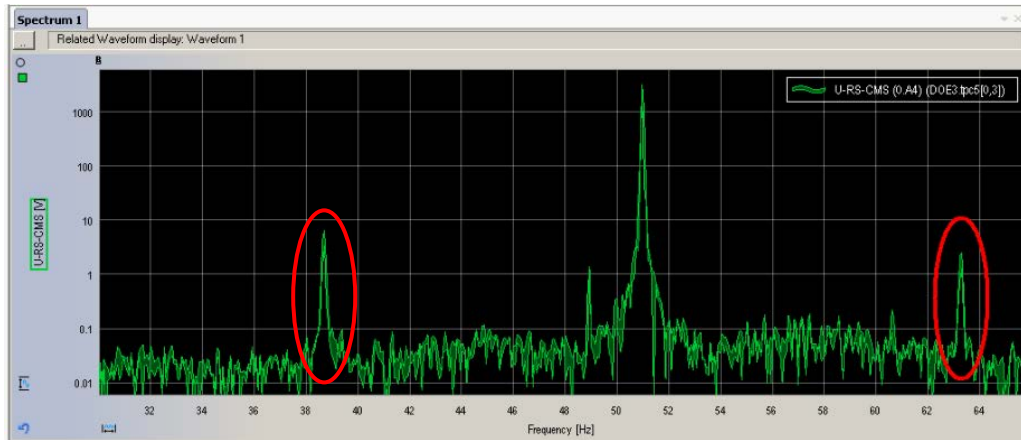

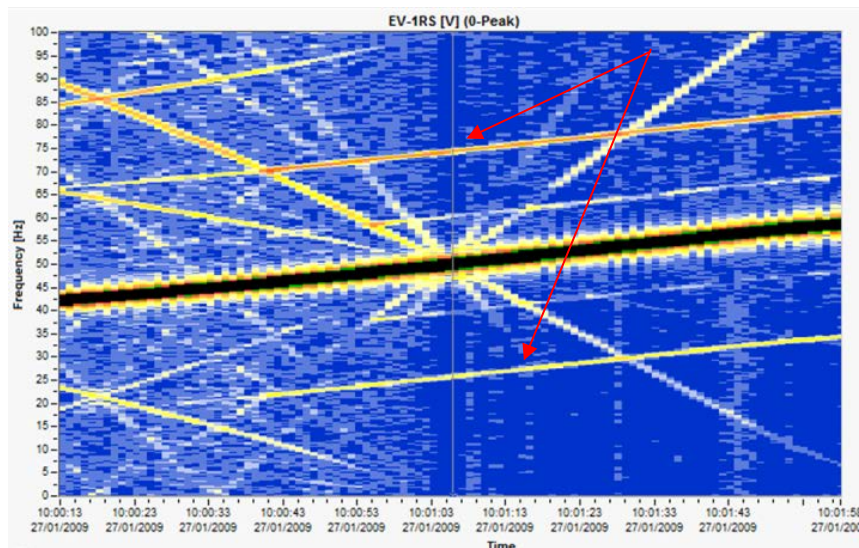Figure 9-3: FFT of motor voltage in steady state condition (1st TNF as sidebands)

Figure 9-4: Waterfall diagram of motor voltage during acceleration (1st TNF as sidebands)
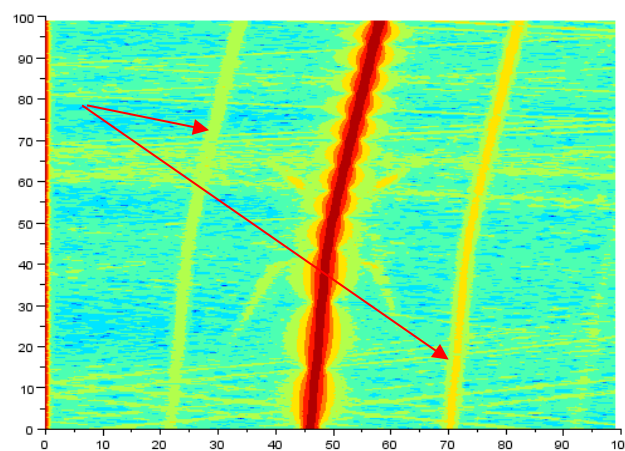
Figure 9-5: Waterfall diagram of motor voltage (1st TNF as sidebands);
x-axis: frequency [Hz], y-axis: time [s]

10 Conclusion

This thesis explains the mechanisms of electro-mechanical interactions in electric variable speed drive systems. A generic model of elastic shaft is developed. This model can be parameterized for any shaft system with lumped inertias and can easily replace simple rigid model. Presented transfer function models enable analytical optimization of speed and current controllers. Passive and active damping functions are proposed. The most perspective algorithms are verified by performing extensive simulations. The results are validated with measurements of several medium voltage drive systems including LCI and VSI drives with power ranging from 1.6 MW up to 20 MW.

One of the main contributions is the torsional damper (also called active damper or active compensator) implemented in current control loop of LCI drives (description in chapter 6.2.6). The torsional vibration is reduced by approx. factor 1.5 - 3.0 when the damper is activated. The functionality was demonstrated by simulations as well as in real operation (string test measurements and measurements on site). In three real systems (Table 7, Table 8 and Table 10) the torsional damper enabled operation at critical speed and expanded the speed range. It provided extended operation flexibility and increased efficiency to the end user. Another major contribution is the modification of pulse pattern (smart switchover) during starting of LCI drive at low speed (0 to approx. 10% nominal speed) that significantly reduces the excitation of dominant torsional natural modes and is very critical for the coupling design. The idea was further developed and patented [A1].

The analytical methods to optimize the speed controller of VSI drives already helped in numerous troubleshooting cases as well as for preparation of commissioning. Early recognition of torsional vibration problems mitigated mechanical failures in concrete cases. The engineering guideline in extended form is used by field service engineers when there is a system sensitive to torsional vibration.

10.1 Main contribution of this thesis

- Explanation of origin of torsional oscillation and vibration in electric drive systems, focusing on torque ripple due to inverter modulation and non-sinusoidal motor current as well as electro—mechanical interaction in the closed loop control system.
- Development of drive simulation model including scalable model of elastic shaft.
- Simulation-based investigations to explore influence of feedback control, interaction among multiple control loops and control damping.
- Investigations of negative damping phenomena.
- Comparison of classical torsional analysis (open loop) and results from closed loop approach.
- Analysis of torsional stability by using frequency characteristics (Bode diagrams) as alternative fast approach to extensive simulations.
- Increase of damping of control circuits for torsional natural frequencies.
- Propose perspective methods for active damping and verify them by means of simulations and on site measurements of real projects.

- Propose and implement control engineering methods and processes to mitigate the risk of torsional vibration during execution stage.
- Issue a guideline for field service engineers how to parameterize variable speed drives in applications sensitive for vibration
- Perform diagnostics of severity of torsional vibration during commissioning stage

10.2 Challenges and perspective directions of future research

Following perspective directions together with associated challenges have been identified:
- Further research on active damping functions on torsional vibration

There is variety of methods for active damping. The principle is often similar, but it differs in implementation. The most suitable methods will probably be those with highest robustness, effectiveness and straightforward commissioning in daily practice.
- Implementation of model predictive control on active torsional damping

Perspective modern control methods such as model predictive control unlock large potential for optimization. The challenge here is mainly the long prediction horizon and estimation of state variables. Suitable algorithms could overcome this obstacle.
- Oscillation damping of direct on-line vs VFD fed induction motor

Natural damping of induction motor when operated in open loop manner brings some advantages that seem to be still not completely understood. A thorough explanation of differences between direct on-line and VFD closed-loop controlled machine could provide hints how to improve VFD control and maximize the electric damping.
- Include effects coming purely from motor design (e.g. spatial harmonics etc.)

Spatial harmonics originate from the winding arrangement of the electric machine. They have typically high frequencies and very low magnitude and can therefore often be neglected. For special cases where very high accuracy is required such effects need to be considered as well.
- Improved modeling of elastic mechanical system

The mechanical model could be potentially extended with non-linear effects and coupling between torsional and lateral vibrations. The latter step is very complex and requires very detailed knowledge of bearing type and it modeling as well as information about stiffness of foundation.
- Automatic identification of parameters of elastic mechanical system (lower priority)

Algorithms for automatic identification have been proposed by several authors. However, these methods are mainly suitable for lower power. The automatic tuning algorithm often requires dynamic tests of the system that may not be acceptable for manufacturer of driven equipment or not supported by the overriding process control system (large amount of instrumentation). The automatic identification would have to be safe from mechanical perspective so that no hardware damages or whatsoever can happen during auto-tuning. In addition, the system would have to accept the fact that some key system parameters might be time variant (e.g. inertia).

List of Figures

List of Tables

References

[1]   H. Devolt, T. Nestli and J. Hurter, "All electric LNG plants," ABB Process Automation, Oslo, Norway / Turgi, Switzerland, 2006.

[2]   D. P. Connors, D. A. Jarc and R. H. Daughtery, "Considerations in applying induction motors with solid state adjustable frequency controllers," in *IEEE Petroleum and Chemical Industry Conference*, 1982.

[3]   ABB Group, "ABB AC Drives: ACS6000c Cycloconverter," [Online]. Available: https://library.e.abb.com/public/2abc426982e203e6c1256e4d004deb49/ACS%206000c%20Cycloconverter.pdf.

[4]   ABB Switzerland, "Giant ABB drive systems boost mining productivity," [Online]. Available: http://www04.abb.com/global/seitp/seitp202.nsf/0/e06911927bb31100c125746d0040f1bd/$file/Giant+ABB+drive+systems+boost+mining+productivity.pdf.

[5]   ABB Group, "MEGADRIVE-LCI," [Online]. Available: https://library.e.abb.com/public/b09e1b7fc1063305c12572490033a751/MEGADRIVE-LCI_for_SoftStarter_Rev0.pdf.

[6]   B. Wu, High-Power Converters and ac Drives, New Jersey: John Wiley & Sons, IEEE Press, 2006.

[7]   TM GE Automation Systems, "Medium Voltage Drive Evolution," [Online].

[8]   A. Nabae, I. Takahashi and H. Akagi, "A new neutral-point-clamped PWM inverter," *IEEE Trans. on Industry Applications,* Vols. IA-17, no. 5, pp. 518 - 523, September/October 1981.

[9]   H. Ismail, A. Jidin, R. Sundram, M. K. Rahim, Y. Tarmizi and A. Razi, "Direct torque control of induction machine using 3-level neutral point clamped inverter," in *IEEE Student Conference on Research and Development*, Kuala Lumpur, 2015.

[10] T. B. Soeiro and J. W. Kolar, "Novel 3-level hybrid neutral-point-clamped converter," in *IECON 2011*, Melbourne, 2011.

[11] J. Rodriguez, S. Bernet, P. K. Steimer and I. E. Lizama, "A survey on neutral-point-clamped inverters," *IEEE Trans. on Industrial Electronics,* vol. 57, no. 7, pp. 2219-2230, 2010.

[12] V. Guenneguez, B. Gollentz, F. Meibody-Tabar, S. Rael and L. Leclere, "A converter topology for high speed motor drive applications," in *European Conference on Power Electronics and Applications*, Barcelona, 2009.

---

[13]   J. Rodriguez, J.-S. Lai and F. Z. Peng, "Multilevel inverters: A survey of topologies, controls and applications," *IEEE Trans. on Industrial Electronics,* vol. 49, no. 4, pp. 724 - 738, 2002.

[14]   C. Z. and W. B., "A novel switching sequence design for five-level NPC/H-bridge inverters with improved output voltage spectrum and minimized device switching frequency," *IEEE Trans. on Power Electronics,* vol. 22, no. 6, pp. 2138-2145, November 2007.

[15]   Z. Cheng and B. Wu, "Dual 18-pulse rectifier for high-power multilevel inverters," in *IECON*, Raleigh, 2005.

[16]   F. Kieferndorf, M. Basler, L. A. Serpa, J.-H. Fabian, A. Coccia and G. A. Scheuer, "A new medium voltage drive system based on ANPC-5L technology," in *IEEE Int. Conference on Industrial Technology*, Vina del Mar (Chile), 2010.

[17]   J. Liao, K. Wan and M. Ferdowski, "Cascaded H-bridge multilevel iinverters - A reexamination," in *IEEE Vehicle Power and Propulsion Conference*, Arlington, 2007.

[18]   G. P. Adam, B. Alajmi, K. H. Ahmed, S. J. Finney and B. W. Williams, "New flying capacitor multilevel converter," in *IEEE Int. Symposium on Industrial Electronics*, Gdansk, 2011.

[19]   A. Lesnicar and R. Marquardt, "An innovative modular multilevel converter topology suitable for a wide power range," in *IEEE Bologna Power Tech Conference Proceedings*, Bologna, 2003.

[20]   R. Marquardt, "Modular multilevel converter - Impact on future applications and semiconductors," *Power electronic components and their applications,* pp. 1 - 10, 2017.

[21]   P. Himmelmann, M. Hiller, D. Krug and M. Beuermann, "A new modular multilevel converter for medium voltage high power oil & gas motor drive applications," *18th European conference on Power Electronics and Applications (EPE'16 ECCE Europe),* pp. 1 - 11, 2016.

[22]   J. Kolb, F. Kammerer and M. Braun, "Dimensioning and design of a modular multilevel converter for drive applications," *15th International Power Electronics and Motion Control Conference (EPE-PEMC 2012 ECCE Europe),* 2012.

[23]   P. Vas, Sensorless vector and direct torque control, Aberdeen, UK: Oxford University Press, 1998.

[24]   D. Ahmadi, K. Zou, C. Li, Y. Huang and J. Wang, "A universal selective harmonic elimination method for high-power inverters," *IEEE Trans. on Power Electronics,* vol. 26, no. 10, pp. 2743-2752, 2011.

[25]   K. Peter and J. Böcker, "Operating electrical high speed drives with pulse patterns of specific harmonic content," in *IEEE Energy Conversion Congress and Exposition*, Montreal, 2015.

[26] T. Geyer, G. Papafotiou and M. Morari, "Model predictive direct torque control - Part I: concept, algorithm, and analysis," *IEEE Trans. on Industrial Electronics,* vol. 56, no. 6, pp. 1894-1905, 2009.

[27] C. Gutscher, N. Oikonomou, P. Karamanakos, F. D. Kieferndorf and T. Geyer, "Model predictive pulse pattern control for the five-level active neutral-point-clamped inverter," *IEEE Trans. on Industry Applications,* vol. 49, no. 6, pp. 2583-2592, 2013.

[28] M. Meyer and J. Schöning, "Power supply stability in large railway networks," ESCARV, 2000.

[29] I. Pendharkar, "Resonance stability in Electrical Railway Systems – a dissipativity approach," *European Control Conference (ECC),* pp. 4574-4579, July 2013.

[30] R. Belmans, K. J. Binns, W. Geyser and A. Vandenput, Vibrations and audible noise in alternating current machines, Kluwer Academic Publishers, 1988.

[31] L. Harnefors, "Analysis of subsynchronous torsional interaction with power electronic converters," *IEEE Trans. on Power Systems,* vol. 22, no. 1, pp. 305 - 313, February 2007.

[32] L. Harnefors, "Proof and application of the positive-net-damping stability criterion," *IEEE Trans. on Power Systems,* vol. 26, no. 1, pp. 481 - 482, February 2011.

[33] The Electric Power Engineering Handbook, Power system stability and control, L. L. Grigsby, Ed., CRC Press, 2012.

[34] R. J. Piwko and E. V. Larsen, "HVDC system control for damping of subsynchronous oscillations," in *IEEE Trans. on Power Apparatus and Systems*, July 1982.

[35] MAN Energy Solutions, "High-Speed Centrifugal Compression & VSD Technology," 20 February 2012. [Online]. Available: http://www.gaselectricpartnership.com/GMANHiSpeed.pdf. [Accessed 09 August 2018].

[36] MAN Energy Solutions, "https://turbomachinery.mandieselturbo.com," 2013. [Online]. Available: https://turbomachinery.mandieselturbo.com/docs/librariesprovider4/Turbomachinery_doc /hofim-technology---oil-free-compression-systems.pdf?sfvrsn=16. [Accessed 22 May 2018].

[37] M. Hernes and B. Gustavsen, "Simulation of shaft vibration due to interaction between turbine-generator train and power electronic converters at the Visund oil platform," *Power Conversion Conference,* 2002.

[38] P. Rotondo, D. Andreo, S. Falomi, P. Jörg, A. Lenzi, T. Hattenbach, D. Fioravanti and S. De Franciscis, "Combined torsional and electromechanical analysis of an LNG compression train

with variable speed drive system," in *Proceedings of the thirty-eighth Turbomachinery Symposium*, 2009.

[39] S. Del Puglia, S. De Franciscis, S. Van de moortel, P. Jörg, T. Hattenbach, D. Sgro, L. Antonelli and S. Falomi, "Torsional interaction optimization in a LNG train with a load commutated inverter," in *8th IFToMM International Conference on Rotordynamics*, Seoul, Korea, 2010.

[40] V. Hütten, R. M. Zurowski and M. Hilscher, "Torsional interharmonic interaction study of 75 MW direct-driven VSDS motor compressor trains for LNG duty," in *Proceedings of the Thirty-Seventh Turbomachinery Symposium*, Houston, Texas, 2008.

[41] V. Hütten, C. Beer, T. Krause, V. A. Ganesan and S. Demmig, "VSDS motor inverter design concept for compressor trains avoiding interharmonics in operating speed range and verification," in *Proceedings of the Forty-Second Turbomachinery Symposium*, Houston, Texas, 2013.

[42] S. Schram, C. Sihler, J. Song-Manguelle and P. Rotondo, "Damping torsional interharmonic effects of large drives," *Power Electronics and Motion Control Conference (IPEMC),* pp. 484 - 490, 2009.

[43] S. Schramm, C. Sihler and J. Song-Manguelle, "A general approach of damping torsional resonance modes in multi-megawatt applications," *IEEE Trans. on Industry Applications,* vol. 47, no. 3, pp. 1390 - 1399, May/June 2011.

[44] J. Song-Manguelle, G. Ekemb, S. Schröder, T. Geyer, J.-M. Nyobe-Yome and R. Wamkeue, "Analytical expression of pulsating torque harmonics due to PWM drives," *IEEE,* 2013.

[45] T. Shimakawa and T. Kojo, "The torsional torque fluctuations of a compressor train with a vector control PWM inverter," in *36th Turbomachinery Symposium*, Houston, TX, 2007.

[46] A. Kocur and J. P. Corcoran, "VFD induced coupling failure," in *37th Turbomachinery Symposium*, Houston, TXyxxxxxxxxxxxxxx, 2008.

[47] J. A. Kocur and M. G. Muench, "Impact of electrical noise on the torsional response of VFD compressor trains," in *Proceedings of the First Middle East Turbomachinery Symposium*, Doha, Qatar, 2011.

[48] K. Tanaka, A. Adachi, N. Takahashi and Y. Fukushima, "Torsional-lateral coupled vibration of centrifugal compressor system at interharmonic frequencies related to control loop frequencies in voltage source inverter," in *38th Turbomachinery Symposium*, Houston, TX, 2009.

[49] M. Tsukakoshi, M. Al Manul, H. Kazunori, H. Hosoda, J. Kasaguchi and L. Ben-Brahim, "Novel torque ripple minimization control for 25MW variable speed drive system fed by multilevel voltage source inverter," in *39th Turbomachinery Symposium*, Houston, TX, 2010.

[50] M. Guidi and A. Pescioni, "Electromechanical optimization against torsional vibrations in O&G electrified trains," in *42nd Turbomachinery Symposium*, Houston, TX, 2013.

[51] C. B. Mayer, P. J. Crescenzo and D. A. Fenton, "Elimination of electromechanical drive system problems during the design process," *IEEE Trans. on Industry Applications,* Vols. IA-20, no. 4, pp. 873 - 880, July/August 1984.

[52] C. B. Mayer, "A recommended new standard electrical supply and control configuration for dual-kiln drives," *IEEE Trans. on Industry Applications,* vol. 25, no. 3, pp. 465 - 474, May/June 1989.

[53] C. B. Mayer, R. M. Johnson and D. J. Gray, "Solution of a serious repetitive vibration problem on a 4500-hp single-pinion synchronous motor ball mill drive," *IEEE Trans. on Industry Applications,* Vols. IA-21, no. 4, pp. 1039 - 1046, July/August 1985.

[54] D. N. Walker, S. L. Adams and R. J. Placek, "Torsional vibration and fatigue of turbine-generator shafts," 1981.

[55] P. Kundur, Power system stability and control, Toronto: McGraw-Hill Inc., 1993.

[56] H. Geng, D. Xu, B. Wu and G. Yang, "Active damping for torsional vibrations in PMSG based WECS," in *25th Annual IEEE Applied Power Electronics Conference*, Palm Springs, CA, 2010.

[57] G. Mandic, E. Ghotbi, A. Nasiri, F. Oyague and E. Muljadi, "Mechanical stress reduction in variable speed wind turbine drivetrains," in *IEEE Energy Conversion Congress and Exposition*, Phoenix, AZ, 2011.

[58] J. Licari, C. E. Ugalde-Loo, J. B. Ekanayake and N. Jenkins, "Comparison of the performance and stability of two torsional vibration dampers for variable-speed wind turbines," *Wind Energy,* 25 May 2014.

[59] M. Tallfors, M. C. Nordin and A. J. Isaksson, "Selection of optimization criterion for speed controlled resonant elastic systems," *Power Electronics and Drive Systems (PEDS 2003),* vol. 1, pp. 642 - 647, 2003.

[60] D. H. E. Butler, M. A. Churches, Y. Anbe and H. Naitoh, "Compensation of a digitally controlled static power converter for the damping of rolling mill torsional vibration," *IEEE Trans. on Industry Applications,* vol. 28, no. 2, pp. 427-433, March/April 1992.

[61] H. Naitoh and K. Suzuki, "Compensation of a GTO-NPC inverter for the damping of rolling mill torsional vibration by ETC (estimated torque feedback control).," in *27th Annual IEEE Power El. Specialists Conf.*, Baveno (Italy), 1996.

[62] P. Belli, S. Bittanti and A. De Marco, "On the origin of torsional vibrations in hot rolling mills and a possible remedy," *ASME Journal on Dynamic Systems, Measurement, and Control,* vol. 126, pp. 811-823, 2004.

[63] P. V. Krot, "Transient torsional vibrations control in the geared drive trains of the hot rolling mills," in *IEEE Control Applications & Intelligent Control*, St. Petersburg, 2009.

[64] T. Tamaoki, M. Takanezawa, Z. Lu, S. Xiao, M. Kimoto and N. Morita, "A study for on-line transfer function analysis, in realizing higher speed response adjustment, in association with variable speed rolling mill motor drive system," in *The 2010 International Power Electronics Conference*, Sapporo, 2010.

[65] I. M. Canay, "A novel approach to the torsional interaction and electrical damping of the synchronous machine, Part II: Application to an arbitrary network," *IEEE Trans. on Power Apparatus and Systems,* Vols. PAS-101, no. 10, pp. 3639 - 3647, 1982.

[66] A. Tabesh and R. Iravani, "Frequency response analysis of torsional dynamics," *IEEE Trans. on Power System,* vol. 19, no. 3, pp. 1430 - 1437, 2004.

[67] A. Tabesh and R. Iravani, "On the application of the complex torque coefficients method to the analysis of torsional dynamics," *IEEE Trans. on Energy Conversion,* vol. 20, no. 2, pp. 268 - 275, June 2005.

[68] S. N. Vukosavic and M. R. Stojic, "Suppression of torsional oscillations in a high-performance speed servo drives," *IEEE Trans. on Industrial Electronics,* vol. 45, no. 1, pp. 108-117, 1998.

[69] K. Szabat and T. Orlowska-Kowalska, "Vibration suppression in a two-mass drive system using PI speed controller and additional feedbacks – Comparative study," *IEEE Trans. on Industrial Electronics,* vol. 54, no. 2, pp. 1193 - 1206, April 2007.

[70] T. Orlowska-Kowalska, K. Szabat and M. Dybkowski, "Neuro-Fuzzy adaptive control of the IM drive with elastic coupling," *13th International Power Electronics and Motion Control Conference (EPE-PEMC),* pp. 2211 - 2218, 2008.

[71] T. Orlowska-Kowalska, M. Dybkowski and K. Szabat, "Adaptive sliding-mode neuro-fuzzy control of the two-mass induction motor drive without mechanical sensors," *IEEE Trans. on Industrial Electronics,* vol. 57, no. 2, pp. 553 - 564, February 2010.

[72] R. Muszynski and J. Deskur, "Damping of torsional vibrations in high-dynamic industrial drives," *IEEE Trans. on Industrial Electronics,* vol. 57, no. 2, pp. 544-552, 2010.

[73] R. Eloundou and W. Singhose, "Saturation compensating input shapes for reducing vibration," *6th International Conference on Motion and Vibration Control,* pp. 625 - 629, August 2002.

[74] S. E. Saarakkala and M. Hinkkanen, "State-space speed control of two-mass mechanical systems: Analytical tuning and experimental evaluation," *IEEE Trans. on Industry Applications,* vol. 50, no. 5, pp. 3428-3437, September/October 2014.

[75] S.-M. Yang and S.-C. Wang, "The detection of resonance frequency in motion control systems," *IEEE Trans. on Industry Applications,* vol. 50, no. 5, pp. 3423-3427, 2014.

[76] L. Harnefors, R. Finger, X. Wang, H. Bai and F. Blaabjerg, "VSC input-admittance modeling and analysis above the Nyquist frequency for passivity-based stability assessment," *IEEE Trans. in Industrial Electronics,* vol. 64, no. 8, pp. 6362-6370, 2017.

[77] A. Dutka and M. Orkisz, "Analysis and remedies for torsional oscillations in rotating machinery," *Power Electronics & Drives (SDEMPED),* pp. 474 - 481, 2011.

[78] J. M. Pacas, A. John and T. Eutenbach, "Automatic identification and damping of torsional vibration in high-dynamic drives," *ISIE'2000,* pp. 201 - 206, 2000.

[79] H. Sarén and O. Pyrhönen, "Active vibration suppression using DTC drive and automatic parameter identification of a two mass system," in *European Power Electronics (EPE)*, Toulouse, 2003.

[80] B. Wu, D. Xu, H. Geng and Y. Geng, "Active damping for torsional vibrations in PMSG based WECS," *Applied Power Electronics Conference and Exposition (APEC),* 2010.

[81] J.-K. Ji and S.-K. Sul, "Kalman filter and LQ based speed controller for torsional vibration suppression in a 2-mass motor drive system," *IEEE Trans. on Industrial Electronics,* vol. 42, no. 6, pp. 564-571, 1995.

[82] C. Sourkounis, "Active damping of torsional vibrations by H-Infinity control," *12th Int. conference on optimization of electrical and electronic equipment, OPTIM 2010,* 2010.

[83] J.-H. Hours, "Active vibration damping in variable speed drive systems (Internship report)," ABB , Dättwil, 2011.

[84] T. J. Besselmann, S. Almer and H. J. Ferreau, "Model predictive control of load-commutated inverter-fed synchronous machine," *IEEE Trans. on Power Electronics,* vol. 31, no. 10, pp. 7384-7393, 2016.

[85] T. J. Besselmann, S. Van de moortel, S. Almer, P. Jörg and H. J. Ferreau, "Model predictive control in the multi-megawatt range," *IEEE Trans. on Industrial Electronics,* vol. 63, no. 7, pp. 4641-4648, 2016.

[86] H. Wertz, S. Beineke, N. Fröhleke, S. Bolognani, K. Unterkofler, M. Zigliotto and M. Zordan, "Computer aided commissioning of speed and position control for electrical drives with identification of mechanical load," 1999.

[87] M. Tallfors, *Parameter estimation and model based control design of drive train systems,* Stockholm: Kungliga Tekniska Högskolan (KTH), 2005.

[88] D. Xu, L. Niu, M. Yang, X. Gui and Z. Liu, "On-line inertia identification algorithm for PI parameters optimization in speed loop," *IEEE Trans. on Power Electronics,* vol. 30, no. 2, pp. 849-859, 2015.

[89] M. Bruha, Modeling of synchronous motor drive (Master thesis), Plzeň/Pilsen: University of West Bohemia, 2011.

[90] Dartmouth College, "System analogies," [Online]. Available: http://www.dartmouth.edu/~sullivan/22files/System_analogy_all.pdf. [Accessed 14 August 2018].

[91] Tutorialspoint, "tutorialspoint.com," [Online]. Available: https://www.tutorialspoint.com/control_systems/control_systems_electrical_analogies_mechanical.htm. [Accessed 14 August 2018].

[92] L. Hu and R. Yacamini, "Harmonic transfer through converters and HVDC links," *IEEE Trans. on Power Electronics,* vol. 7, no. 3, pp. 514-525, 1992.

[93] A. Ekström and Y. Jiang, "General analysis of harmonic transfer through converters," *IEEE Trans. on Power Electronics,* vol. 12, no. 2, pp. 287-293, 1997.

[94] F. C. Nelson, "Rotor dynamics without equations," vol. 10, no. 3, pp. 2 - 10, 2007.

[95] R. Gasch and H. Pfützner, Rotordynamics (in Czech), Prague: SNTL, 1980.

[96] J. J. Simond, A. Sapin, M. Tu Xuan, R. Wetter and P. Burmeister, "12-pulse LCI synchronous drive for a 20 MW compressor modeling, simulation and measurements," *Fourteenth IAS Annual Meeting, Industry Applications Conference,* vol. 4, pp. 2302 - 2308, October 2005.

[97] T. Holopainen, J. Niiranen, P. Jörg and D. Andreo, "Electric motors and drives in torsional vibration analysis and design," in *Proceedings of the Forty-Second Turbomachinery Symposium*, Houston, Texas, 2013.

[98] P. Jörg, A. Lenzi and V. Depau, "Optimization of transient behavior of complex turbocompressor shaft lines," in *IEEE IAS Annual Meeting*, Orlando, Florida, 2011.

[99] T. Wymann and P. Jörg, "Power loss ride-through in a variable speed drive system," in *PCIC Europe*, Amsterdam, 2014.

[100] M. Kita, T. Hataya and Y. Tokimasa, "Study of a rotordynamic analysis method that considers torsional and lateral coupled vibrations in compressor trains with a gearbox," in *Proceedings of thirty-sixth Turbomachinery Symposium*, 2007.

[101] A. Muszynska, Rotordynamics, Boca Raton, Florida: CRC Press, Taylor & Francis group, 2005.

[102] J. Huster, L. Eckert and F. Pohle, "Calculation and measurement of torsionals in large steam turbosets," *ABB Review,* pp. 31-40, June 1998.

[103] P. Jörg, "Load Oscillation Damping Functions in the VSD Control," ABB Switzerland Ltd, Turgi, 2015.

[104] L. Harnefors, L. Zhang and M. Bongiorno, "Frequency-domain passivity-based current control design," *IET Power Electronics,* vol. 1, no. 4, pp. 455-465, 2008.

[105] L. Harnefors, A. G. Yepes, A. Vidal and J. Doval-Gandoy, "Passivity-based stabilization of resonant current controllers with consideration of time delay," *IEEE Trans. on Power Electronics,* vol. 29, no. 12, pp. 6260-6263, 2014.

[106] L. Harnefors, A. G. Yepes, A. Vidal and J. Doval-Gandoy, "Passivity-based controller design of grid-connected VSCs for prevention of electrical resonance instability," *IEEE Trans. on Industrial Electronics,* vol. 62, no. 2, pp. 702-710, 2015.

[107] M. Rossi, "Torsional vibrations in medium voltage electrical drives: Analysis and control design (dissertation)," Politecnico di Milano / ABB Switzerland, Turgi, 2015.

[108] I. N. Kar, T. Miyakura and K. Seto, "Bending and torsional vibration control of a flexible plate structure using H-infinity based robust control law," *IEEE Trans. on Control Systems Technology,* vol. 8, no. 3, pp. 545-553, 2000.

[109] P. Jörg and C. Stulz, "Technical note: Modeling of DTC MV drive for analysis of system dynamics," ABB Switzerland (MV drives), Turgi, 2005.

[110] M. A. Corbo and C. P. Cook, "Torsional vibration analysis of synchronous motor-driven turbomachinery," in *29th Turbomachinery Symposium*, Houston, TX, 2000.

[111] D. Buzzini and M. Zago, "Testing large ASDS," in *PCIC Europe*, Prague, 2012.

[112] P. Jörg, A. Tresch and M. Bruha, "A model based approach to optimize controls of a large LCI VSD for minimal grid-side sub-synchronous torsional interaction," *PCIC Europe 2013 - Petroleum & Chemical Industry Conference,* vol. 10, pp. 1-7, May 2013.

[113] M. Leader and R. Kelm, "Practical implementation of torsional analysis and field measurement," in *National technical training symposium of the Vibration Institute*, 2004.

[114] L. A. Kilgore, D. G. Ramey and M. C. Hall, "Simplified transmission and generation system analysis procedures for subsynchronous resonance problems," in *IEEE Trans. on Power Apparatus and Systems*, 1977.

[115] J. S. Joyce, T. Kulig and D. Lambrecht, "Torsional fatigue of turbine-generator shafts caused by different electrical system faults and switching operations," in *IEEE Trans. on Power Apparatus and Systems*, 1978.

[116] P. Zizliauskas, "Subsynchronous torque interaction in HVDC Light B - a theoretical description," Lund University.

[117] API 684 Rotordynamic Tutorial, *Lateral critical speeds, unbalance response, stability, train torsionals and rotor balancing,* second ed., Washington: API Publishing Services, 2005.

[118] H. Weiss, "Adjustable speed AC drive systems for pump and compressor applications," *Industry Applications, IEEE Transactions on,* no. 1, pp. 162-167, 1974.

[119] E. Douville, "Selection and Application of Variable Speed Motor Drive Systems," *Industry Applications, IEEE Transactions on,* no. 6, pp. 698-702, 1982.

[120] E. Turner and C. Lemone, "Adjustable-speed drive applications in the oil and gas pipeline industry," *Industry Applications, IEEE Transactions on,* vol. 25, no. 1, pp. 30-35, 1989.

[121] R. Hanna and S. Prabhu, "Medium-voltage adjustable-speed drives-users' and manufacturers' experiences," *Industry Applications, IEEE Transactions on,* vol. 33, no. 6, pp. 1407-1415, nov/dec 1997.

[122] J. Rodriguez, S. Bernet, B. Wu, J. Pontt and S. Kouro, "Multilevel voltage-source-converter topologies for industrial medium-voltage drives," *Industrial Electronics, IEEE Transactions on,* vol. 54, no. 6, pp. 2930-2945, 2007.

[123] B. Schmitt and R. Sommer, "Retrofit of fixed speed induction motors with medium voltage drive converters using NPC three-level inverter high-voltage IGBT based topology," in *Industrial Electronics, 2001. Proceedings. ISIE 2001. IEEE International Symposium on*, 2001.

[124] ABB, *Load Oscillation Damping Functions in VSDs,* ABB Switzerland.

[125] V. Vondrasek, J. Langhammer, A. Peroutka, J. Mesicek and J. Molnar, Projektovani vykonovych polovodicovych menicu - vybrane stati (in Czech), Designing of Power Semiconductor Converters - Selected parts (in Czech), Plzen: University of West Bohemia, 2008.

[126] M. Hudeczek, Increasing the reliability of asynchronous electromotors including driven machines (in Czech), Ostrava: Hudeczek Service, 2011.

[127] K. Zeman, Z. Peroutka and M. Janda, Automatic regulation of asynchronous motor drives, J. Flajtingr, Ed., Pilsen: University of West Bohemia, 2007.

[128] M. Pittermann, Overview of converters for electric drives (in Czech), 1. ed., Plzen: University of West Bohemia, 2015, p. 259.

[129] J. Rodriguez, J.-S. Lai and F. Z. Peng, "Multilevel inverters: A survey of topologies, controls and applications," in *IEEE Trans. on Industrial Electronics*, August 2002.

[130] P. Jörg, "Phase behaviour of torque pulsations of load-commutated inverters," ABB Switzerland, Turgi, 2009.

Author's publications

List of author's granted patents

[A1] M. Bruha, T. Besselmann, P. Joerg, S. Almer, *Method for reduced harmonic excitation during pulse mode operation of load commutated inverters,* ID No. CH-1605101, No. 16199635.0.

List of author's publications presented at international conferences

[A2] P. Jörg, A. Tresch, M. Bruha, „A model based approach to optimize controls of a large LCI VSD for minimal grid-side sub-synchronous torsional interaction", *PCIC Europe 2013 – Petroleum & Chemical Industry Committee*, Istanbul, Turkey, 2013.

[A3] M. Bruha, Z. Peroutka, „Torsional vibration in large variable speed drive systems: Origin and mitigation methods", *EPE'15 ECCE-Europe – 17th European Conference on Power Electronics and Applications*, Geneve, Switzerland, 2015.

[A4] M. Mauri, M. Rossi, M. Bruha, „Generation of torsional excitation in a variable-speed-drive-system", *SPEEDAM 2016 – International Symposium on Power Electronics, Electrical Drives, Automation and Motion ,* Capri island, Italy, 2016.

[A5] M. Bruha, „Importance of control engineering to minimize torsional vibration in variable speed drive systems", *PCIC Europe 2016 – Petroleum & Chemical Industry Committee*, Berlin, Germany, 2016.

[A6] M. Bruha, M. Byrtus, K. Pietilaeinen, M. Rossi, and M. Mauri, „Torsional issues related to variable frequency control of elastic drive systems" *IECON 2016 - 37th Annual Conference on IEEE Industrial Electronics Society*, Florence, Italy, 2016, pp. 2981 - 2987.

[A7] M. Bruha, M. Sirovy, V. Kindl, "*Methodology for complex energy efficiency evaluation of high-power variable speed drive applications*", 17th International Conference on Mechatronics – Mechatronika (ME), 2016

[A8] M. Bruha, M. Visser, J. von Sebo, E. Virtanen, P. Tallinen, "Protection of VSD transformers", Petroleum and Chemical Industry Conf. Europe (PCIC Europe), Vienna 2017, pp. 1 - 12

[A9] M. Bruha, V. Kindl, K. Hruska, "Motor friendliness of variable frequency drives with output transformer", European Power Electronics (EPE) conference, Warsaw 2017

List of author's proceedings presented at national conferences

[A10] M. Brůha, „Vybraná specifika pohonu s vysokonapěťovým měničem ACS5000", Elektrické pohony – XXXIII. konference o elektrických pohonech, Plzeň, 2013.

[A11] M. Brůha, M, von Sebo, J.: „Intelligent protection of VSD transformers", Elektrické pohony – XXXV. konference o elektrických pohonech, Plzeň, červen 2017

List of author's scripts and models

[A12] M. Bruha, *make_waterfall_speed, make_waterfall_torque,* Matlab scripts to generate waterfall diagrams based on measured or simulated data, 2013

[A13] M. Bruha, *Bode_ACS_drive_with_DTC*, Matlab script to plot Bode diagram of speed controlled drive system with DTC for rigid or elastic mechanics, 2014.

[A14] M. Bruha, *LCI_CurrentCtrlLoop_RevC*, Matlab script to plot Bode diagram of LCI current control loop with several control variables, 2014

[A15] M. Bruha, *Campbell_Diagram_script_Rev0,* Matlab script to plot project specific Campbell diagram*,* 2016.

[A16] M. Bruha, *Elastic_mechanics_RevC.slx,* Matlab model to investigate torsional response of ealstic mechanics to various kind of excitation signals, 2016

List of author's research reports

[A17] M. Bruha, *Transient torsional study of geared turbo-compressor train*, ABB research report No. ATDAD 111010-3, ABB Switzerland Ltd, Turgi 2011

[A18] M. Bruha, *Electro-mechanical interaction*, ABB research report No. 3BHS399110, ABB Switzerland Ltd, Turgi 2012

[A19] M. Bruha, *Closed loop simulations of LCI drive and compressor mechanical train*, ABB research report No. 3BHS542269, ABB Switzerland Ltd, Turgi 2013

[A20] M. Bruha, *Air gap torque analysis of ACS6000 LSU drive with DTC: Closed loop versus Open loop*, ABB research report No. 3BHS553671, ABB Switzerland Ltd, Turgi 2014

[A21] M. Bruha, *Stability of speed control loop*, ABB research report No. DMDR-A1 141014-3, ABB Switzerland Ltd, Turgi 2014

[A22] M. Bruha, *Parameterization of MV drives in applications sensitive for torsional vibration*, Engineering guideline, ABB doc. no. 3BHS828037 ZAB E01, December 2015

List of author's training courses and seminars

[A23] M. Corbo, E. Swanson, M. Leader, *Practical Rotordynamics for Real Machinery*

- 5-Day Seminar with certificate
- Experts from No Bull Engineering und X-Dot Engineering
- Location: Charlottesville, Virginia, USA, Date: March 2012

[A24] Measurement of torque and force (HBM Seminar)

- Topics: Force and torque measurement, Data acquisition systems (amplifiers, filters, sampling methods etc.)
- Experts from HBM Academy
- Location: Lenzburg, Switzerland, Date: March 2015

[A25] J. Schmied, A. Fuchs, M. Perucchi, F. Gaulard, *Rotor Dynamic Seminar*

- 2-Day seminar with certificate plus 1-Day hands-on MADYN 2000
- Experts from Delta JS
- Location: Zurich, Switzerland, Date: April 2016

[A26] Noise and vibrations due to magnetic forces in electrical machines

- Webinar organized by EOMYS Engineering
- Noise, Vibration and Harshness (NVH) issues in electrical systems
- Introduction of MANATEE software
- Date: March 2017

Appendix 1 – Oscillations across power electronic systems

A) Oscillations in traction application

A converter installed in a rolling stock application is likely to cause grid instability because:

- The train moves along the grid cables, meaning the grid parameters constantly change for the converter, because the position of the converter changes constantly in time. The train is 'scanning the grid for a resonance' by moving from position A to B.
- The damping effect is higher in 16.7 Hz grids than in 50 Hz grids (X/R ratio is close to 1 whereas in 50 Hz grids this ratio is closer to 10…20).

In Switzerland, the Swiss Federal Authority for Transportation requires as of 2013 that all traction converters must be passive above 102 Hz, but in future it is planned to reduce this number to 82 Hz.

Case: Collapse of Swiss railway system

This issue is also known as "165 Hz instability". It happened on Saturday, 9th April 1995. All modern locomotives of series Re 450 and Re 460 switched off at the same time. A large 165 Hz oscillation in the traction line supply has been present all over Switzerland [28]. The root cause of the large oscillations is an interaction between modern inverter fed traction vehicle and the corresponding traction line supply. The power electronic traction vehicle has to be considered as a vehicle active at certain frequencies. When the excitation frequency of traction vehicle matches the resonance frequency of the supply network, oscillations will occur. The control system of the vehicle might further amplify the oscillations. These are the conditions where the power supply instability develops. The phenomenon has been studied and confirmed by several tests in the Swiss railway network.
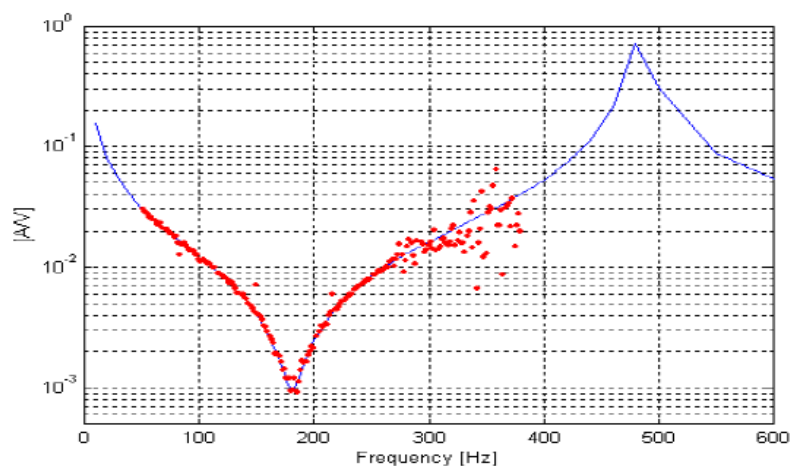
Modelled (blue) and measured (red) line admittance [28]
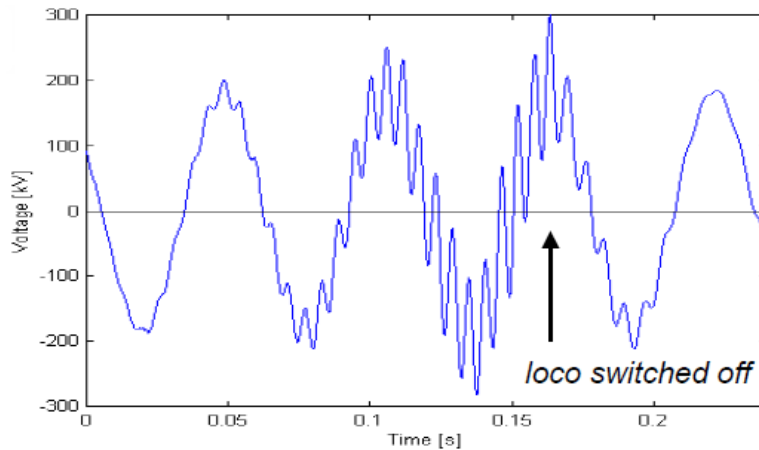
Instability in 132 kV network (up to 60% overvoltage) [28]

The problem in Switzerland has been solved by software changes on the locomotives of Re 460 series. However, as the report [28] states, there is still no guideline how to determine the degree of stability. The analysis is so far only possible by means of simulations or calculations. The measurement principle is depicted in Appendix 2 – Measurement of input admittance: Principle scheme.

The approach of vehicle input impedance/admittance can predict the instability. The modelled results match very well real measurements – see figure above.

B) Oscillations in conventional power generation

The types of interaction are described in chapter 2.1.2.4. The sub-synchronous resonance, induction generator effect and torsional interaction phenomena are closely coupled. The induction generator effect can be explained by using basic equivalent circuit diagram of induction machine. Although the generator is typically a synchronous machine, the damper winding or the rotor surface itself act during transients in similar way like the squirrel cage rotor (see [114] for more details). The same effect happens also in case of non-synchronous frequencies in stator current and/or voltage. We might imagine the physics as a superposition of steady state synchronous generator operation and imposed induction generator effect for sub-synchronous frequency. E_i is the voltage induced from oscillations of rotor.
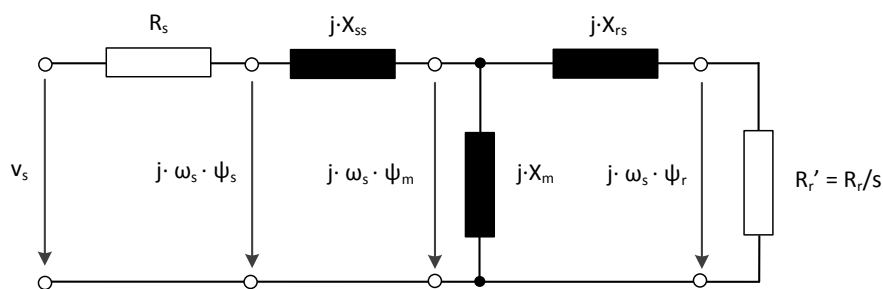
Equivalent circuit of induction machine
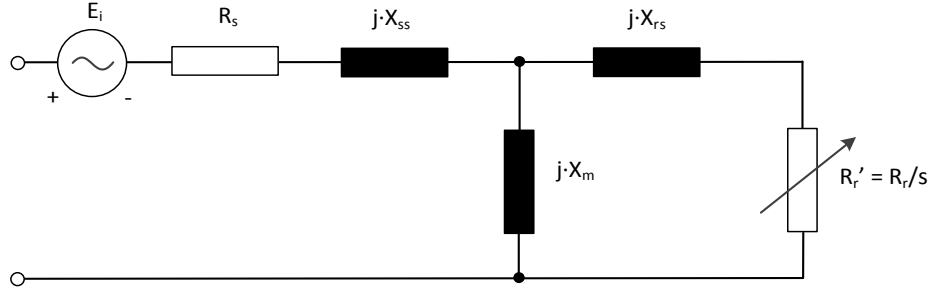
Simplified equiv. circuit diagram for synchronous machine at non-synchronous frequency [114]

The effective rotor resistance as seen from stator terminals is:

$$R'_r = \frac{R_r}{s} \tag{55}$$

R'_r is the equivalent rotor resistance

R_r is the physical rotor resistance

s is the slip

The slip is defined in (56). As slip is relative quantity, it can be expressed using angular frequencies or electric frequencies:

$$s = \frac{\omega_0 - npp.\,\omega_m}{\omega_0} = \frac{\omega_r}{\omega_0} = \frac{f_r}{f_0} \tag{56}$$

ω_0 is the synchronous angular frequency (frequency of magnetic field of stator)

npp is number of pole pairs

ω_m is the mechanical angular frequency of rotor

ω_r is the rotor angular (electrical) frequency

Series capacitor compensated electric systems inherently have a subsynchronous resonance frequency f_{er}. During disturbances in the electric grid there will be currents flowing in the stator of generator (armature) at frequency f_{er}. The positive sequence component of these currents will produce a rotating magnetic field an angular frequency $2\pi f_{er}$ while the machine's rotor keeps rotating at synchronous angular frequency $2\pi f_0$. A current of frequency $f_r = f_{er} - f_0$ will be induced into rotor windings and corresponding electromagnetic torque component at frequency f_r will be developed. The torque component corresponds to slip as per (3):

$$s = \frac{f_{er} - f_0}{f_{er}} \tag{57}$$

By combination (55) and (57) we obtain:

$$R'_r = \frac{R_r \cdot f_{er}}{f_{er} - f_0} \tag{58}$$

Since f_{er} is subsynchronous, then per definition $f_{er} < f_0$ and therefore $R'_r < 0$. The effective resistance for this particular component viewed from stator terminals will always be negative. If this equivalent resistance exceeds the sum of positive armature resistance and system resistance at the resonance frequency f_{er}, the armature current can be sustained or growing. The phenomenon is

known as induction generator effect [33] or self-excitation effect. A similar effect can potentially appear in some variable speed drive systems. Therefore, it is worth to mention the problematic here. The torque component developed on the generator rotor contributes to torsional interaction with turbine-generator shaft string. The phenomenon is known as torsional interaction or more specifically sub-synchronous torsional interaction and involves both electrical and mechanical systems. The torsional interaction can be triggered from both sides:

> a) Generator rotor oscillations at torsional natural frequency f_{TNF} induce sub-synchronous voltage components in the stator (armature) of sub-synchronous frequency $f_{en}^- = f_0 - f_{TNF}$ and super-synchronous frequency $f_{en}^+ = f_0 + f_{TNF}$.
>
> Note: f_{en}^- and f_{en}^+ are often referred to as sidebands (synchronous frequency plus/minus the mechanical oscillation frequency).
>
> b) Electric grid disturbance excites the resonance frequency f_{er} causing currents at this frequency to flow through stator (armature) windings of generator. A rotating magnetic field at frequency f_{er} is developed and the interaction between this field generator rotor field at frequency f_0 creates a torque component at frequency $f_0 - f_{er}$. If this torque component coincides with the torsional natural frequency f_{TNF} of the turbine-generator shaft and the magnitude exceeds the damping torque, sustained or growing oscillations can occur.
>
> In case of severe faults in the electric system (especially short circuits) a significant sub-synchronous torsional excitation can develop. If the frequency of this sub-synchronous transient torque corresponds to the torsional natural frequency of turbine-generator shaft, a large cyclic shaft torque will appear. Such torque oscillations have the potential to damage the shaft components [115], [54].

C) Oscillations in wind power generation

Passivity-based design

Admittance analysis method as a learning from traction becomes state of the art. The excitation is the grid voltage and the response is the converter current. Admittance is a transfer function that gives the current answer to a voltage excitation. The admittance approach is only possible for linear and time invariant systems. A real converter is never a linear system, but as long as there is no strange control function deviating the linear assumption, the approximation can be made. Converter is also inherently time variant as there are many adjustable control parameters that modify the response. Therefore the parameter settings need to be frozen when determining the admittance. The admittance, with respect to grid stability, is not equally important in all frequency regions. One approach used in the industry is enforced passivity within the frequency band of interest.

Torsional vibration in wind turbine-generator shaft

Damping strategies employ either passive or active damping systems. Passive systems use mechanical components with increased damping, e.g. rubber elements. Active systems utilize pitch control (adjustment of blades) or software algorithms to modify the torque of generator. The latter one is the preferred method with two available solutions: conventional method with fixed parameter band-pass filters and model based damper structure.

D) Oscillations in power transmission (HVDC)

In late 1970s the risk of sub-synchronous torsional interaction was discovered for the first time during commissioning and operation of HVDC links (keyword Square Butte project in North Dakota). The HVDC system has a potential to interact adversely with turbine-generator torsional vibration modes and destabilize them. Rigorous test plans and extensive studies followed in order to understand the phenomena and design and verify control systems that prevent such dangerous interaction. The negative damping of HVDC increases with transmitted power (destabilization) while at the same time the inherent damping of turbine-generator mode increases with output power. Therefore, it is difficult to define the worst-case condition.

The control strategy of firing the semiconductors pays role for the damping performance as explained e.g. in [116]. The two basic methods for generation of firing pulses are:

- Individual phase control (IPC)

This is the older method used in early HVDC installations. The pulse generator for each phase or semiconductor is independent of each other. The major drawback of IPC scheme is a harmonic stability problem, characterized by magnification of noncharacteristic harmonics in steady state.

- Equidistant pulse control (EPC)

The firing pulses are generated in steady state at equal intervals. There are three variations of the EPC scheme: Pulse frequency control (PFC), Pulse period control and Pulse phase control (PPC).

E) Sub-synchronous torsional interaction (SSTI)

Sub-synchronous interaction can appear in power systems between the turbine-generator and load. There are several types of load capable to destabilize the torsional mode of turbine-generator.

In general, any device that controls or responds rapidly to power or speed variations in the sub-synchronous frequency range is a potential source of excitation of sub-synchronous oscillations [33]. Among such devices belong:

- Excitation systems of generators with Power System Stabilizers
- HVDC converter controllers
- Variable speed motor controllers

There are two forms of instability [55]:

- steady increase in generator rotor angle due to lack of *synchronizing torque*
- rotor oscillations of increasing amplitude due to lack of sufficient *damping torque*.

Appendix 2 – Measurement of input admittance: Principle scheme

Messung der Eingangsadmittanz: Prinzipschema
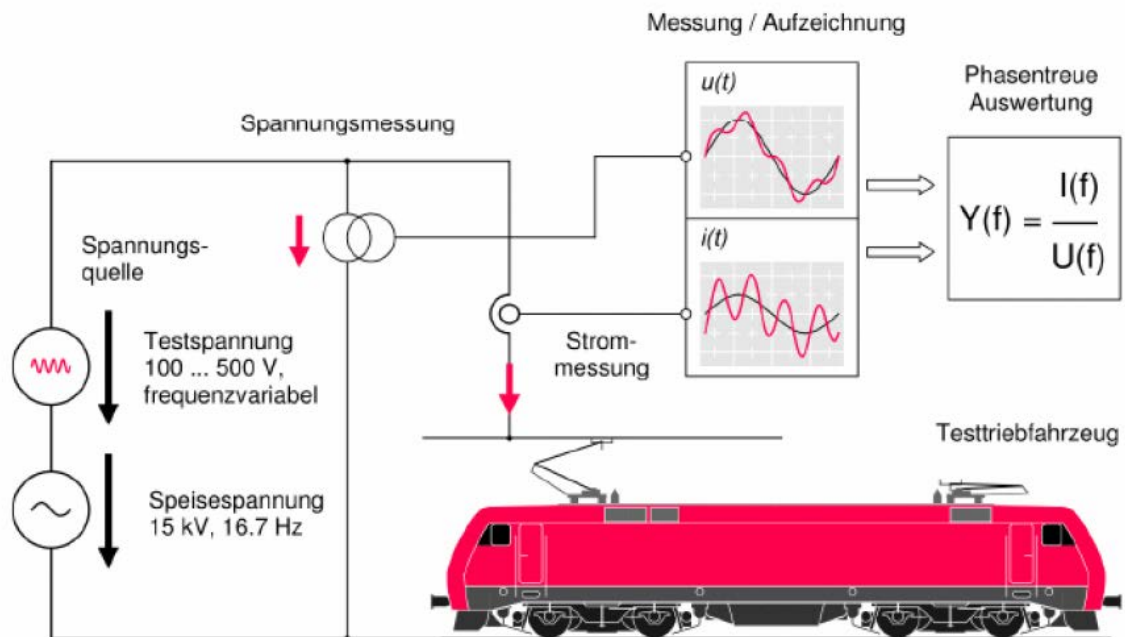
Figure in German language; translation provided below:

Messung	=	measurement
Aufzeichnung	=	recording
Phasentreue Auswertung	=	true phase evaluation
Spannungsmessung	=	voltage measurement
Strommessung	=	current measurement
Spannungsquelle	=	voltage source
Testspannung	=	test voltage
frequenzvariabel	=	variable frequency
Speisespannung	=	supply voltage
Teststriebfahrzeug	=	traction unit under test

The principle evolved from traction vehicles to wind converters and motor drives (especially drives with active rectifiers where several units operate in parallel).

Appendix 3 – System analogies between electrical and mechanical systems

When observing an object from mechanical point of view, the main properties typically are the mass or inertia, elasticity and friction. These three properties can be realized through separate idealized building elements

- inertial, but stiff and without friction → mass
- elastic, but without mass and friction → spring
- dissipative, but stiff and without mass → damper

In electrical world there are also three basic building elements used:

- capacitance → capacitor
- inductance → inductor (coil)
- resistance → resistor

The analogies differ depending on the literature source.

In translational systems the mass can be replaced with capacitance, spring with inductance and damping (friction) with resistance. Force is equivalent to current. Rotational systems have inertia instead of mass and torsional spring instead of linear spring.

- Mass m is equivalent to inductance L
- Stiffness k is equivalent to electric elastance $\frac{1}{C}$
- Damping (friction) b is equivalent to resistance R
- Excitation Q is equivalent to rate of change of voltage $\frac{dv}{dt}$
- Deflection q is equivalent to current I
- velocity v is equivalent to rate of change of current $\frac{di}{dt}$
- acceleration a is equivalent to second derivative of current $\frac{d^2 i}{dt^2}$

Each rotational equipment as a system of second or higher order has certain eigenfrequencies. These eigenfrequencies can be obtained as a solution of eigenvalue problem.

A system can oscillate if there are at least two energy storages so that the energy can be periodically exchanged or transformed. In rotordynamics there is the torsional disc as a storage (accumulator) of kinetic energy and the torsional spring as a storage of potential energy.

A comprehensive comparison is summarized on the last page of [90].

Appendix 4 – Unbalance, coupling misalignment and shaft eccentricity

A) Unbalance

Ideal stiff rotor has no or very small torque fluctuation and the centrifugal forces are compensated by axis symmetry. In reality, the mass distribution is not completely symmetrical due to manufacturing tolerances. The rotor is out of balance when the center of mass (gravity) does not coincide with the center of rotation. Effects of unbalance are vibration, noise, decreased life of bearings, reduced machine lifetime and increased maintenance.

The centrifugal force acting on the eccentric center of gravity is calculated according to (59).

$$F_c = m \cdot \varepsilon \cdot \omega^2 \tag{59}$$

Elastic (flexible) rotor:

The centrifugal forces increase with speed. Above certain speed the elastic deformation of rotor ρ_H has to be taken into account because it increases the forces. Overall centrifugal force is given by (60):

$$F_c = m \cdot (\varepsilon + \rho_H) \cdot \omega^2 \tag{60}$$

$$\varepsilon \dots \text{Eccentricity}$$

$$\rho_H \dots \text{Elastic deformation}$$

We talk about elastic rotor when the elastic deformation is not negligible compared to eccentricity. An Imagination about behavior of elastic shaft is obtained by defining the condition of equilibrium of acting forces. The returning force is in balance with centrifugal force:

$$F_r = k \cdot \rho_H = F_c = m \cdot (\varepsilon + \rho_H) \cdot \omega^2 \tag{61}$$

$$F_r \dots \text{Returning force}$$

$$k \dots \text{Bending stiffness}$$

Based on condition (61) the elastic deformation can be expressed as (62):

$$\rho_H = \frac{\left(\frac{\omega}{\Omega}\right)^2}{1 - \left(\frac{\omega}{\Omega}\right)^2} \cdot \varepsilon \tag{62}$$

where Ω is the undamped eigenfrequency given by relationship (63):

$$\Omega = \sqrt{\frac{k}{m}} \tag{63}$$

At low speed ($\omega < \frac{1}{2}\Omega$) the bending of the shaft increases proportionally with centrifugal force $m \cdot \varepsilon \cdot \omega^2$, because the impact of the term $m \cdot \rho_H \cdot \omega^2$ in (60) is very small. For $\omega = \frac{1}{2}\Omega$ the shaft deformation reaches the value of eccentricity ε. For $\omega = \Omega$ the critical speed appears where the shaft bending (by assumptions of undamped system) is infinitely large. At very high speed ($\omega \gg \Omega$) the self-centering effects apply.
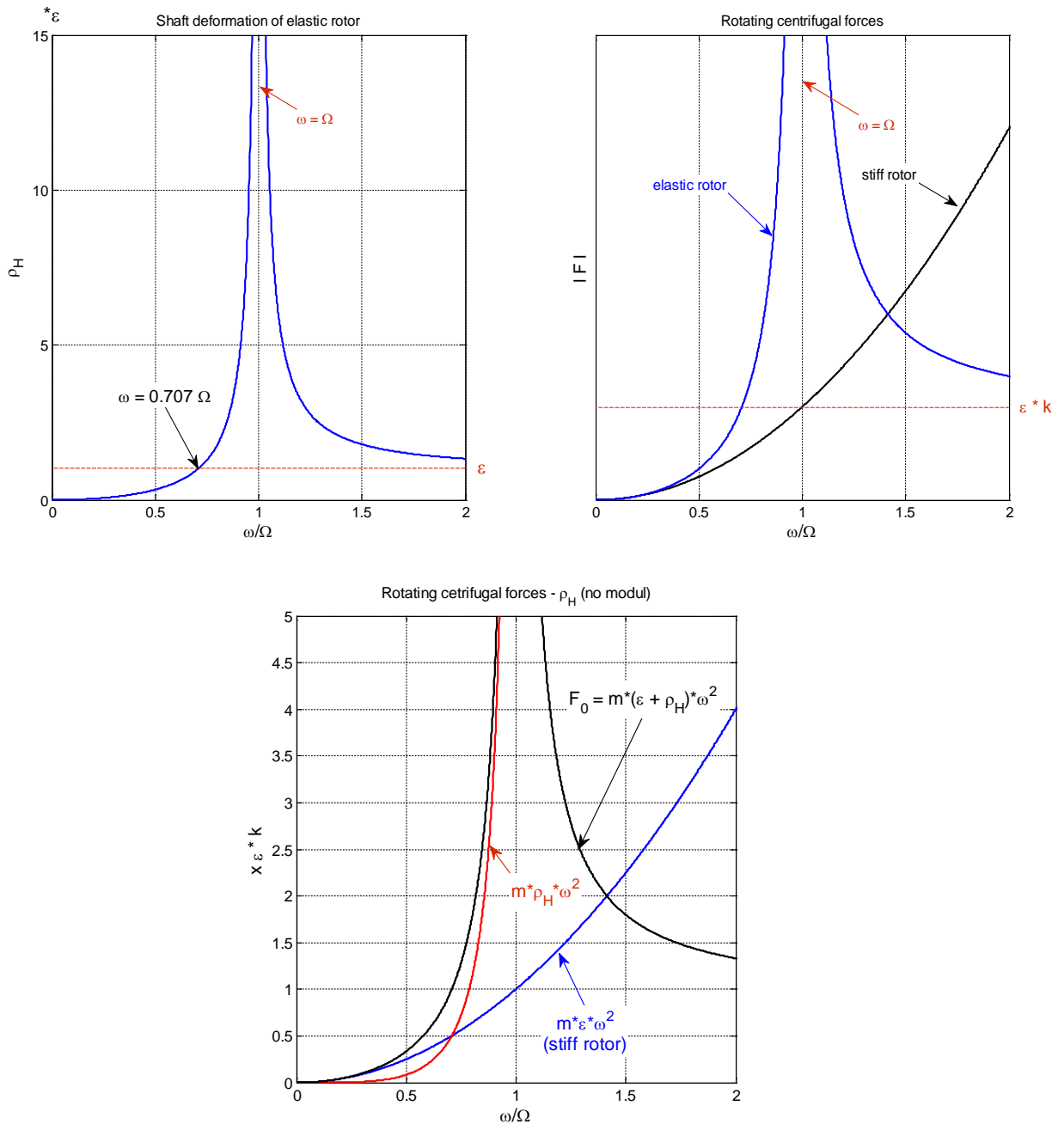
Shaft deformation and centrifugal forces due to unbalance

The force F_c causes reactions F_l and F_p inside the bearings. These forces increase with the square of the shaft speed ($F_l, F_p \sim \omega^2$). Centrifugal forces and forces in bearings can be minimized by attaching masses in two selected balancing planes. This procedure is called rotor balancing.

Rotor balancing is an important task in design and testing of rotating equipment, particularly in turbomachinery, and strict limits apply. Despite of this fact, every rotor has some residual unbalance. The excitation frequency from unbalance corresponds to the fundamental rotor frequency (sometimes called "1X"). Maximum allowed magnitudes are defined in international standards such as ISO,

API or VDI. The magnitude of excitation is determined at the beginning of torsional analysis. Typical values are 1% or 2% of nominal transmitted torque.

B) Coupling misalignment

Similar as unbalance, the couplings are in reality never perfectly aligned. Misalignment is a condition where the centerlines of the coupled shafts do not coincide. The misalignment is radial, axial, angular or a combination of all of them. Parallel (radial or axial) misalignment occurs in case the shaft centerlines are parallel, but not coincident. Angular misalignment is the situation where the misaligned shafts meet at a point, but are not parallel. Modern couplings tolerate certain degree of misalignment so for them it is not a primary concern. However, it causes additional forces in bearings. Therefore, misalignment shall be minimized. The excitation frequency is the fundamental rotor frequency and twice this frequency (sometimes called "1X" and "2X"). Parallel misalignment has dominant 2X component with smaller 1X component. Angular misalignment has largest 1X component, but 2X and eventually 3X are present as well.

The recommended amplitude of excitation torque due to misalignment with shaft speed ("1X") is typically 1% of the transmitted torque, whereas that of 2X shaft speed ("2X") is assumed 0.5% of the transmitted torque.

Radial Misalignment   Axial Misalignment   Angular Misalignment
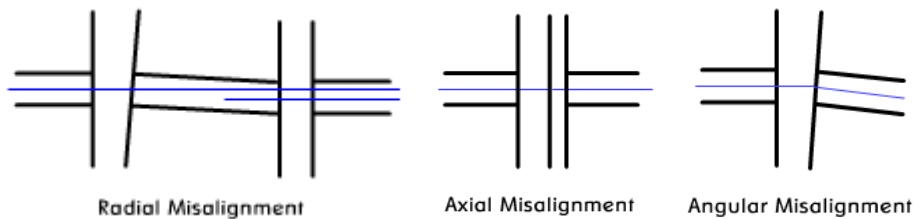
Radial, axial and angular misalignment between the shafts

C) Shaft eccentricity

Shaft eccentricity is a condition in which the geometric center of the rotating shaft moves from the true center (the center the assembly tries to rotate around naturally). Most often root cause of shaft eccentricity is bow or bend. It can be developed when the rotor is sitting idle e.g. during overhaul or it has been inadvertently stopped during coast down (mechanical bow / temporary thermal bow / gravity bow).

Appendix 5 – Campbell diagram for LCI and VSI drives

A) LCI drives

MOS = Minimum operating speed

MCS = Maximum continuous speed

Magenta dots – intersections of excitation frequency and torsional natural frequency
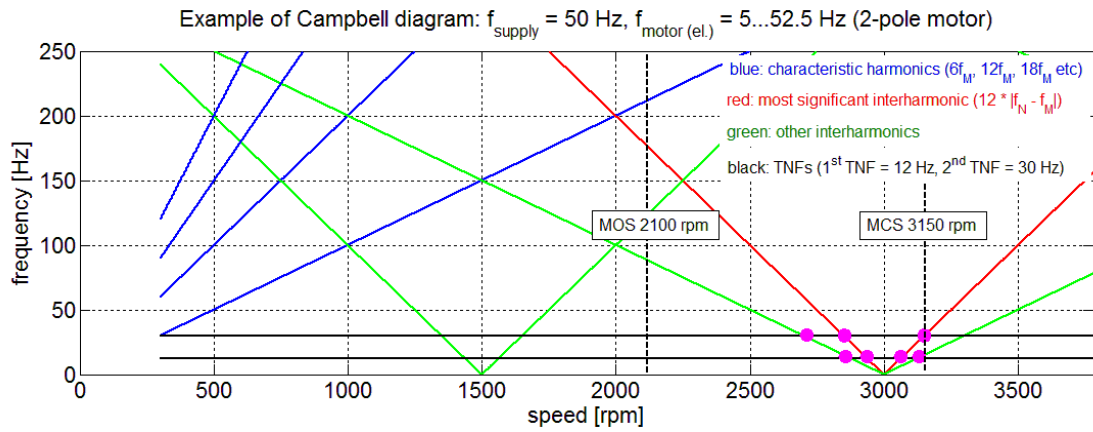
Campbell diagram for 50 Hz supply and 50 Hz motor (2-pole)
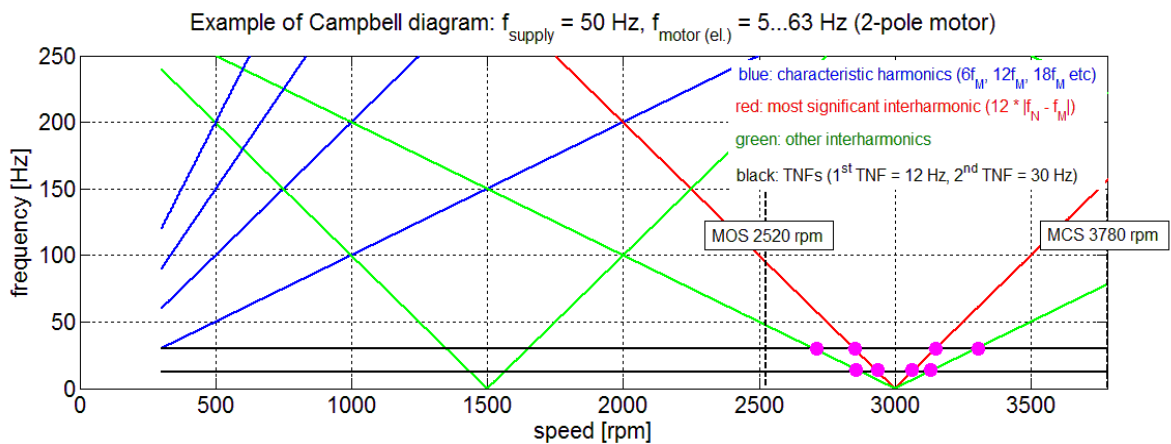
Campbell diagram for 50 Hz supply and 60 Hz motor (2-pole)
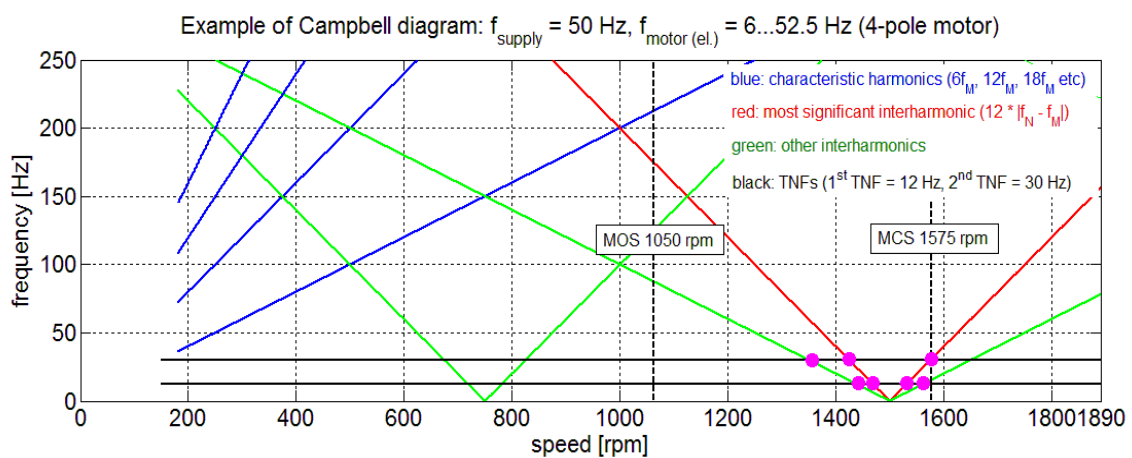
Campbell diagram for 50 Hz supply and 50 Hz motor (4-pole)
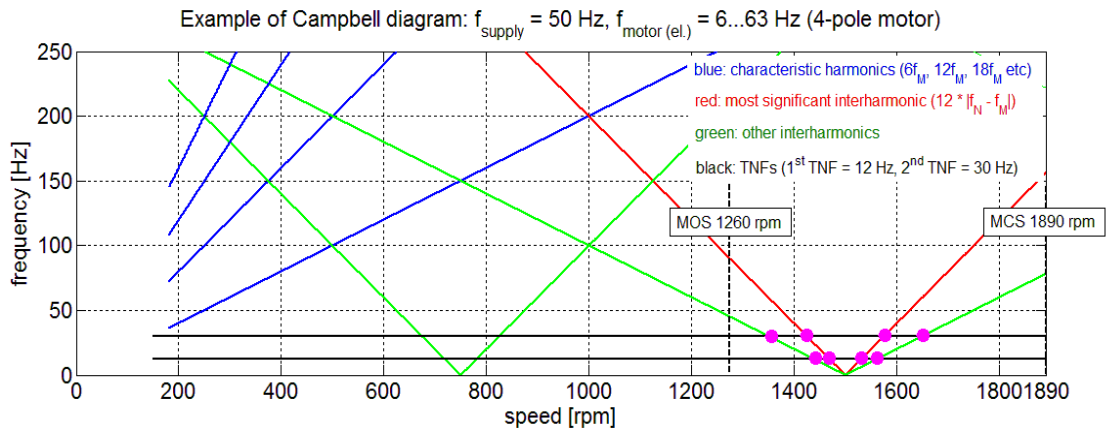
Campbell diagram for 50 Hz supply and 60 Hz motor (4-pole)
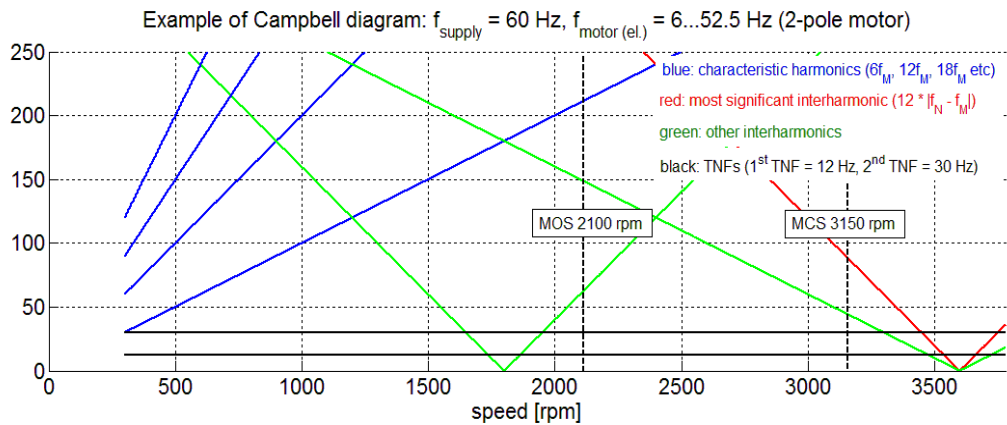
Campbell diagram for 60 Hz supply and 50 Hz motor (2-pole)
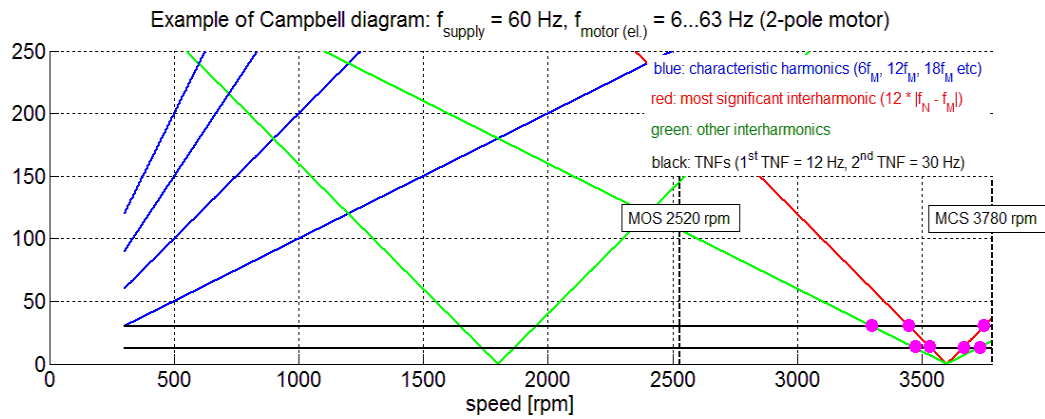
Campbell diagram for 60 Hz supply and 60 Hz motor (2-pole)
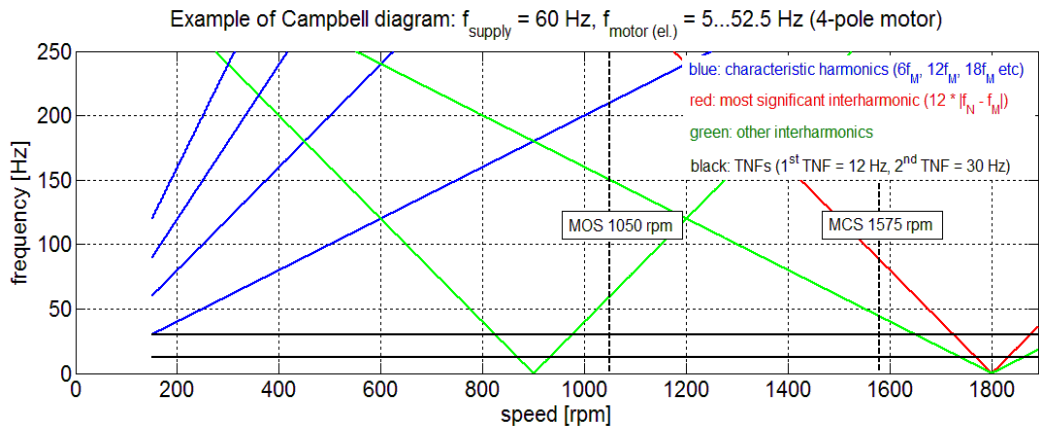
Campbell diagram for 60 Hz supply and 50 Hz motor (4-pole)
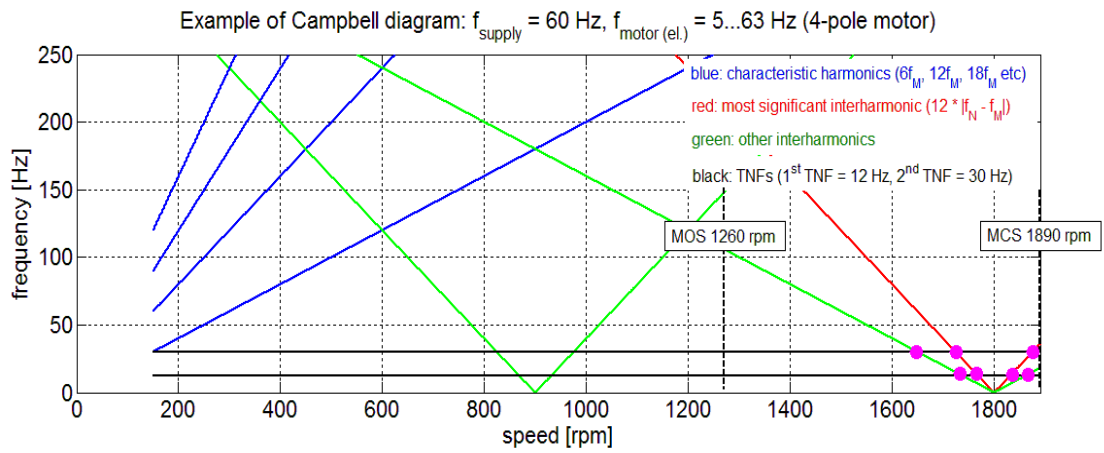
Campbell diagram for 60 Hz supply and 60 Hz motor (4-pole)

B) VSI drives

Project specific Campbell diagram

Legend

– – – (blue dashed)	Characteristic torque harmonics due to VFD operation, magnitude range 1…2.5% rated torque
– – – (grey dashed)	Torque excitation due to mechanical reasons as recommended by API standards
—— (red)	Torsional natural frequency (15 Hz just as example)

Notes/Comments

1. MOS… Minimum Operation Speed (continuous)
2. MCS… Maximum Continuous Speed
3. Characteristic torque harmonics due to VFD operations have magnitude 1…2.5%
4. Non-Characteristic torque harmonics due to VFD operation («white noise») have very low magnitude in the range 0.1…0.3%

Appendix 6 – Introduction in rotordynamics and torsional analysis

A) Rotordynamics

There are three basic types of dynamics:

- lateral (radial, tranverse)
    - complex models including foundations etc.
    - measurable with state of the art instrumentation
    - adjustable alarm and trip limits
- torsional (twist)
    - relatively simple models
    - difficult to measure, usually not instrumented
    - limited observability
    - dangerous (problems can grow until failure)
- axial
    - less of a concern for most machines
    - important for magnetic bearing machinery
- structural
    - disk or blade vibration

Shortly summarized: Lateral vibration is easy to measure and difficult to predict. Torsional vibration is difficult to measure and easy to predict.

The simplest elastic model that allows to study rotordynamic behavior is called "Laval rotor" (German literature) or "Jeffcott rotor" (English literature). It is a single DOF model with one single rigid disk mounted on a circular flexible shaft.

- The disk has certain mass and inertia and is ideally stiff (rigid)
- The shaft element is mass-less and has a finite stiffness, i.e. is elastic (flexible)

Such model is of course an extreme simplification. However, it is possible to describe and explain almost all phenomena relevant in practical use (however insufficient for torsional issues).

The model can be easily extended by increasing the number of disk and shaft elements. In order to study torsional behavior at least two disks are needed.

Rotordynamic Terms:

- <u>Eigenfrequency:</u> An "Eigenfrequency" of a system is a frequency at which the system vibrates if affected by an impact force.
- <u>Resonance:</u> When the frequency of a periodic forcing phenomenon (excitation) applied to a rotor system (torsional vibration) or rotor-bearing support system (lateral vibration) coincides with an eigenfrequency of that system, the system will be in a state of resonance.
- <u>Critical speed:</u> A shaft rotational speed at which the rotor system (torsional) or rotor-bearing-support system (lateral) is in a state of resonance. According API the critical speed is defined as resonance with amplification factor greater than or equal 2.5.

The main objectives of a rotordynamics analysis are:

1. Predict critical speeds
2. Determine design modifications to change the critical speeds
3. Predict natural frequencies of torsional vibration (TNFs)
4. Calculate balance correction masses and locations from measured vibration data
5. Predict amplitudes of synchronous vibration caused by rotor imbalance
6. Predict threshold speeds and vibration frequencies for dynamic instability
7. Determine design modifications to suppress dynamic instabilities

ad 1) Speeds at which vibration due to rotor imbalance is a maximum can be calculated from design data, so as to avoid them in normal operation of the machine.

ad 2) Whenever design engineers fail to avoid critical speeds or the operating speed range is changed, design modifications might be required to change the critical speeds.

ad 3) This objective usually applies to the entire drive train system in which the turbomachine is employed. TNFs are calculated for the whole shaft string, TNFs of individual string components are not much of interest.

ad 4) This capability allows "in-place" rotor balancing -> reduction of amplitude of synchronous vibration.

ad 5) One of the most difficult objectives! The amplitude of rotor whirling depends on two factors which are both very difficult to measure:

      a) distribution of imbalance along the rotor

      b) rotor-bearing system damping

What can be done is to predict relative effects of rotor imbalance and system damping at specific locations.

ad 6) Another challenging objective - lot of destabilizing forces that are not yet fully understood. Instability caused by journal bearings (sleeve bearings) can be predicted quite accurately.

ad 7) Computer simulations can predict the relative stabilizing effect of various hardware modifications, even if the models for destabilizing force are only approximations.

B) Torsional analysis

The torsional response characteristics of rotating equipment should be analyzed and evaluated to ensure system's reliability. Torsional analysis is a mandatory design check for majority of shaft systems, especially in turbomachinery. The goal is to verify that the system can operate within the required speed range without excessive vibration and torsional stress. According [117] the classical torsional design consists of the following steps:

- Machine selection and pre-selection of coupling
- Calculation of undamped torsional natural frequencies
- Definition of torsional excitation
- Campbell diagram to identify resonances
- Forced response analysis
- Resonance conditions
- Transient torsional response
    - o motor starting
    - o fault conditions

Torsional analysis

The coupling design is an iterative process. A pre-selection of the coupling is done in early stage in order to calculate the undamped torsional natural frequencies and corresponding mode shapes (e.g. using Eigenvector-Eigenvalue method). As the damping in torsional systems is small, it has very little effect on the natural frequencies. Therefore, the torsional natural frequencies and mode shapes may be calculated assuming the damping is zero. The Campbell diagram (also called interference diagram) shows if there is any resonance. Required separation margin shall be taken into account. Forced vibration response is performed to calculate the shaft torsional stresses and results are compared with proposed criteria. Holzer method and the Eigenvector-Eigenvalue procedure are the major analysis techniques. A parametric analysis can identify sensitive elements that may be adjusted to modify the torsional response. Afterwards, the coupling selection can be optimized. Coupling stiffness can eventually be modified e.g. to move the resonance outside of the operating speed range.

C) Vibration sources in electric variable speed drive systems

Overview of vibration sources and their influence on stability

Root cause of oscillation, mechanism	Influence on			Excitation frequency	
	eigenfre-quency	stability		ω (1x)	$\nu \cdot \omega$ (multiple x)
		unstable	stable		
Unbalance (mechanical)				***	
Elastic bearings	***				
External damping	*		***		
Internal damping	*	**	**		
Sleeve bearings	**	***	***		
Non-circularity of shaft	**	**			***
Orthotropic bearings	**		***		
Gyroscopic forces	**			**	
Magnetic forces	**			**	**
Couplings				**	**
Deformed shaft (bending)				***	
Gear (teeth shape, oil quality etc)	Note 1	Note 1	Note 1	Note 1	Note 1
Roller element bearings	**			***	**
Groove effect	*	***			
Network disturbances	**	**		Note 2	Note 2
Process disturbances (e.g. inlet gas flow)	*/**	*			
Motor slot harmonics					*/**
Motor drive (VSDS)				**	**

*	negligible influence
**	medium influence
***	strong influence

Note 1: Impact of gear on stability of rotor system is very complex and exceeds author's knowledge and practical experience. Author only knows that the shape of teeth inside gearbox significantly influence the lateral-torsional vibration transfer and oil properties influence vibration level.

Note 2: Character of network disturbance is very generic (influence of other non-linear loads, grid faults, unbalance etc). Projects are known where heavily distorted network voltage induced pulsating torques in direct on-line machine driving e.g. blower in metals plant.

Appendix 7 – Vector control and direct torque control schemes

A) Simplified torque control core
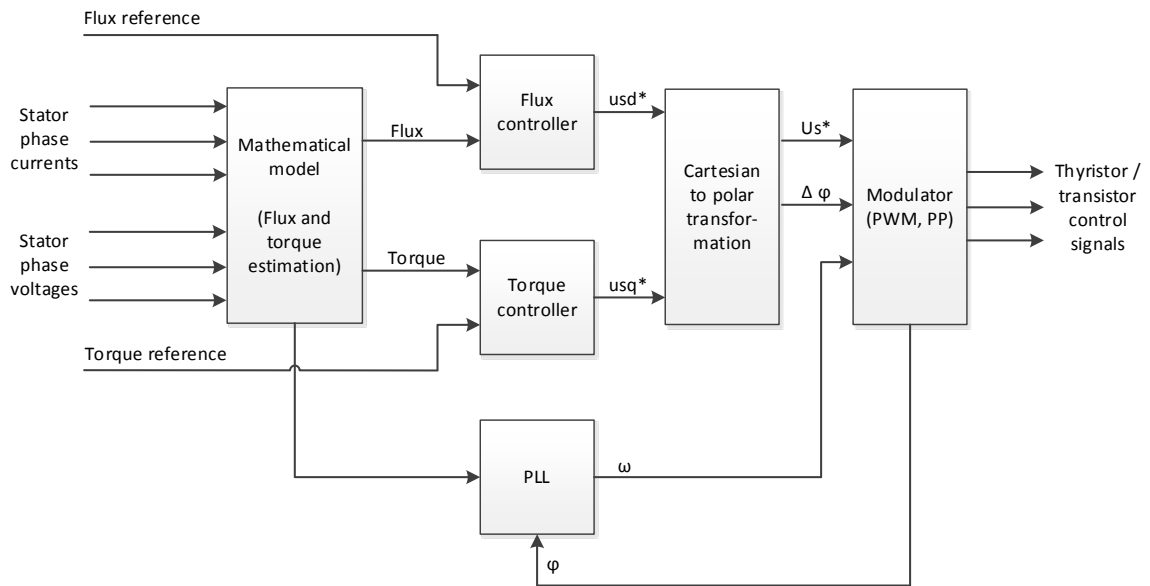
Torque control part in vector control
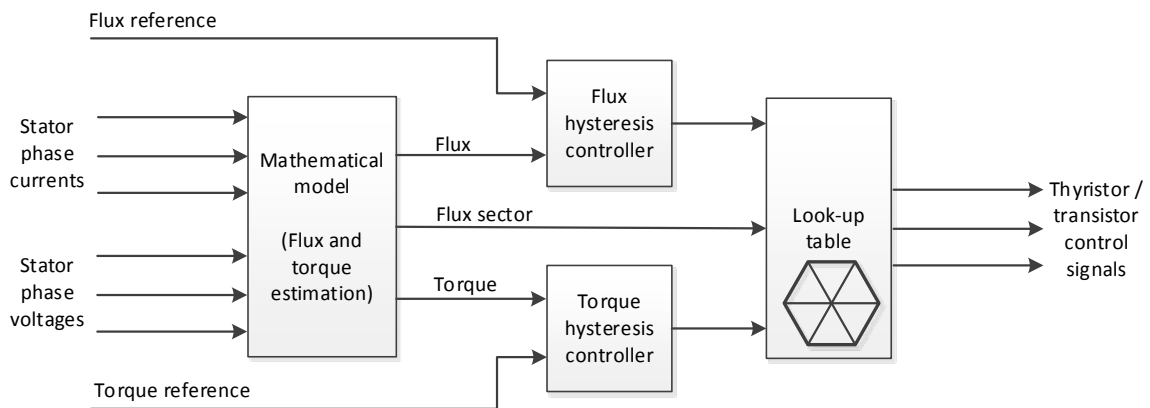
Torque control part in direct torque control (DTC)

B) Overview scheme of Direct Torque Control (DTC)
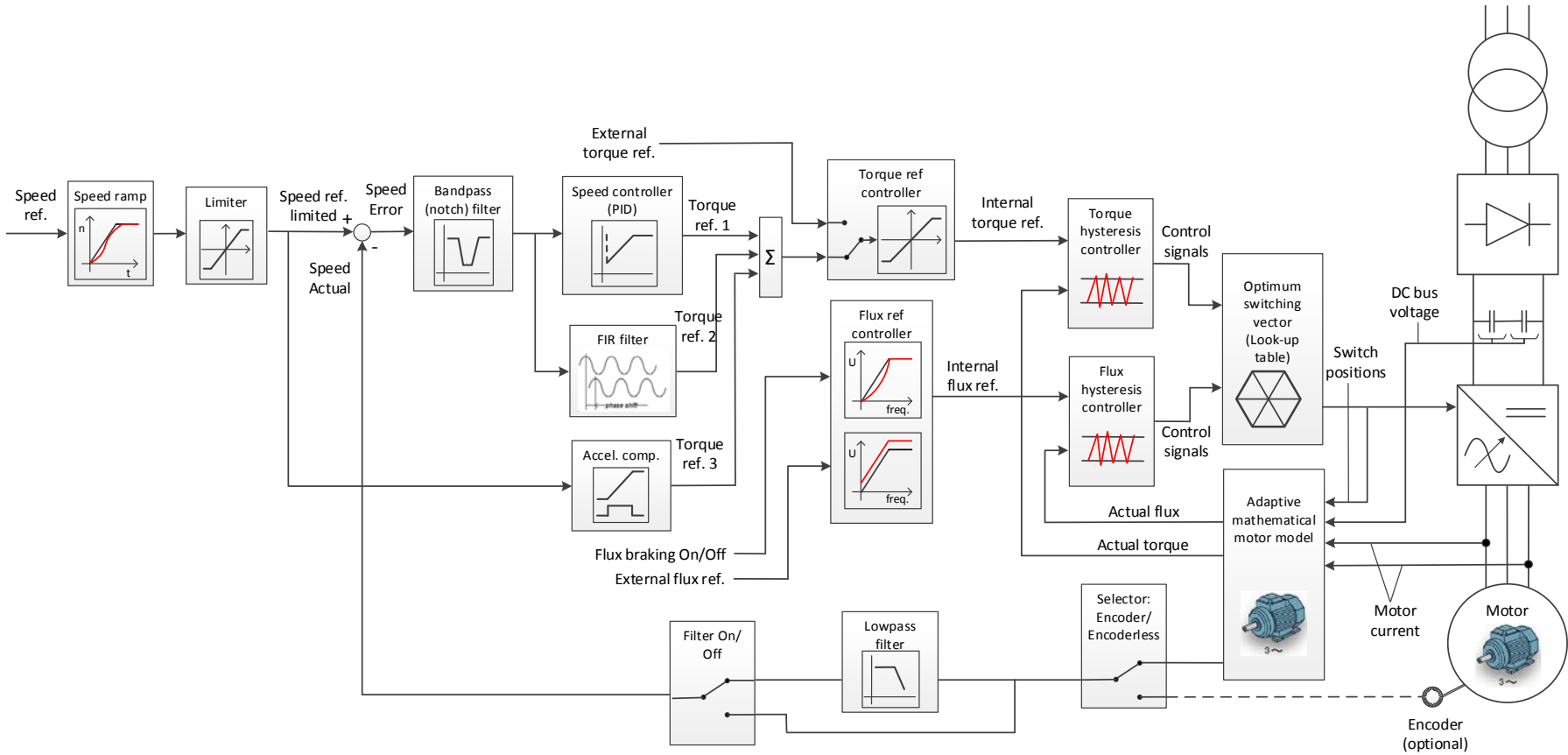
Overview speed of speed and torque control loops with DTC

Appendix 8 – Air gap torque comparison: PWM versus DTC modulator
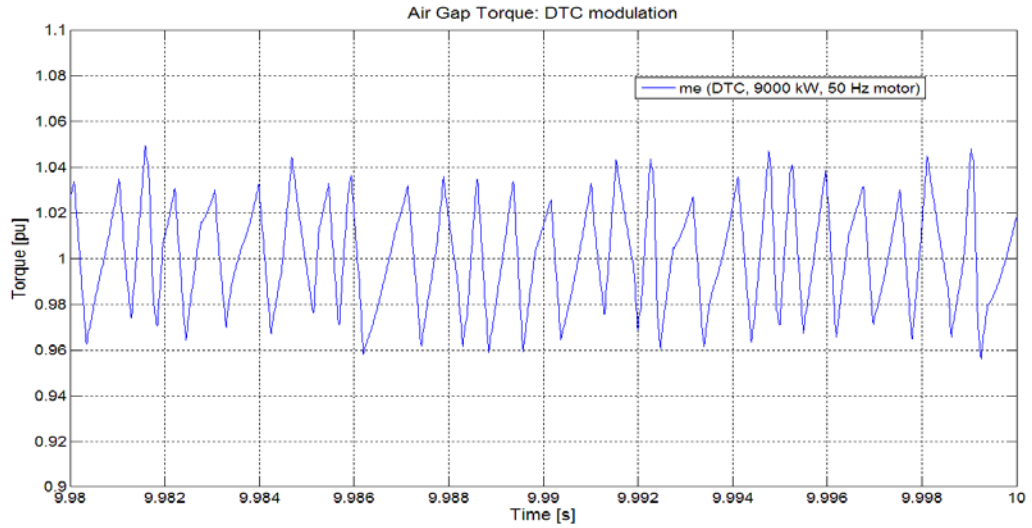
Air gap torque with DTC modulation
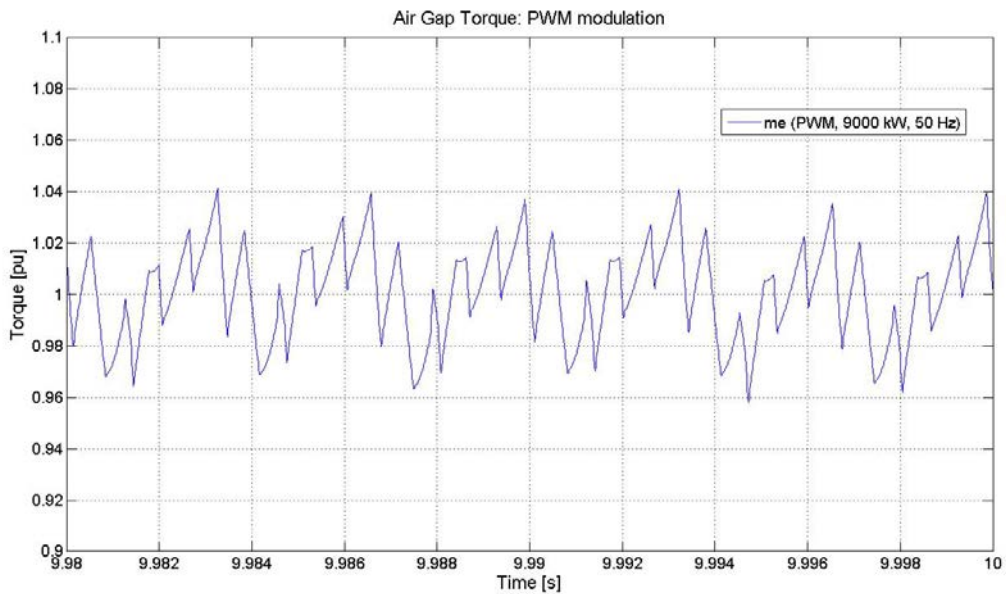
Air gap torque with PWM modulation

Appendix 9 – Air gap torque spectrum: white noise

Motor air gap torque with hysteresis torque controller ("DTC")

Spectrum of air gap torque (interval of 1 second)

Total Distortion   = 3.0985%

DC magnitude: = 0.9998

Fundamental frequency = 0Hz

Spectrum of air gap torque (interval of 10 seconds)

Total Distortion   = 3.0838%

DC magnitude: = 0.99964

Fundamental frequency = 0Hz
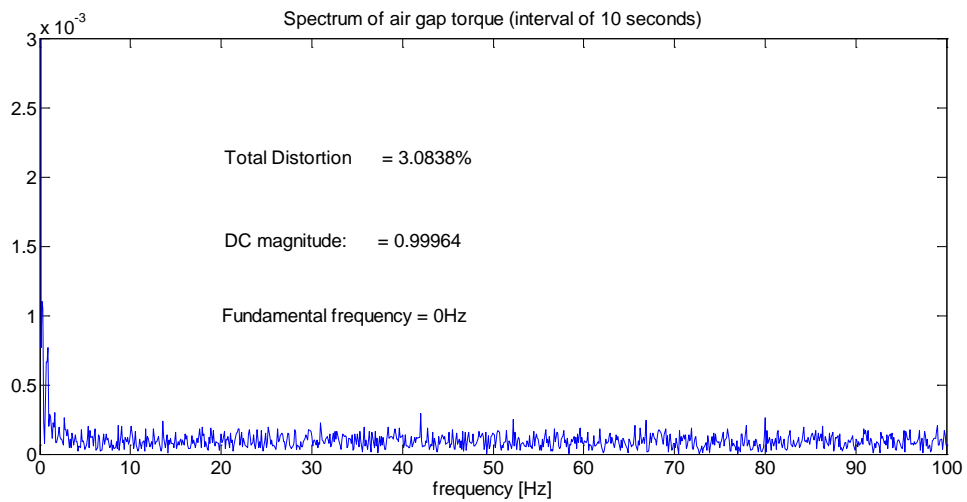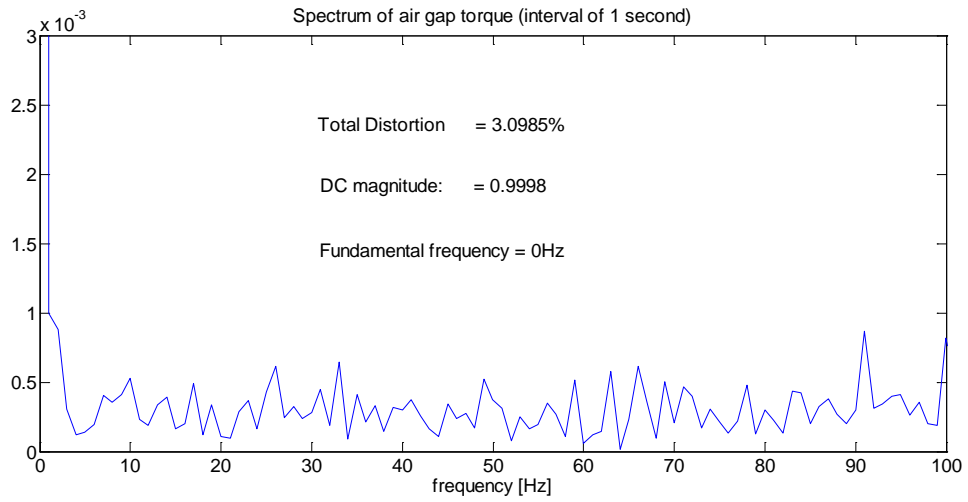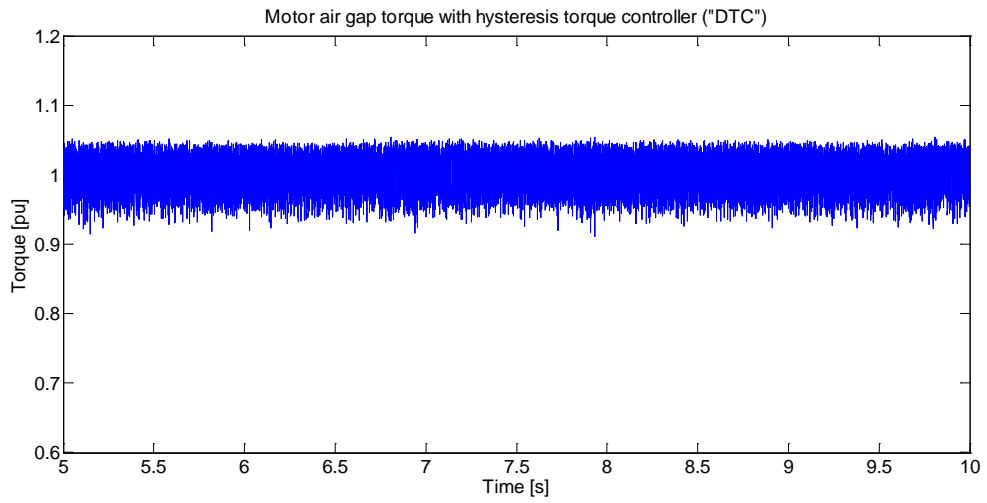
Appendix 10 – Mechanical shaft strings of real projects

This is an overview of torsional demanding projects where the author was involved. The table below shows torsional natural frequencies (first, second and third) and corresponding modes for typical compressor trains. All data is based on real projects executed together with six world leading compressor OEMs (Europe, Japan and North America). Project names and customer names are not displayed due to confidentiality. The author does not know all details of each project, but available information is shown.

Application (driven load)	Rated motor power [kW]	Motor type	VFD model	Rated speed [rpm] Load side	Rated speed [rpm] Motor side	Gear [Yes/No]	Speed range [rpm]	1st TNF freq [Hz]	1st TNF location	2nd TNF freq [Hz]	2nd TNF location	3rd TNF freq [Hz]	3rd TNF location
Compressor	8'700	Asynchronous	ACS5000	8'910	1'410	Yes	1'128 … 1'480						
Compressor	20'600	Synchronous	LCI.DR	7'654	4'300	Yes		14.90	Coupling between LP compressor and gear (LS)	21.80	Coupling between motor and LP compressor (LS)	85.80	Coupling between gear and HP compressor (HS)
Compressor and gas turbine	20'000	Synchronous	LCI.DR		3'636	No		9.93	Coupling between GT and compressor	18.68	Coupling between axial and centrifugal compressors	39.05	Inside gas turbine (Internal)
Blower	8'400	Asynchronous	ACS5000	5'204	1'492	Yes		16.91		50.49			
Blower	8'400	Asynchronous	ACS5000	5'313	1'492	Yes	1'191 … 1'530	16.76	HS coupling	49.42	LS coupling	159.79	Motor internal
Compressor	6'000	Synchronous	LCI.DR	7'547	1'500	Yes	1'050 … 1'575	15.01		77.80		342.68	
Compressor	9'910	Asynchronous	ACS6000	7'548	1'500	Yes							
Compressor	21'000	Synchronous	LCI.DR	7'548	1'500	Yes		17.60		60.10		221.92	

Application (driven load)	Rated motor power [kW]	Motor type	VFD model	Rated speed [rpm] Load side	Rated speed [rpm] Motor side	Gear [Yes/No]	Speed range [rpm]	1st TNF freq [Hz]	1st TNF location	2nd TNF freq [Hz]	2nd TNF location	3rd TNF freq [Hz]	3rd TNF location
Compressor	13'580	Synchronous	LCI.DR	11'006	1'500	Yes	1'050 ... 1'575	11.20		30.80			
Compressor	18'211	Synchronous	LCI.DR		1'500	Yes	1'050 ... 1'576						
Compressor	17'000	Synchronous	LCI.DR	11'195	1'714	Yes	1'076 ... 1'800	10.80		71.60		213.60	
Compressor	37'000	Synchronous	LCI.DR	7'927	1'800	Yes	1'260 ... 1'890	17.40	LS coupling	58.20	HS coupling	202.80	LS coupling
Compressor	17'400	Asynchronous	ACS5000	4'216	1'500	Yes	1'441 ... 1'575	12.73	LS coupling	36.33	HS coupling		
Compressor	6'100	Asynchronous	ACS6000	10'249	1'429	Yes	1'000 ... 1'500	14.89	LS coupling	56.45	HS coupling	347.95	
Compressor	6'100	Asynchronous	ACS6000	10'249	1'429	Yes	1'000 ... 1'500	17.92	LS coupling	56.70	HS coupling	462.30	
Compressor	1'200	Asynchronous	ACS1000		1'450	Yes	1'050 ... 1'572	23.17	LS coupling	79.40	HS coupling	606.90	between motor and coupling
Compressor	1'500	Asynchronous	ACS1000		1'422	Yes	1'050 ... 1'573	22.01	LS coupling	69.70	HS coupling	629.40	between motor and coupling
Compressor	3'400	Asynchronous	ACS5000		1'463	Yes	1'050 ... 1'575	22.15	LS coupling	67.40	HS coupling	594.60	between motor and coupling
Compressor	900	Asynchronous	ACS1000		2'997	Yes	2'400 ... 3'150	20.89	LS coupling	125.80	HS coupling	758.70	between gear and HS coupling
Compressor	1'300	Asynchronous	ACS1000		1'499	Yes	1'200 ... 1'575	24.27	LS coupling	79.70	HS coupling	585.40	between motor and coupling
Compressor	9'000	Asynchronous	ACS5000		1'500	Yes	1'200 ... 1'575	13.85	HS coupling	50.20	HS coupling (mainly) and LS coupling	464.60	between motor and coupling
Compressor	11'500	Asynchronous	ACS5000		1'500	Yes	1'200 ... 1'575	15.56	LS coupling (between LS coupling and gear)	29.30	HS coupling 1 and LS coupling	57.30	HS coupling 2 (slightly also LS coupling and HS coupling 1)
Compressor	5'950	Asynchronous	ACS5000					13.30	HS coupling	69.10	LS coupling & HS coupling	399.50	

Application (driven load)	Rated motor power [kW]	Motor type	VFD model	Rated speed [rpm] Load side	Rated speed [rpm] Motor side	Gear [Yes/No]	Speed range [rpm]	1st TNF freq [Hz]	1st TNF location	2nd TNF freq [Hz]	2nd TNF location	3rd TNF freq [Hz]	3rd TNF location
Compressor	15'100	Synchronous	ACS5000					10.35	LS coupling 1	15.60	LS coupling 2	26.93	HS coupling 1
Compressor	1'100	Asynchronous	ACS1000					23.40	LS coupling	75.24	HS coupling		
Compressor				8'891	1'490	yes	1'044 ... 1'566	29.17	LS coupling - gear	62.03	HS coupling	178.23	inside motor
Compressor	13'057	Synchronous	LCI.DR		1'498			18.98		61.49			
Compressor	30'889	Synchronous	LCI.DR		1'500			13.51		39.24			
Compressor	7'000	Asynchronous	ACS5000		1'500			19.49	HS coupling	76.99	LS cooupling & HS coupling	817.50	
Compressor	10'300	Asynchronous	ACS5000		1'500			17.10	LS coupling	37.10	HS coupling	224.70	inside gear
Compressor	2'500	Asynchronous	ACS1000		1'680		1'176 ... 1'764	17.00	LS coupling	65.47	HS coupling	599.10	
Compressor	2'300	Asynchronous	ACS5000		1'800			26.10	LS coupling				
Compressor	350	Asynchronous	ACS1000i		1'500		1'050 ... 1'575	26.10	LS coupling	100.04	HS coupling		
Compressor	2'200	Asynchronous	ACS5000i		1'680		1'680 ... 1'800	27.90	LS coupling	61.12	HS coupling		

Appendix 11 – Motor transient torques

A) 5'500 kW induction machine at min. speed (36.2 Hz/1'080 rpm) and max. speed (63.3 Hz/1'890 rpm)
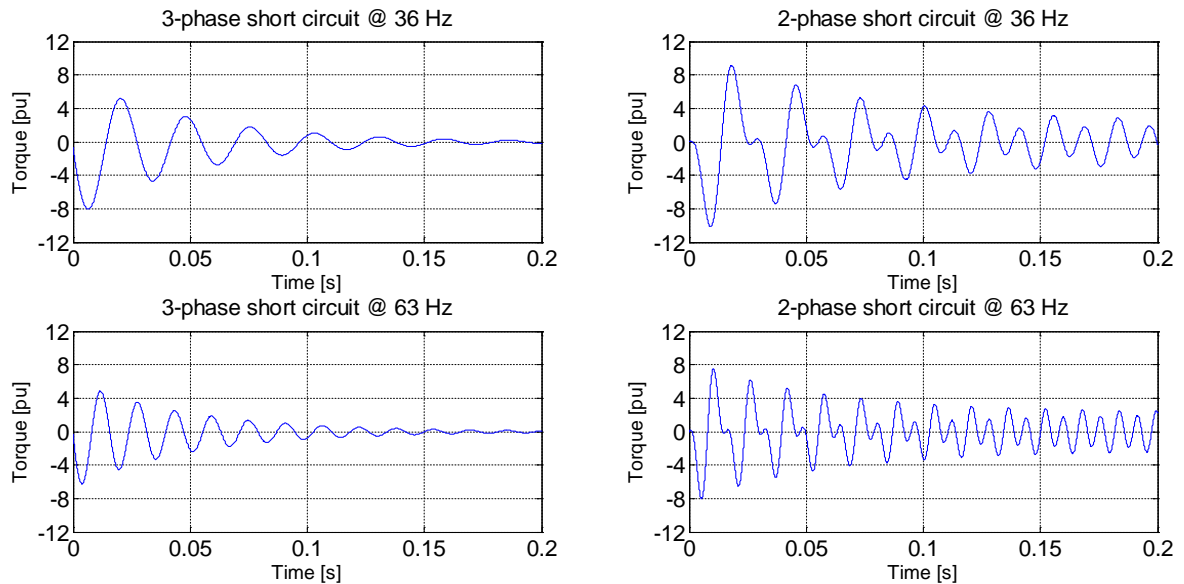
Air gap torque at 3-phase short circuit at min. speed: -8.04 T_N at t = 6.91 ms

Air gap torque at 2-phase short circuit at min. speed: -10.5 T_N at t = 8.98 ms

Air gap torque at 3-phase short circuit at max. speed: -6.27 T_N at t = 3.95 ms

Air gap torque at 2-phase short circuit at max. speed: -8.2 T_N at t = 5.53 ms

B) 7'000 kW induction machine at nominal speed (50.2 Hz/1'500 rpm)
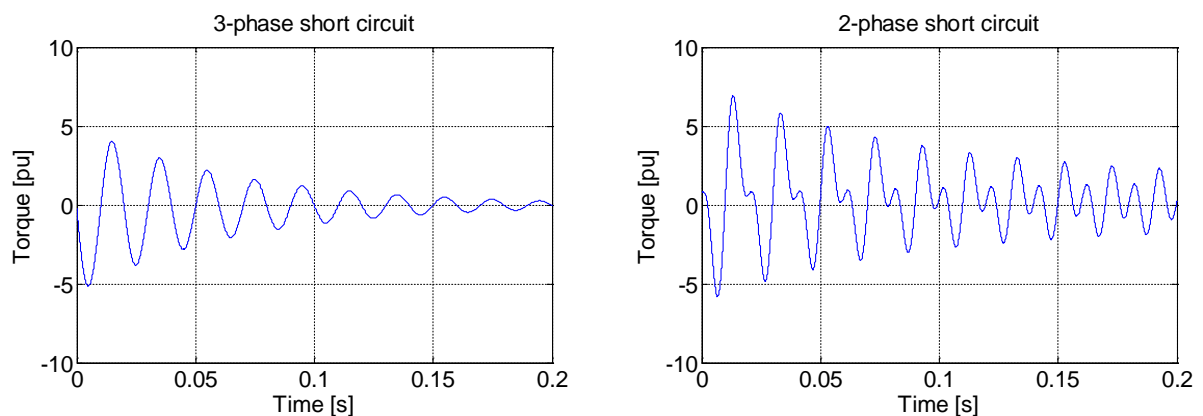
Air gap torque at 3-phase short circuit at nom. speed: -5.16 T_N at t = 5.0 ms

Air gap torque at 2-phase short circuit at nom. speed: 6.92 T_N at t = 13.3 ms

C) 13'600 kW induction machine at nominal speed (49.2 Hz/980 rpm)
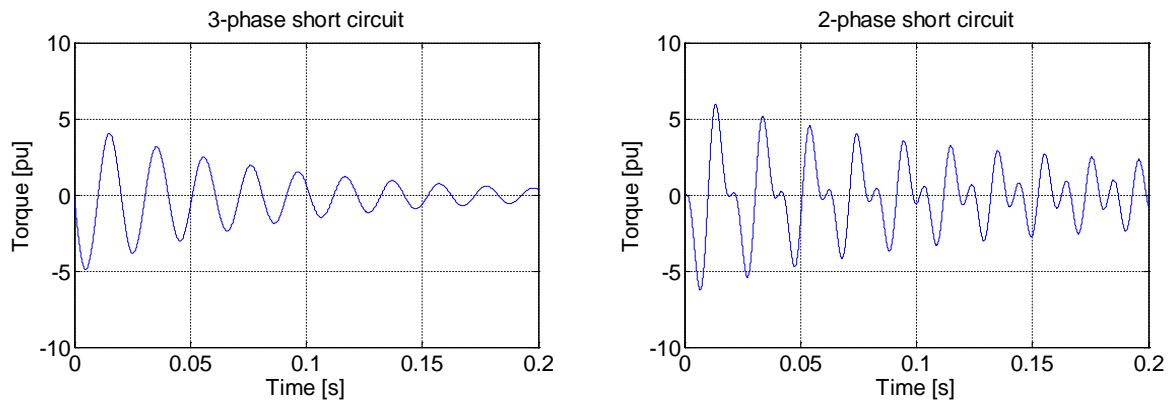
Air gap torque at 3-phase short circuit at nom. speed: -4.89 T_N at t = 5.08 ms

Air gap torque at 2-phase short circuit at nom. speed: -6.38 T_N at t = 6.61 ms

D) 8'700 kW induction machine at nominal speed (43.9 Hz/1'318 rpm) incl. coupling torques
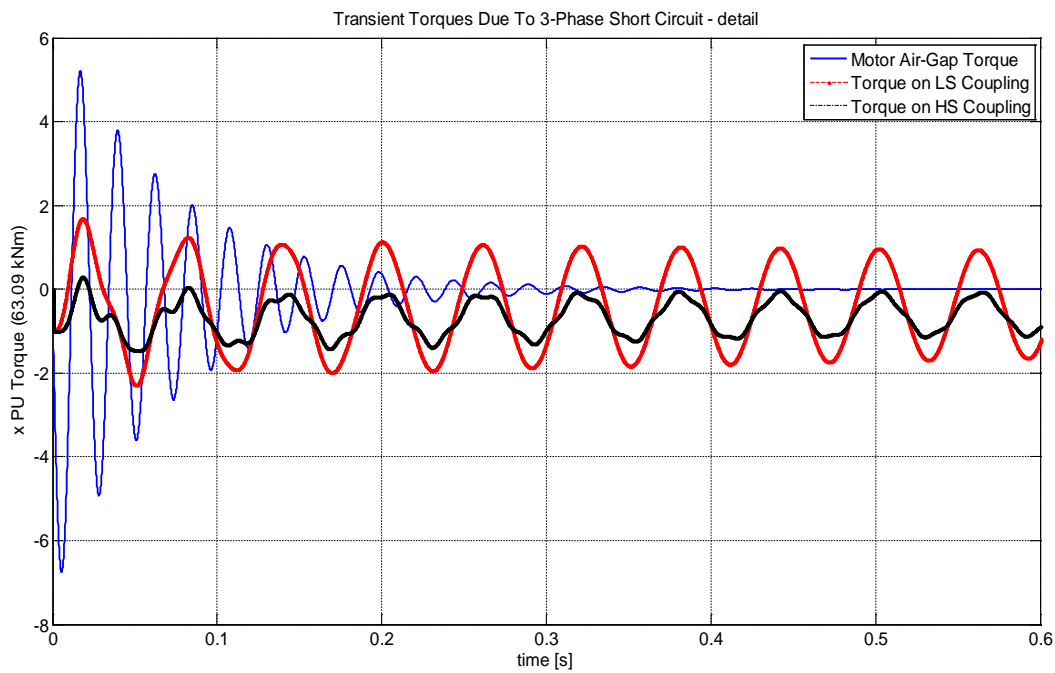
Transient torques during 3-phase short circuit (air gap torque, torque on low-speed coupling, torque on high-speed coupling)
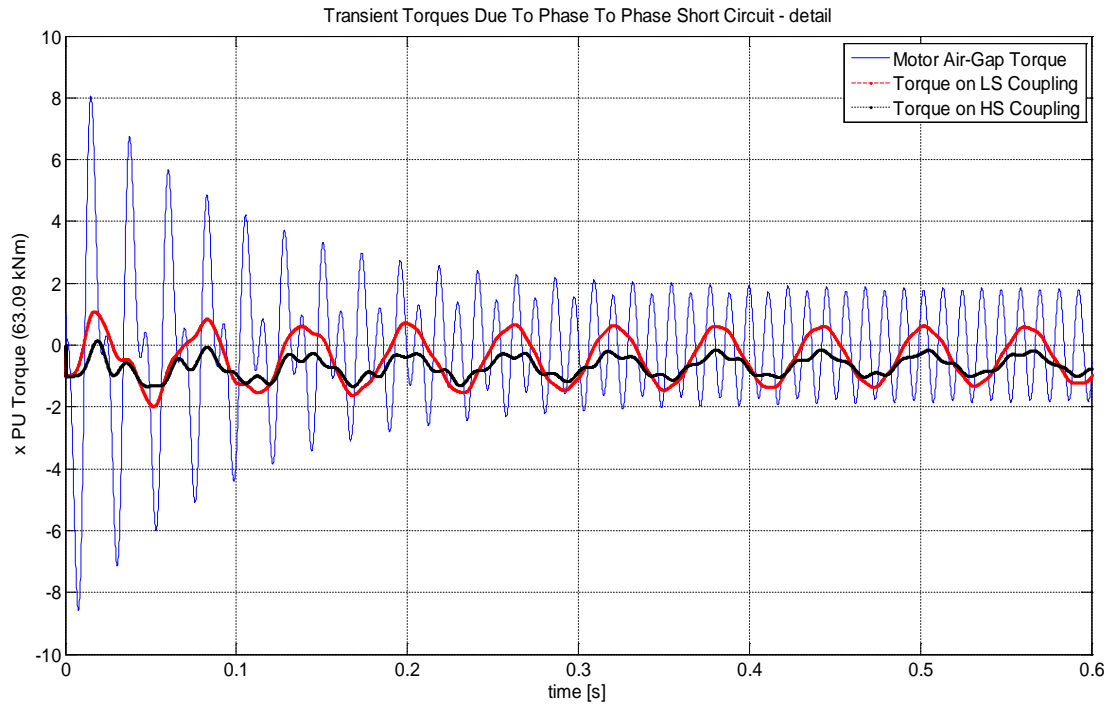
Transient torques during 2-phase short circuit (air gap torque, torque on low-speed coupling, torque on high-speed coupling)

D) Overview of induction motor transient torques across wide power range - both direct on-line (DOL) and VFD driven motors

Motor type	Motor power	Motor voltage	Shaft height	Pole number	Rated speed	2-phase short circuit	3-phase short circuit	High-speed reclosing	Stator reactance X_1	Total reactance	Supply
Asynchronous	350 kW	3.3 kV	400 mm	4-pole	1'500 rpm	-9.01 * TN	-6.71 * TN	n.a.	0.102 pu	0.204 pu	VFD
Asynchronous	1'100 kW	4.0 kV	450 mm	4-pole	1'800 rpm	-6.08 * TN	-4.62 * TN	n.a.	0.172 pu	0.278 pu	VFD
Asynchronous	1'300 kW	3.3 kV	450 mm	4-pole	1'490 rpm	-7.79 * TN	-5.92 * TN	n.a.	0.138 pu	0.241 pu	VFD
Asynchronous	2'200 kW	6.6 kV	500 mm	4-pole	1'680 rpm	-9.26 * TN	-7.11 * TN	n.a.	0.110 pu	0.187 pu	VFD
Asynchronous	2'500 kW	3.0 kV	500 mm	4-pole	1'489 rpm	-6.12 * TN	-4.69 * TN	-12.1 * TN	0.141 pu	0.247 pu	DOL
Asynchronous	2'500 kW	6.0 kV	500 mm	4-pole	1'490 rpm	-7.08 * TN	-5.42 * TN	-14.2 * TN	0.147 pu	0.238 pu	DOL
Asynchronous	2'600 kW	6.6 kV	560 mm	4-pole	1'559 rpm	-7.74 * TN	-5.93 * TN	n.a.	0.139 pu	0.220 pu	VFD
Asynchronous	2'800 kW	6.3 kV	560 mm	4-pole	1'492 rpm	-7.42 * TN	-5.72 * TN	n.a.	0.183 pu	0.259 pu	VFD
Asynchronous	2'800 kW	6.0 kV	630 mm	4-pole	1'494 rpm	-9.43 * TN	-7.10 * TN	-21.0 * TN	not known	not known	DOL
Asynchronous	3'000 kW	3.0 kV	560 mm	4-pole	1'488 rpm	-5.24 * TN	-4.01 * TN	-10.2 * TN	0.204 pu	0.317 pu	DOL
Asynchronous	3'000 kW	6.0 kV	560 mm	4-pole	1'490 rpm	-7.05 * TN	-5.40 * TN	-14.2 * TN	0.153 pu	0.234 pu	DOL
Asynchronous	3'639 kW	3.3 kV	560 mm	2-pole	3'600 rpm	-6.01 * TN	-4.61 * TN	n.a.	0.179 pu	0.260 pu	VFD
Asynchronous	3'728 kW	4.0 kV	710 mm	8-pole	893 rpm	-8.53 * TN	-6.46 * TN	-11.6 * TN	0.118 pu	0.205 pu	DOL
Asynchronous	4'500 kW	3.0 kV	560 mm	4-pole	1'490 rpm	-6.27 * TN	-4.80 * TN	-12.4 * TN	0.172 pu	0.272 pu	DOL
Asynchronous	4'500 kW	6.0 kV	560 mm	4-pole	1'490 rpm	-7.17 * TN	-5.49 * TN	-14.3 * TN	0.149 pu	0.245 pu	DOL
Asynchronous	4'500 kW	6.0 kV	560 mm	4-pole	1'490 rpm	-6.67 * TN	-5.10 * TN	-13.4 * TN	0.156 pu	0.262 pu	DOL
Asynchronous	4'500 kW	6.0 kV	560 mm	4-pole	1'491 rpm	-7.50 * TN	-5.73 * TN	-15.2 * TN	0.137 pu	0.239 pu	DOL
Asynchronous	4'620 kW	6.0 kV	710 mm	4-pole	1'489 rpm	-7.78 * TN	-4.74 * TN	-9.62 * TN	0.225 pu	0.369 pu	DOL
Asynchronous	4'750 kW	6.6 kV	560 mm	2-pole	3'437 rpm	-6.96 * TN	-5.33 * TN	n.a.	0.258 pu	0.287 pu	VFD
Asynchronous	5'000 kW	6.0 kV	560 mm	4-pole	1'492 rpm	-5.60 * TN	-4.29 * TN	-11.3 * TN	0.193 pu	0.305 pu	DOL
Asynchronous	5'235 kW	3.1 kV	630 mm	4-pole	1'489 rpm	-6.02 * TN	-4.59 * TN	-11.9 * TN	0.182 pu	0.299 pu	DOL
Asynchronous	5'500 kW	3.0 kV	630 mm	4-pole	1'584 rpm	-8.20 * TN	-6.27 * TN	n.a.	0.114 pu	0.184 pu	VFD
Asynchronous	5'900 kW	10.0 kV	800 mm	10-pole	597 rpm	not known	not known	not known	0.167 pu	0.294 pu	DOL
Asynchronous	5'950 kW	6.6 kV	710 mm	4-pole	1'500 rpm	-6.52 * TN	-5.00 * TN	n.a.	0.156 pu	0.243 pu	VFD

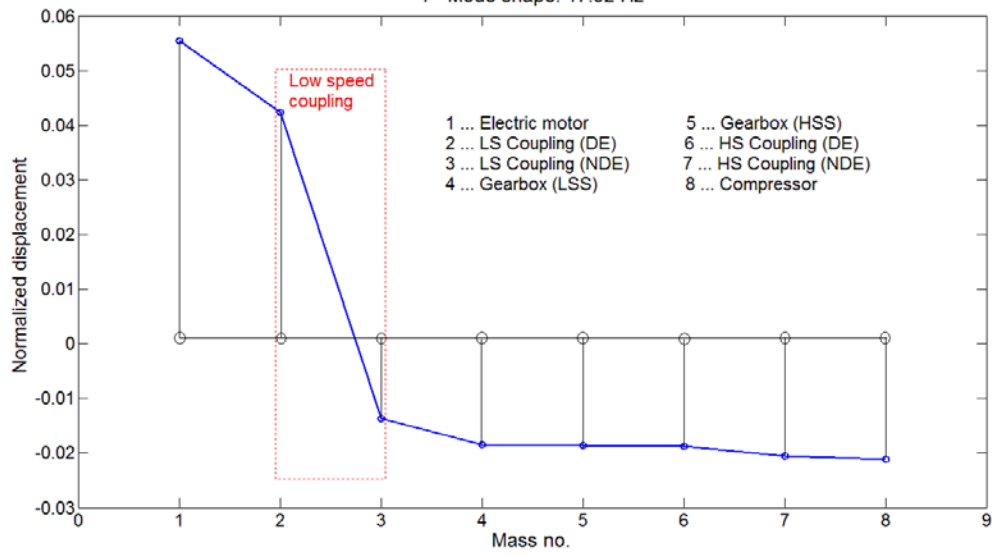| Motor type	Motor power	Motor voltage	Shaft height	Pole number	Rated speed	2-phase short circuit	3-phase short circuit	High- speed reclosing	Stator reactance X1	Total reactance	Supply
Asynchronous	6'000 kW	3.0 kV	630 mm	4-pole	1'492 rpm	-6.35 * TN	-4.86 * TN	-12.5 * TN	0.169 pu	0.270 pu	DOL
Asynchronous	6'000 kW	6.0 kV	630 mm	4-pole	1'491 rpm	-6.29 * TN	-4.82 * TN	-12.4 * TN	0.171 pu	0.272 pu	DOL
Asynchronous	6'300 kW	3.0 kV	630 mm	4-pole	1'491 rpm	-6.05 * TN	-4.63 * TN	-11.9 * TN	0.178 pu	0.284 pu	DOL
Asynchronous	6'300 kW	6.0 kV	630 mm	4-pole	1'491 rpm	-5.99 * TN	-4.59 * TN	-11.8 * TN	0.180 pu	0.286 pu	DOL
Asynchronous	6'400 kW	6.9 kV	710 mm	6-pole	1'000 rpm	-8.46 * TN	-6.46 * TN	n.a.	0.150 pu	0.236 pu	VFD
Asynchronous	6'500 kW	6.6 kV	630 mm	4-pole	1'500 rpm	-6.52 * TN	-4.99 * TN	n.a.	0.171 pu	0.267 pu	VFD
Asynchronous	6'500 kW	6.6 kV	630 mm	4-pole	1'500 rpm	-7.71 * TN	-5.90 * TN	n.a.	0.146 pu	0.228 pu	VFD
Asynchronous	6'800 kW	6.6 kV	not known	4-pole	1'480 rpm	-7.00 * TN	-5.38 * TN	n.a.	0.181 pu	0.269 pu	VFD
Asynchronous	7'000 kW	6.6 kV	710 mm	4-pole	1'493 rpm	-6.72 * TN	-5.16 * TN	-12.5 * TN	0.143 pu	0.235 pu	VFD
Asynchronous	7'100 kW	3.0 kV	630 mm	4-pole	1'492 rpm	-7.45 * TN	-5.70 * TN	-14.9 * TN	0.148 pu	0.230 pu	DOL
Asynchronous	7'100 kW	6.0 kV	630 mm	4-pole	1'490 rpm	-5.69 * TN	-4.36 * TN	-11.0 * TN	0.185 pu	0.299 pu	DOL
Asynchronous	7'400 kW	6.6 kV	630 mm	4-pole	1'622 rpm	-7.84 * TN	-6.01 * TN	-14.4 * TN	0.144 pu	0.230 pu	VFD
Asynchronous	7'400 kW	13.8 kV	800 mm	4-pole	1'778 rpm	-7.59 * TN	-5.66 * TN	-13.4 * TN	0.136 pu	0.218 pu	DOL
Asynchronous	7'800 kW	6.6 kV	630 mm	4-pole	1'935 rpm	-7.75 * TN	-5.94 * TN	n.a.	0.128 pu	0.198 pu	VFD
Asynchronous	8'000 kW	3.0 kV	630 mm	4-pole	1'491 rpm	-6.70 * TN	-5.13 * TN	-13.2 * TN	0.163 pu	0.255 pu	DOL
Asynchronous	8'000 kW	6.0 kV	710 mm	4-pole	1'493 rpm	-6.10 * TN	-4.68 * TN	-12.1 * TN	0.168 pu	0.223 pu	DOL
Asynchronous	8'000 kW	6.6 kV	710 mm	4-pole	1'500 rpm	-6.60 * TN	-5.06 * TN	n.a.	0.162 pu	0.250 pu	VFD
Asynchronous	8'700 kW	6.6 kV	800 mm	4-pole	1'318 rpm	-8.84 * TN	-6.74 * TN	n.a.	0.117 pu	0.219 pu	VFD
Asynchronous	8'700 kW	6.6 kV	900 mm	4-pole	1'380 rpm	-7.06 * TN	-5.40 * TN	n.a.	0.151 pu	0.243 pu	VFD
Asynchronous	9'000 kW	6.0 kV	710 mm	4-pole	1'494 rpm	-6.42 * TN	-4.92 * TN	-12.9 * TN	0.162 pu	0.252 pu	DOL
Asynchronous	9'000 kW	6.6 kV	710 mm	4-pole	1'494 rpm	-7.54 * TN	-5.78 * TN	n.a.	0.136 pu	0.225 pu	VFD
Asynchronous	10'000 kW	6.0 kV	710 mm	4-pole	1'494 rpm	-6.25 * TN	-4.79 * TN	-12.4 * TN	0.168 pu	0.258 pu	DOL
Asynchronous	10'300 kW	6.6 kV	800 mm	4-pole	1'500 rpm	-7.36 * TN	-5.63 * TN	-14.6 * TN	0.141 pu	0.227 pu	VFD
Asynchronous	11'200 kW	6.0 kV	800 mm	4-pole	1'493 rpm	-6.94 * TN	-5.31 * TN	-9.89 * TN	0.148 pu	0.239 pu	DOL
Asynchronous	11'500 kW	6.6 kV	800 mm	4-pole	1'494 rpm	-6.58 * TN	-5.04 * TN	n.a.	0.158 pu	0.255 pu	VFD

Motor type	Motor power	Motor voltage	Shaft height	Pole number	Rated speed	2-phase short circuit	3-phase short circuit	High-speed reclosing	Stator reactance X1	Total reactance	Supply
Asynchronous	12'447 kW	6.6 kV	800 mm	4-pole	1'343 rpm	-6.64 * TN	-5.08 * TN	n.a.	0.167 pu	0.257 pu	VFD
Asynchronous	12'500 kW	6.0 kV	800 mm	4-pole	1'494 rpm	-7.83 * TN	-5.99 * TN	-11.2 * TN	0.132 pu	0.215 pu	DOL
Asynchronous	13'600 kW	3.0 kV	900 mm	6-pole	980 rpm	-6.38 * TN	-4.89 * TN	n.a.	0.161 pu	0.276 pu	VFD
Asynchronous	14'000 kW	6.0 kV	900 mm	4-pole	1'494 rpm	-7.47 * TN	-5.72 * TN	-11.2 * TN	0.138 pu	0.216 pu	DOL
Asynchronous	15'286 kW	6.9 kV	900 mm	4-pole	1'343 rpm	-8.61 * TN	-6.57 * TN	n.a.	0.122 pu	0.221 pu	VFD
Asynchronous	16'000 kW	6.0 kV	800 mm	4-pole	1'494 rpm	-7.32 * TN	-5.60 * TN	-10.4 * TN	0.143 pu	0.232 pu	DOL
Asynchronous	16'000 kW	6.0 kV	900 mm	4-pole	1'495 rpm	-9.09 * TN	-6.96 * TN	-13.7 * TN	0.115 pu	0.181 pu	DOL
Asynchronous	16'556 kW	6.6 kV	1'000 mm	4-pole	1'791 rpm	-5.19 * TN	-4.15 * TN	-11.0 * TN	not known	not known	VFD
Asynchronous	17'400 kW	6.6 kV	900 mm	4-pole	1'494 rpm	-6.32 * TN	-4.85 * TN	n.a.	0.172 pu	0.262 pu	VFD
Asynchronous	17'400 kW	6.6 kV	900 mm	4-pole	1'494 rpm	-6.32 * TN	-4.85 * TN	n.a.	0.172 pu	0.262 pu	VFD
Asynchronous	18'000 kW	6.0 kV	900 mm	4-pole	1'492 rpm	-5.58 * TN	-4.28 * TN	-8.11 * TN	0.189 pu	0.294 pu	DOL
Asynchronous	18'000 kW	6.0 kV	900 mm	4-pole	1'494 rpm	-7.47 * TN	-5.72 * TN	-11.2 * TN	0.139 pu	0.219 pu	DOL
Asynchronous	18'000 kW	6.0 kV	900 mm	4-pole	1'495 rpm	-8.44 * TN	-6.46 * TN	-12.4 * TN	0.127 pu	0.198 pu	DOL
Asynchronous	18'000 kW	6.0 kV	800 mm	4-pole	1'795 rpm	-8.76 * TN	-6.71 * TN	-13.1 * TN	0.120 pu	0.198 pu	DOL
Asynchronous	20'000 kW	6.0 kV	900 mm	4-pole	1'494 rpm	-7.13 * TN	-5.46 * TN	-10.5 * TN	0.148 pu	0.227 pu	DOL
Asynchronous	20'000 kW	6.0 kV	900 mm	4-pole	1'494 rpm	-7.60 * TN	-5.82 * TN	-11.0 * TN	0.141 pu	0.220 pu	DOL
Asynchronous	20'000 kW	6.0 kV	900 mm	4-pole	1'494 rpm	-6.98 * TN	-5.34 * TN	-10.3 * TN	0.152 pu	0.237 pu	DOL
Asynchronous	22'000 kW	6.0 kV	900 mm	4-pole	1'493 rpm	-6.34 * TN	-4.86 * TN	-9.23 * TN	0.168 pu	0.262 pu	DOL
Asynchronous	23'000 kW	6.6 kV	900 mm	4-pole	1'494 rpm	-7.75 * TN	-5.93 * TN	-11.3 * TN	0.134 pu	0.216 pu	DOL
Asynchronous	24'000 kW	6.6 kV	900 mm	4-pole	1'494 rpm	-7.43 * TN	-5.68 * TN	-10.8 * TN	0.140 pu	0.226 pu	DOL
Asynchronous	24'000 kW	6.6 kV	900 mm	4-pole	1'793 rpm	-5.64 * TN	-4.33 * TN	-8.38 * TN	0.154 pu	0.297 pu	DOL
Asynchronous	24'000 kW	6.0 kV	900 mm	4-pole	1'795 rpm	-7.60 * TN	-5.83 * TN	-11.3 * TN	0.122 pu	0.224 pu	DOL
Asynchronous	24'500 kW	6.6 kV	900 mm	4-pole	1'494 rpm	-7.27 * TN	-5.57 * TN	-10.6 * TN	0.143 pu	0.231 pu	DOL
Asynchronous	27'000 kW	6.0 kV	900 mm	4-pole	1'794 rpm	-6.62 * TN	-5.08 * TN	-9.7 * TN	0.138 pu	0.257 pu	DOL
Asynchronous	28'000 kW	6.0 kV	900 mm	4-pole	1'794 rpm	-6.38 * TN	-4.9 * TN	-9.31 * TN	0.144 pu	0.267 pu	DOL

Appendix 12 – Torsional natural frequencies and mode shapes in variable speed drive systems

1'200 kW compressor drive
1st Mode shape: 23.17 Hz

1 ... Electric motor
2 ... LS Coupling (DE)
3 ... LS Coupling (NDE)
4 ... Gearbox (LSS)
5 ... Gearbox (HSS)
6 ... HS Coupling (DE)
7 ... HS Coupling (NDE)
8 ... Compressor

1'200 kW compressor drive
2nd Mode shape: 79.35 Hz

1 ... Electric motor
2 ... LS Coupling (DE)
3 ... LS Coupling (NDE)
4 ... Gearbox (LSS)
5 ... Gearbox (HSS)
6 ... HS Coupling (DE)
7 ... HS Coupling (NDE)
8 ... Compressor

6'100 kW compressor drive
1st Mode shape: 17.92 Hz

1 ... Electric motor
2 ... LS Coupling (DE)
3 ... LS Coupling (NDE)
4 ... Gearbox (LSS)
5 ... Gearbox (HSS)
6 ... HS Coupling (DE)
7 ... HS Coupling (NDE)
8 ... Compressor

Low speed coupling

6'100 kW compressor drive
2nd Mode shape: 56.70 Hz

1 ... Electric motor
2 ... LS Coupling (DE)
3 ... LS Coupling (NDE)
4 ... Gearbox (LSS)
5 ... Gearbox (HSS)
6 ... HS Coupling (DE)
7 ... HS Coupling (NDE)
8 ... Compressor

High speed coupling

11'500 kW compresssor drive
1st Mode shape: 15.56 Hz

1 ... Electric motor
2 ... LS coupling (DE)
3 ... LS coupling (NDE)
4 ... Gearbox LSS
5 ... Gearbox HSS
6 ... HS2 coupling (DE)
7 ... HS2 coupling (NDE)
8 ... Compressor 2
9 ... HS1 coupling (DE)
10 ... HS1 coupling (NDE)
11 ... Compressor 1

11'500 kW compresssor drive
2nd Mode shape: 29.28 Hz

1 ... Electric motor
2 ... LS coupling (DE)
3 ... LS coupling (NDE)
4 ... Gearbox LSS
5 ... Gearbox HSS
6 ... HS2 coupling (DE)
7 ... HS2 coupling (NDE)
8 ... Compressor 2

9 ... HS1 coupling (DE)
10 ... HS1 coupling (NDE)
11 ... Compressor 1

15'100 kW compressor drive
1st Mode shape: 10.35 Hz

Low speed
coupling 1

1 ... Compressor 3
2 ... HS Coupling 3 (NDE)
3 ... HS Coupling 3 (DE)
4 ... Gearbox 2 (HSS)
5 ... Gearbox 2 (LSS)
6 ... LS Coupling 2 (NDE)
7 ... LS Coupling 2 (DE)
8 ... Electric motor
9 ... LS Coupling 1 (DE)
10 ... LS Coupling 1 (NDE)
11 ... Gearbox 1 (LSS)
12 ... Gearbox 1 (HSS)

13 ... HS Coupling 2 (DE)
14 ... HS Coupling 2 (NDE)
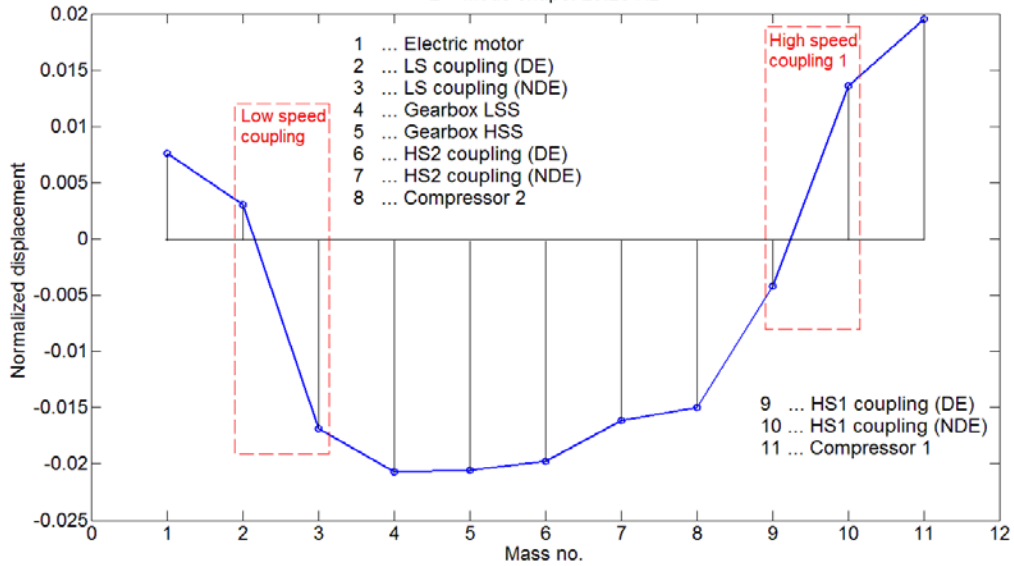15 ... Compressor 2
16 ... HS Coupling 1 (DE)
17 ... HS Coupling 1 (NDE)
18 ... Compressor 1

15'100 kW compressor drive
2nd Mode shape: 15.60 Hz

Low speed
coupling 2

High speed
coupling 2

1 ... Compressor 3
2 ... HS Coupling 3 (NDE)
3 ... HS Coupling 3 (DE)
4 ... Gearbox 2 (HSS)
5 ... Gearbox 2 (LSS)
6 ... LS Coupling 2 (NDE)
7 ... LS Coupling 2 (DE)
8 ... Electric motor
9 ... LS Coupling 1 (DE)
10 ... LS Coupling 1 (NDE)
11 ... Gearbox 1 (LSS)
12 ... Gearbox 1 (HSS)

13 ... HS Coupling 2 (DE)
14 ... HS Coupling 2 (NDE)
15 ... Compressor 2
16 ... HS Coupling 1 (DE)
17 ... HS Coupling 1 (NDE)
18 ... Compressor 1

15'100 kW compressor drive
3rd Mode shape: 26.93 Hz

1 ... Compressor 3
2 ... HS Coupling 3 (NDE)
3 ... HS Coupling 3 (DE)
4 ... Gearbox 2 (HSS)
5 ... Gearbox 2 (LSS)
6 ... LS Coupling 2 (NDE)
7 ... LS Coupling 2 (DE)
8 ... Electric motor
9 ... LS Coupling 1 (DE)
10 ... LS Coupling 1 (NDE)
11 ... Gearbox 1 (LSS)
12 ... Gearbox 1 (HSS)

13 ... HS Coupling 2 (DE)
14 ... HS Coupling 2 (NDE)
15 ... Compressor 2
16 ... HS Coupling 1 (DE)
17 ... HS Coupling 1 (NDE)
18 ... Compressor 1

High speed
coupling 1

Low speed
coupling 1

Low speed
coupling 2

17'400 kW compressor drive
1st Mode shape: 12.73 Hz

1 ... Electric motor
2 ... LS Coupling (DE)
3 ... LS Coupling (NDE)
4 ... Gearbox (LSS)
5 ... Gearbox (HSS)
6 ... HS Coupling (DE)
7 ... HS Coupling (NDE)
8 ... Compressor

17'400 kW compressor drive
2nd Mode shape: 36.33 Hz

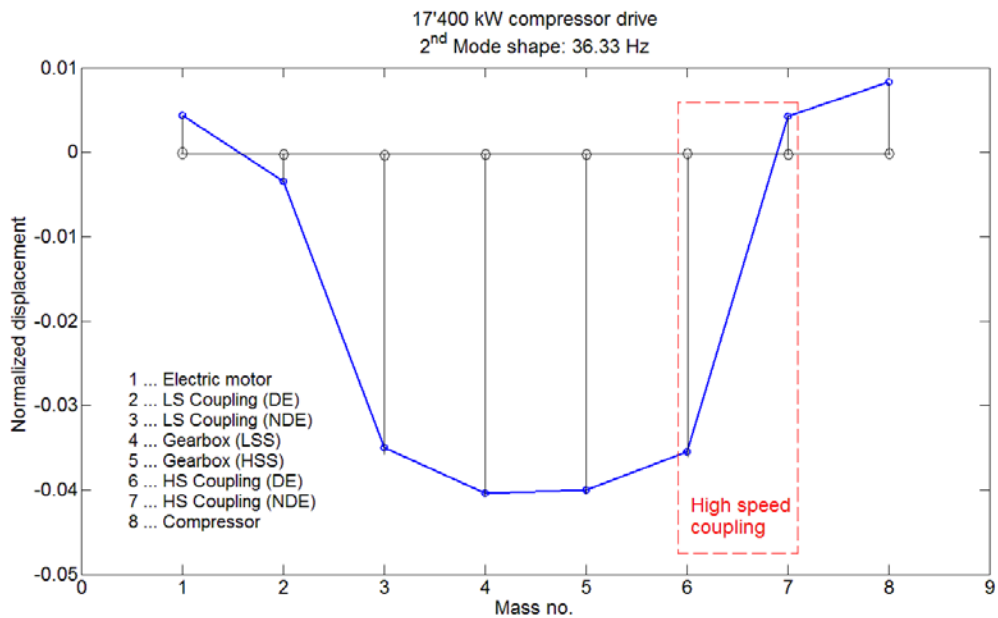1 ... Electric motor
2 ... LS Coupling (DE)
3 ... LS Coupling (NDE)
4 ... Gearbox (LSS)
5 ... Gearbox (HSS)
6 ... HS Coupling (DE)
7 ... HS Coupling (NDE)
8 ... Compressor

Note:

For the investigations of electro-mechanical interactions the finite element model is not practical and a simplified lumped inertia model can be used instead. The detailed model is reduced to several dominant masses. Only the lowest torsional natural frequencies need to be considered. Higher torsional modes are much better damped and they are outside the bandwidth of the VFD controllers. Therefore the simplified model needs to reproduce correctly the lowest two or three torsional modes (more than three modes only in special cases with very complex shaft string). The simplest model of elastic shaft is a two mass model. Such model is easy to understand and might be good enough for certain qualitative considerations. An eight mass model shown in a case study seems to be sufficient for most investigations.

# Appendix 13 – Elastic mechanical model (example with 8 inertial masses)

A) Lump inertia model with 8 inertial masses
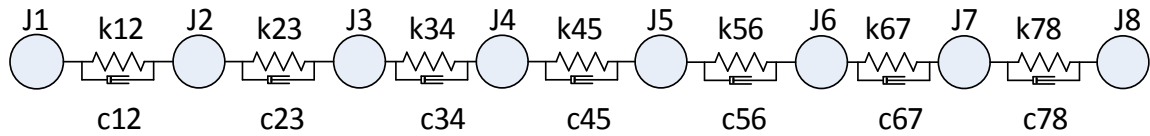
J ... moment of inertia (torsional disc) [kg*m2]
K ... stiffness (torsional spring) [Nm/rad]
C ... damping (torsional damper) [Nm*s/rad]

J1 ... Electric motor, J2 ... Low speed coupling (driving end), J3 ... Low speed coupling (non-driving end), J4 ... Gear (low speed side), J5 ... Gear (high speed side), J6 ... High speed coupling (driving end), J7 ... High speed coupling (driving end), J8 ... compressor
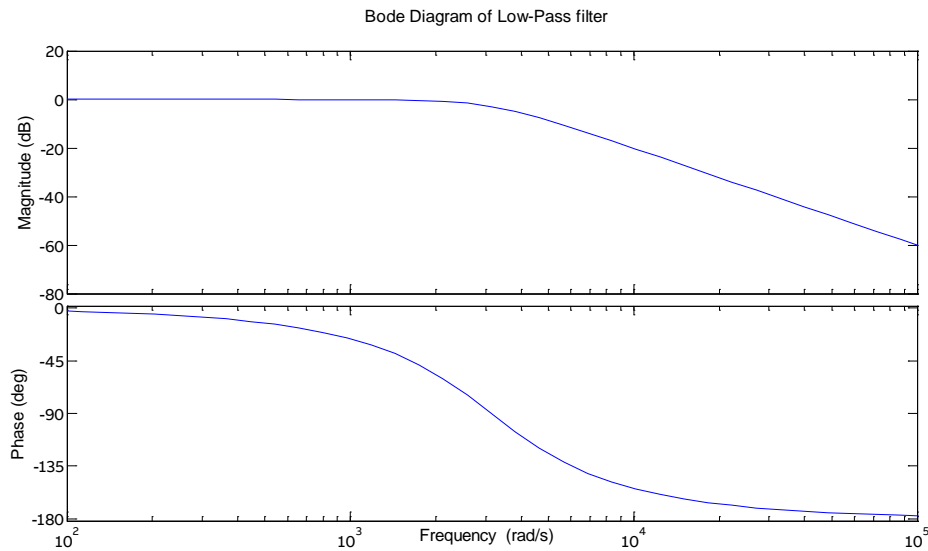
B) Simulink implementation with state-space modeling
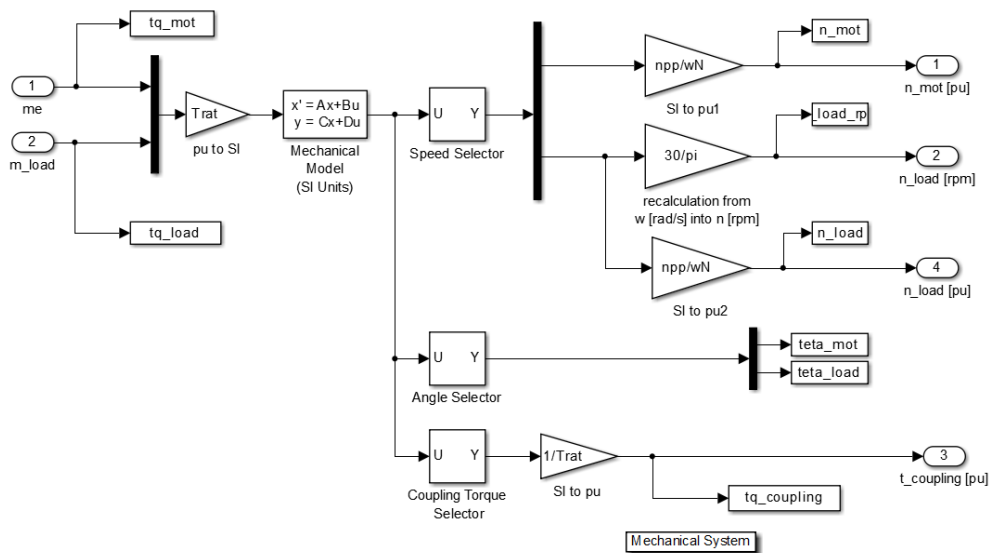
Appendix 14 – Software filters

The most common second order filters are described with transfer function (where ω_c is the cut-off frequency and δ represents the damping) and corresponding Bode diagram.
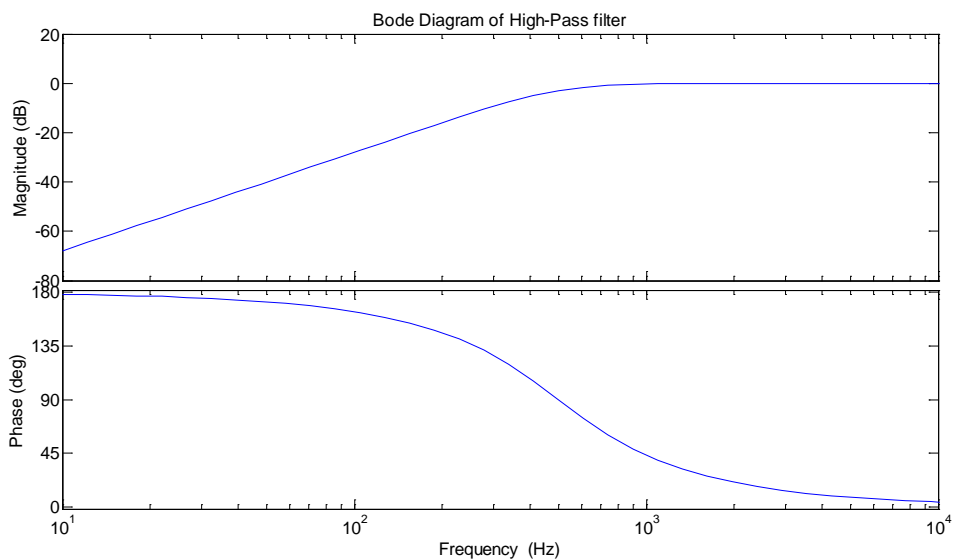
- Low pass filter (LP)

  Transfer function $\qquad F_{LP}(s) = \dfrac{1}{1 + \frac{2 \cdot \delta \cdot s}{\omega_c} + \left(\frac{s}{\omega_c}\right)^2}$

Bode Diagram of Low-Pass filter

Usage of LP filter: Reduction or elimination of high frequency components, e.g. to remove ripple from measured signal and get just fundamental component.
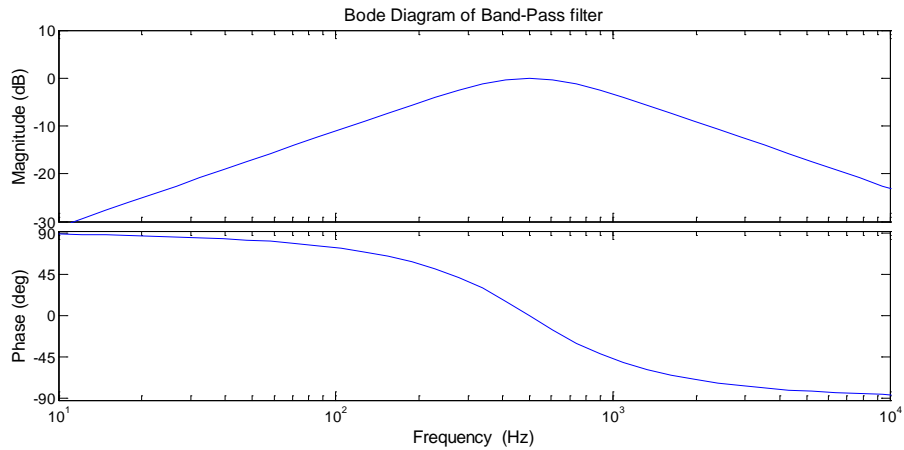
- High pass filter (HP)

  Transfer function $\qquad F_{HP}(s) = \dfrac{\left(\frac{s}{\omega_c}\right)^2}{1 + \frac{2 \cdot \delta \cdot s}{\omega_c} + \left(\frac{s}{\omega_c}\right)^2}$

Bode Diagram of High-Pass filter

Usage of HP filter: Reduction or elimination of low frequency components, e.g. to remove DC component or fundamental harmonic.
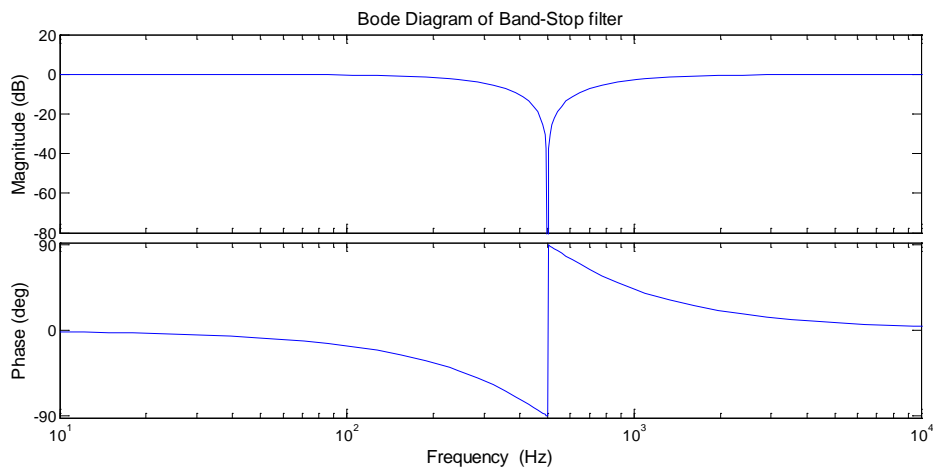
- Band pass filter (BP)

    Transfer function
    $$F_{BP}(s) = \frac{\frac{2 \cdot \delta \cdot s}{\omega_c}}{1 + \frac{2 \cdot \delta \cdot s}{\omega_c} + \left(\frac{s}{\omega_c}\right)^2}$$

Bode Diagram of Band-Pass filter

Usage of BP filter: Block (remove) the whole frequency spectrum besides a defined frequency range.

- Band stop filter (BS)

    Transfer function
    $$F_{BS}(s) = \frac{1 + \left(\frac{s}{\omega_c}\right)^2}{1 + \frac{2 \cdot \delta \cdot s}{\omega_c} + \left(\frac{s}{\omega_c}\right)^2}$$

Bode Diagram of Band-Stop filter

Usage of BS filter: Remove specific frequency or narrow frequency range from measured spectrum.

Passive control damping functions require only few fundamental data of the driven equipment such as e.g. the values of torsional natural frequencies.

The shape (frequency characteristic) of above filters is significantly impacted by the damping value. This is illustrated on the examples of band-pass filter below for damping values 0.16, 1.0 and 3.0.
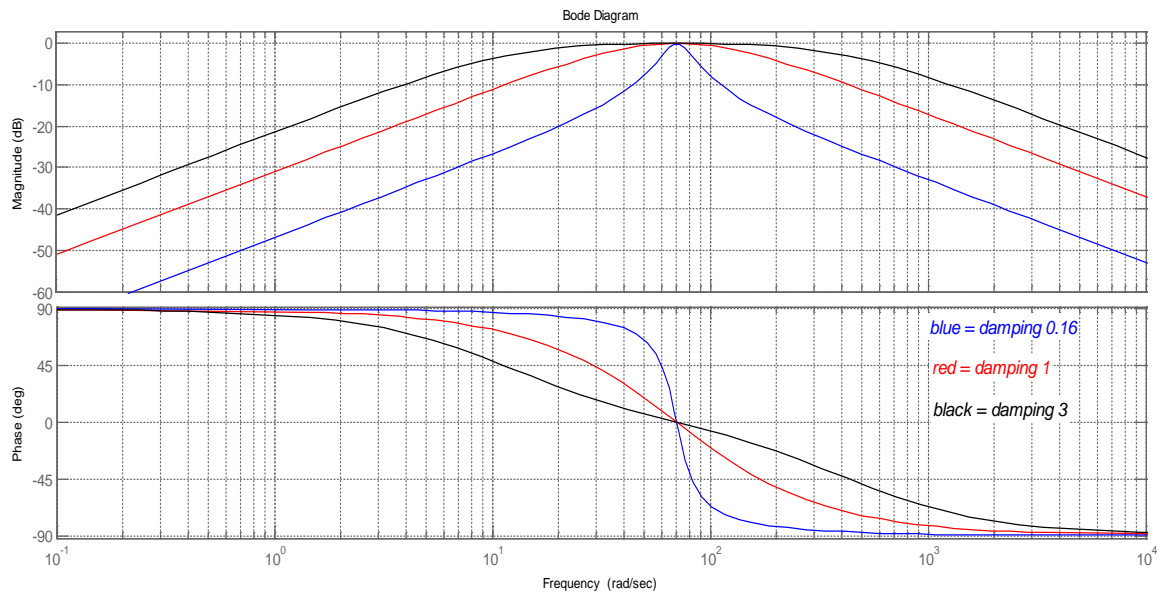
Appendix 15 – Background on waterfall plots

The waterfall plots shown in submitted thesis are mostly "2-dimensional", i.e. one axis is time (usually x-axis) and the other axis is the frequency (usually y-axis). The magnitude of the frequency components is represented by a colorbar. The waterfall plot actually consists of a series of FFTs over the time domain signal; the principle is a moving window with certain overlap (see figures below).

Typical settings of waterfall plot:

Window length: 1, 2 or 4 seconds (dynamic processes require shorter length while for steady state or quasi steady state trends longer window can be used)

Step size: 0.1 to 0.5 seconds (smaller step size provides smoother diagram)

Overlap: In order to get a smooth trend, an overlap of time windows is required. Presented figures use high overlap up to 90-98%.

overlap = (window length – step size) / window length * 100%

Windowing function: Hann, Hanning, Hamming or Blackmann-Harris windows
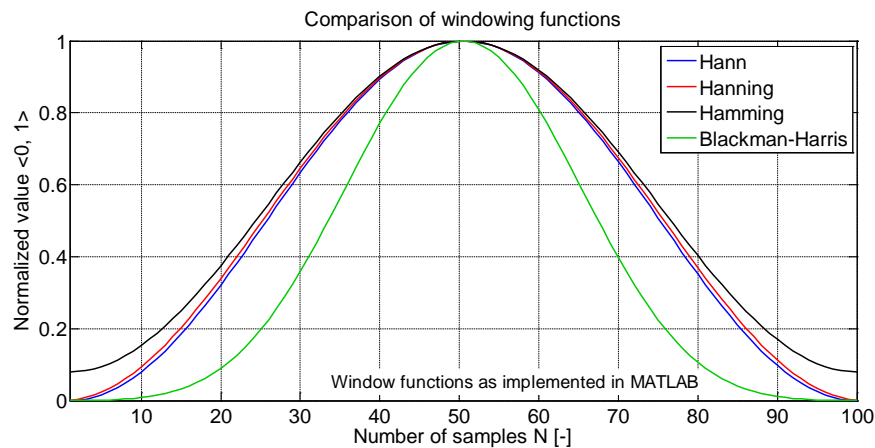

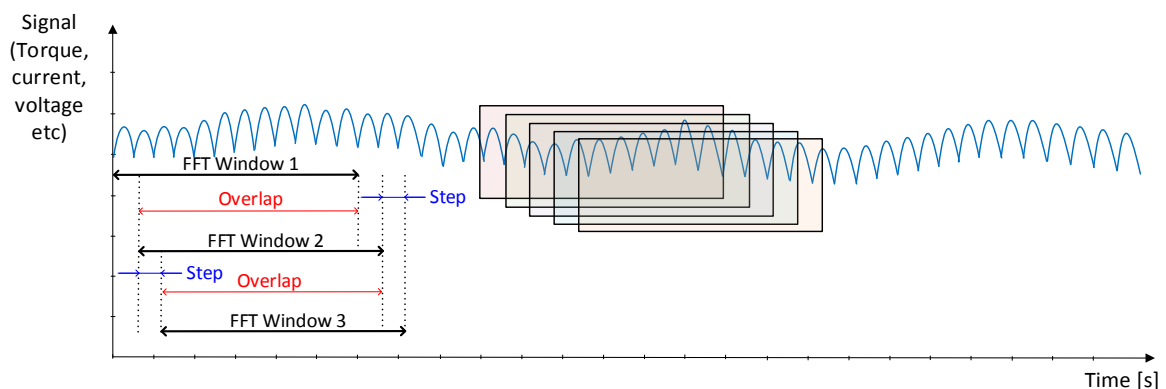Figure A9.1 – Comparison of most frequent windowing functions

Figure A9.2 – Principle of generation of waterfall plot by using a moving FFT window

The author has positive experience with window length of 4 seconds for slowly changing trends and length of 1 to 2 seconds for a bit faster trends (step size in both cases 0.1 seconds). Longer window length provides better resolution of frequency (y-axis), but suppresses transients due to averaging.

Short window length makes transients better visible, but it influences the frequency axis. Selection of window length is therefore always a compromise. This is illustrated in figure below.
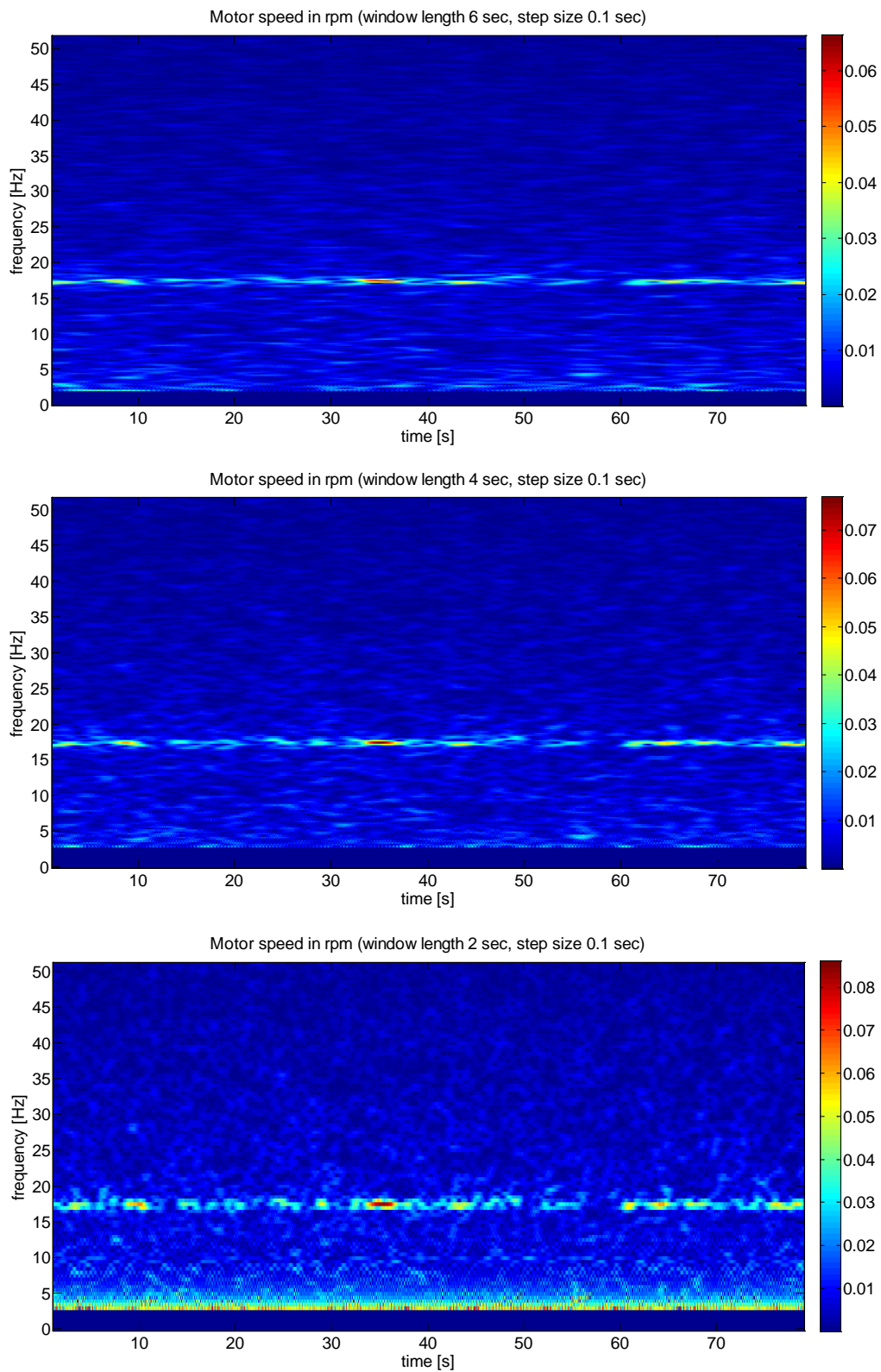

Figure A9.3 – Waterfall diagrams of identical signal; upper – window length 6 seconds, middle – window length 4 seconds, lower – window length 2 seconds

Appendix 16 – Slip of VFD driven induction machine at rated point

Shaft power [kW]	Rated speed [rpm]	Stator freq. [Hz]	Rated torque [Nm]	Rated slip [%]	Breakdown torque [pu]
900	2'997.0	50.4	2'868	0.89%	not known
1'200	1'450.0	48.7	7'903	0.75%	1.90
1'500	1'422.5	47.7	10'070	0.59%	2.10
2'100	1'499.9	50.3	13'370	0.60%	2.80
2'300	1'799.8	60.3	12'203	0.51%	2.40
3'400	1'463.0	49.0	22'192	0.48%	2.90
4'750	3'437.0	57.6	13'197	0.55%	2.30
6'100	1'429.6	47.9	40'746	0.51%	2.40
6'500	1'500.2	50.3	41'375	0.58%	2.40
7'000	1'500.0	50.2	44'563	0.40%	2.40
7'370	3'590.0	60.2	19'604	0.61%	2.90
8'700	1'380.0	46.2	60'202	0.43%	2.20
8'700	3'588.4	60.0	23'152	0.32%	2.59
9'000	1'500.0	50.2	57'296	0.40%	2.50
9'000	3'602.1	60.3	23'859	0.44%	2.05
10'300	1'500.0	50.2	65'572	0.40%	2.60
11'500	1'500.0	50.2	73'211	0.40%	2.30
15'290	1'800.0	60.3	81'116	0.50%	2.90
17'400	1'500.0	50.2	110'772	0.40%	2.20
21'250	1'775.0	59.4	114'323	0.39%	2.20
21'700	1'807.0	60.5	114'676	0.44%	2.10

Slip at rated point versus shaft power